FIRE RESEARCH AND DEVELOPMENT TECHNICAL REPORT

Considerations for Fire Service Response to Residential Battery Energy Storage System Incidents

December 4, 2023

Alex Schraiber, PE
Adam Barowy*
Ben Gaudet, PE
Veronica Kimmerly, PhD
*UL Fire Safety Research Institute

Prepared for the International Association of Fire Fighters

Executive Summary

As the installation of residential energy storage systems (ESS) increase, the frequency of fire incidents involving these products will increase. To date, at least 60 residential ESS fire events have been documented globally, including 19 incidents in 2022 and 21 incidents at the time of this publication in 2023. In response to this new and evolving hazard for the fire service, the International Association of Fire Fighters partnered with UL Solutions and UL Fire Safety Research Institute to conduct a series of large-scale tests sponsored by the U.S. Department of Energy. This test series was designed to characterize the challenges for fire fighters responding to fires involving residential energy storage systems with a focus on developing size-up and tactical considerations to support the fire service in navigating the modern fireground.

This project included four large scale tests including one baseline test and three tests utilizing a mockup of a residential lithium-ion battery energy storage system installed in a representative two-car garage. The ESS was constructed with three units with an equivalent energy capacity of 17 kWh per unit. The impact if ventilation operations were considered for scenarios batteries enter thermal runaway without prompt ignition, as well as scenarios where batteries are involved in a surrounding room and contents fire.

This testing demonstrated the impact of lithium-ion battery involvement on fire growth rate. For the firefighter, this means incipient fires, well-developed fires, and explosion hazards followed by fires, and rapid-fire growth should all be included in their mental models considered when responding to li-ion battery-initiated incidents. Unburned battery gas, if present in a ventilation limited fire, will increase the flammability of the smoke and can contribute to increased risk of backdraft, as demonstrated in Tests 3 and 4. This reinforces the potential impact of ventilation that could result in deflagration or a rapid transition to flashover. Deflagration scenarios in a residential garage are considered in three cases: partial volume deflagration, full volume deflagration, and backdraft.

Lithium-ion battery thermal runaways without active fire may be recognizable by distinct white/gray battery gas leaking from the structure and forming low-hanging clouds. Should thermal runaways occur after fire fighters enter, thermal runaways can be indicated by a two-layer accumulation of whitish/gray lighter gases near the ceiling and heavier gases and vapors along the floor. However, there are no reliable visual, thermal imaging, or portable gas meter indicators to confirm battery involvement in a room and contents fire. Additional indicators for battery involvement should be considered beyond smoke appearance. Other common detection methods (smoke alarms, CO alarms, heat alarms) may be able to detect thermal runaway but may not be viable to detect all thermal runaway scenarios and may be susceptible to nuisance.

The timing and severity of a battery gas explosion is unpredictable. An explosion hazard begins the instant batteries undergo thermal runaway and release gas without burning. A significant explosion hazard can develop before any exterior indicators (visual or measurable) are shown. Additionally, unburned battery gas ignites readily and can increase the flammability of the smoke in a ventilation-limited fire. Firefighters are at

greatest risk for explosion hazards in the driveway and at doors, windows, and other vent points. The fire apparatus should not be parked in front of the garage door to avoid this hazard.

Portable gas meters are not effective for determining whether a garage fire involves li-ion batteries. The structure should not be approached or entered to take gas meter measurements if there is a suspected case of batteries in thermal runaway and there are no indicators of a concurrent fire. Full structural PPE (Level D ensemble) with full SCBA should be donned before performing size-up. In all cases when li-ion thermal runaways are suspected, hose lines should be pre-deployed, charged, and ready for operations before ventilation or entry.

Notice

The issuance of this Report does not constitute an endorsement of any proposed amendment and in no way implies Certification, Listing, Classification or other recognition by UL and does not authorize the use of UL Certified, Listed or Classified Marks or any other reference to UL on, or in connection with, the product. This report can be used and referenced in alignment with our customer marketing guidelines available at https://marks.ul.com/about/ul-listing-and-classification-marks/promotion-and-advertising-guidelines/testing-inspection-auditing-software-and-test-tools-marketing-guidelines/.

UL LLC, its employees and its agents shall not be responsible to anyone for the use or nonuse of the information contained in this Report, and shall not incur any obligation or liability for damages, including consequential damages, arising out of or in connection with the use of, or inability to use, the information contained in this Report.

This material is based upon work supported by the U.S. Department of Energy's Office of Energy Efficiency and Renewable Energy (EERE) under the Solar Energy Technologies Office Award Number DE-EE0009454.

Acknowledgements

UL Solutions thanks Sean DeCrane and Kelly Opert for their project administration, technical input and leadership in obtaining the grant opportunity. UL Solutions also thanks Greg Sutter and Mark Hojnacki for their technical expertise in the design and execution of the test program.

UL Solutions thanks the members of the project advisory panel, listed below, for providing technical input to planning of this project, contributing valuable feedback during the execution of the tests, and in representing the concerns and inputs of the firefighter community.

Tom Abbott	Surprise Fire Department
Dave Bernzweig	International Association of Fire Fighters (IAFF)
John Cassidy	Fire Department of the City of New York (FDNY)
Hunter Clare	Peoria Fire Department
Ningshengjie Gao	Fire Department of the City of New York (FDNY)
Mike Gorin	National Fire Protection Association (NFPA)
Steve Kerber	UL Fire Safety Research Institute
Andrew Klock	National Fire Protection Association (NFPA)
Brian Kokkila	Pittsburgh Fire Department
Kevin Kuntz	Verisk/ISO
Michael Maiz	Fire Department of the City of New York (FDNY)
Michael O’Brian	Brighton Area Fire Authority
Matt Paiss	Pacific Northwest National Laboratory
Paul Rogers	International Association of Fire Fighters (IAFF)
Larry Sherwood	Interstate Renewable Energy Council
Paul Shoemaker	Next Level Extrication
Rick Swan	International Association of Fire Fighters (IAFF)
Bob Zalosh	Firexplo LLC

UL Solutions also recognizes and thanks Mountain View Fire Rescue for sharing explosion incident narrative and video footage.

This report is dedicated to the memory of Professor Bob Zalosh.

Table of Contents

Executive Summary ii
Notice iv
Acknowledgements vi
Table of Contents x
Table of Tables xii
Table of Figures xiv
1 Introduction 20
1.1 Objectives 20
1.2 Scope 20
1.3 Technical Plan 21
1.4 Glossary 21
2 Literature Review 23
2.1 Growth of Energy Storage Systems 23
2.2 ESS Incidents 25
2.3 ESS Safety Standards 37
2.4 Survey of Residential ESS Products 40
2.5 Garage Construction 41
2.6 Garage Firefighting Tactics 42
2.7 Summary 43
3 Test Setup 44
3.1 Large-Scale Test Facility 44
3.2 Construction 45
3.3 Instrumentation 54
3.4 Simulation of Ventilation Operations 66
4 Procedure 71

5 Results 74
5.1 Test 1 74
5.2 Test 2 95
5.3 Test 3 123
5.4 Test 4 150
6 Discussion of Results 178
6.1 Impact of Li-ion Battery Involvement on Fire Growth Rate 178
6.2 Impact of Battery Gas on Smoke Flammability 179
6.3 Impact of Ventilation 180
6.4 Deflagration Hazards 180
6.5 Visual Indications of Li-Ion Battery Involvement in Fire 184
6.6 Detection of Thermal Runaways with Portable Gas Meters 185
6.7 Detection of Residential Explosion Hazards 186
6.8 Detection of Hydrogen Fluoride (HF) 187
7 Fire Service Size-Up and Tactical Considerations 188
8 References 198
Appendix A: Development Tests of ESS Unit 203
Module 203
Unit 204
Appendix B: Portable Gas Meter Technologies 217

Table of Tables

Table 1 – Cell, module, and unit characteristics. 50
Table 2 – Cell level thermal runaway properties. 52
Table 3 – Gas measurement equipment. 58
Table 4 – Gas sensor technologies. 65
Table 5 – Sensors and Sensor Cross-Sensitivities Listed for RAE Systems Sensors 65
Table 6 – Ventilation sequence. 70
Table 7 – Thermal runaway propagation summary for Test 2. 103
Table 8 – Thermal runaway propagation summary for Test 3. 129
Table 9 – Thermal runaway propagation summary. 159
Table 10 – Minimum ignition energies [38]. 179
Table 11 – Estimated battery gas volume in garage at ignition based on gas concentration measurements. 181
Table 12 – Pressure damage thresholds [42]. 183
Table 13 – Gas concentrations measured at the time of venting or deflagration (Test 2), and the peak gas concentration measured prior to that time in parentheses. 185
Table 14 – Concentration thresholds for HF. 187
Table 15 – Timing of thermal runaway and major test events in Scenario 1. 208
Table 16 – Timing of thermal runaway and major test events in Scenario 2. 214
Table 17 – Correction factors for a catalytic bead LEL sensor calibrated for Methane. 219

Table of Figures

Figure 1 – Trends for global residential energy storage in USD billions [7]. 23
Figure 2 – Trends in US residential ESS installations [9]. 24
Figure 3 – Annual US electric generating capacity additions [10] 24
Figure 4 – Breakdown of battery application across 141 lithium-ion battery ESS incidents. 25
Figure 5 – Breakdown of failure type within 141 ESS lithium-ion battery failure incidents. 25
Figure 6 – Global distribution of residential ESS incidents. 26
Figure 7 – Breakdown of failure type within 60 residential ESS lithium-ion battery incidents. 26
Figure 8 – Year over year trends in ESS lithium-ion battery failure events (pink denotes residential ESS). 27
Figure 9 – Damage to window during incident [16]. 28
Figure 10 – Burning ESS after removal from residence [17]. 29
Figure 11 – ESS unit condition after firefighting operations [11]. 29
Figure 12 – Garage condition following incident [19]. 30
Figure 13 – Concrete bunker where ESS incident occurred [20]. 31
Figure 14 – Aftermath of Adelaide incident [21]. 32
Figure 15 – Window damaged by explosion [23]. 33
Figure 16 – Fire service responding to incident [23]. 33
Figure 17 – Battery condition following incident [23]. 33
Figure 18 – Fire damage to property following lithium ion battery thermal runaway [24]. 34
Figure 19 – Conditions after fire caused by residential ESS [25]. 35
Figure 20 – Responding firefighting crew [26]. 36
Figure 21 – Garage door location following garage explosion [26]. 36
Figure 22 – Manufacturer market share in US in 2020 [9]. 40
Figure 23 – Garages in Single-Family Homes Built by Year, based on US Census Bureau data [31] 41
Figure 24 – Test facility layout. 44
Figure 25 – Naming convention for the different exterior sides of the garage. 45
Figure 26 – Test structure (A-side). 46
Figure 27 – Test structure (B-side). 46
Figure 28 – Test structure (C-side). 47
Figure 29 – Test structure (D-side). 47
Figure 30 – Test structure (Garage door interior). 48
Figure 31 – ESS layout in Test 2 through Test 4. 49
Figure 32 – Module construction. 50
Figure 33 – Unit construction with modules (left), expanded metal insert layer (center), and sheet steel cover (right). 51
Figure 34 – Rack storage of commodity along C-side wall (left) and D-side wall (right). For Test 2 – 4, the center rack on the D-side wall was replaced with residential ESS units. 53
Figure 35 – Cut away of single box showing cups. 53

Figure 36 – Exterior instrumentation key. 54
Figure 37 – Exterior instrumentation plan view. 54
Figure 38 – Interior instrumentation key. 55
Figure 39 – Interior instrumentation plan view. 55
Figure 40 – Thermocouple array (outlined in orange). 56
Figure 41 – Location of ceiling gas probe (outlined in orange). 57
Figure 42 – Location of gas probe in front of garage door (outlined in orange, sampling location near bottom of rectangle). 57
Figure 43 – HD camera (left) and TIC camera (right) installed through garage door. 58
Figure 44 – Initiating module constructed from 18650 cells. 59
Figure 45 – Initiating Unit instrumentation layout (module TCs marked in red, outer enclosure TCs marked in blue). 60
Figure 46 –Target Unit instrumentation layout. 61
Figure 47 – Heat flux gauge placement (outlined in orange). 62
Figure 48 – Schmidt-Boelter heat flux gauge. 62
Figure 49 – Measurement locations for HF. 63
Figure 50 – Example of tunable diode laser emitter and reflector. 63
Figure 51 – Fire service portable gas meter locations. 64
Figure 52 – Exterior camera locations. 66
Figure 53 – Inverted-V cutting operation with rotary rescue powered saw. 67
Figure 54 – Spark fountain positioning. 68
Figure 55 – Spark fountain operation. 69
Figure 56 – Ignition location on the D-side wall for Test 1. 71
Figure 57 – Location of thermal runaway within Unit 1, shown on D-side wall for Test 2 and Test 4. 72
Figure 58 – Location of thermal runaway within Unit 1, shown on D-side wall for Test 3. 73
Figure 59 – Ignition of Group A commodity using an electric match at resultant fire growth. 74
Figure 60 – Sequence of events between 3 and 6 minutes of test time in Test 1. 75
Figure 61 – Sequence of events occurring between 6 and 20 minutes of test time. 76
Figure 62 – Suppression of the test at 21 minutes. 77
Figure 63 – Temperature measurements inside the garage for Test 1. 78
Figure 64 – Interior upper layer gas measurements for Test 1. 79
Figure 65 – Heat flux measurement in Test 1. 80
Figure 66 – Exterior gas measurements at the garage door in Test 1. 81
Figure 67 – HF measurements in Test 1. 81
Figure 68 – Images from commodity ignition (00:00). 83
Figure 69 – Images from first external signs of smoke (03:00). 84
Figure 70 – Images from first gerb operation (05:30). 85
Figure 71 – Images from 1 minute post-ventilation (07:00). 86
Figure 72 – Images of visible flaming in vent plume and ‘breathing’ pattern (17:40). 87
Figure 73 – Images from test termination and suppression (21:00). 88
Figure 74 – CO Concentration measurement by all portable gas meters. 89
Figure 75 – Portable gas meter readings at garage door. 90

Figure 76 – Portable gas meter readings at garage door (zoomed in on low concentrations). 90
Figure 77 – Portable gas meter readings 20 ft in front of garage door. 91
Figure 78 – Portable gas meter readings 20 ft in front of garage door (zoomed in on low concentrations). 91
Figure 79 – Portable gas meter readings 40 ft in front of garage door. 92
Figure 80 – Portable gas meter readings 40 ft in front of garage door (zoomed in on low concentrations). 92
Figure 81 – Portable gas meter readings at C-side service door. 93
Figure 82 – Portable gas meter readings at C-side service door (zoomed in). 94
Figure 83 – Thermal runaway initiation and propagation through initiating unit. 95
Figure 84 – Gas release and heat development in ESS unit enclosure at 29:43 (TR + 09:13). 96
Figure 85 – Deflagration and resultant smoke plume from the garage at 36:26 (TR + 15:56). 96
Figure 86 – Test events between 36 and 49 minutes of test time in Test 2. 97
Figure 87 – Fire growth and test termination in Test 2 (post 49 minutes). 98
Figure 88 – Temperature measurements in the initiating battery module (“Unit1Init2”). 98
Figure 89 – Temperature measurements within the initiating unit (Unit 1) of Test 2. 99
Figure 90 – Status of Unit 1 modules at the time of deflagration (36:26, TR + 15:56) 99
Figure 91 – Thermal images of thermal runaway propagation through Unit 1 in Test 1 100
Figure 92 – Unit 1 enclosure exterior temperatures in Test 2. 100
Figure 93 – Unit 2 enclosure exterior temperatures in Test 2. 101
Figure 94 – Temperature measurements within the center unit (Unit 2) of Test 2. 101
Figure 95 – Unit 3 enclosure exterior temperatures in Test 2. 102
Figure 96 – Temperature measurements within the rightmost unit (Unit 3) of Test 2. 102
Figure 97 – Temperature inside the garage for Test 2. 104
Figure 98 – Temperature inside the garage between 0 and 36 minutes for Test 2. 105
Figure 99 – Temperature inside the garage between 36 and 37 minutes for Test 2. 105
Figure 100 – Interior upper layer gas measurements for Test 2. 106
Figure 101 – Thermal image sequence of ignition and deflagration (36:24 to 36:26). 107
Figure 102 – Exterior effects of deflagration in Test 2. 108
Figure 103 – Exterior gas measurements at the garage door in Test 2. 109
Figure 104 – HF measurements in Test 2. 110
Figure 105 – Gas accumulation from battery thermal runaway (24:45, TR + 4:45). 111
Figure 106 – Early exterior smoke showing (25:50, TR + 5:20). 112
Figure 107 – Exterior view during propagating thermal runaway (30:50, TR + 10:20). 113
Figure 108 – Visual conditions immediately prior to deflagration (36:26, TR + 15:56). 114
Figure 109 – Conditions 10 seconds after deflagration (36:36, TR + 16:06). 115
Figure 110 – Conditions 1 minute after deflagration (37:26, TR + 16:56). 116
Figure 111 – Conditions 5 minutes after deflagration (41:26, TR + 20:56). 117
Figure 112 – View during suspected thermal runaway propagation (44:42, TR + 24:12). 118
Figure 113 – All portable meter CO measurements in Test 2. 119
Figure 114 – Portable meter measurements at garage door in Test 2. 120

Figure 115 – Portable meter measurements at garage door in Test 2 (zoomed in). ... 120
Figure 116 – Portable meter measurements at driveway 20 ft location in Test 2. 121
Figure 117 – Portable meter measurements at driveway 40 ft location in Test 2. 121
Figure 118 – Portable meter measurements at C-side service door in Test 2............ 122
Figure 119 – Ignition of Group A commodity using an electric match at time 00:01. ... 123
Figure 120 – Sequence of events in Test 3 leading up to 19 minutes of test time. 124
Figure 121 – Sequence of events occurring between 19 and 53 minutes of test time. 125
Figure 122 – Suppression of the test at 53 minutes and 41 seconds. 126
Figure 123 – Surface temperatures of cells inside of residential ESS unit #1. 127
Figure 124 – Surface temperatures of cells inside the initiating module of residential ESS unit #1. 127
Figure 125 – Surface temperatures of cells contained in residential ESS Unit 1......... 128
Figure 126 – Surface temperatures of cells in residential ESS Unit #2. 130
Figure 127 – Surface temperatures of cells in residential ESS Unit #3. 130
Figure 128 – Gas temperatures measured in the center of the garage during Test 3, from 0 to 50 minutes test time. 131
Figure 129 – 90 second sequence of infrared images showing diminishment of burning in Group A commodity and increase in thermal runaway events. 132
Figure 130 – Gas temperatures measured in the center of the garage during Test 3, from 51 to 54 minutes test time. 133
Figure 131 – Gas temperatures measure in the garage door vent during Test 3, from 51 to 54 minutes test time. 134
Figure 132 – Sequence of photographs showing period of transition into vent-limited burning from 11 to 28 minutes of test time. 135
Figure 133 – Gas concentrations measured in the garage during Test 3. 136
Figure 134 – Heat flux measured in front of the garage door in Test 3. 138
Figure 135 – Exterior gas measurements at the garage door in Test 3...................... 139
Figure 136 – Images from first cell thermal runaway (19:14). 140
Figure 137 – Images from first module thermal runaway (32:11). 141
Figure 138 – Images from after at least 6 modules experienced thermal runaway within 90 seconds (43:56)......... 142
Figure 139 – Short lived transient pressure increase affecting neutral plane height. .. 143
Figure 140 – All portable meter CO measurements in Test 3 (0-2000 ppm). 144
Figure 141 – All portable meter CO measurements in Test 3 (0-200 ppm). 145
Figure 142 – All portable meter CO measurements in Test 3, for the period between 51 and 60 minutes (0-2000 ppm). 145
Figure 143 – Garage door meter measurements during Test 3. 146
Figure 144 – Garage door meter measurements during Test 3, for the period between 51 and 60 minutes......... 146
Figure 145 – Garage door meter measurements during Test 3, for the period between 51 and 60 minutes, zoomed in for lower gas concentrations......... 147
Figure 146 – C-side service door meter measurements during Test 3. 148
Figure 147 – C-side service door meter measurements during Test 3, for the period between 51 and 60 minutes. 148
Figure 148 – Portable meter measurements at driveway 20 ft location during Test 3. 149
Figure 149 – Portable meter measurements at driveway 40 ft location during Test 3. 149

Figure 150 – Test events between 25 and 28 minutes of Test 4. 150
Figure 151 – Battery gas ignition at 27:41 (TR + 02:20). 151
Figure 152 – Test events between 27 and 36 minutes in Test 4. 152
Figure 153 – Test events between 40 and 52 minutes of Test 4. 153
Figure 154 – Conditions at test termination (54 minutes) in Test 4. 153
Figure 155 – Temperature measurements in the initiating battery module (“Unit1Init1”). 154
Figure 156 – Temperature measurements within the initiating unit (Unit 1) of Test 4. 155
Figure 157 – Unit 1 enclosure exterior temperatures in Test 4. 155
Figure 158 – Unit 2 enclosure exterior temperatures in Test 4. 156
Figure 159 – Temperature measurements within the center unit (Unit 2) of Test 4. 157
Figure 160 – Unit 3 enclosure exterior temperatures in Test 4. 157
Figure 161 – Temperature measurements within the rightmost unit (Unit 3) of Test 4. 158
Figure 162 – Temperature inside the garage for Test 4. 160
Figure 163 – Temperature inside the garage between 25 and 45 minutes for Test 4. 161
Figure 164 – Interior upper layer gas measurements for Test 4. 161
Figure 165 – Exterior effects of deflagration (Left – Initial, Right – Peak deflection) in Test 4. 162
Figure 166 – Heat flux measurement in Test 4. 163
Figure 167 – Exterior gas measurements at the garage door in Test 4. 164
Figure 168 – HF measurements in Test 4. 164
Figure 169 – Gas accumulation before ignition (27:40, TR + 02:19). 166
Figure 170 – Flaming observed at penetrations (27:42, TR + 02:21). 167
Figure 171 – Battery fire growth (28:27, TR + 03:06). 168
Figure 172 – Ignition and gas stratification (32:26, TR + 07:05). 169
Figure 173 – Conditions prior to opening C-side door (43:21, TR + 18:00). 170
Figure 174 – Conditions immediately after opening door (43:23, TR + 18:02). 171
Figure 175 – Conditions prior to backdraft (44:03, TR + 18:42). 172
Figure 176 – All CO measurements in Test 4. 173
Figure 177 – Measurements at garage door in Test 4 (0-300 ppm). 174
Figure 178 – Measurements at garage door in Test 4 (zoomed in to 0-50 ppm). 174
Figure 179 – Measurements at driveway 20 ft location in Test 4. 175
Figure 180 – Measurements at driveway 40 ft location in Test 4. 175
Figure 181 – Measurements at C-side rear door in Test 4. 176
Figure 182 – Measurements at C-side service door in Test 4 (zoomed in). 177
Figure 183 – Increasing explosion hazard with ongoing thermal runaway propagation. 189
Figure 184 – Still image of garage door contacting incident commander during explosion incident in Erie, CO. 191
Figure 185 – Sequence of images from different instances of accumulated battery gas leaking from structures. 192
Figure 186 – Visual indication of thermal runaways in Test 4: hot gas layer developing at ceiling and a clearly defined smoke layer remains at the floor. 193
Figure 187 – Module construction (left) and assembly (right). 203
Figure 188 – Module heat release rate. 203
Figure 189 – Photo of module at peak heat release rate. 204

Figure 190 – Interior of ESS units (left) and complete test setup (right) for Scenario 1. 205
Figure 191 – Initiating unit instrumentation layout. 206
Figure 192 – Left target unit instrumentation layout used in Scenario 1 and Scenario 2. 207
Figure 193 – Heat release rate from the first cell thermal runaway to the end of the test in Scenario 1. 208
Figure 194 – Images showing test progression in Scenario 1. 209
Figure 195 – Post-test condition of ESS units and Commodity boxes in Scenario 1... 210
Figure 196 – ESS unit interior (left) and complete setup (right). 211
Figure 197 – Heat release rate from the first cell thermal runaway to the end of the test in Scenario 2. 212
Figure 198 – Images showing test progression in Scenario 2. 215
Figure 199 – Post-test condition of ESS unit and Commodity boxes in Scenario 2. ... 216

1 Introduction

Renewable energy sources (e.g., rooftop photovoltaics, wind turbines) are capable of addressing our grid-level energy challenges by reducing environmental impacts, increasing resiliency, and increasing the supply of input energy. However, renewable energy sources alone are not a complete solution. The generation of power from major renewable energy sources fluctuates with the weather, creating significant challenges in matching electrical power generation to electrical power consumption. The value of renewable power generation sources is multiplied when paired with battery energy storage systems (ESS), which can store excess power generated from renewable energy sources when it is not consumed and deliver that power later when demand exceeds base power generation.

Residential ESS units are frequently installed to support renewable energy initiatives by storing energy from intermittent sources such as photovoltaic panels. Residential ESS units also offer an alternative to gas-powered generators or other backup power means. Lithium-ion batteries are the most common residential ESS technology due to their affordability and energy density. Though lithium-ion systems come with benefits, there is also a risk of thermal runaway within this technology which can result in flammable gas release, fire, and explosion.

As the installations of these products increase, the frequency of response to fire incidents involving these products will increase. In response to this new and evolving hazard, UL Solutions (ULS) and UL Fire Safety Research Institute (FSRI) have partnered with the International Association of Fire Fighters (IAFF) to conduct a series of large-scale tests sponsored by the US Department of Energy to characterize the challenges for fire fighters responding to fires involving residential energy storage systems. The project focuses on developing size-up and tactical considerations to support the fire service in navigating the evolving modern fireground.

1.1 Objectives

The test series was conducted with the following objectives:

1. Determine how the contribution of lithium-ion battery gas generated by thermal runaway in a residential energy storage system impacts compartment fire dynamics.
2. Develop fire fighter size-up and tactical considerations for incidents that may involve residential energy storage systems with lithium-ion batteries.

1.2 Scope

The scope of this investigation was limited to a UL-designed mockup of a residential battery energy storage system (ESS) that used lithium-ion cells with lithium nickel cobalt aluminum oxide (NCA) cathode chemistry and had a total system energy capacity of 51 kWh (17 kWh per unit, 3 units) installed in a two-car garage. The impact of a single ventilation operation was evaluated. Operations involving coordinated ventilation were not assessed. The impact of suppression operations was outside the scope of this project.

1.3 Technical Plan

Four tests were conducted in this test program. All four tests were conducted in a test structure representing an attached two-car garage. All four tests utilized a standardized commodity (Group A cartoned unexpanded plastic) to represent the multitude of combustible fuels that may be present in a residential garage. Three out of four tests included a mockup residential energy storage system comprised of three individual units.

Test 1 was a baseline test to characterize ventilation-limited conditions resulting from burning commodity fuel. Test 1 did not include a mockup ESS. Test 2 through Test 4 included a mockup ESS positioned between the commodity fuel. Test 2 characterized an event initiated by thermal runaway in the ESS, a delayed ignition of battery gases, and a subsequent fire. Test 3 characterized an event started with a commodity fire and later involving thermal runaway of the ESS units. Test 4 characterized an event initiated by thermal runaway in the ESS, a prompt ignition of battery gases, and a resultant fire. All four tests included simulated fire department ventilation operations following ventilation-limited conditions inside the garage.

Further detail is included in both Section 3 Test Setup and Section 4 Procedure.

1.4 Glossary

BACKDRAFT – A turbulent deflagration and external fireball caused by a fresh-air gravity current propagating through accumulated unburned gaseous fuel in an under-ventilated compartment fire and creating a mixed, flammable region that travels to an ignition source within the compartment. The influx of the gravity current is due to the creation of a ventilation opening in the compartment [1].

BATTERY GAS – A mixture of gases and vapors generated from lithium-ion battery thermal runaway. May include heavier gases and electrolyte aerosols which remain close to the ground, as well gases lighter than air or neutrally buoyant in air which rise upwards. The gases tend to be mixtures of hydrogen (H_2), carbon monoxide (CO), carbon dioxide (CO_2) and hydrocarbons.

BATTERY ENERGY STORAGE SYSTEM (BESS) – Stationary equipment that receives electrical energy and then utilizes batteries to store that energy to supply electrical energy at some future time. The BESS at a minimum consists of one or more modules, including a power conditioning system (PCS), a battery management system (BMS), and a balance of plant components [2].

CELL – The basic functional electrochemical unit containing an assembly of electrodes, electrolyte, separators, container, and terminals. It is a source of electrical energy by direct conversion of chemical energy [2].

DEFLAGRATION – Propagation of a combustion zone at a velocity less than the speed of sound in the unreacted medium [3]. The unreacted medium may entail a flammable mixture of an oxidizer and flammable gases, aerosols or dusts.

ELECTROLYTE – Usually a liquid- or gel-based solution that the anode and cathodes are immersed in which acts as a conductor allowing the lithium-ions to move between the cathode and anode. The electrolyte is typically a hydrocarbon-based mixture that includes multiple additives. [4]

IMMEDIATELY DANGEROUS TO LIFE OR HEALTH (IDLH) – An atmospheric concentration of any toxic, corrosive, or asphyxiant substance that poses an immediate threat to life or would interfere with an individual’s ability to escape from a dangerous atmosphere [5], [6].

MODULE – A subassembly that is a component of a BESS that consists of a group of cells or electrochemical capacitors connected in a series and/or parallel configuration (sometimes referred to as a block) with or without protective devices and monitoring circuitry [2].

PARTIAL VOLUME DEFLAGRATION - A deflagration explosion developed from a flammable cloud of gas, aerosol, or dust that occupies only part of the volume in a confined space [3].

THERMAL RUNAWAY – When an electrochemical cell increases its temperature through self-heating in an uncontrollable fashion. The thermal runaway progresses when the cell’s generation of heat from the chemical reaction occurs at a higher rate than the heat it can dissipate. This may lead to fire, explosion, and gas evolution [2].

UNIT – A frame, rack, or enclosure that consists of a functional BESS that includes components and subassemblies, such as cells, modules, battery management systems, ventilation devices, and other ancillary equipment [2].

VENTING – Cell venting occurs when sufficient internal pressure is generated, typically from the vaporization of liquid electrolyte, to operate a safety vent or otherwise rupture a cell casing/container.

SMOKE – Gaseous products and suspended particulates generated from combustion.

2 Literature Review

The literature review presented below describes the growth of ESS installations, a series of field incidents of ESS failure including residential systems, an overview of the residential ESS market, a summary of the relevant product and installation codes and standards, a review of residential garage construction, and a description of residential garage firefighting tactics.

Based on the literature review, a 20 ft by 20 ft two-car attached residential garage with a wall-mounted ESS was determined to be the representative hazard scenario for this research project. The representative ESS for testing had an energy capacity of 17 kWh per unit and 51 kWh aggregate. These capacities represent the upper end of energy capacity, but do not exceed the quantities permitted by NFPA 855. Common firefighter ventilation methods including the inverted-V cut and approach through the dwelling were utilized for the test scenarios.

2.1 Growth of Energy Storage Systems

Energy storage systems are seeing rapid growth around the world, due to decreasing technology costs and governmental incentivization of “green” energy production. In the global market, the lithium-ion segment is the fastest growing due to decreasing costs, pressure from environmental policies, and greater efficiency when compared to lead-acid batteries. As shown in Figure 1, the Asia-Pacific region is forecasted to be the largest market from 2019 to 2024, with the North America region coming in second [7].

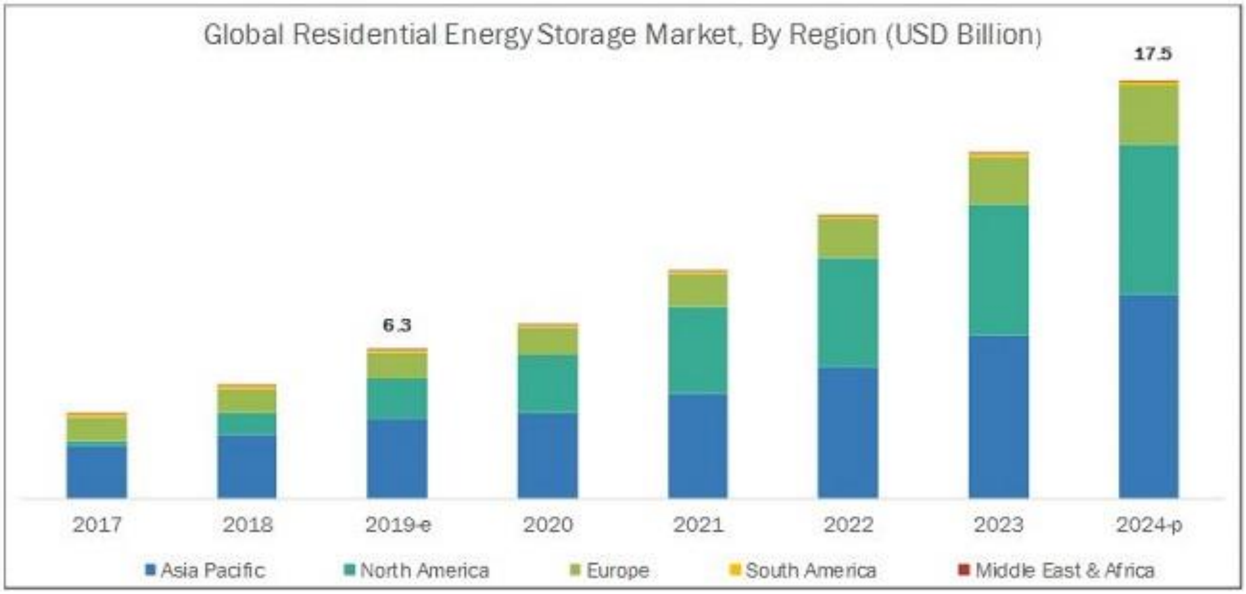

Figure 1 – Trends for global residential energy storage in USD billions [7].

The global market is forecasted to grow from $11 billion to $30 billion by 2029 (a 16.3% annual growth rate). In 2021, lithium-ion batteries were 98% of the global ESS market share. The use of ESS in residential settings is driven by governmental directives to increase solar power installations at the residential level [8].

The residential ESS market in the US has undergone rapid growth in the last few years. From 2017 to 2020, the US residential energy storage market grew from 29 MWh to 540 MWh, as shown in Figure 2 [9].

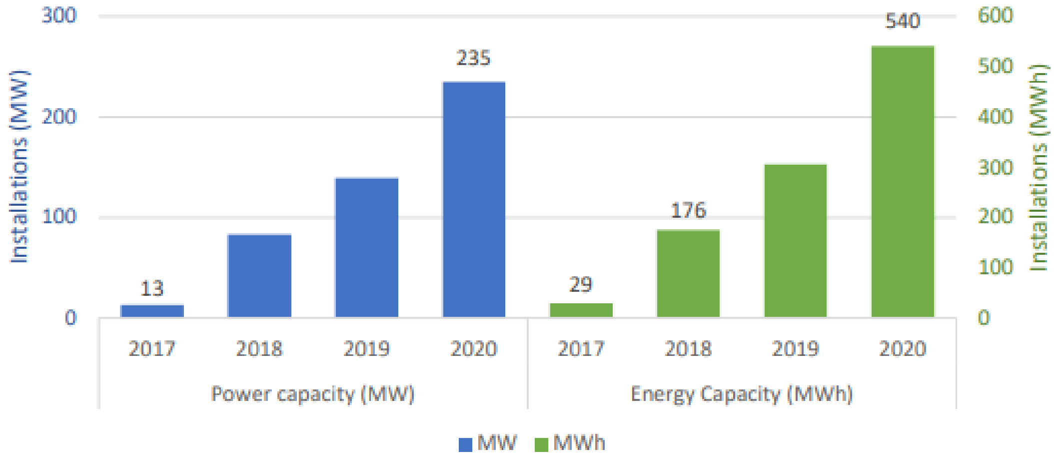

Figure 2 – Trends in US residential ESS installations [9].

In 2021, battery storage capacity in the U.S. significantly increased with 3.1 GW added to the grid (a 200% increase) due to a combination of tax credits and falling technology costs. From 2022 to 2023, power plant developers/operators expect to add 85 GW of new generating capacity to the grid, 60% of which will be solar power and battery storage projects. In 2023 and 2024, it is expected that an additional 10 GW of battery storage capacity, with 60% associated with solar power plants, will be added to the grid [10]. Figure 3 illustrates these numbers.

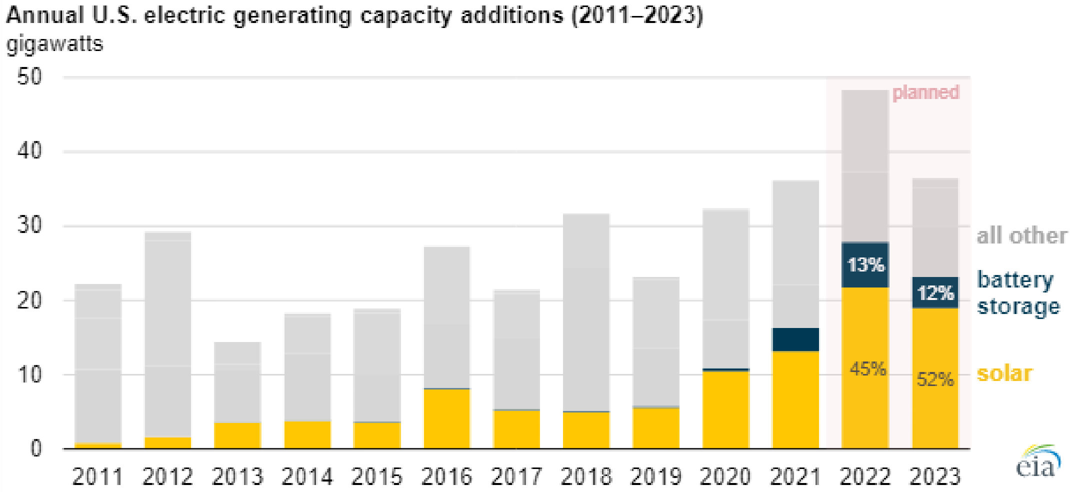

Figure 3 – Annual US electric generating capacity additions [10]

2.2 ESS Incidents

With the rapid rise of both residential and commercial ESS installations, within the US and globally, a concurrent increase in ESS safety incidents has been observed. To develop a clearer picture of the incidents being reported, an aggregate database of lithium-ion battery incidents (fires, explosions, etc.) was developed by UL Solutions from public databases, news articles, and government issued documents from around the world. At the time of writing, this database has identified over 8000 lithium-ion battery failure events, including 141 energy storage system events. Of these, 60 are residential ESS events, as shown in Figure 4 and Figure 5.

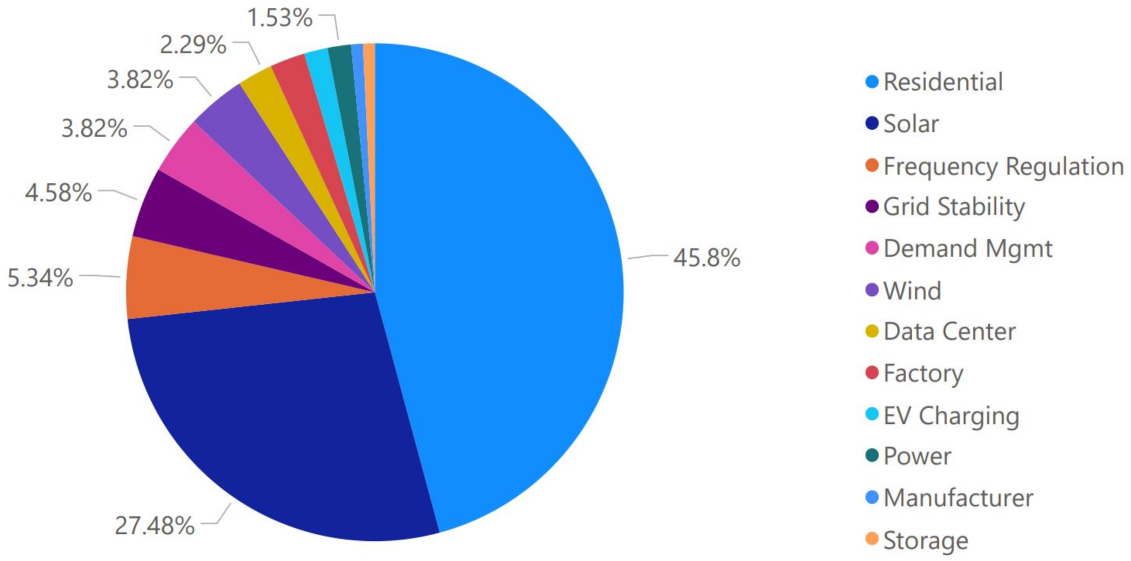

Figure 4 – Breakdown of battery application across 141 lithium-ion battery ESS incidents.

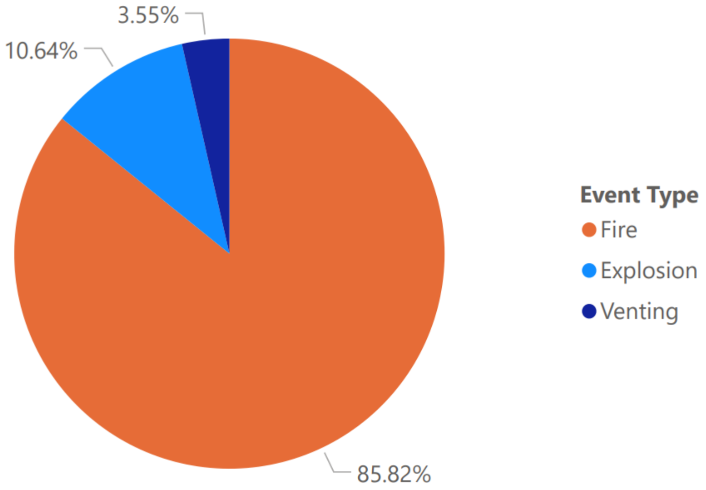

Figure 5 – Breakdown of failure type within 141 ESS lithium-ion battery failure incidents.

Figure 6 shows that residential ESS events have mainly been found in Europe and Asia, but events have been recorded in India, Australia, Japan, the United States, and Chad.

Figure 6 – Global distribution of residential ESS incidents.

Residential ESS systems have been found to experience fires, explosions, and venting due to thermal runaway. A breakdown is shown in Figure 7. These events have been reported during normal operation of the devices, pointing towards issues with the battery management systems (leading to electrical abuse) or manufacturing defects in the batteries that degrade the cell separator.

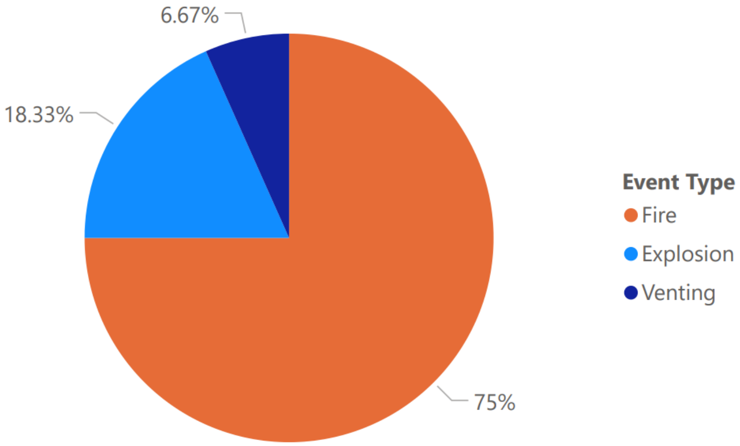

Figure 7 – Breakdown of failure type within 60 residential ESS lithium-ion battery incidents.

The frequency of residential ESS events increasing, with one incident in 2018, one in 2019, seven in 2020, 10 in 2021, 19 in 2022, and 21 in 2023 (as of this publication), as is shown in Figure 8. This is attributed to the growing adoption of residential solar systems across the world.

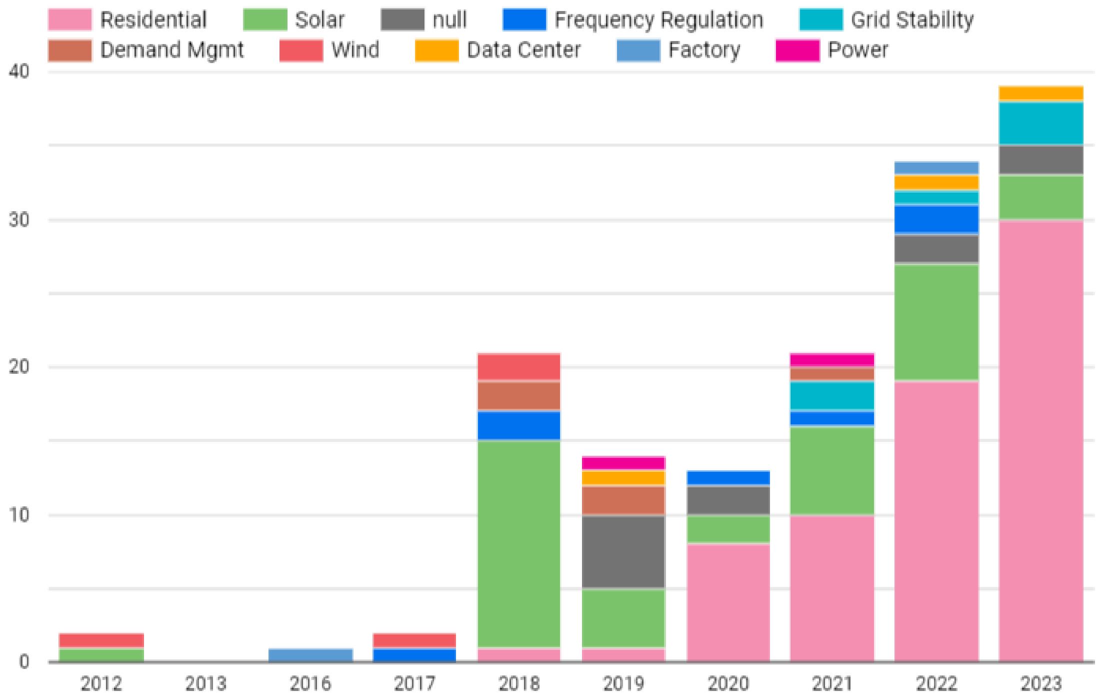

Figure 8 – Year over year trends in ESS lithium-ion battery failure events (pink denotes residential ESS).

In the sections below, several residential ESS case studies and two garage explosions due to electric vehicles will be described. Though the construction of an ESS and electric vehicles differ, the hazards of battery thermal runaway in a residential garage structure are consistent.

2.2.1 SENEC Solar Residential ESS Incidents in Germany

The week of March 10, 2022, the German ESS manufacturer SENEC announced that it had remotely switched all its residential ESS in Germany to a stand-by mode where the batteries would no longer store energy. This remote shutdown was due to reports of three explosions in houses with SENEC products [11]. The company described this as a “purely precautionary measure” and said this did not indicate a technical problem in their systems. SENEC started the process of bringing the ESS back online on March 21 [12] with full restoration by May 12 [13]. The press release for the shutdown mentions three explosions associated with SENEC systems one of which was in Bodnegg [11] and a second article says there are four incidents involving SENEC systems in Germany [14].

July 18, 2018 – Theilheim, Germany

A woman who was alone in her house reported that she heard a loud explosion from the basement and immediately fled the house and called the fire service. A fire followed the explosion, and the cause was found to be the recently installed ESS for the solar system. Firemen from five different brigades were called to contain the fire to the basement and protect the house. No one was injured but €100,000 of damage is reported [15].

September 3, 2020 – Grub am Forst, Germany

At approximately 5:20 pm a woman reported a fire in the basement of a house in the Coburg area. The fire service was able to bring the fire under control, but an explosion occurred during this process. The source of the fire was later identified as a technical defect in the ESS of a solar system. The two residents had initially attempted to fight the fire themselves and were later taken to the hospital for smoke inhalation [16]. Figure 9 shows some of the damage following the explosion and fire fighter operations.

Figure 9 – Damage to window during incident [16].

March 3, 2022 – Bodnegg, Germany

According to police investigation, at around 2 pm the ESS of a solar system exploded in the basement of a house in Bodnegg, Germany. The cause is suspected to be a technical defect in the system. The explosion was strong enough to push out several doors and windows and to lift the entire roof structure. No one was injured but the building was rendered uninhabitable with an estimated €250,000 of damages. The fire service sent five vehicles and 30 firefighters to fight the fire [17]. A technician from the local electrical utility service came to switch off power to the building and a master electrician pulled the fuses allowing the fire service to remove the ESS from the house. According to the fire service, the system reignited as it was brought outside and it was finally extinguished and put in a tank of water to cool it down and prevent further reignition [11]. This sequence of events is shown in Figure 10 and Figure 11.

Figure 10 – Burning ESS after removal from residence [17].

Figure 11 – ESS unit condition after firefighting operations [11].

April 27, 2022 – Sommerkahl, Germany

The Aschaffenburg fire brigade reported smoke associated with an ESS in the basement of a residential building but did not report a fire. The fire brigade used CO_2 to cool the batteries and cleared the smoke out with a fan. No one was injured in this incident. SENEC issued a statement regarding this fire and stated that they are still investigating the cause of this incident [18].

2.2.2 Battery Fire Incidents in Residences (ESS and EV)

Seven additional examples of residential battery fire incidents are described below.

July 27, 2019 – Montreal, Canada

On July 27, 2019 a Hyundai Kona was parked in a residential garage in Île-Bizard, Montreal, Canada when it caught fire and later caused an explosion [19]. The car was purchased in March 2019 and was not plugged in according to the owner. He called the fire service at 1 pm after seeing dark smoke coming from the closed garage and turning off the breaker to the garage. No one was injured but the owner said “If we were in front of the garage door, we could have been in the hospital.” The fire service reported that they could find no other sources inside the garage besides the car that could have caused the explosion. Figure 12 shows the position of the garage door as encountered upon arrival of the first due engine company.

Figure 12 – Garage condition following incident [19].

October 2, 2019 – Brown's Canyon, Colorado, United States

October 2, 2019 a fire broke out in a concrete bunker that contained the ESS for a residential solar and wind system. When the fire department arrived, black smoke was pouring out of the bunker around the metal garage door [20]. The batteries were in the back of the bunker (approximately 15 or 20 feet from the door) and the fire service used foam to extinguish the fire. No one was injured and the damage was confined to the bunker. Figure 13 is a photograph of the bunker ESS installation.

Figure 13 – Concrete bunker where ESS incident occurred [20].

February 12, 2022 – Adelaide, Australia

A resident of Burton, a suburb of Adelaide, was woken at 3 am on February 12, 2022 by his smoke alarm and bangs coming from the roof of his house. He called the fire service and then evacuated the house with the other residents. The fire started in the ESS for the solar system which was in the garage. No one was injured but the damage is estimated at $200,000 AUD and the garage is a total loss [21]. Damages are shown in Figure 14.

Figure 14 – Aftermath of Adelaide incident [21].

February 25, 2022 – Yokohama, Japan

Late at night on February 25, 2022, a fire was reported in the bedroom of a two-story wood structure in Yokohama City, Japan. The fire was reported to be coming from the storage battery of a solar panel in the bedroom. No one was injured but the bedroom was fully destroyed by the fire [22].

May 9, 2022 – Althengstett, Germany

On May 9, 2022, the fire service was called due to reports of white smoke coming out of a house’s basement where an ESS for a solar system was located. An explosion occurred shortly before the fire service arrived. The explosion blew out the basement windows and doors, and the doors in the house as well. No one was injured but the damages are estimated at €400,000 to €500,000 and the house is uninhabitable [23]. The fire operations manager said, “I'm so glad the explosion happened before my attack squads entered the house. I can't imagine what could have happened there.” The fire was brought under control and the remains of the ESS were submerged in water to cool it and prevent reignition. A sequence of key images is shown in Figure 15 - Figure 17.

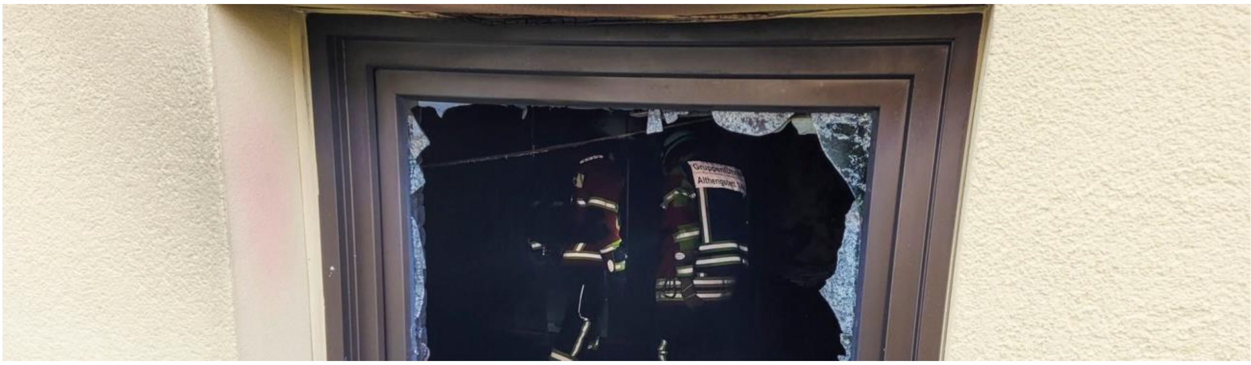

Figure 15 – Window damaged by explosion [23].

Figure 16 – Fire service responding to incident [23].

Figure 17 – Battery condition following incident [23].

December 17, 2022 – Sanbornton, New Hampshire, United States

On Saturday, December 17, 2022, one woman was injured in a fire resulting from a battery backup system that was utilized during a power outage. The battery system was installed in a mechanical room and constructed from three used lithium-ion batteries repurposed from Chevy Volt cars [24]. When the homeowner investigated a "popping" sound, she described the battery as "bubbling over" and when she returned with a fan, the battery was on fire with flame extension to the ceiling, at which point the local fire department was called. Figure 18 is a photograph of the incident after the fire.

Figure 18 – Fire damage to property following lithium ion battery thermal runaway [24].

February 15, 2023 – Epping, Sydney, Australia

A fire on 15 February 2023 in Epping, Sydney, Australia was found to be caused by a faulty li-ion battery by Fire and Rescue New South Wales. No one was injured but the house experienced significant damage. This incident highlights the challenges of second-life batteries in residential ESS systems due to the unknown history of the battery and how that affects the probability of it experiencing thermal runaway [25]. Figure 19 shows the condition of the home after the fire.

Figure 19 – Conditions after fire caused by residential ESS [25].

April 11, 2023 – Erie, Colorado, United States

On the morning of April 11, 2023, Mountain View Fire Rescue responded to a reported structure fire. There was no smoke showing at the time the crews arrived. Firefighters searched the first floor of the home to identify the source of the smoke. Smoke was found to be coming from the secondary garage. Within the garage, a Jeep Wrangler 4XE hybrid was smoking and a dense smoke condition had formed. An explosion involving the burning of this dense smoke layer occurred while firefighters applied water to the vehicle. The explosion propelled the garage door 30 ft into the yard. No one was injured [26], though the garage door came into contact with the helmet of the incident commander as it traveled through the air. Figure 20 shows the condition of the garage after the explosion. Figure 21 shows the position of the garage door after the explosion.

Figure 20 – Responding firefighting crew [26].

Figure 21 – Garage door location following garage explosion [26].

2.3 ESS Safety Standards

2.3.1 International Residential Code and International Fire Code – 2021 Editions

The International Residential Code, 2021 Edition, includes requirements for the installation of battery energy storage systems in residential applications in Chapter R328. Section R328.4 limits installation locations:

> "ESS shall be installed only in the following locations:
>
> 1. Detached garages and detached accessory structures
> 2. Attached garages separated from the dwelling unit living space in accordance with Section R302.6
> 3. Outdoors or on the exterior side walls located not less than 3 feet from doors and windows directly entering the dwelling unit
> 4. Enclosed utility closets, basements, storage or utility spaces within swelling units with finished or noncombustible walls and ceilings. Walls and ceilings of unfurnished wood-framed construction shall be provided with not less than 5/8-inch Type X gypsum wallboard.
>
> ESS shall not be installed in sleeping rooms, or closets or spaces opening directly into sleeping rooms" [27].

Section R328.5 limits energy ratings for ESS installations:

> "Individual ESS units shall have a maximum rating of 20 kWh. The aggregate rating of the ESS shall not exceed:
>
> 1. 40 kWh within utility closets, basements and storage or utility spaces.
> 2. 80 kWh in attached or detached garages and detached accessory structures.
> 3. 80 kWh on exterior walls.
> 4. 80 kWh outdoors on the ground.
>
> ESS installations exceeding the permitted individual or aggregate ratings shall be installed in accordance with Section 1207 of the International Fire Code" [27].

Section 1207 of the International Fire Code includes requirements for electrical energy storage systems [28]. Section 1207 includes requirements for battery energy storage systems exceeding threshold quantities based on energy capacity. For lithium-ion batteries, the threshold quantity is 20 kWh. A hazardous mitigation analysis is required to determine the following:

> "1. Fires will be contained within unoccupied ESS rooms or areas for the minimum duration of the fire-resistance-rated separations identified in Section 1207.7.4.

> 2. Fires in occupied work centers will be detected in time to allow occupants within the room or area to safety evacuate.
>
> 3. Toxic and highly toxic gases released during fires will not reach concentrations in excess of the IDLH level in the building or adjacent means of egress routes during the time deemed necessary to evacuate occupants from any affected area.
>
> 4. Flammable gases released from ESS during charging, discharging and normal operation will not exceed 25 percent of their lower flammability limit (LFL).
>
> 5. Flammable gases released from ESS during fire, overcharging, and other abnormal conditions will be controlled through the use of ventilation of the gases, preventing accumulation, or by deflagration venting."

A large-scale fire test, per UL 9540A, *Test Method for Evaluating Thermal Runaway Fire Propagation in Battery Energy Storage Systems*, is required for ESS to "show that a fire involving one ESS will not propagate to an adjacent ESS, and where installed within buildings, enclosed areas and walk-in units will be contained within the room, enclosed area, or walk-in unit for a duration equal to the fire-resistance rating of the room separation" [2]. Furthermore, the International Building Code requires listing to UL 9540, *Standard for Energy Storage Systems and Equipment*.

2.3.2 UL 9540, Standard for Energy Storage Systems and Equipment, 2nd Edition (2020)

UL 9540 is a product safety standard for energy storage systems that can be used for certifying and listing ESSs. UL 9540 includes multiple technologies including electrochemical, mechanical, thermal, and chemical energy storage systems. Like the International Fire Code, UL 9540 requires a system safety analysis. UL 9540 includes electrical, mechanical, environmental, and production performance tests. The standard also requires a UL 1741-certified inverter and a UL 1973-certified battery [29].

UL 9540 Section 1.6 limits the maximum energy capacity for residential use electrochemical ESS units to 20 kWh and non-residential use electrochemical ESS units to 50 kWh. There are provisions for the non-residential limit to be exceeded based on UL 9540A testing and compliance with the cell, unit, or installation level performance criteria [29]. No such provision is included for residential use electrochemical systems.

2.3.3 UL 9540A, Test Method for Evaluating Thermal Runaway Fire Propagation in Battery Energy Storage Systems, 4th Edition (2019)

UL 9540A is a test method utilized to evaluate the fire and explosion hazards associated with propagating thermal runaway in battery energy storage systems. UL 9540A is structured in four levels, cell, module, unit, and installation, to address the scaling of the hazards and determine at which level the hazards are contained. UL 9540A testing results in a test report which includes the data needed to determine the fire and explosion protection required for an installation.

The cell is the smallest battery component of the ESS. The cell level tests determine whether a specific battery technology is susceptible to thermal runaway and measures the components and flammability of the thermal runaway effluent gases. The module is an assembly of electrically connected cells. The module level test utilizes the thermal runaway initiation methodology determined at the cell level and evaluates the cell-to-cell propagation of thermal runaway and measures the resultant gas release, heat release, and smoke release from the module.

The unit is a rack or enclosure that consists of a functional ESS including modules, BMS, and other ancillary equipment. The unit level tests utilize the thermal runaway initiating methodology from the module level tests and assesses module-to-module as well as unit-to-unit thermal runaway propagation. Additionally, the unit test measures gas release, heat release, and smoke release. Finally, if necessary, the installation level test is provided to assess the effectiveness of the building-integrated fire suppression systems to mitigate the fire and explosion hazards of thermal runaway. The test is initiated in the same manner as the unit level test, but incorporates a representative test structure and fire protection systems [2].

UL 9540A divides residential use BESS into four categories: indoor floor mounted, outdoor ground mounted, indoor wall mounted, and outdoor wall mounted. UL 9540A Table 9.1 lists performance criteria for residential systems tested at the unit level. For indoor floor mounted and indoor wall mounted:

> “a) Flaming outside the initiating BESS unit is not observed as demonstrated by no flaming or charring of the cheesecloth indicator;
>
> b) Surface temperatures of modules within the target BESS units adjacent to the initiating BESS unit do not exceed the temperature at which thermally initiated cell venting occurs, as determined [at the cell level];
>
> c) For BESS units intended for installation locations with combustible construction, surface temperature measurements on wall surfaces do not exceed 97 °C (175 °F) of temperature rise above ambient;
>
> d) Explosion hazards are not observed, including deflagration, detonation or accumulation (to within the flammability limits in an amount that can cause a deflagration) of battery vent gases; and
>
> e) The concentration of flammable gas does not exceed 25% LFL in air for the smallest specified room installation size” [2].

For outdoor wall mounted units, criteria A, B, C, and D above apply. For outdoor ground mounted, criteria B, C, and D apply. Additionally, separation distances between exposures are determined by greatest flame extension and heat flux in the accessible means of egress may not exceed 1.3 kW/m^2 [2].

2.3.4 NFPA 855, Standard for the Installation of Stationary Energy Storage Systems – 2020 Edition

NFPA 855 is the North American installation standard for stationary energy storage systems. For lithium-ion ESS technologies, it applies to installations with an aggregate capacity exceeding 20 kWh. While the majority of NFPA 855 does not apply to residential applications, Chapter 15 addresses one- and two-family dwellings and townhouse units. NFPA 855 Chapter 15 requires ESS of 1 kWh or greater to be listed to UL 9540. Section 15.5 requires separation distances between units of at least 3 ft unless demonstrated by large-scale fire testing per UL 9540A and AHJ approval. NFPA 855 limits ESS installations to the same locations and energy capacities as the International Residential Code [30].

2.4 Survey of Residential ESS Products

Tesla has the largest market share of the US residential energy storage system (ESS) market in 2020. However, in the second half of 2020 ESS imports started rapidly increasing, with South Korea as the largest foreign residential ESS supplier to the US [9]. In the US, residential ESS systems range from 5 to 30 kWh, with the 13.5 kWh Tesla Powerwall being the most commonly installed in 2020 [9]. Figure 22 shows the breakdown of the U.S. domestic supply of residential ESS.

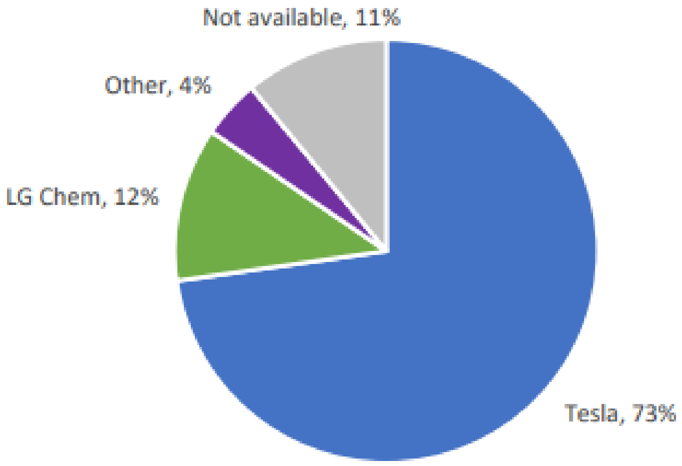

Figure 22 – Manufacturer market share in US in 2020 [9].

A survey was taken of 84 commercially available residential energy storage products. The survey included portable, wall mounted, and floor mounted designs. The survey included multiple lithium-ion chemistries. Product weights ranged from 5 lb. to over 950 lb. per unit. Product energy capacities ranged from 1 to 38 kWh (the 2021 International Residential Code however limits maximum unit capacity to 20 kWh).

Wall mounted products ranged from 4 to 20 kWh per unit and included LFP, LMO, and NMC chemistries. Products weighed between 110 and 952 lbs. Wall mounted unit profiles are typically shallow to be minimally invasive into a space. The surveyed product depths ranged from 7.5 to 20 inches deep and 17 to 60 inches wide. Product heights ranged from 19 to 66 inches. Most products included some openings for dedicated vents or conduit connections.

Based on this survey, the representative residential ESS constructed for this research test program measured nominally 21 inches wide, 66 inches tall, and 4 inches deep and enclosed an electrical capacity of 17 kWh.

2.5 Garage Construction

Consumer trends indicate that most homebuyers want garage space to accommodate at least two cars, according to a survey of 24,000 new home buyers. US Census Bureau data indicates 65% of single-family homes built in 2017 included two car garages, making the two car garage the most common residential garage, as shown in Figure 23. Side-by-side parking is the most common layout of two-car garages. A typical two car garage measures nominally 20 ft wide by 24 ft deep. Surveys also indicate that car storage is not the only function that homeowners anticipate for their garages. Most intend to also use garages for storage, typically with 24-inch cabinets [31].

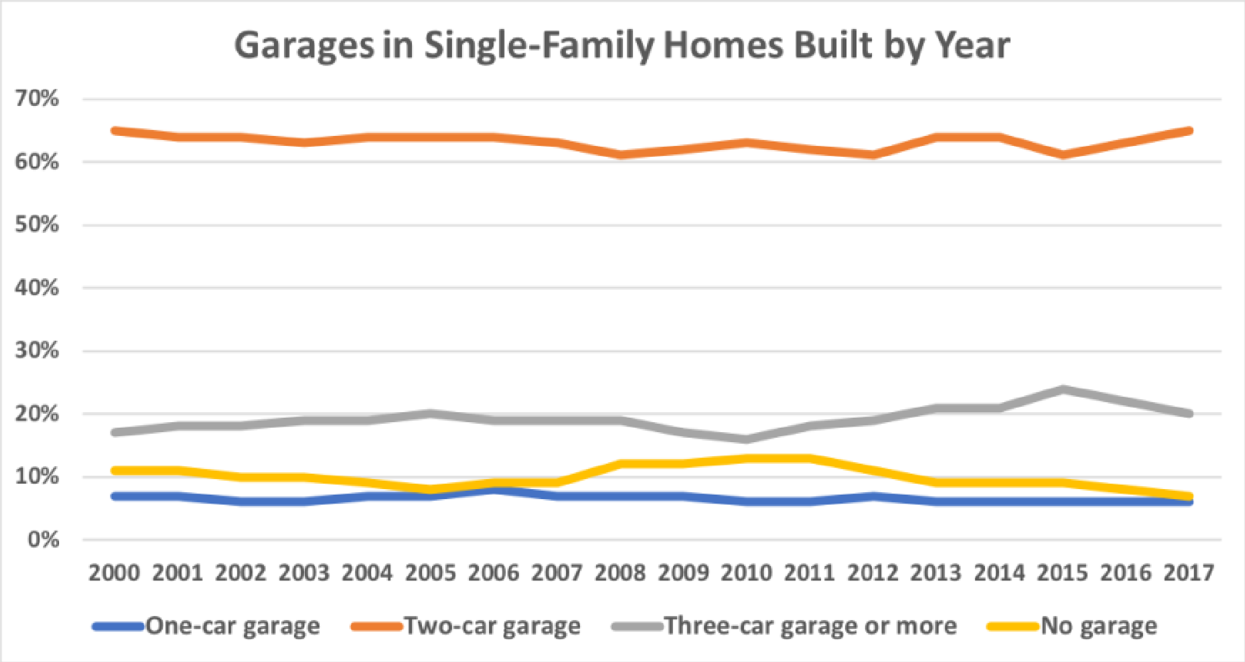

Figure 23 – Garages in Single-Family Homes Built by Year, based on US Census Bureau data [31] .

Due to allowances in the International Residential Code, as well as proximity to electrical panels, photovoltaic panels, and electric vehicles, it is likely that residential ESS will be installed within the garage of a home.

2.6 Garage Firefighting Tactics

Garages often include flammable and combustible liquids, oxidizers, aerosols, and other chemicals. The presence of these chemicals that may be actively burning or exposed nearby create hazards for firefighters. The addition of residential energy storage, electric vehicles, and other li-ion battery containing products compounds the hazards found in garages. Furthermore, there may be limited, if any, fire-rated separation between the garage structure and the rest of the dwelling.

The US Fire Administration estimates that there is an annual average of 6,600 residential garage fires per year. These fires result in an annual average of 30 deaths, 400 injuries, and $457 million in property loss. 93% of these fires occur in one- and two-family dwellings and electrical malfunction is considered the leading cause of these fires [32]. Typically, residential garages are constructed without smoke detection and the delay in response without automatic detection allows fire time to develop before intervention. Only 13% of residential garage fires are limited to the object of origin, suggesting the propensity for fire spread. Only 35% of residential garage fires are limited to the room of origin. Another 35% of residential garage fires are limited to the building of origin, contributing to significant property damage and likelihood of injury or fatality [32].

Limited and conflicting guidance is published for residential garage firefighting tactics due to the wide range of contents that may be present and the relative infrequency of these fires relative to other residential fires [33] [34].

There are several possible points of ventilation present with a garage. While some advise venting the roof, feedback from this project’s technical panel emphasized that the venting through the roof in parallel with hose-line attack through the garage is inadvisable due to the risk for potential explosion hazards involved in battery fires, as demonstrated by the incidents reviewed in Section 2.2 ESS Incidents [34]. Some garages may have service doors, but fire fighters should consider that homeowners may obstruct the door with stored materials. Similarly, some suggest suppressing from the dwelling using handlines (i.e., “attacking from the unburned side”) [34]. Fire Engineering University encourages that this door be protected with a hose-line, but that the door not be opened at all if there is no fire extension into the house so that the door can protect the house interior for as long as possible [33]. The technical panel further emphasized the importance of entering from the exterior to protect the attached residence for as long as possible.

If there are no accessible service doors to enter the garage, the overhead garage door may be lifted or otherwise breached. If the garage door is opened, Fire Engineering University recommends it be wedged open with a tool to prevent accidental closure which could trap firefighters inside [33]. To breach the garage door, the panels may be knocked out with axes or cut with a powered rotary saw. Two styles of ventilation cut were reviewed with the technical panel. One style of cut is the “inverted-V cut” where a triangular opened is cut from above the head of the operator all the way to the floor [33]. The second style was the “inverted-L cut” which involves making one vertical cut through several door panels and a horizonal cut spanning most of the door width, followed by opening the large flap that this creates. It was panel consensus that the inverted-V cut is likely the more common approach used in North America.

2.7 Summary

Battery energy storage system installations are becoming increasingly popular in residential settings. Within the United States, attached two-car garages are a popular location for energy system installations due to residential code provisions, construction prevalence, and installation practicality. These factors have all driven the design of the test articles and structure, as well as the selection of firefighting tactical considerations and approaches.

3 Test Setup

3.1 Large-Scale Test Facility

The large-scale fire test building used for this investigation houses four fire test areas that are used to develop data on the fire growth and fire suppression characteristics. A schematic of the test facility is shown in Figure 24.

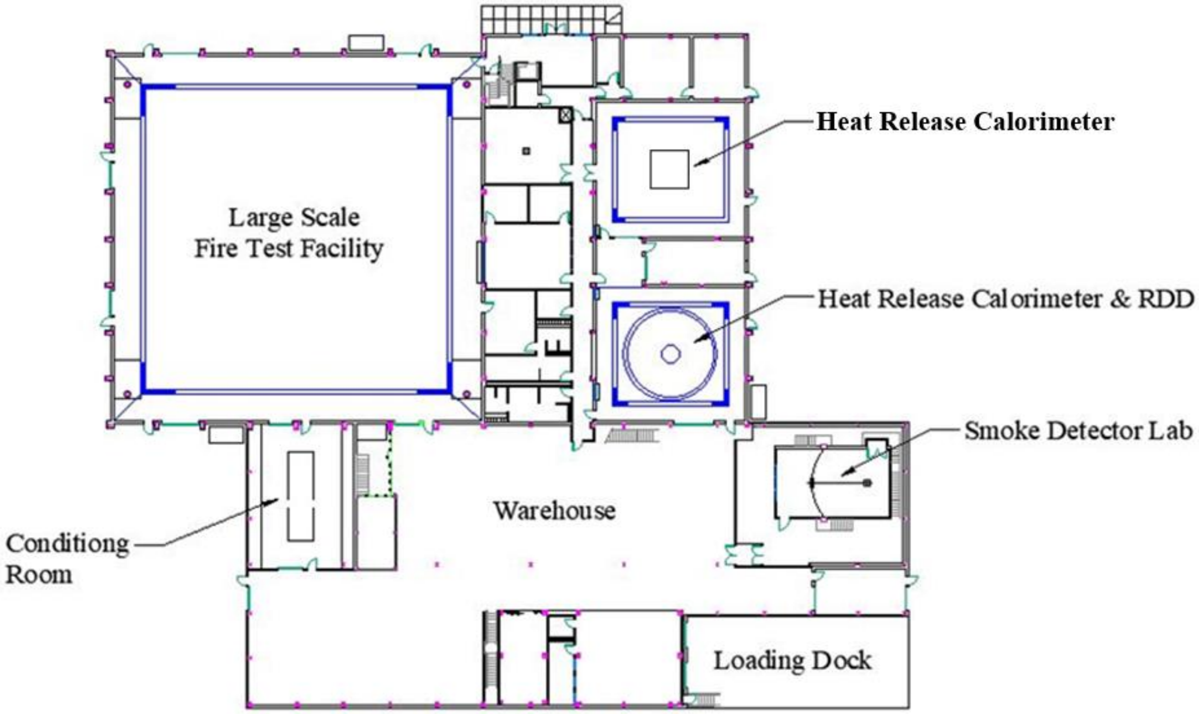

Figure 24 – Test facility layout.

The test was conducted in the 120 ft by 120 ft main fire test cell that is equipped with a 100 ft by 100 ft adjustable height ceiling. The center of the floor of the test facility is 100-ft by 100 ft., is smooth and flat and is surrounded with a grated drainage trench to insure adequate water drainage from the test area.

The large-scale test cell used in this investigation is equipped with an exhaust system capable of a maximum flow of 60,000 cubic feet per minute through a smoke abatement system. Fresh air was provided through four inlet ducts positioned along the wall of the test facility. The fresh air was released into the room approximately 10 ft above the floor level through straightening screens. This ventilation arrangement provides adequate air so that the fire growth occurs naturally. All products of combustion from the tests were contained within the test facility and processed through a regenerative thermal oxidizing system.

3.2 Construction

Four tests were conducted in a test structure representing an attached two-car garage. All four tests utilized a standardized commodity (Group A cartoned unexpanded plastic [35]) to represent the multitude of combustible fuels that may be present in a residential garage. Three out of four tests included a mockup residential energy storage system comprised of three individual units. The construction of the test structure, mockup energy storage system units, and standardized commodity fuel package are described below.

3.2.1 Test Structure

The test structure was designed to represent an attached two-car garage. Exterior measurements of the garage were 20 ft. by 20 ft. The interior height of the garage was 10 ft. A 16 ft x 7 ft garage door was installed centrally on the front (A-side) with two access doors on the B-side and C-side walls, as shown in Figure 25. The access doors were outfitted with Brixon latches to regulate the force required for opening and to allow the doors to be opened remotely. Photos of the garage exterior are included in Figure 26 through Figure 29. The garage interior is pictured in Figure 30.

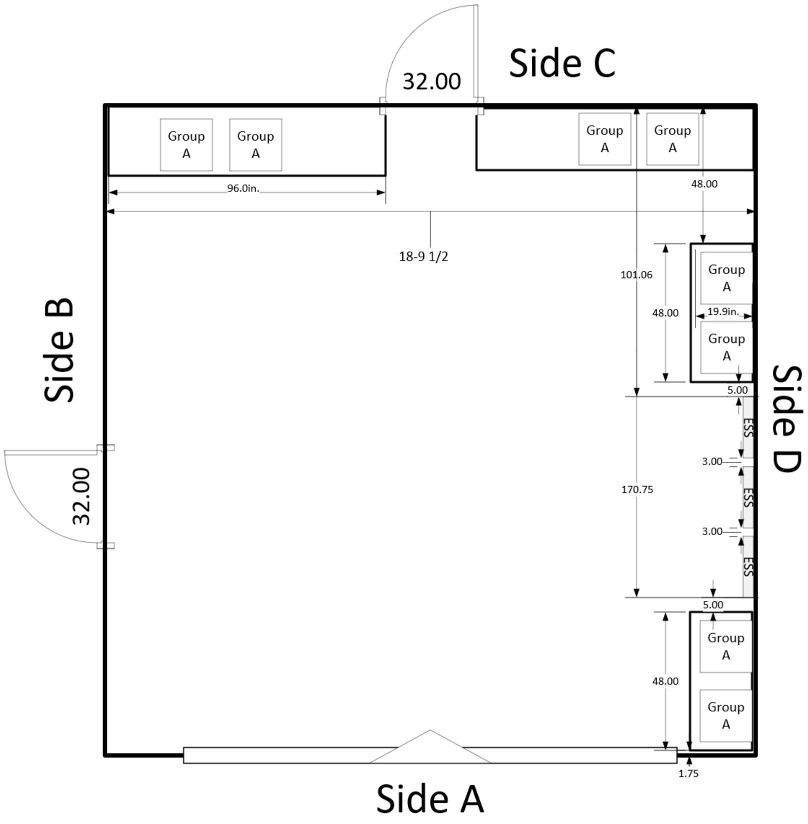

Figure 25 – Naming convention for the different exterior sides of the garage.

Figure 26 – Test structure (A-side).

Figure 27 – Test structure (B-side).

Figure 28 – Test structure (C-side).

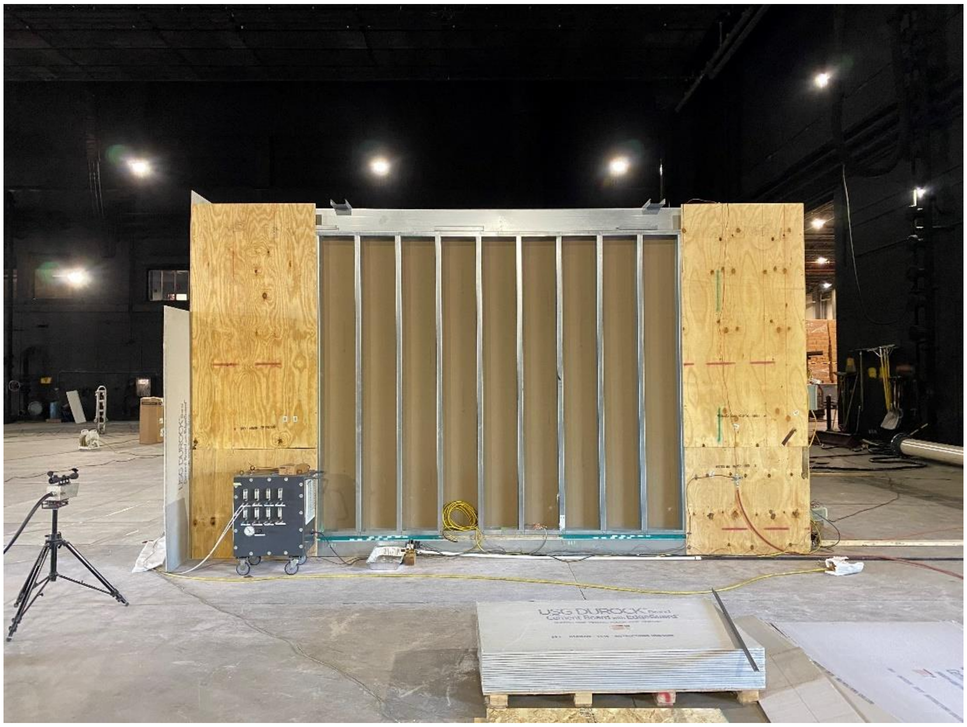

Figure 29 – Test structure (D-side).

Figure 30 – Test structure (Garage door interior).

To manage the potential explosion hazard within the large-scale test facility, the test structure was designed for an enclosure strength of at least 1 psig. The test structure frame was fabricated from steel joists. The flooring included two layers of 3/4 in. plywood with sheet rock cover. The walls were constructed from 3/4 in. plywood with two layers of 5/8 in. Type X gypsum. The ceiling was constructed from two layers of 5/8 in. gypsum with 1/2 in. sheet rock cover.

The garage door was modified to function as a deflagration vent designed to operate at 0.12 psig. Instead of installing on a traditional track, the garage door was installed with a hinge on the bottom axis, reinforced with metal flat stock for rigidity, and outfitted with explosion-venting fasteners along the top axis. The washer system was protected with ceramic wool insulation to protect the fasteners from thermal exposure.

3.2.2 Energy Storage System Units

All units were designed to create a condition of cell-to-cell propagating thermal runaway following the first cell thermal runaway within the unit. Three units were installed for each test that included ESS. The units were installed 3 inches apart and 6 inches off the floor. The installation is pictured in Figure 31.

Figure 31 – ESS layout in Test 2 through Test 4.

The units included 48 modules, each filled with thirty 18650-format cells (Table 1) with NCA cathode chemistry. All cells in all units were charged to 100% state of charge. For these tests, unlike UL 9540A standard tests, the cells and modules were not electrically connected. Based on the previous cell, module, and unit test series, this configuration demonstrated the potential hazards of ESS installations effectively without requiring additional electrical connections.

Table 1 – Cell, module, and unit characteristics.

Feature	Cell	Module	Unit
Picture		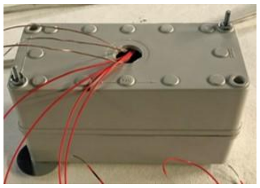	
Capacity	3.3 Ah (12 Wh)	99 Ah (356 Wh)	4,752 Ah (17,088 Wh = 17 kWh)
Quantity of 18650 li-ion cells	1	30	1440
Dimensions	0.7 in (18 mm) diameter x 2.6 in (65 mm) length	6.8 in (172 mm) x 3.6 in (92 mm) x 3.6 in	16.1 in (0.41 m) x 53.1 in (1.35 m) x 3.1 in (0.08 m)

The enclosures for the modules were made of UL 94 HB-rated ABS plastic. The enclosure of the unit was constructed from solid sheet steel panels with perforated steel shelves to support each set of cells (Figure 33). An expanded metal panel and sheet steel cover were fixed to the front of each unit to fully enclosure the unit. Two 2-inch vents were located on the sides of the units above the top row of modules to represent the locations for cooling fans or conduit installations. Two 1-inch vents were located on the sides of the units near above the second row of modules for instrumentation passthroughs. A 40 in. space was left open on the top of the unit to represent the space where a BMS would be located.

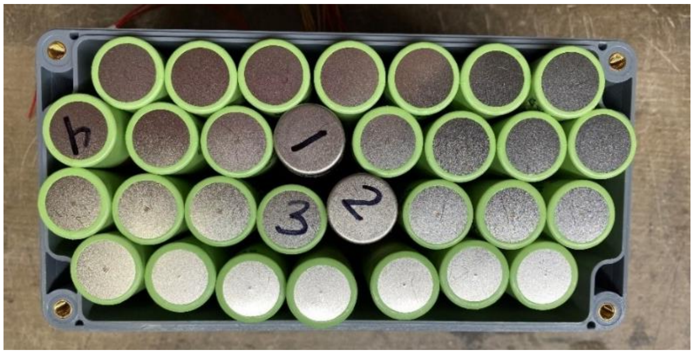

Figure 32 – Module construction.

Figure 33 – Unit construction with modules (left), expanded metal insert layer (center), and sheet steel cover (right).

The cell design was characterized by cell level UL 9540A testing. Properties of the cell are presented in Table 2.

Table 2 – Cell level thermal runaway properties.

Property	Measurement
Cell vent temperature	130 °C
Thermal runaway temperature	204 °C
Gas volume	7.1 L per 18650
Gas composition	36.2 v% carbon monoxide; 22.1 v% carbon dioxide; 31.7 v% hydrogen; 10.0 v% hydrocarbons <u>Hydrocarbon breakdown</u> 7.4 v% methane; 0.92 v% ethylene; 0.61 v% ethane; 0.22 v% propylene; 0.04 v% propane; 0.07 v% C4-hydrocarbons; 0.24 v% benzene; 0.03 v% toluene; 0.38 v% dimethyl carbonate
Gas LFL	10.8 v% [36]
Gas UFL	50.3 v% [36]
Gas Pmax	97.2 psig [36]
Gas burning velocity	59 cm/s [36]

The mock-up ESS was comprised of two different configurations: Initiating Units and Target Units, depending on the test configuration. Initiating and Target units are labeled in the test specific layouts described in Section 4 of this report. The construction of the units was identical; only the instrumentation locations within the units varied, as described in Section 3.3.2.

3.2.3 Cartoned Unexpanded Group A Plastic Commodity

Standardized commodity was installed on racking along the C-side and D-side walls of the garage, as pictured in Figure 34, to represent the wide range of items that may be stored in a residential garage.

Figure 34 – Rack storage of commodity along C-side wall (left) and D-side wall (right). For Test 2 – 4, the center rack on the D-side wall was replaced with residential ESS units.

The boxes used as standardized commodity were extracted from pallets of Cartoned Unexpanded Group A Plastic Commodity [35]. The boxes were single layer cardboard boxes featuring an arrangement of 125 plastic cups and cardboard. Each box contained five tiers of twenty-five cups. Each cup was separated by one layer of cardboard. The nominal external dimensions of the commodity were 21 inches wide by 21 inches deep by 21 inches tall. The cups used in the cartoned, unexpanded Group A commodities were manufactured from polystyrene. A photograph of the box and cups is shown in Figure 35.

Figure 35 – Cut away of single box showing cups.

3.3 Instrumentation

The overall instrumentation layout is illustrated in Figure 37 and Figure 39 with instrumentation keys included in Figure 36 and Figure 38. Instrumentation was positioned to characterize conditions inside the garage, to consider exterior gas detection approaches, to monitor the extent of thermal runaway propagation, and to provide data to develop firefighter size-up considerations.

All video feeds were recorded continuously at 30 fps. Data was recorded at 1 Hz.

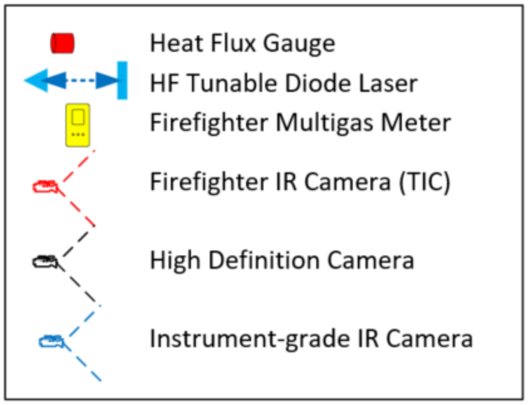

Figure 36 – Exterior instrumentation key.

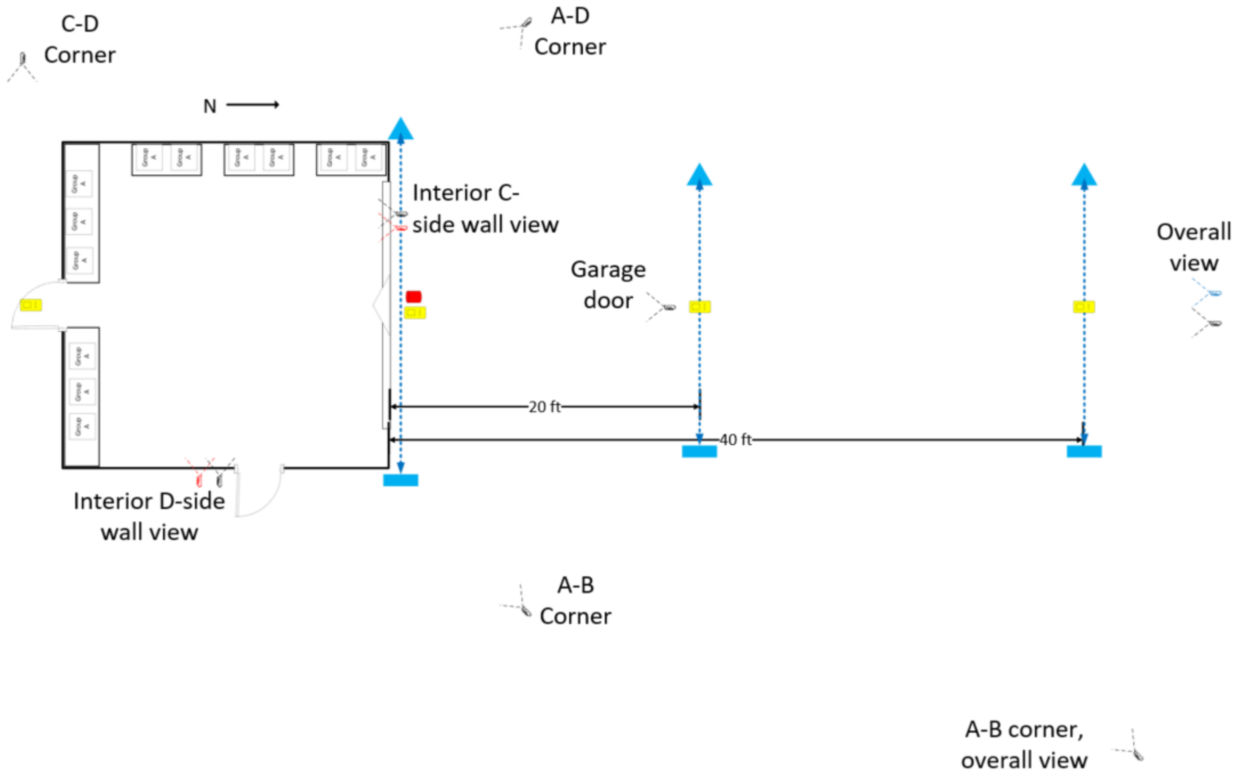

Figure 37 – Exterior instrumentation plan view.

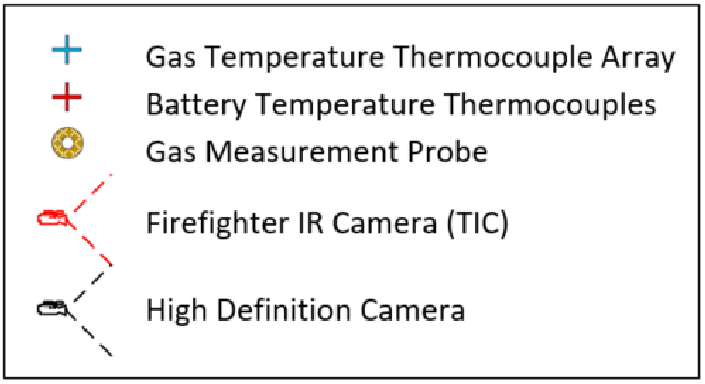

Figure 38 – Interior instrumentation key.

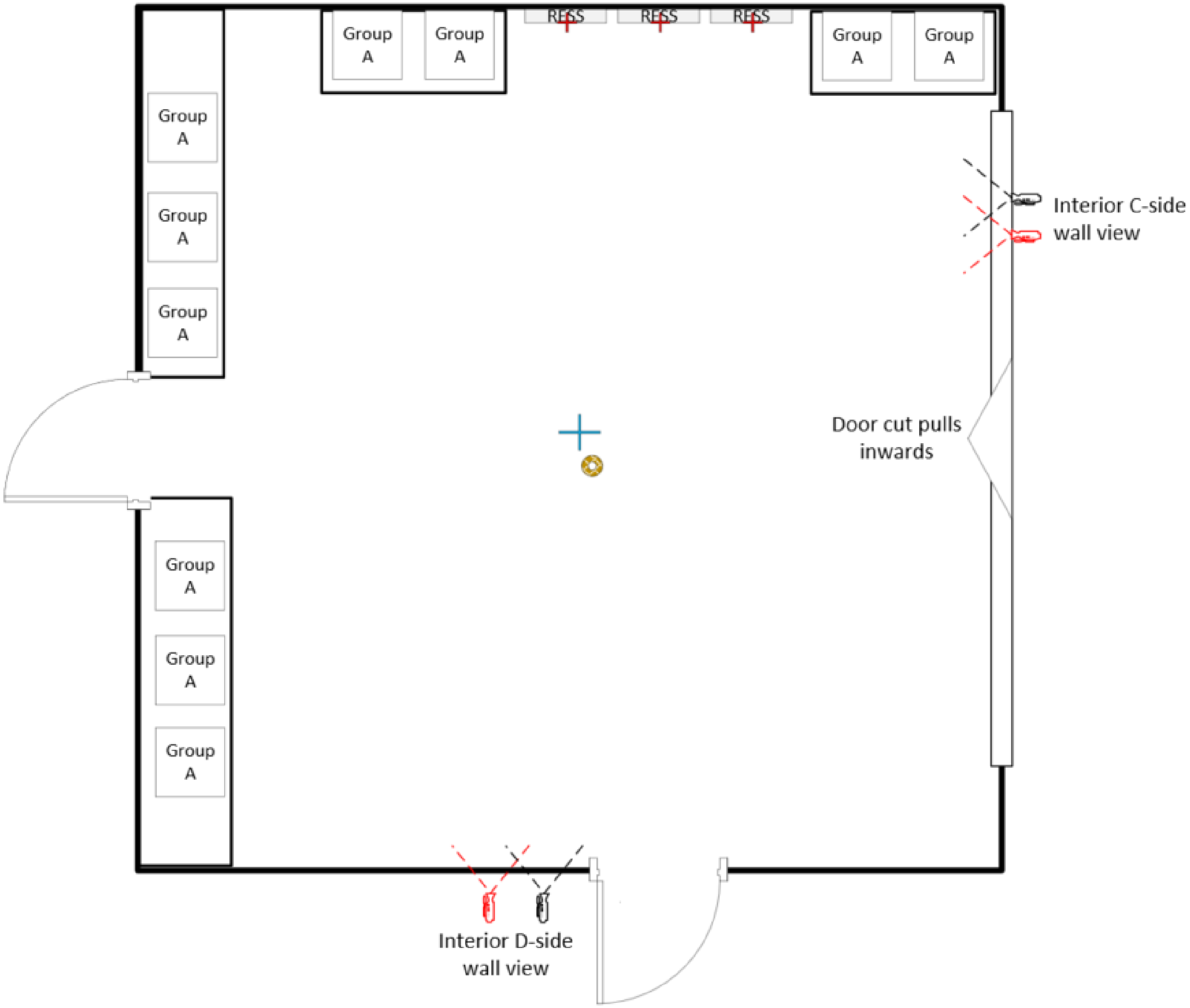

Figure 39 – Interior instrumentation plan view.

3.3.1 Structure

Instrumentation was installed in the garage structure to assess the interior conditions in terms of temperature and gas composition.

Thermocouples

In addition to the thermocouple measurements in the ESS units described in Section 3.1.2, thermocouples were installed in the center of the garage to monitor interior air and gas temperatures and the development of a hot gas layer. Container gas temperatures were monitored using a thermocouple array. Array thermocouples were 24 American Wire Gauge (AWG) Type K. The array included 10 thermocouples spaced every 12 inches beginning 1 ft above the floor and ending 1 inch below the ceiling. The array is shown in Figure 39**.**

Figure 40 – Thermocouple array (outlined in orange).

Gas Analysis

A combination of analytical instruments was used to characterize the gas composition inside the compartment, as summarized in Table 3.

Gas samples were extracted at two locations and transported to analytical equipment: near the ceiling (sampling across the top 24 inches) and immediately outside the garage door at an elevation of 3 ft. The sample from inside the compartment was transported by heated lines. The sample line from outside the garage was transported by an unheated line. The sample from the ceiling was analyzed for oxygen, carbon monoxide, carbon dioxide, and total hydrocarbon concentrations. The sample taken near the garage door was analyzed for oxygen, carbon monoxide, and carbon dioxide. Measurement locations are pictured in Figure 41 and Figure 42.

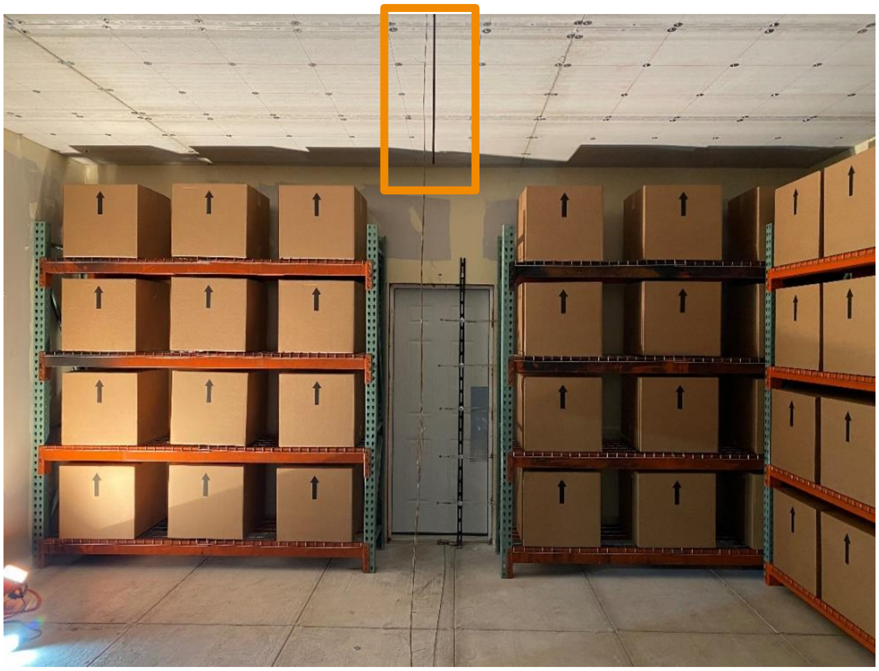

Figure 41 – Location of ceiling gas probe (outlined in orange).

Figure 42 – Location of gas probe in front of garage door (outlined in orange, sampling location near bottom of rectangle).

Table 3 – Gas measurement equipment.

Gas	Measurement Location	Measurement Principle
Oxygen	Ceiling probe; Garage door exterior	Paramagnetic
Carbon dioxide	Ceiling probe; Garage door exterior	Nondispersive Infrared (NDIR)
Carbon monoxide	Ceiling probe; Garage door exterior	NDIR
Total hydrocarbons	Ceiling probe	Flame ionization detection (FID)

Gas analysis for the interior of the garage near ceiling level used a custom-built gas sampling system that would periodically cycle between drawing sample gases and producing a brief pulse of positive pressure by injecting nitrogen gas. The pressure pulse would effectively clean the sample probe orifices and prevent clogging from high concentrations of particulates within the fire environment of the tests. The system produced artifacts in the gas data the appeared as brief, rolling spikes and depressions. However, the approach prevents complete loss of sampling due to soot obstruction throughout the duration of the tests.

Interior Cameras

Interior conditions were monitored by two high-definition (HD) cameras and two fire service thermal imaging (IR) cameras. The HD cameras used in the experiments were HD-SDI CCTV cameras and the fire service thermal imaging cameras used were Bullard Model T3Xs. The HD and thermal imaging cameras were co-located, as shown in Figure 43.

Figure 43 – HD camera (left) and TIC camera (right) installed through garage door.

One pair of cameras was installed with a view through the B-side wall towards the D-side wall interior. These cameras were positioned approximately 3 ft off the floor. One pair of cameras was installed with a view through the garage door towards the C-side wall interior. These cameras were located approximately 1 ft off the floor. The layout is summarized above in Figure 39.

3.3.2 ESS Units

Initiating Modules

Within the Initiating Module, flexible film heaters were wrapped around two individual 18650-format cells. One cell was heated to initiate the first thermal runaway event, and the second cell was available for the unlikely occurrence of a malfunction with sending the first cell into thermal runaway. The instrumented cell(s) were heated at a rate of 10.8 °F/min (6 °C/min). Thermocouple locations within the initiating module are shown in Figure 44.

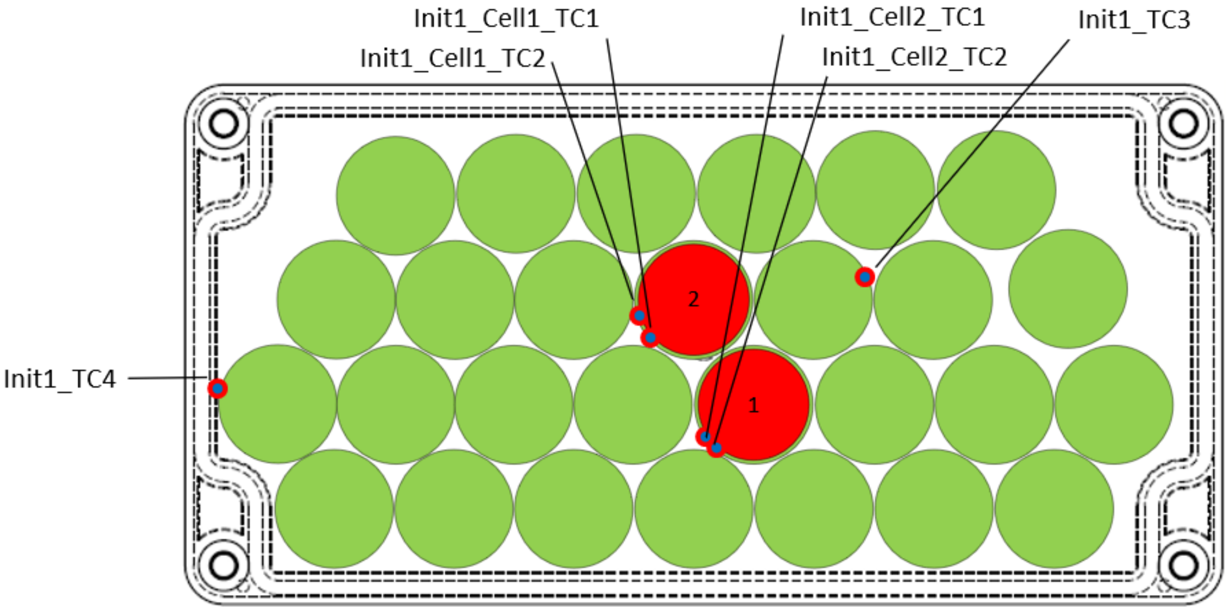

Figure 44 – Initiating module constructed from 18650 cells.

Non-Initiating Instrumented Modules

All instrumented modules within the unit, besides the initiating modules, included one thermocouple on the center of the metal plate within the ABS enclosure. These thermocouples are named “UnitX_ModY” with X and Y denoting the specific unit and module location.

Initiating Units

The Initiating Module (Figure 44) was installed in the position second from the bottom in the Initiating Unit (Figure 45). The Initiating Unit included two Initiating Modules for the unlikely occurrence of a malfunction with the first module. The numbering convention for modules is shown in Figure 45. Two thermocouples were welded on the outer surfaces of the two sides of the enclosure to monitor exterior temperatures. The outer thermocouples were installed at 1/3 and 2/3 heights of the portion of the unit that included live modules and are denoted with blue crosses. Non-initiating, instrumented modules are denoted with red crosses. A ½" diameter copper tube, not picture here, was inserted into the top of the unit and connected to a ¾" hose to enable water injection into the unit for rapid termination of thermal runaway propagation at the conclusion of the tests.

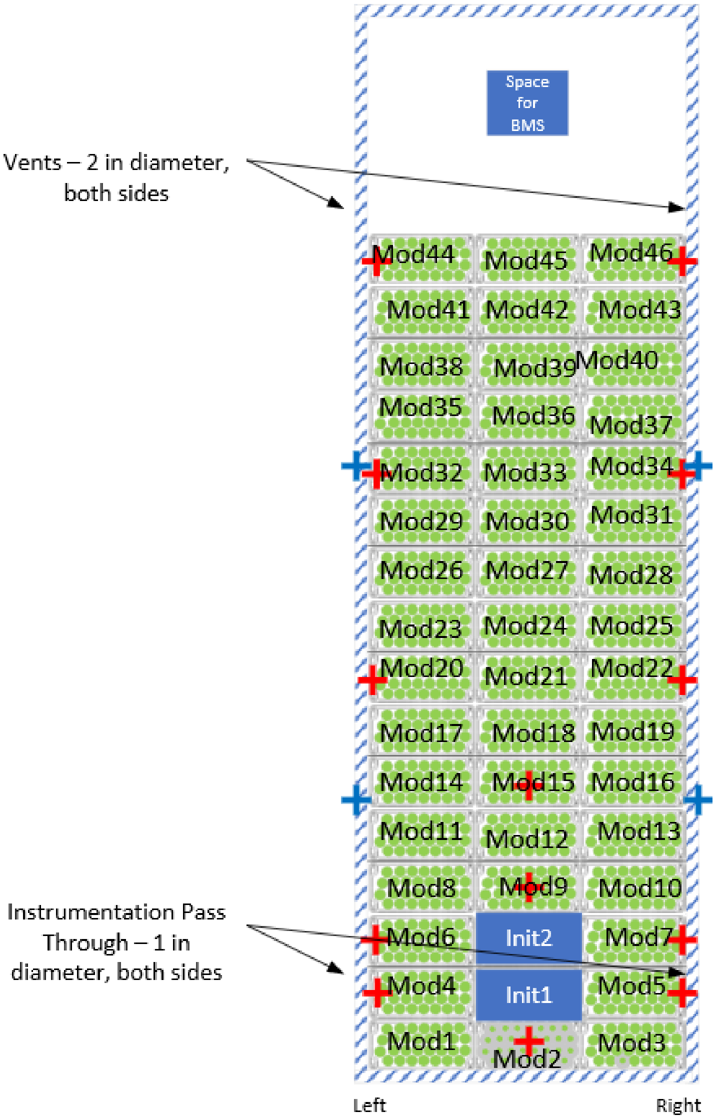

Figure 45 – Initiating Unit instrumentation layout (module TCs marked in red, outer enclosure TCs marked in blue).

Target Units

The construction of the Targets units was consistent with the Initiating Unit, except the instrumentation layout is as shown in Figure 46. Each target included one initiating module as a backup to the initiating unit. These initiating modules were not heated during this test series, so they can be considered as any other instrumented module. Two thermocouples were welded on the outer surfaces of the two sides of the enclosure to monitor exterior temperatures. The outer thermocouples were installed at 1/3 and 2/3 heights of the portion of the unit that included live modules and are denoted with blue crosses. Non-initiating, instrumented modules are denoted with red crosses. A ½" diameter copper tube, not picture here, was inserted into the top of the unit and connected to a ¾" hose to enable water injection into the unit for rapid termination of thermal runaway propagation at the conclusion of the tests.

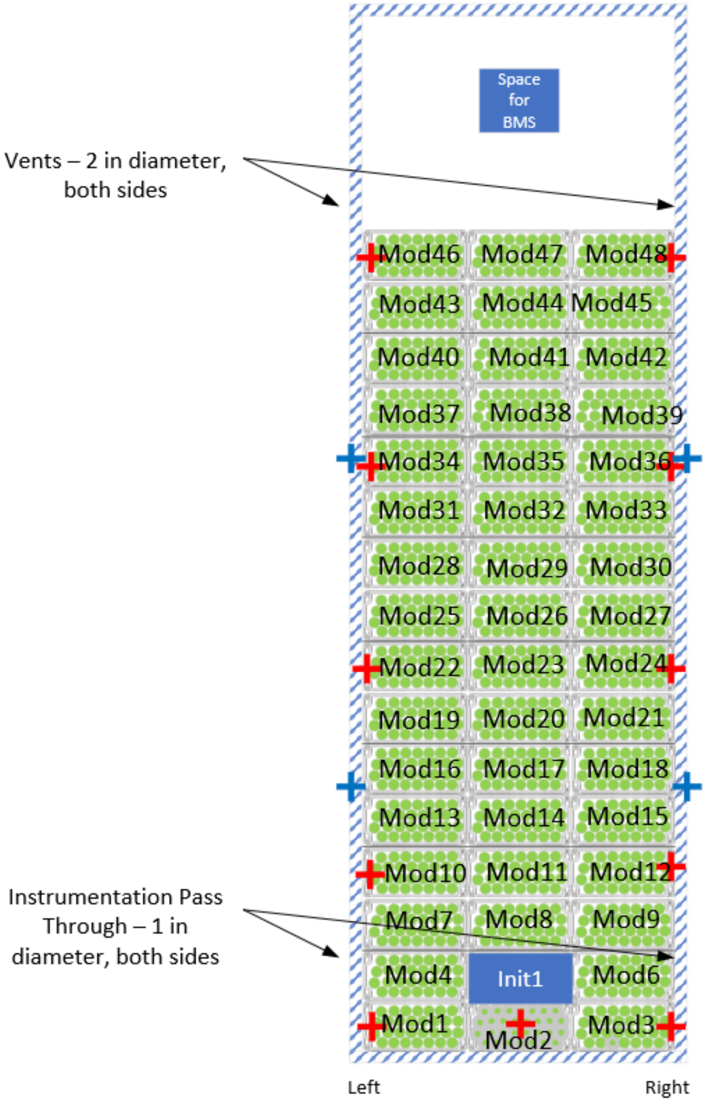

Figure 46 –Target Unit instrumentation layout.

3.3.3 Exterior Measurements and Fire Service Size-up Equipment

Instrumentation was installed outside the garage structure to assess the exterior conditions in terms of thermal exposure and gas composition. Additional cameras and gas meters were installed outside the garage to develop size-up considerations for firefighters.

Heat Flux

One Schmidt-Boelter heat flux gauge was facing the garage door at an elevation 5 ft off the floor and a position approximately 6 inches from the garage door. The location is pictured in Figure 47 with an example gauge pictured in Figure 48.

Figure 47 – Heat flux gauge placement (outlined in orange).

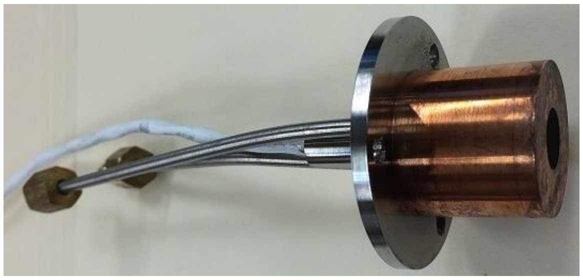

Figure 48 – Schmidt-Boelter heat flux gauge.

Tunable Diode Laser Absorption Spectrometer

Hydrogen fluoride (HF) concentration was measured across the width of the driveway at three distances from the garage door: 1 ft, 20 ft, and 40 ft using an open path Tunable Diode Laser Absorption Spectrometer (TDLAS) from Boreal Laser Inc. [37]. The concentration was averaged across the path length between the laser emitter and reflector. The minimum detection limit of the instrument as configured is 0.8 ppm. The instruments were mounted 3 ft off the ground to be collocated with the portable gas meters described in the next section. Measurement locations are described in Figure 49 and an example of the instrument is shown in Figure 50.

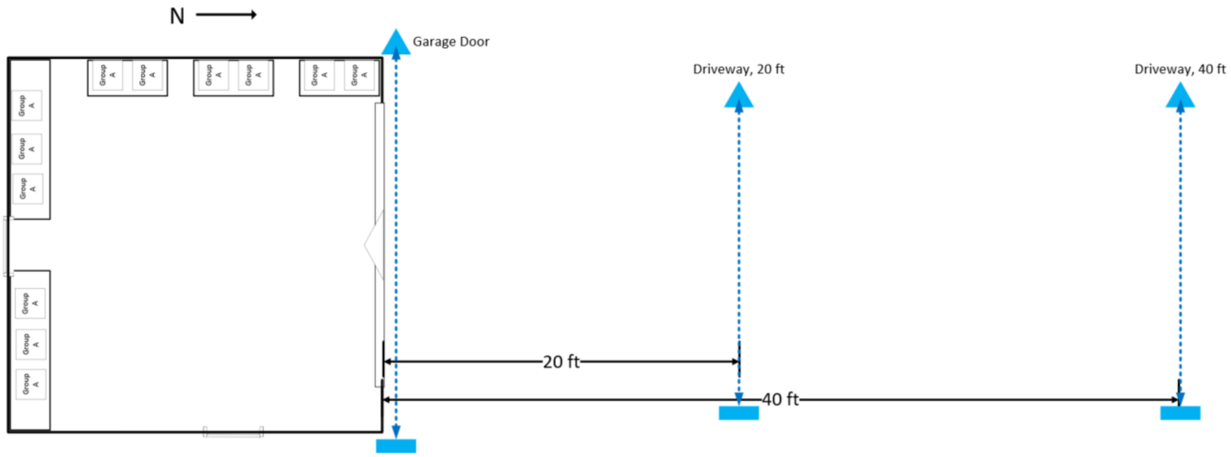

Figure 49 – Measurement locations for HF.

Figure 50 – Example of tunable diode laser emitter and reflector.

Portable Gas Meters

Four fire service portable gas monitors were placed at locations on the exterior of the garage to assess their ability to discern battery thermal runaway effluent gases and inform fire service size-up decisions. Figure 51 shows meter locations within the test setup. These locations are described as follows:

- At the center of the garage door exterior, approximately 1 ft from the surface of the door ("Garage Door")
- At the C-side access door of the garage, approximately 2 ft from the surface of the door ("C-side Access Door")
- 20 ft in front of the center of the garage door ("Driveway, 20ft")
- 40 ft in front of the center of the garage door ("Driveway, 40ft").

All meters were elevated 3 ft above the ground to simulate firefighters sampling the ambient environment while holding the meter near their waist.

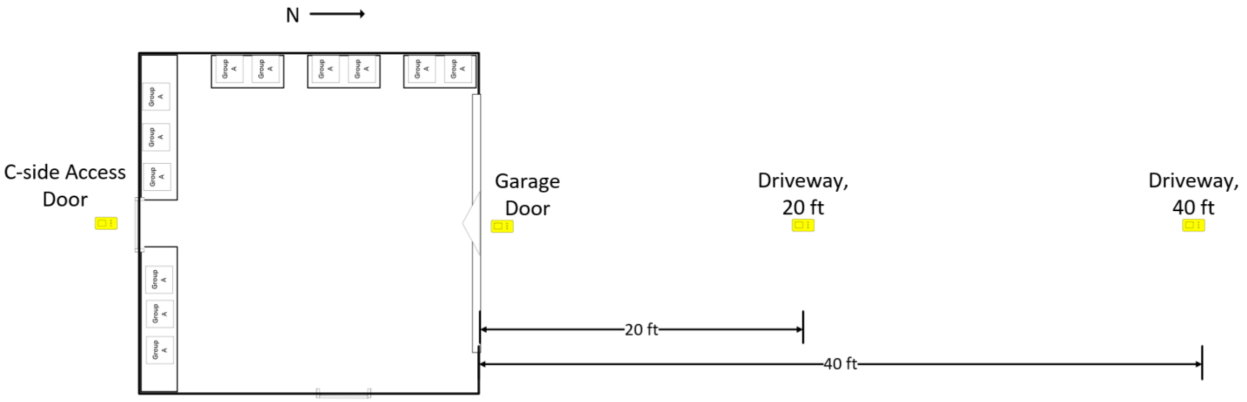

Figure 51 – Fire service portable gas meter locations.

A range of gas sensor technologies commonly utilized by fire service and hazardous materials personnel were used to monitor the experiments. The meters contained a variety of sensors and included both pumped and diffusion style. The pumped meters included a sampling pump that can extract a sample from the ambient for analysis. Diffusion style meters require the sensors to have direct contact with the gas atmosphere to sample. Only the diffusion style meter was designed to measure hydrogen.

Three models of meters were used. Table 4 lists these meters, the labels that will refer to them in this document, and the quantities they measured.

Table 4 – Gas sensor technologies.

Meter Label		**Garage Door**	**Driveway, 20ft**	**Driveway, 40ft**	**C-side Access Door**
Manufacturer		RAE Systems	RAE Systems	MSA	RAE Systems
Model		MultiRAE Lite	MultiRAE Lite	Altair 5X	MultiRAE Lite
Style		Pumped	Pumped	Pumped	Diffusion
Measurements	**Technology**				
O2	Electrochemical		X	X	X
CO	Electrochemical	X	X	X	X
HCN	Electrochemical	X	X	X	
H_2S	Electrochemical		X		X
H_2	Electrochemical				X
Volatile Organic Compounds	PID	X			
LEL (Calibrated to methane)	Catalytic Bead	X*	X*		X*

* calibrated to LEL of methane gas

Cross-sensitivities of the sensors used in the meters, based on listed data for the meters and sensors, are also provided in Table 5 and Appendix B.

Table 5 – Sensors and Sensor Cross-Sensitivities Listed for RAE Systems Sensors.

Sensor Type	**O_2**	**CO**	**HCN**	**LEL****	**H_2S**	**H_2**
Sensor Part Number	C03-0942-000	C03-0906-000	C03-0949-000	C03-0911-000	C03-0907-001	C03-0981-000
Sensor Type	Electro chem	Electro chem	Electro chem	Catalytic bead	Electro chem	Electro chem
Cross-Sensitive Gas/Vapor	**Relative Sensitivity (ppm of false reading per ppm of cross-sensitive gas)***					
O_2	N/A	N/A	N/A	N.A	N/A	N/A
CO	N/A	N/A	0.05	0.83	0.005	0.2
HCN	N/A	N/A	N/A	N/A	N/A	0.3
H_2S	N/A	N/A	6	N/A	N/A	0.2
H_2	-2	0.4	N/A	0.83	N/A	N/A
Volatile Organic Compounds***	N/A	Acetylene (1)	Ethylene (0.25)	Phosphine (3.85)	Methyl mercaptan (0.4)	Ethylene (0.8)

*Relative sensitivity is calculated by dividing the listed response value of the sensor in terms of its measured quantity by the listed concentration value for the cross-sensitive gas.

**In the case of LEL sensors, relative sensitivity is given in terms of a multiple of the Methane response

***Multiple VOCs may be listed in a sensor's sensitivity data. The single most sensitive is listed here.

The breadth of specific gases and measurement ranges for the sensors enable correlation of the conditions inside the garage to the measurements yielded by fire service personnel conducting 360-degree size-ups. Appendix B provides technical background on the sensor technologies.

Exterior Cameras

Exterior conditions were monitored by 6 HD cameras and one instrument grade thermal imaging camera (FLIR model t560) to monitor test conditions and capture visual cues for fire service size-up considerations. Figure 52 shows the camera locations on the exterior of the garage.

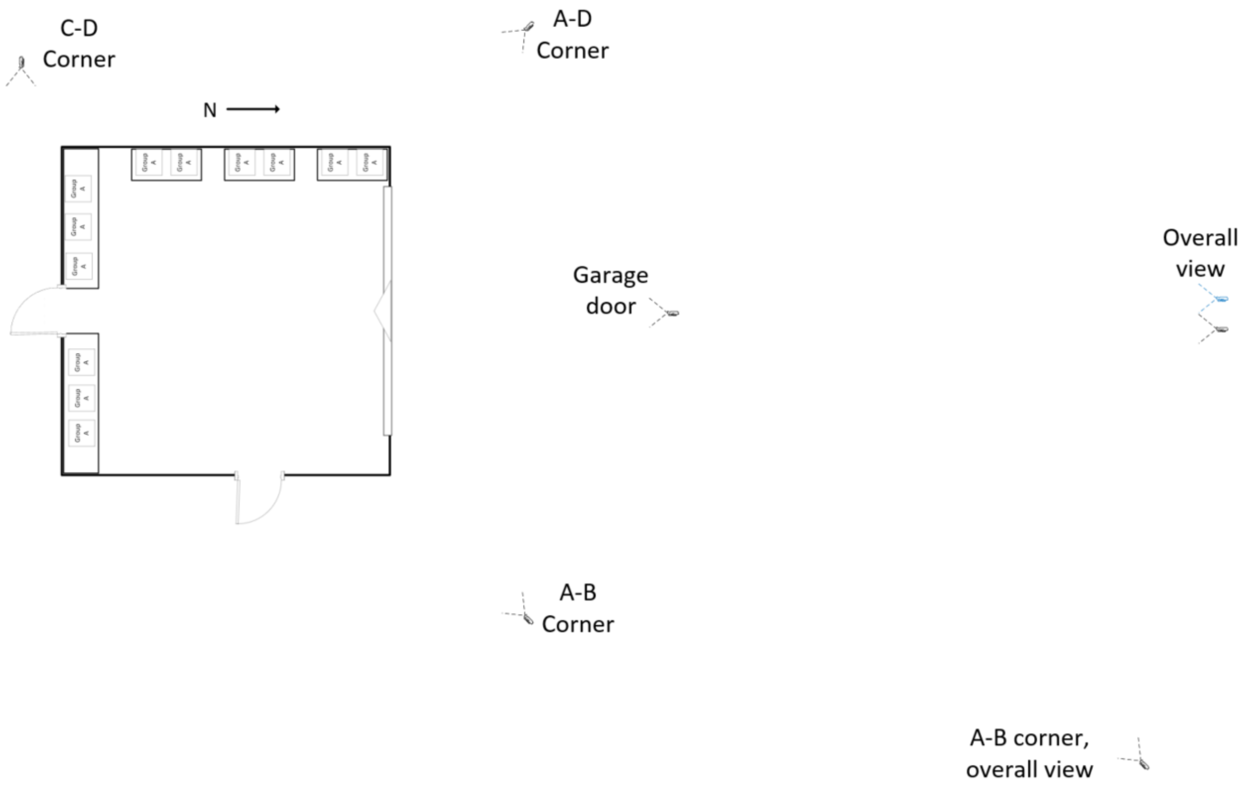

Figure 52 – Exterior camera locations.

The thermal imaging camera was collocated with a HD camera 60 ft in front of the garage door to monitor the whole scene.

3.4 Simulation of Ventilation Operations

For three out of four tests, firefighter intervention tactics and ventilation operations were simulated to represent the common approach of an “inverted-V cut”. The operations were simulated such that testing staff did not need to directly approach the structure during a test due to the potential explosion hazard. This approach also provided test-to-test consistency. The inverted-V was pre-cut into the garage door with a rotary rescue battery-powered saw before each test. A sequence of images from this preparation process are included in Figure 53.

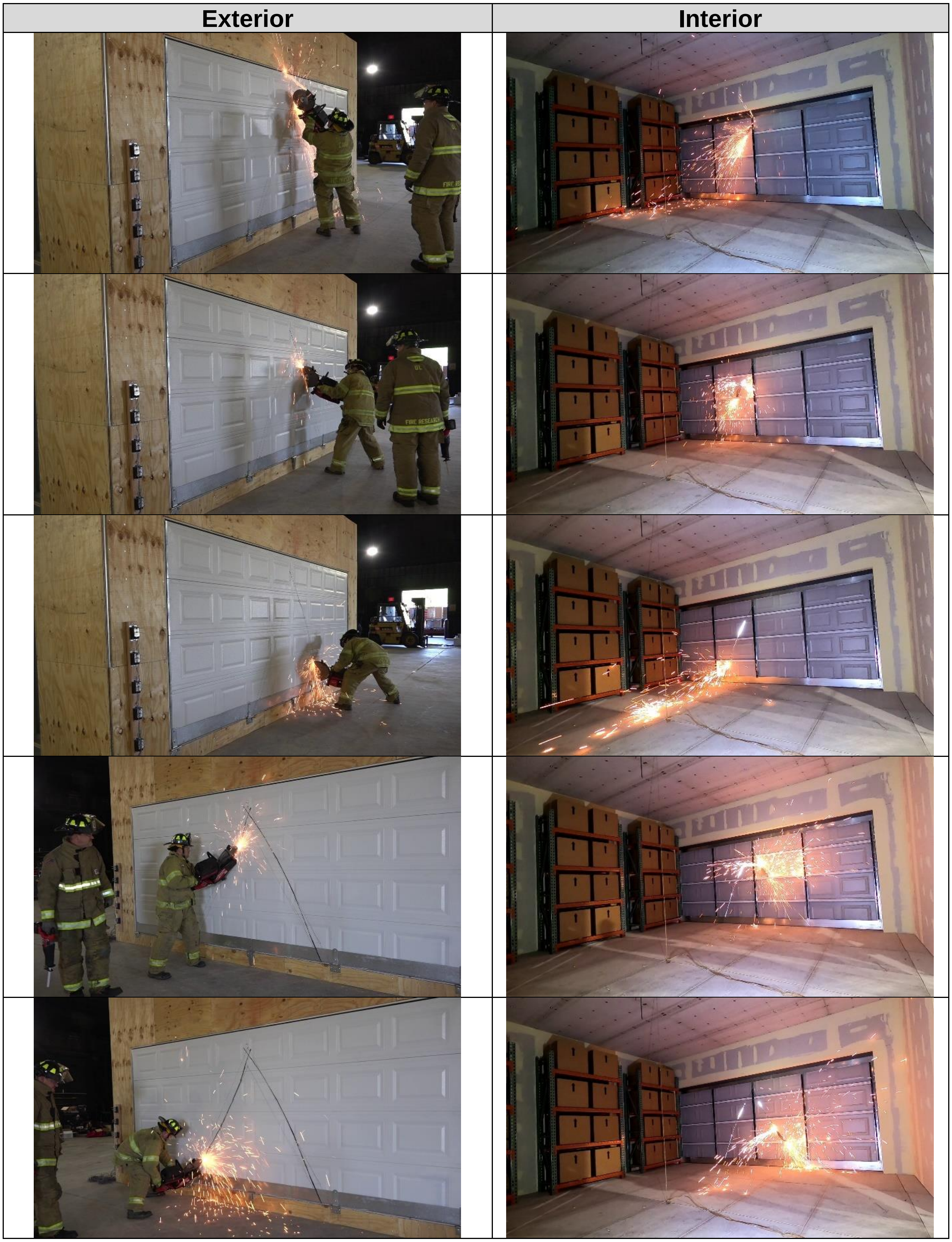

Figure 53 – Inverted-V cutting operation with rotary rescue powered saw.

From this preparation, it was evident that the operation of cutting through the metal door with a powered saw could throw sparks along the cutting path (kerf) on both the interior and exterior of the structure. This phenomenon was simulated during the tests with the activation of a spark fountain ("gerb") in sequence along each kerf. The positioning of the spark fountains is pictured in Figure 54. Images of gerb operation are included in Figure 55. The gerbs were positioned to distribute sparks outside of and into the garage through the kerfs in the garage door. The gerb was not capable of projecting sparks as far into the garage as did the actual saw cutting operation despite several trials. However, it was estimated that ignition of any flammable mixture would occur near to the kerfs where sparks traveling into the garage would pass through regions of higher gas concentration battery gas/smoke mixtures and sparks remaining outside the garage would have greater dilution with air. Given that the purpose of including the sparks was to demonstrate qualitatively whether the flammability of the smoke had been increased, the severity of any deflagration or flame spread that followed was considered important data but outside the scope of these experiments.

Figure 54 – Spark fountain positioning.

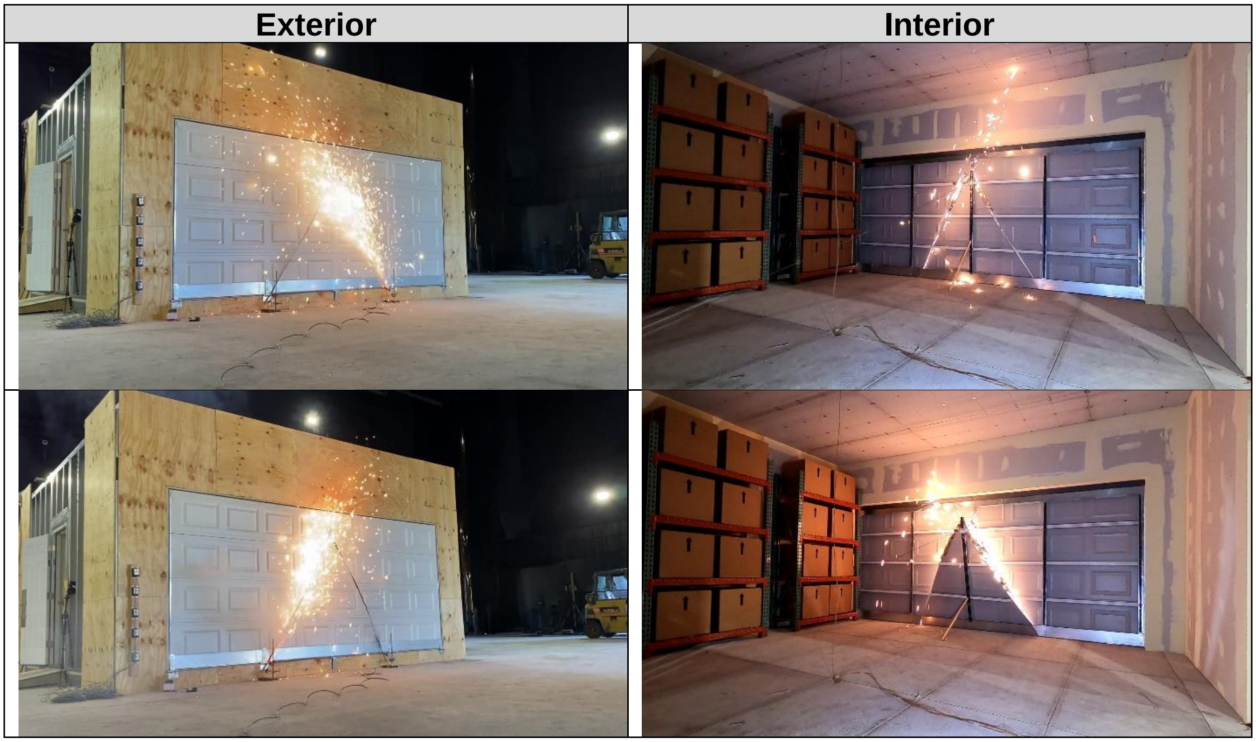

Figure 55 – Spark fountain operation.

Following the initiation of the gerbs, the garage door section was pulled into the garage with a remotely operated winch. The sequence timing is summarized in

Table 6.

Table 6 – Ventilation sequence.

Action	Estimated Duration	Timing	Visualization
Spark fountain #1	15 seconds	Beginning of simulated fire department response	
Spark fountain #2	15 seconds	Immediately after Spark Fountain #1 completes	
Movement of garage section	30 seconds	Initiated simultaneously with Spark Fountain #2	

4 Procedure

Prior to each test, each analytical gas instrument was field calibrated. Every fire service gas meter was checked for proper operation with appropriate calibration gases.

Regarding simulated fire department interventions, is unlikely that homeowners will be alerted to a garage fire (i.e., because there are no requirements for fire detection devices). Therefore, fire department arrival time and ventilation operations thereafter were assumed to occur after the fire reached a ventilation-limited condition in all tests.

Each test was initiated differently. For Test 1, the test began by remotely igniting an ignitor package with an electric match at the center of the bottom edge of the lowest Group A commodity box on the bottom right of the leftmost commodity array (Figure 56). The ignitor package consisted of a tightly wrapped cylinder of gauze and tissue paper soaked in 8 fl oz of gasoline. Fire spread proceeded without intervention until ventilation-limited fire conditions were established. Fire department vent operations were simulated at this time with the gerb ignition and remote ventilation sequence described in Section 3.4. The influence of ventilation of fire development was observed. One minute after flames were visible from ventilation openings, the test was terminated.

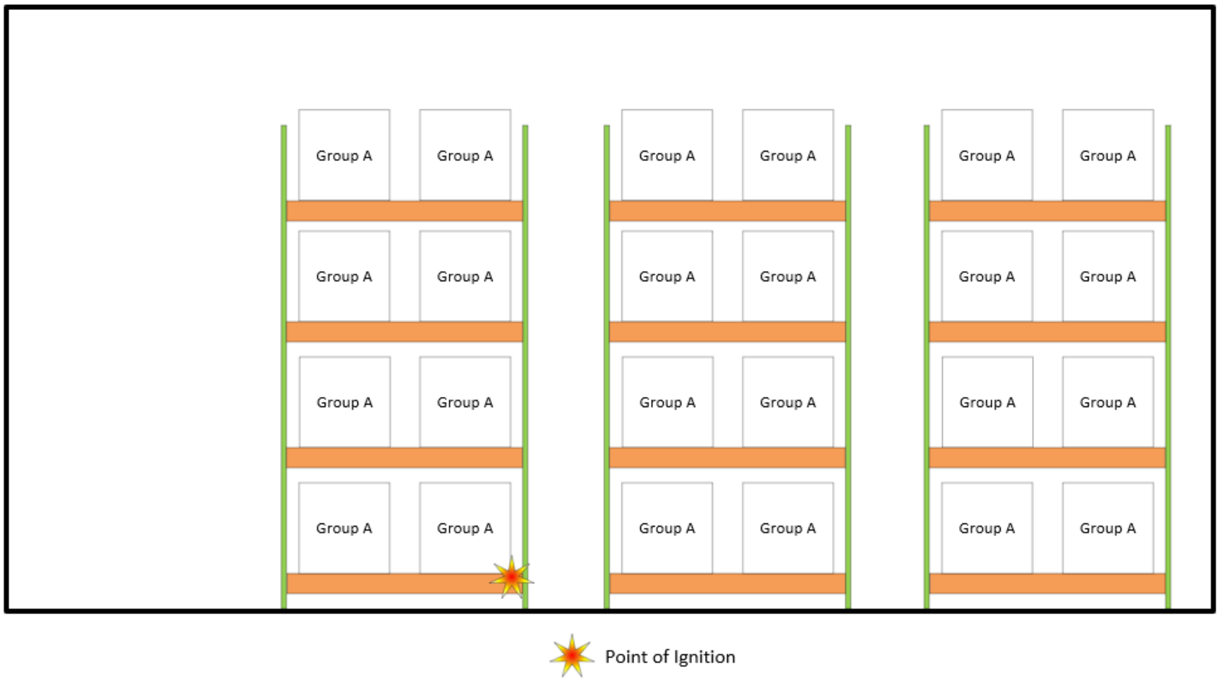

Figure 56 – Ignition location on the D-side wall for Test 1.

For Test 2, the test began by energizing a flexible film heater installed on one component 18650 cell (Figure 57). Power was automatically controlled to provide 10.8 °F/min (6 °C/min) of temperature rise on the initiating component cell surface. Heating continued at this rate until thermal runaway was observed, at which point the heater was de-energized. Thermal runaway behavior was confirmed by a rapid increase in cell surface temperature exceeding 18 °F/s (10 °C/s) to a maximum temperature in excess of 930 °F (500 °C) for the 18650 cell at 100% state of charge. Thermal runaway propagation proceeded without intervention. Battery thermal runaway naturally ignited the accumulated gases and resulted in sustained fire growth. Fire spread proceeded without intervention until ventilation-limited fire conditions were established. Fire department vent operations were simulated at this time with the gerb ignition and remote ventilation sequence described in Section 3.4. One minute after flames were visible from ventilation openings, the test was terminated.

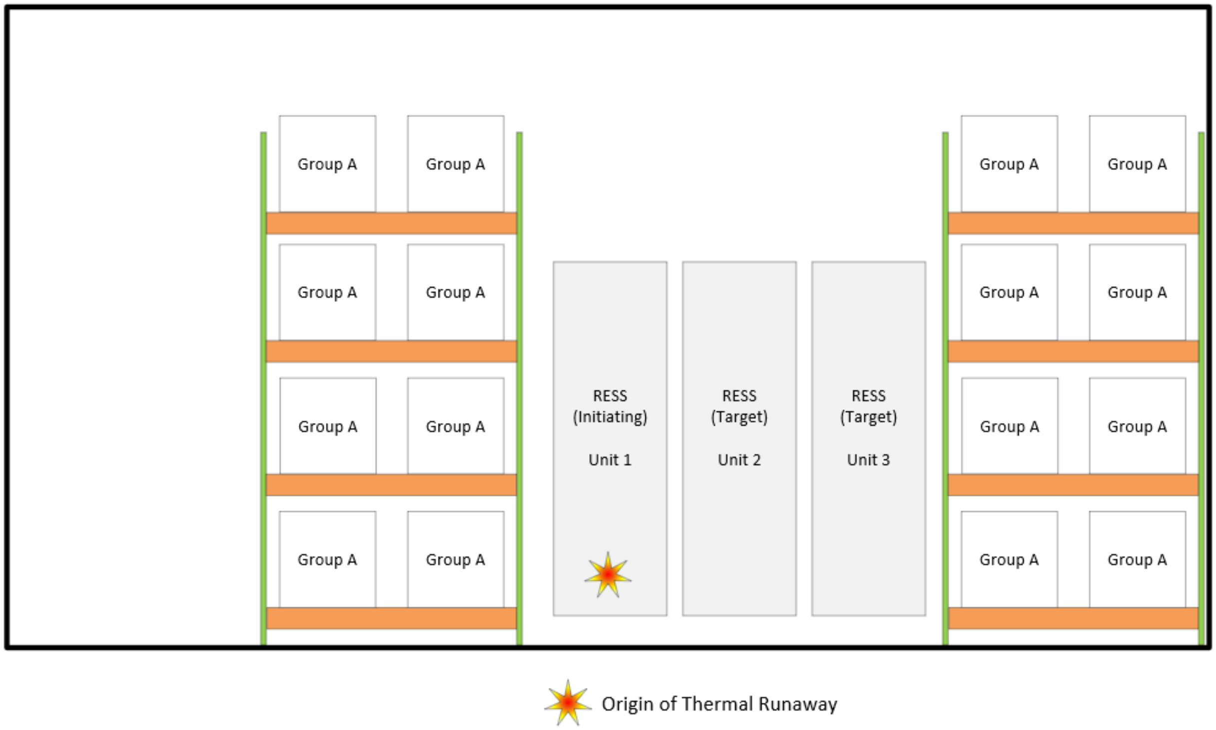

Figure 57 – Location of thermal runaway within Unit 1, shown on D-side wall for Test 2 and Test 4.

For Test 3, the test began by remotely igniting an ignitor package with an electric match at the center of the bottom edge of the lowest Group A commodity box on the bottom right of the leftmost commodity array (Figure 58). The ignitor package consisted of a tightly wrapped cylinder of gauze and tissue paper soaked in 8 fl oz of gasoline. This is the same location as Test 1 and is nearest the leftmost residential ESS unit. Fire spread proceeded naturally until flame vitiation caused a steady reduction in burning. The batteries of the ESS units had not yet gone into thermal runaway. Approximately 10 minutes after test start, a heater installed on a single 18650 cell inside the leftmost ESS was energized and controlled to heat the cell at a rate of 10.8 °F/min (6 °C/min) to ensure battery involvement to achieve test objectives. Thermal runaway propagation proceeded without further intervention. When it was determined that battery gas concentration within the fire environment was near its peak, fire department vent operations were simulated with the sequence described in Section 3.4. The test was terminated one minute after the ventilation sequence.

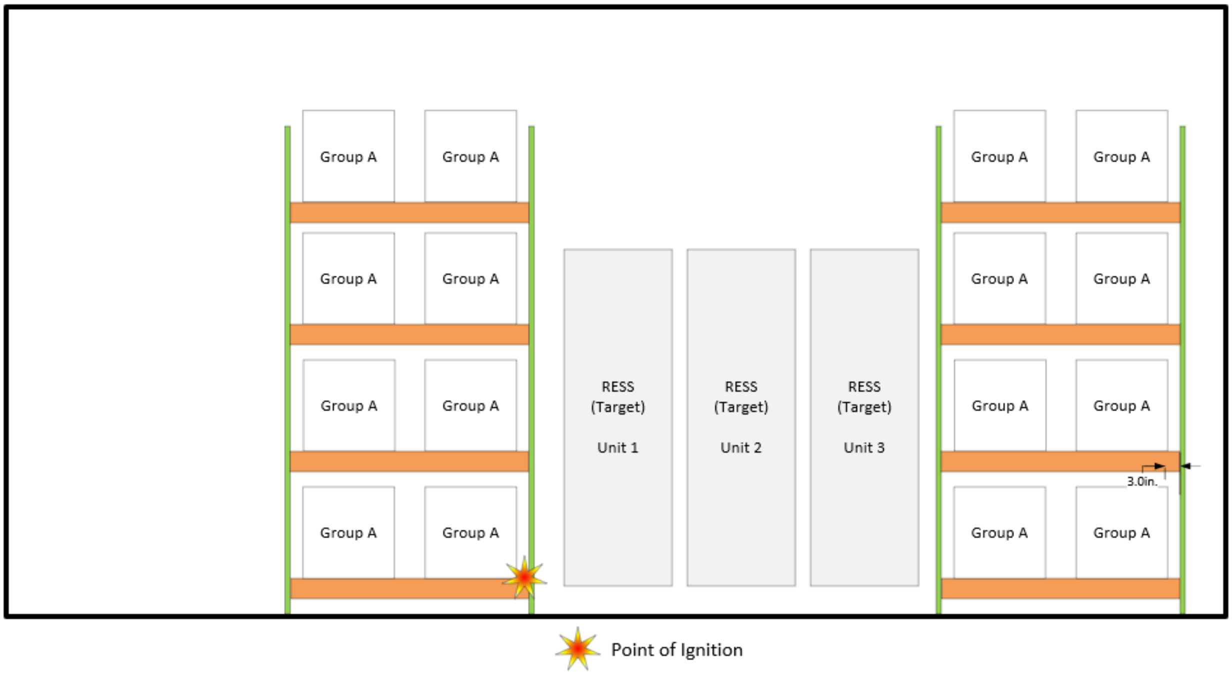

Figure 58 – Location of thermal runaway within Unit 1, shown on D-side wall for Test 3.

For Test 4, the test began with the same setup and procedure as Test 2, by energizing a flexible film heater installed on one component 18650 cell (Figure 57). Power was automatically controlled to provide 10.8 °F/min (6 °C/min) of temperature rise on the initiating component cell surface. Heating continued at this rate until thermal runaway was observed, at which point the heater was de-energized. After cell-to-cell thermal runaway propagation was observed, a gerb was activated to ignite the accumulated battery gases and transition the thermal runaway event to a flaming condition. Thermal runaway propagation and fire growth was then permitted to proceed without further intervention. When it was determined that thermal runaway propagation was complete through Unit 1 and Unit 2, fire department vent operations were simulated by remotely operating the C-side door to represent the scenario where firefighting operations approach an attached garage from within the residence. Fire growth proceeded with the additional ventilation. The test was terminated after there were no further fire department actions to simulate and the room was fully involved in fire.

In all tests, test termination procedures involved remotely opening both access doors and applying a firefighting hose stream through the B-side door until the fire was sufficiently controlled such that the firefighters could enter the structure and achieve final extinguishment.

5 Results

5.1 Test 1

5.1.1 Timeline

Figure 59 through Figure 62 are a visual sequence of the events that occurred during Test 1. Test 1 was initiated remotely with an electric match and ignitor package at the center of the bottom edge of the lowest Group A commodity box on the bottom right of the leftmost commodity array on the D-side wall. The ignition location is shown in Figure 59. The fire spread vertically through all 4 vertical tiers of stored array Group A commodity within 3 minutes of ignition.

Ignition (C-side wall interior and C-D corner)

Ignition (Infrared view of D-side wall interior)

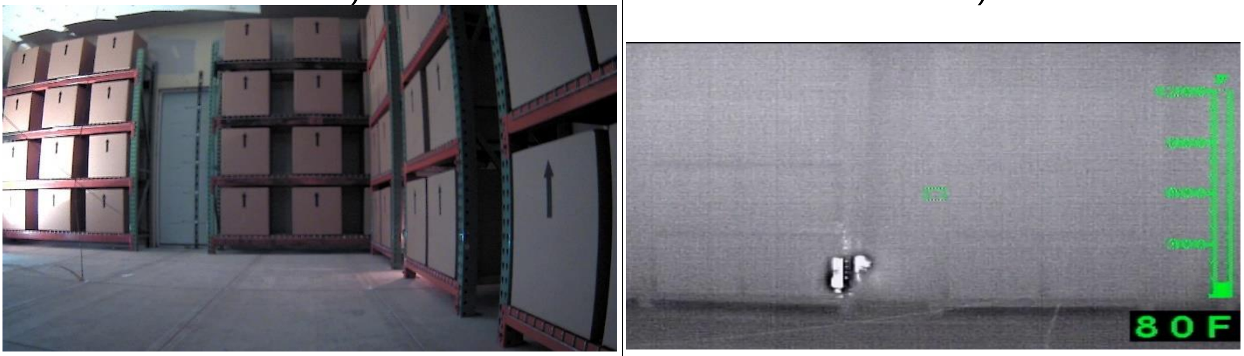

00:04

00:04

Fire spread to 4th box of 1st column

Fire spread to 4th box of 1st column (Infrared view)

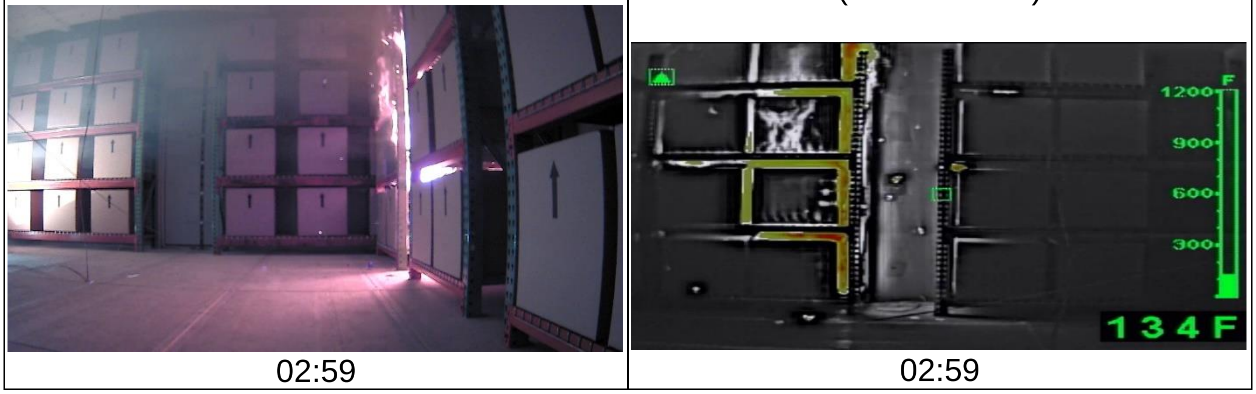

02:59

02:59

Figure 59 – Ignition of Group A commodity using an electric match at resultant fire growth.

As shown in Figure 60, within 3 seconds of fire growth into the top row of commodity boxes, smoke became visible outside the structure. Approximately 30 seconds later, fire spread to the second column of commodity boxes in the storage rack of origin. Five minutes after ignition, the smoke layer visibly reached the floor of the garage. By this point, the fire had reached its peak heat release rate and vitiation of the flames caused a steady reduction in burning. The top right photo in Figure 60 shows the exterior conditions of the smoke from the ventilation-limited fire at 5 minutes and 18 seconds. Smoke was visible around the border of the garage door and saw kerfs at the bottom center of the garage door.

Fire department vent operations were simulated at 5 minutes and 30 seconds after ignition since the temperature profile indicated ventilation-limited fire conditions were occurring. Simulated vent operation began with igniting the gerb on the right-hand side of the pre-cut opening, as pictured in Figure 61. Sparks were observed ejecting from the gerb on the inside and outside of the garage door within 1-2 seconds from commanded ignition of the gerbs. No gas or smoke ignition was observed during the operation of the first gerb. The second gerb was operated after the completion of the first gerb, at 5 minutes and 42 seconds. While the second gerb was active, the pre-cut opening was remotely operated to simulate ventilation of the garage. No ignition of smoke or combustion gases was observed during the operation of the second gerb.

Smoke becomes visible outside structure at garage door seams and pre-cut.	Increased smoke exhausts around seams of garage door
	
03:02	05:18
First gerb operation	Second gerb operation and ventilation begins
	
05:30	05:47

Figure 60 – Sequence of events between 3 and 6 minutes of test time in Test 1.

Following the simulated ventilation, a dark colored and opaque smoke plume exited from the opening as well as from the seams around the garage door, as shown in Figure 61. The additional ventilation increased oxygen supply to the smoldering commodity boxes and burning steadily increased. As burning increased, the smoke plume increased in both size and opacity. At 17 minutes and 40 seconds, approximately 12 minutes after vent operation, flames became visible at the top of the pre-cut opening in the garage door. The flaming was difficult to see within the thick black smoke plume. Fire growth continued in a cyclic pattern where fresh air entered the bottom of the pre-cut opening, flaming increased, and then smoke output increased (decreasing air intake) before cycling again. Less than two minutes after flames were visible at the garage door, a small amount of flames were visible at the bottom of the C-side door which represented the entryway into the residence.

Exterior smoke plume 10 seconds after ventilation begins  05:57	Exterior smoke plume as first flames become visible out of ventilation opening  17:40
Flaming observed from ventilation opening  19:27	Small flame observed at bottom of C-side service door  19:29

Figure 61 – Sequence of events occurring between 6 and 20 minutes of test time.

The test was terminated one minute after flames were visible at the C-side door by remotely opening the B-side and C-side doors, and initiating manual suppression, as pictured in Figure 62.

Figure 62 – Suppression of the test at 21 minutes.

5.1.2 Thermal Runaway Propagation

Batteries were not included in Test 1.

5.1.3 Conditions Inside Garage

Gas Temperature

Gas temperatures measured in the center of the garage were used to characterize the fire growth inside the compartment. Temperatures increased until 4 minutes and 23 seconds after ignition before they decreased again, as described in Figure 63. The peak at 4 minutes and 23 seconds indicates the beginning of a ventilation limited fire condition. After ventilation was initiated at 5 minutes and 30 seconds, the compartment temperatures steadily increased to a maximum of 700 °C at the ceiling. After 17 minutes and 40 seconds, flames were visible through the garage door vent. This is correlated with an increase in temperatures near the floor and subsequent steady state conditions until test termination and suppression operations. Between 17 minutes and 40 seconds and test termination, the compartment fire was considered fully developed and once again ventilated-limited.

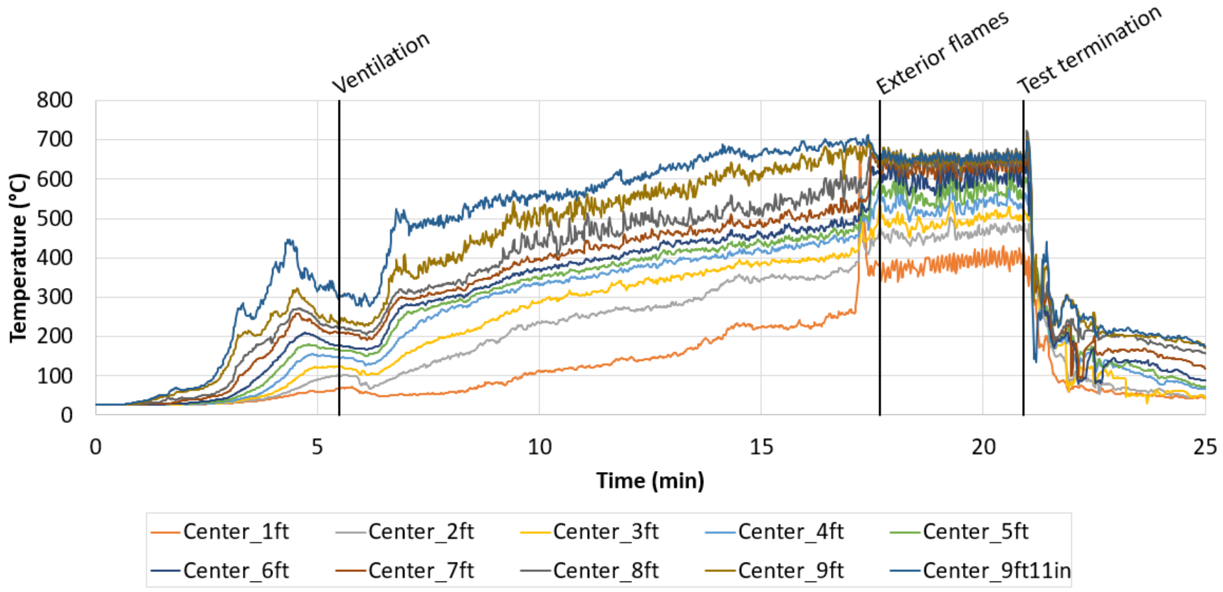

Figure 63 – Temperature measurements inside the garage for Test 1.

Gas Concentrations

Leakage of fresh air in through gas sampling system fitting in Test 1 resulted in an artificial smoothing, reduced response time, and under-reported gas concentration measurements for the interior gas sampling system. The exterior gas sampling system was not impacted. The interior gas sampling system was repaired for Test 2, Test 3, and Test 4. Interior gas sampling during Test 1 can be used as an indicator of interior behavior, but quantitative analysis is not appropriate.

Oxygen concentration in the garage decreased during the period between ignition and operation of the garage door vent, as shown in Figure 64. In this same period, carbon monoxide, carbon dioxide, and total unburned hydrocarbons increased as products of incomplete combustion.

For the period between ventilation operations and flaming, oxygen concentration decreased while CO_2, CO, and THC increased as products of incomplete combustion.

As flaming conditions resumed interior and exterior to the garage, quantities of unburned fuel, including CO and THC decreased. Oxygen increased and CO_2 increased. Gas measurements were discontinued shortly after test termination and suppression operations commenced.

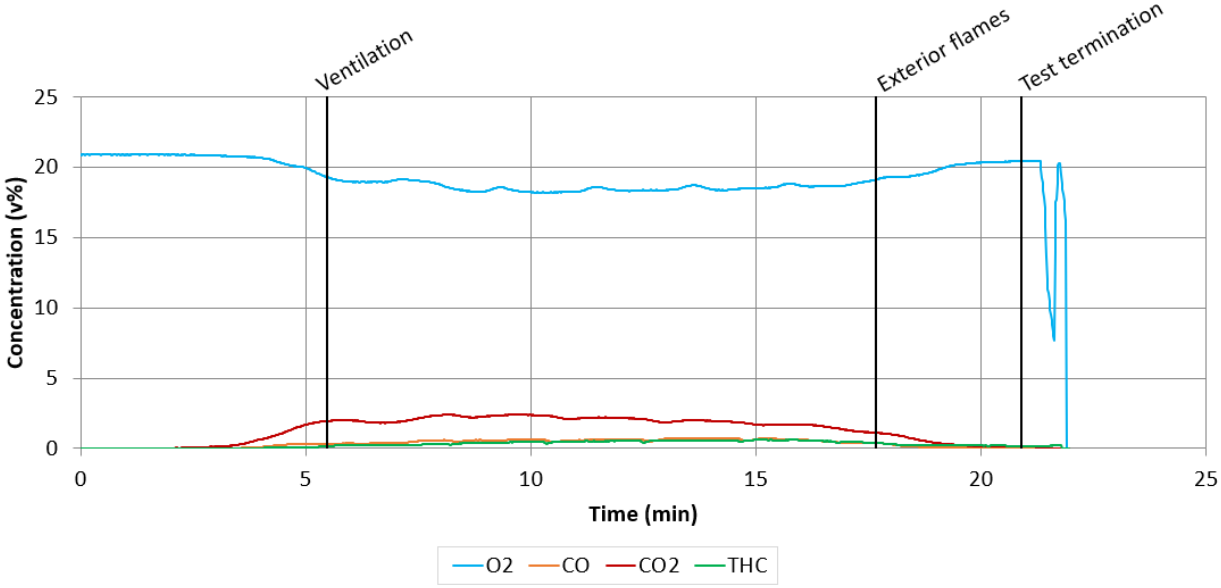

Figure 64 – Interior upper layer gas measurements for Test 1[1].

Explosion Hazards

No deflagration or explosion events were observed during Test 1.

5.1.4 Conditions Exterior to Garage

Heat Flux

Heat flux was measured facing the garage door at an elevation 5 ft above the floor (near the top of the ventilation cut) and a position approximately 6 inches from the garage door. The first spike in heat flux at 4 minutes and 17 seconds measured 2.1 kW/m^2 and corresponded to a small ejection of smoke plume around the garage door kerf, as plotted in Figure 65. Heat flux remained below 5 kW/m^2 before the garage was ventilated. Heat flux increased rapidly following ventilation operations when the heat flux gauge was immersed in the smoke plume. Heat flux peaked at 23 kW/m^2 between 9 and 13 minutes at which point heat flux began to decrease to 15 kW/m^2. Heat flux rises as combustion increases between 17 minutes and 18 seconds and 17 minutes and 40 seconds as flames become visible on the exterior of the garage door. Heat flux remained stable at this point until test termination. Because the gauge was no longer directly immersed in the fire plume during this period, the maximum heat flux was lower than what was observed near 9 minutes and 13 seconds. Heat flux spiked to 25 kW/m^2 during test termination as the contents of the garage rapidly ignited when the B-side and C-side doors were opened, and suppression activities began. Heat flux decreased to ambient as the fire was manually extinguished.

---

[1] Note: Plot should be used for qualitative assessment. System leakage prohibited quantitative analysis.

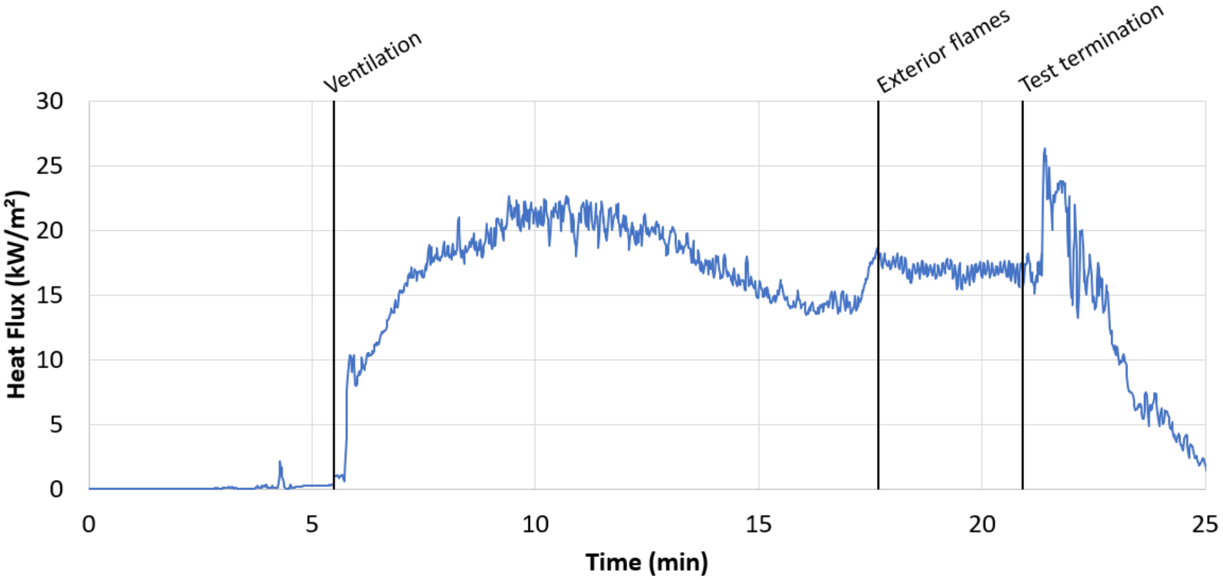

Figure 65 – Heat flux measurement in Test 1.

Gas Measurements

Oxygen concentration outside the garage door remained at ambient concentration prior to ventilation of the garage, as shown in Figure 66. Peak CO_2 and CO concentrations prior to ventilation were 0.2 v% and 0.03 v%, respectively, which align with typical ambient conditions. Following ventilation operations, the sampling probe became immersed in the hot gas plume exiting the garage. Oxygen concentration in the plume dropped to a minimum of 11.5 v% at 8 minutes and 42 seconds. At the same point, CO_2 and CO measured 6.5 v% and 1.8 v%, respectively. Between 12 and 18 minutes, gas concentrations in the plume were approximately steady at 15 v% O_2, 5 v% CO_2, and 2 v% CO. As flames became visible in the plume, O_2 dropped further to 9.8 v%, CO_2 increased to 7.4 v%, and CO increased to 3.6 v%. Within one minute of test termination and suppression operations, gas concentrations at the garage door returned to initial ambient conditions.

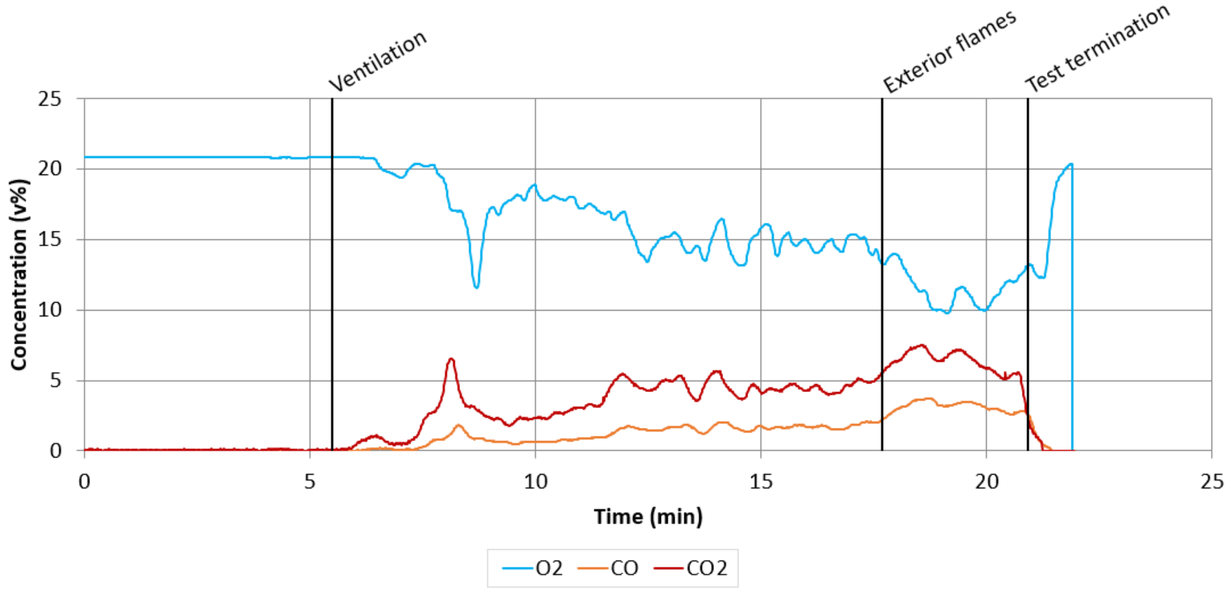

Figure 66 – Exterior gas measurements at the garage door in Test 1.

Hydrogen fluoride gas was not measured above the minimum detection limit (0.8 ppm) of the hydrogen fluoride measurement instruments in Test 1.

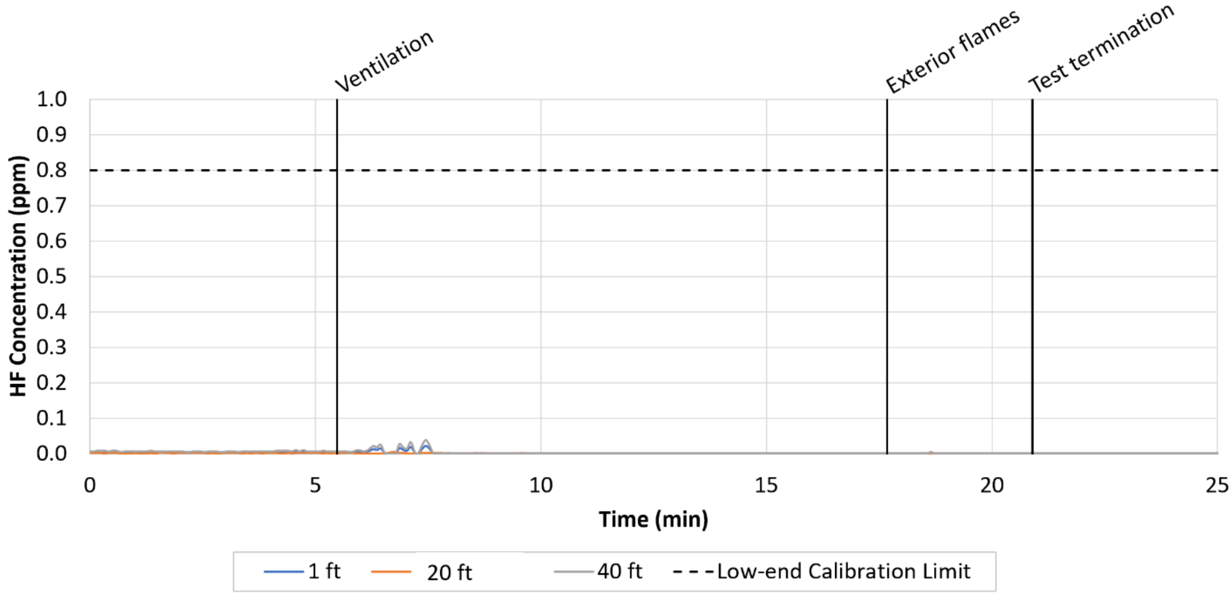

Figure 67 – HF measurements in Test 1.

5.1.5 Size-up Indicators

Visual Indicators

Because no batteries were involved in Test 1, this section provides a baseline of visual compartment fire indicators to compare observations from Tests 2 - 4. Size up indicators include unaided visual observations and thermal imaging.

TICs directed at the burning commodity were able to provide imagery of the events inside the garage for approximately 3 minutes longer than the visual cameras before hot smoke obscured all observation into the garage.

The TIC directed through the garage door at the commodity boxes along the C-side and D-side wall provided the most direct and prolonged view of commodity ignition and burning. Views from this camera were compared with different camera angles from around the exterior of the garage. The sequence of images shown in Figure 68 - Figure 73 compares the TIC view with key external camera views, including the A-side of the garage (garage door side) and the C/D-side corner (C-side service door), which provided the best views of smoke leakage from the garage and primary points of entry for the fire service. The FLIR TIC viewpoint of the A-side of the garage is also included. A series of major test events are chronicled from these viewpoints.

The first externally visible indicator of a fire in the garage is smoke leakage from the garage door seams approximately 3 minutes after ignition. At this point, within the garage, fire had spread to the top row of commodity boxes above the ignition point and a smoke layer was forming. Similar visual leakage continued at slowly increasing intensity up to the point of garage door ventilation. After ventilation, a plume was formed at the garage door vent. At this point, a small plume of smoke leakage was also observed out the top gap of the C-side door. The plume slowly increased in opacity until the flaming was first observed within the plume and the plume began to pulsate. The flaming was partially concealed by the high opacity of the plume.

By the time of suppression, visibility in the test lab was very low due to smoke diffusion and filling within the lab space.

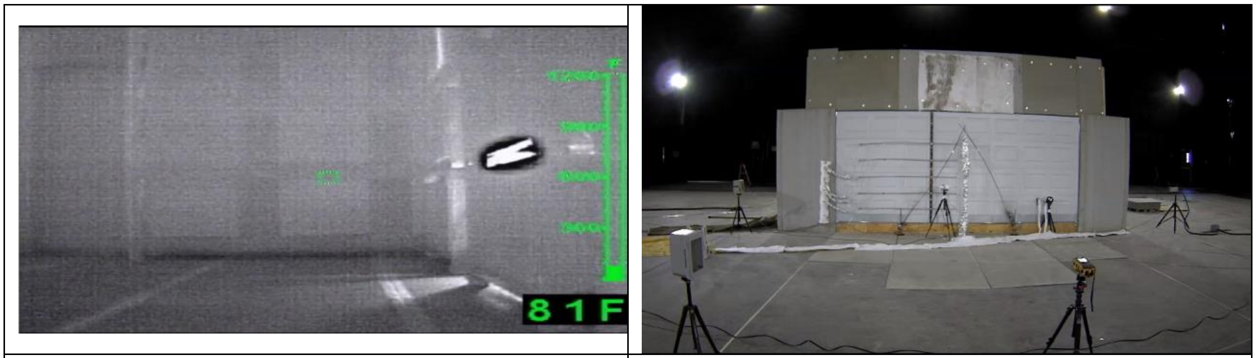

(a) IR image of interior C-D corner

(b) Overall view

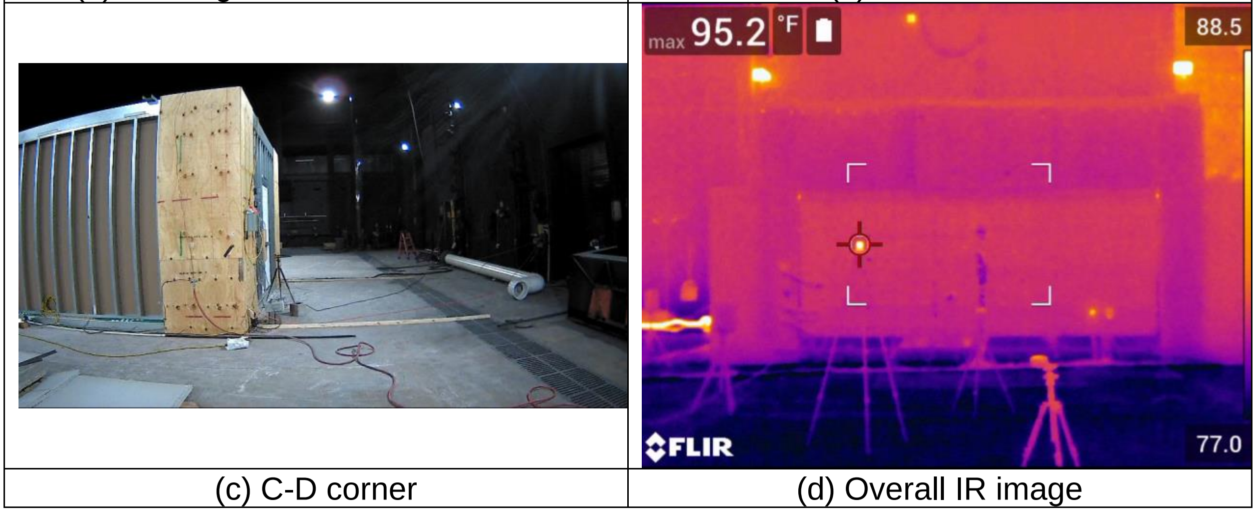

(c) C-D corner

(d) Overall IR image

Figure 68 – Images from commodity ignition (00:00).

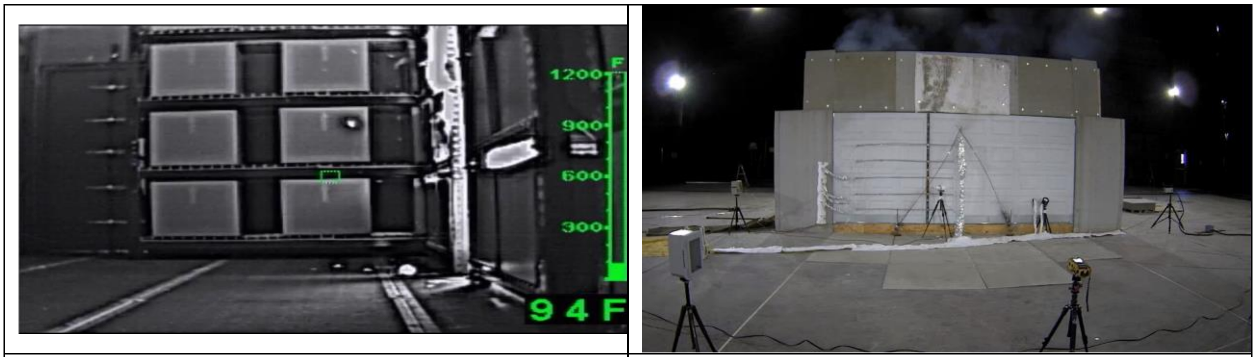

(a) IR image of interior C-D corner

(b) Overall view

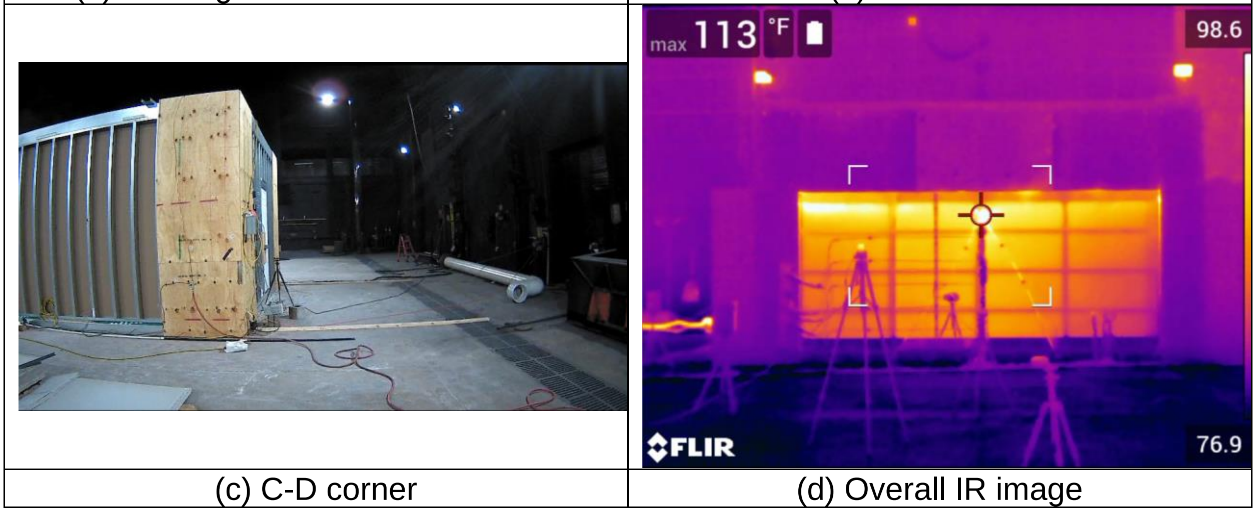

(c) C-D corner

(d) Overall IR image

Figure 69 – Images from first external signs of smoke (03:00).

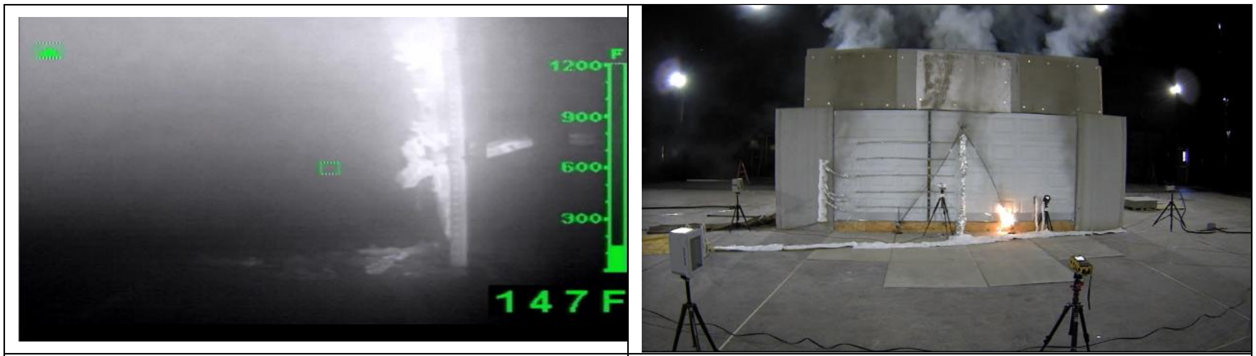

(a) IR image of interior C-D corner

(b) Overall view

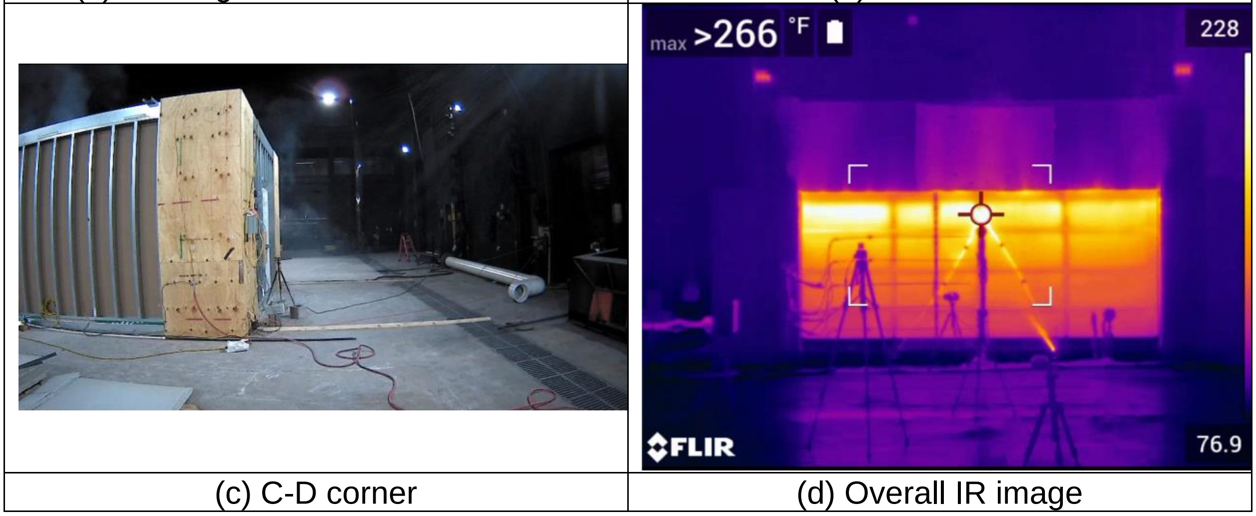

(c) C-D corner

(d) Overall IR image

Figure 70 – Images from first gerb operation (05:30).

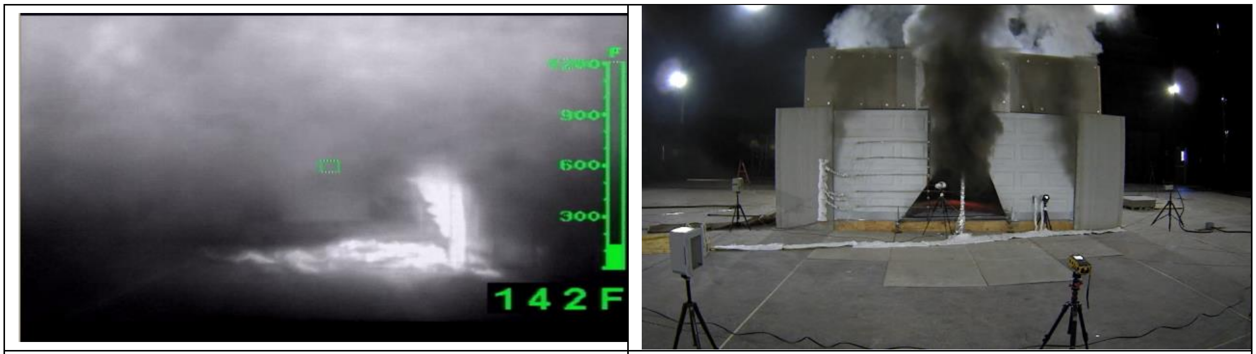

(a) IR image of interior C-D corner

(b) Overall view

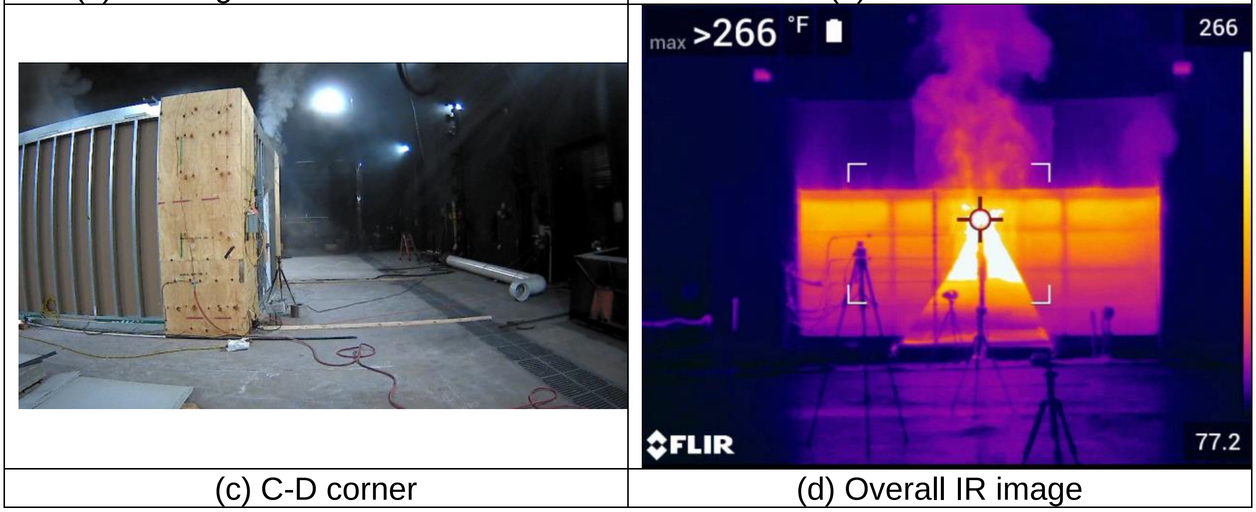

(c) C-D corner

(d) Overall IR image

Figure 71 – Images from 1 minute post-ventilation (07:00).

N/A - TIC removed to protect equipment

(a) IR image of interior C-D corner

(b) Overall view

(c) C-D corner

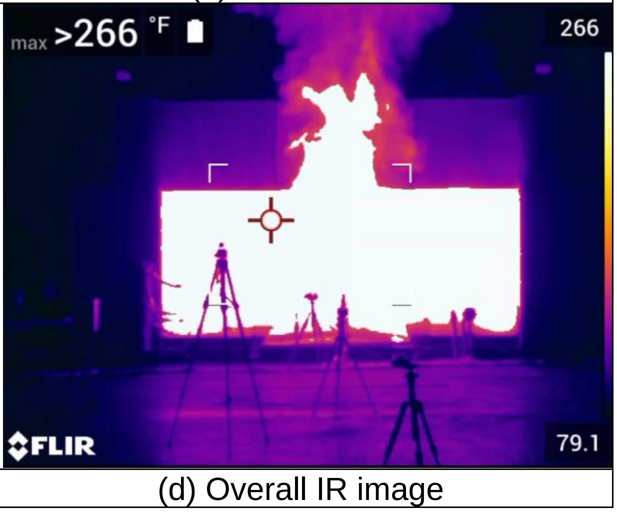

(d) Overall IR image

Figure 72 – Images of visible flaming in vent plume and ‘breathing’ pattern (17:40).

N/A - TIC removed to protect equipment	
(a) IR image of interior C-D corner	(b) Overall view
	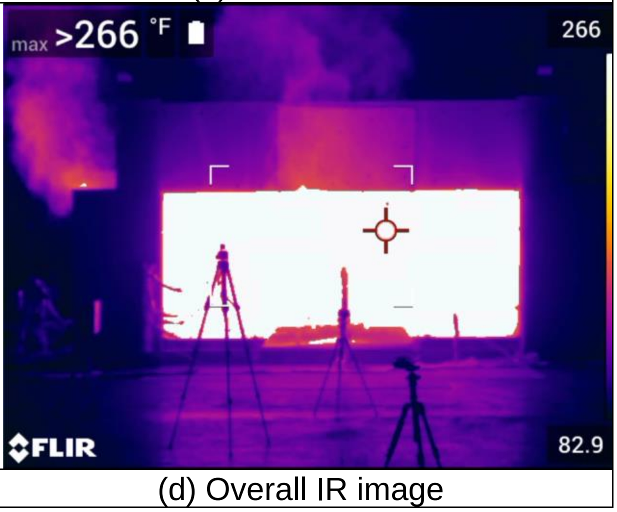
(c) C-D corner	(d) Overall IR image

Figure 73 – Images from test termination and suppression (21:00).

Portable Gas Meters

During Test 1, O_2 concentrations where the portable gas meters were located, 3 ft above the floor, remained at ambient pre-test measurements for the duration of the test.

Measurements from the four meters, given in Figure 74, indicated that within 30 seconds of ventilation, CO concentrations near the garage door rapidly increased and reached sensor saturation (2000 ppm) within 30 seconds. Prior to the ventilation, the CO concentration near the garage door had reached a peak of approximately 180 ppm. The meter located near the C-side access door measured between 10 and 70 ppm for the duration of the test, starting 4 minutes after ignition.

The two meters along the driveway measured a steady increase in CO from near 0 ppm up to approximately 250 ppm by the end of the test. The fact that both meters measured increases at the same rate indicates that they were measuring ambient increases caused by smoke diffusion into the test lab. It is therefore not realistic to expect that meters in these positions would measure this increasing CO concentration in a real incident, where smoke would not be confined by the large laboratory used in these experiments.

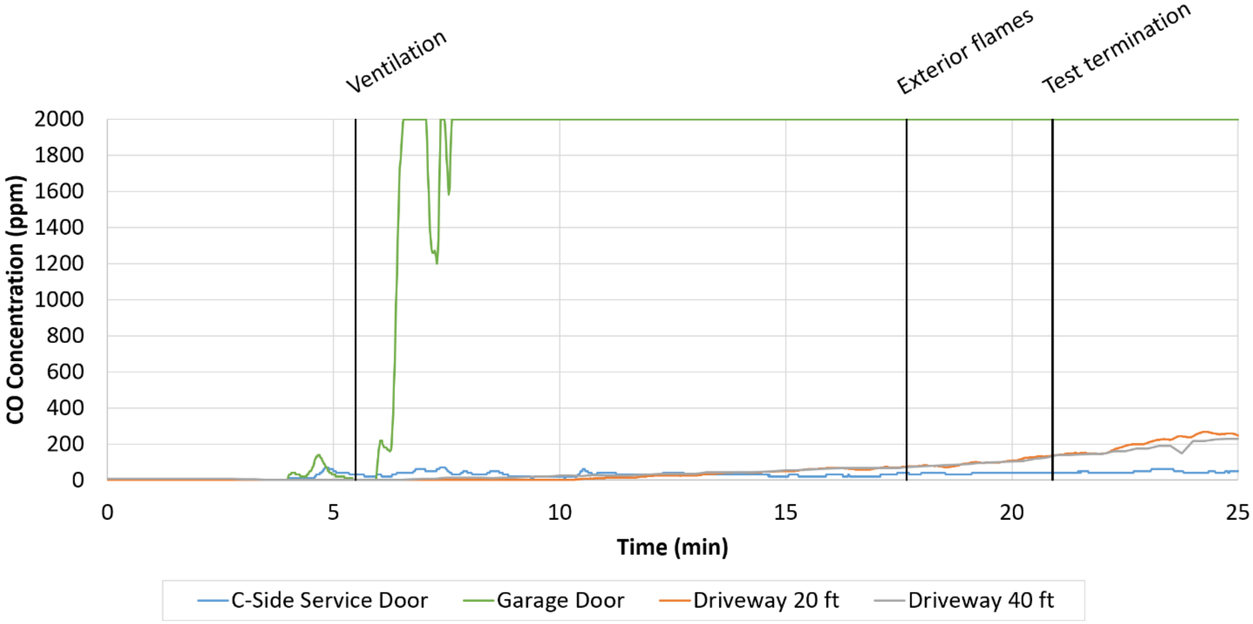

Figure 74 – CO Concentration measurement by all portable gas meters.

The meter in front of the garage door measured HCN, VOCs, and LEL of flammable gases in addition to CO. The concentrations of VOCs and HCN began to increase following the initiation of ventilation, as indicated in Figure 75 and Figure 76. Within 30 seconds, the HCN sensor had saturated at 50 ppm and VOCs began to increase. At approximately 3 minutes and 30 seconds after start of ventilation, VOCs peaked near 750 ppm before decreasing again, increasing to saturation at 1000 ppm. The signal dropped to zero at 12 minutes and 55 seconds. Video review did not suggest a reason for the signal drop of the VOC sensor, which was calibrated and measured normally in subsequent tests. At 17 minutes and 50 seconds into the test, the meter was remotely pulled from its location to prevent heat damage from the garage door plume.

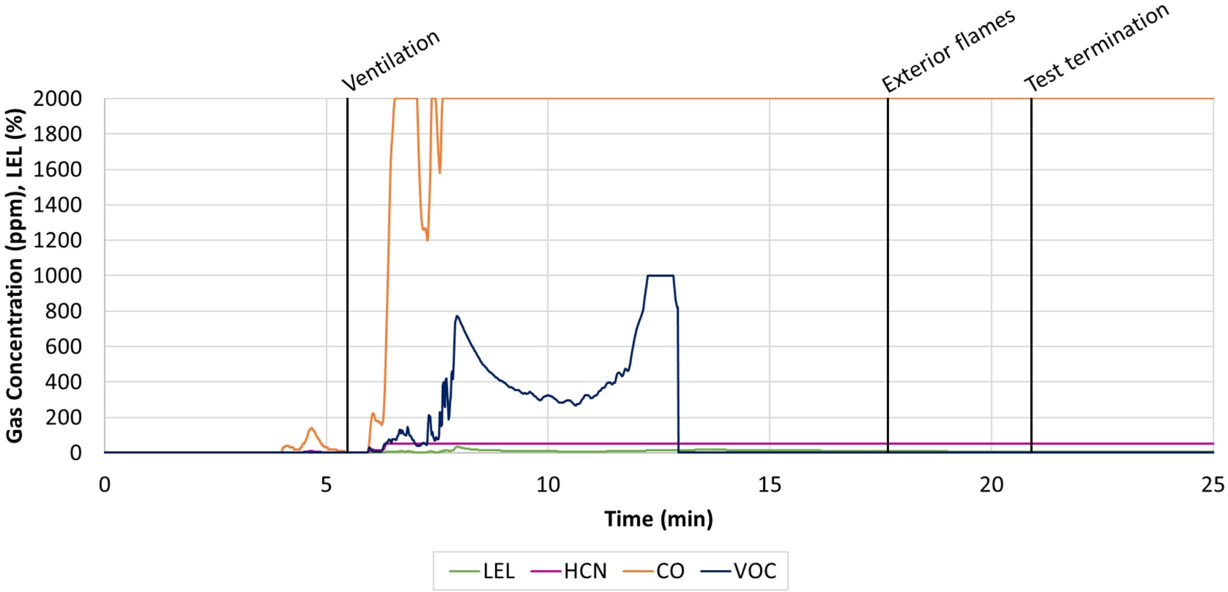

Figure 75 – Portable gas meter readings at garage door.

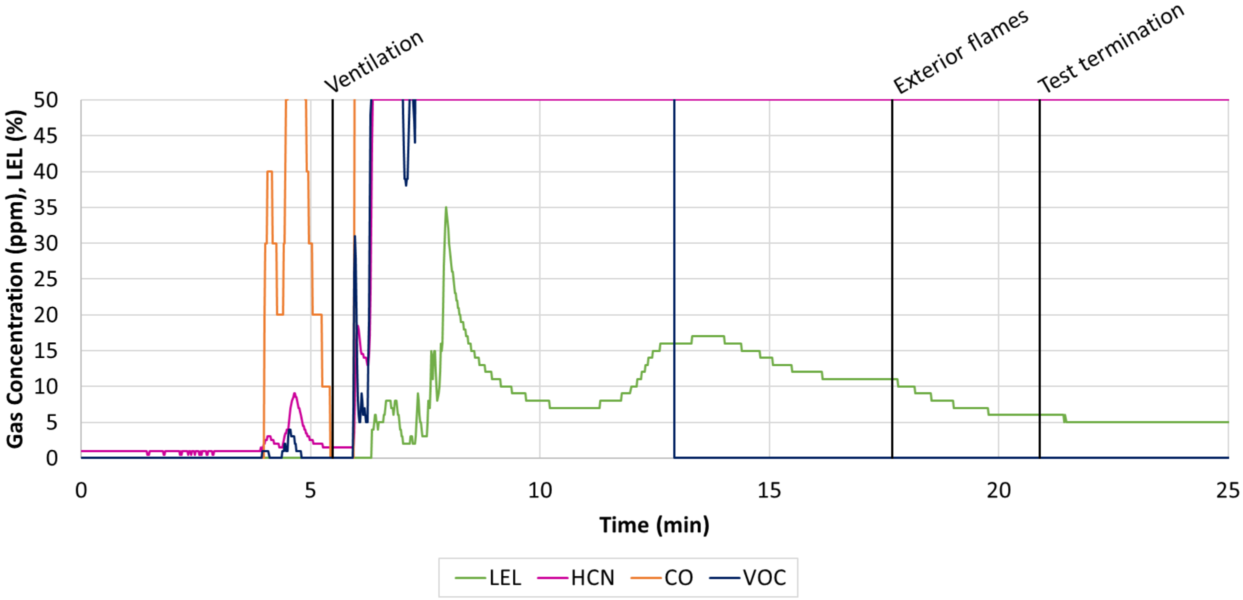

Figure 76 – Portable gas meter readings at garage door (zoomed in on low concentrations).

The meter 20 ft in front of the garage door measured HCN, and H_2S in addition to CO. Figure 77 and Figure 78 indicate that the meter began to register CO and HCN approximately 5 minutes after the start of ventilation. Both measurements then steadily increased. HCN measurement saturated at 50 ppm approximately 2 minutes after the start of test termination and suppression activities. H_2S measurement remained zero for the majority of the test. A peak of 2 ppm registered during the last 5 minutes of the test. There was no clear cause for this minor increase in H_2S.

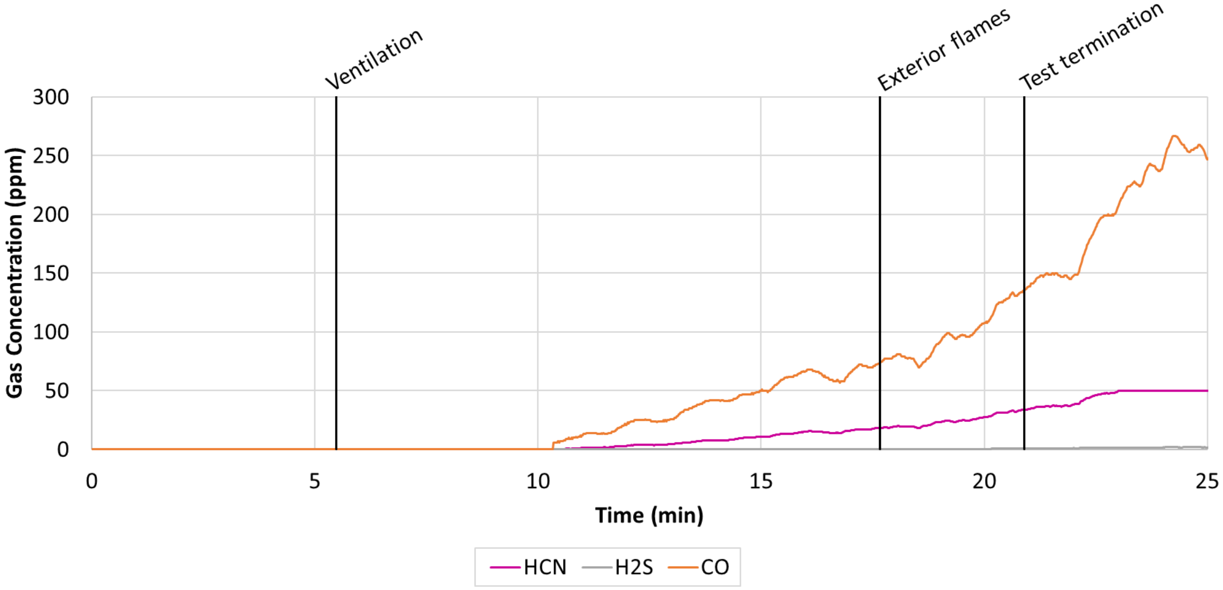

Figure 77 – Portable gas meter readings 20 ft in front of garage door.

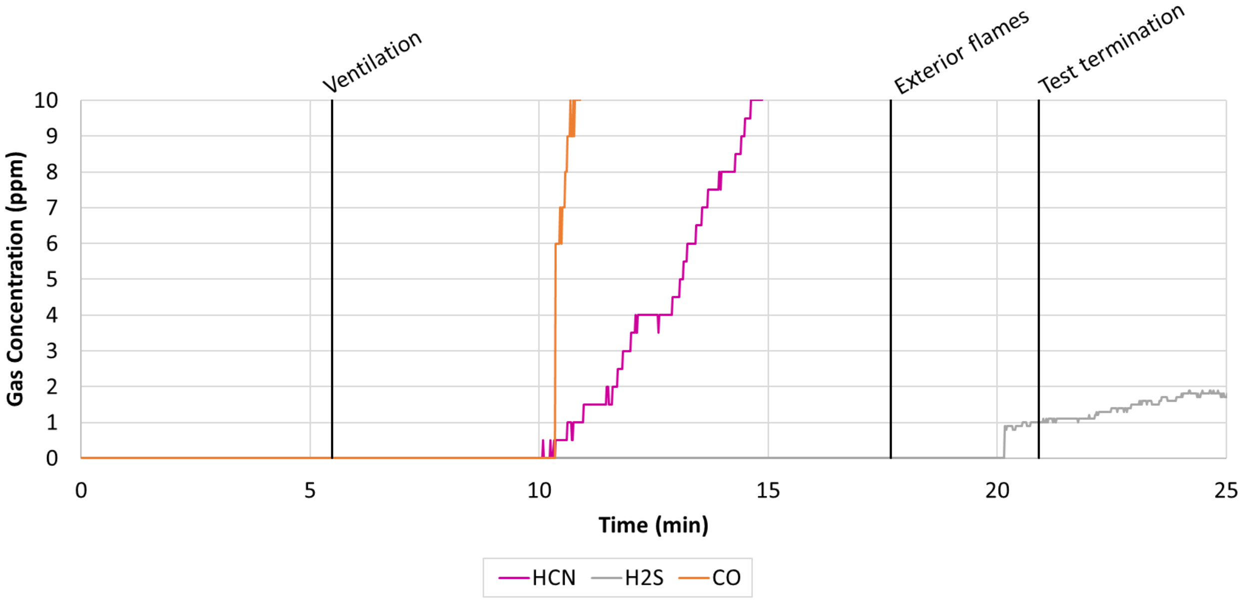

Figure 78 – Portable gas meter readings 20 ft in front of garage door (zoomed in on low concentrations).

The meter 40 ft in front of the garage door has sensors for measuring HCN in addition to CO (Figure 79 and Figure 80). CO readings began to occur 1 minute after the start of ventilation and then steadily increased for the duration of the test (similar to the meter at

20 ft in front of the garage). Within 30 seconds after test termination, HCN was measured between 0.5 and 2 ppm. This is likely due to the increase in HCN in the lab atmosphere caused by opening the doors to the garage and performing suppression, which released cooled less dense smoke into the lab. This likely increased local HCN concentrations around the meter in addition to the overall background HCN concentration in the lab.

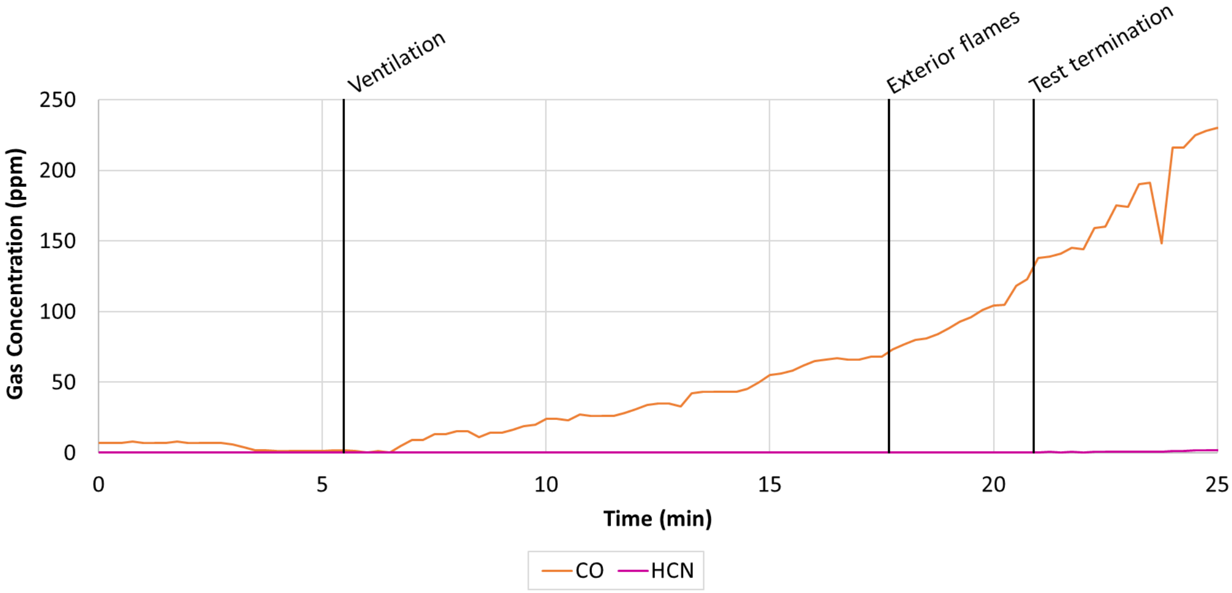

Figure 79 – Portable gas meter readings 40 ft in front of garage door.

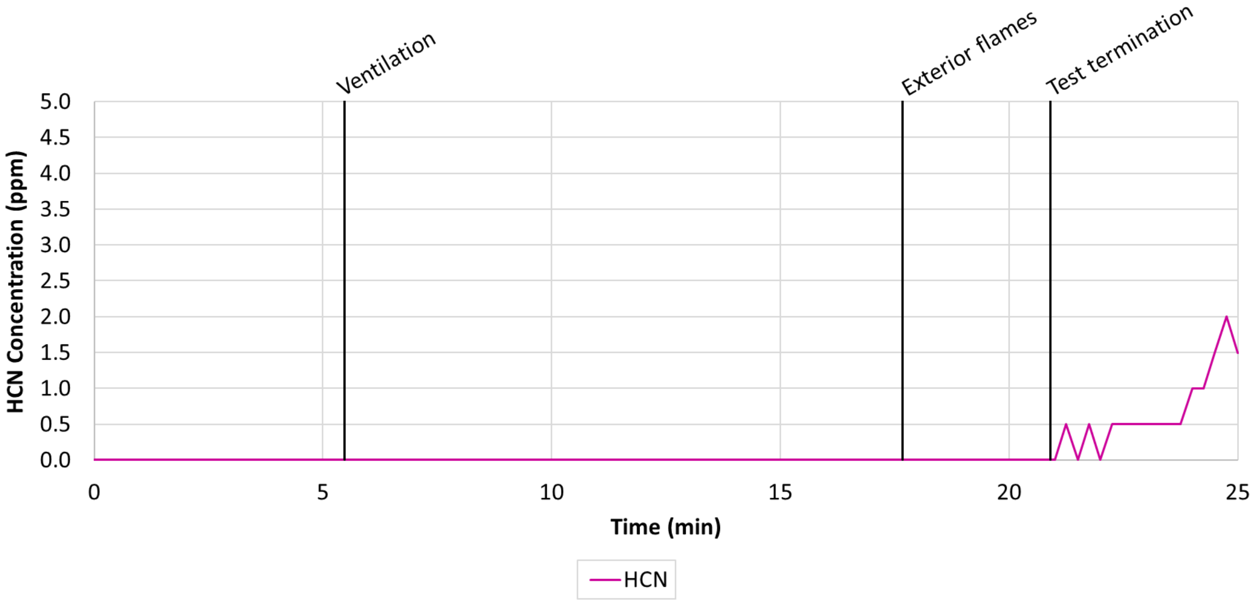

Figure 80 – Portable gas meter readings 40 ft in front of garage door (zoomed in on low concentrations).

The meter at the access door on the C-side of the garage has sensors for measuring H_2 and H_2S in addition to CO. Hydrogen between 10 and 60 ppm was measured from approximately 4 minutes after ignition to the end of the test (Figure 81). However, the hydrogen measurements are likely the result of cross-sensitivity to CO. No batteries were present in Test 1, so there was no signifiant source of H_2. Up to 1.2 ppm of H_2S was sporadically registered during the test (Figure 82). The majority of H_2S readings were present after the start of ventilation.

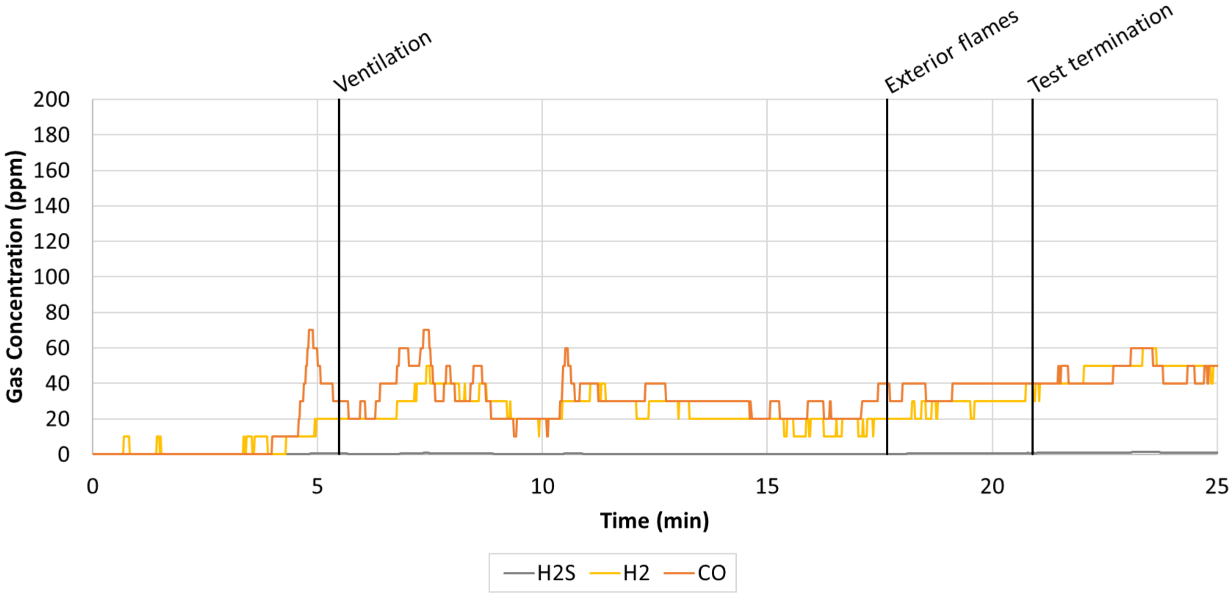

Figure 81 – Portable gas meter readings at C-side service door.

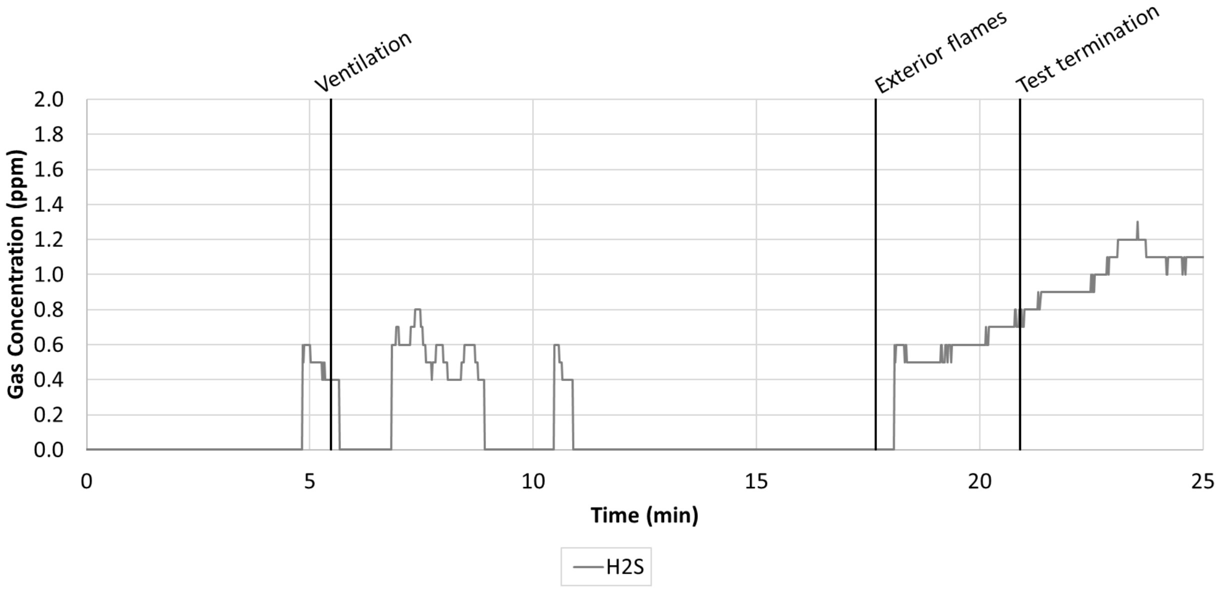

Figure 82 – Portable gas meter readings at C-side service door (zoomed in).

5.2 Test 2

5.2.1 Timeline

Figure 83 - Figure 87 show a visual sequence of the most significant events that occurred during Test 2.

Test 2 was initiated by heating a single 18650 component cell within a module to thermal runaway at a steady rate of 6°C/min. After 20 minutes and 30 seconds of heating, the heated 18650 component cell experienced thermal runaway. Five seconds after the first cell thermal runaway, a small amount of battery gas is visible outside the unit enclosure, as shown in Figure 83. Three minutes and 22 seconds later, cell-to-cell propagation occurred within the remaining twenty-nine 18650 component cells of the initiating module and a large plume of gas extended from all openings on the unit enclosure. The plume stratified with heavy white vapors pooling low on the floor and lighter gases swirling and accumulating near the ceiling. Two minutes after thermal runaway propagation of the initiating module, the first traces of thermal runaway effluent gas are visible outside the structure around the garage door.

Signs of smoke following first cell thermal runaway	Gas release during propagation through initiating module (Front view)
	
20:35 (TR + 00:05)	24:31 (TR + 04:01)
Gas release during propagation through initiating module (Side view)	First signs of pale smoke emission from garage door
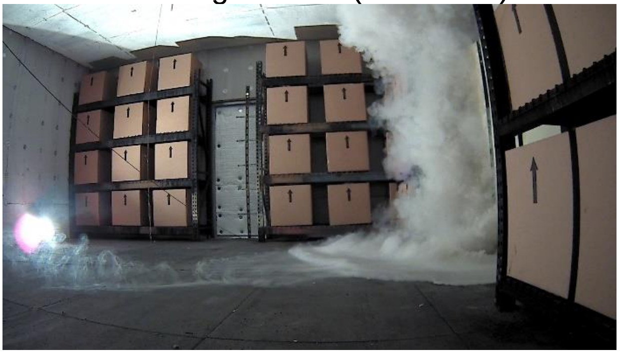	
24:31 (TR + 04:01)	25:50 (TR + 05:52)

Figure 83 – Thermal runaway initiation and propagation through initiating unit.

Five minutes after thermal runaway propagation through the initiating module, the module directly beneath the initiating module (“Unit1Init1”) experienced thermal runaway. Heat accumulated within the unit enclosure and additional modules underwent thermal runaway, advancing upwards through the unit, as pictured in Figure 84. As additional modules experienced thermal runaway, battery gas ejected from the unit and battery gas was vented from the garage structure at all leakage points. Stratification of the gases was observed.

Figure 84 – Gas release and heat development in ESS unit enclosure at 29:43 (TR + 09:13).

Fifteen minutes and 32 seconds after the first cell thermal runaway, 36 minutes and 2 seconds into the test, ignition of the gases within the compartment occurred. Thermal imaging identified the point of ignition near the bottom left corner of Unit 1. A deflagration of the accumulated battery vent gases followed. At this time, it is estimated that 70% of the 48 modules within the unit enclosure had experienced thermal runaway. Pressure rise was sufficient to cause the pre-cut garage door opening to be partially blown out of the garage door. Flames vented from the opening and gas and smoke was ejected across a 60-70 ft span of the laboratory as pictured in Figure 85.

Figure 85 – Deflagration and resultant smoke plume from the garage at 36:26 (TR + 15:56).

The deflagration of the accumulated battery gases resulted in the immediate ignition and sustained burning of the garage contents. Within 10 seconds of the deflagration all remaining batteries in the initiating unit experienced thermal runaway. Approximately 3 minutes after the deflagration, battery modules within the center ESS unit on the side nearest the initiating unit began to undergo thermal runaway.

The fire was allowed to burn until reaching a steady under-ventilated condition. This behavior was coupled with an increase in smoke production observed from the partially dislodged vent and garage door perimeter. Thermal runaway propagation continued in the center ESS unit (“Unit 2”). When it appeared likely that the batteries had reached a peak amount of thermal runaway propagation, fire department intervention was simulated with ventilation of the pre-cut opening.

Ignition of commodity boxes adjacent to initiating ESS unit (View of C-D corner)	Continued gas release and flaming of ESS contents (View of D-side wall)
	
36:30 (TR + 16:00)	37:12 (TR + 16:42)
Exterior smoke plume intensifies	Operation of second gerb ignition source
	
42:00 (TR + 21:30)	48:33 (TR + 28:03)

Figure 86 – Test events between 36 and 49 minutes of test time in Test 2.

The gerb did not cause immediate ignition of the vented smoke and gas plume. The increased ventilation from the opening, however, did result in fire growth and flaming out of the vent less than one minute after ventilation, as shown in Figure 86 and Figure 87. After approximately one minute of fire growth, the test was terminated by remotely opening the B-side and C-side doors, and initiating remote suppression.

Flaming out of the garage door	Suppression and test termination
	
49:19 (TR + 28:49)	50:21 (TR + 29:51)

Figure 87 – Fire growth and test termination in Test 2 (post 49 minutes).

5.2.2 Thermal Runaway Propagation

Test 2 was initiated by heating one cell (“Unit1Init2_Cell1”) at 6°C/min for 20 minutes and 30 seconds, at which time thermal runaway occurred. Surface temperature on the cell measured 155 °C at the onset of thermal runaway. Heater operation was discontinued at this time. Thermal runaway propagation through the rest of the cells in this module (“Unit1Init2”) occurred 3 minutes and 27 seconds later, as shown in Figure 88.

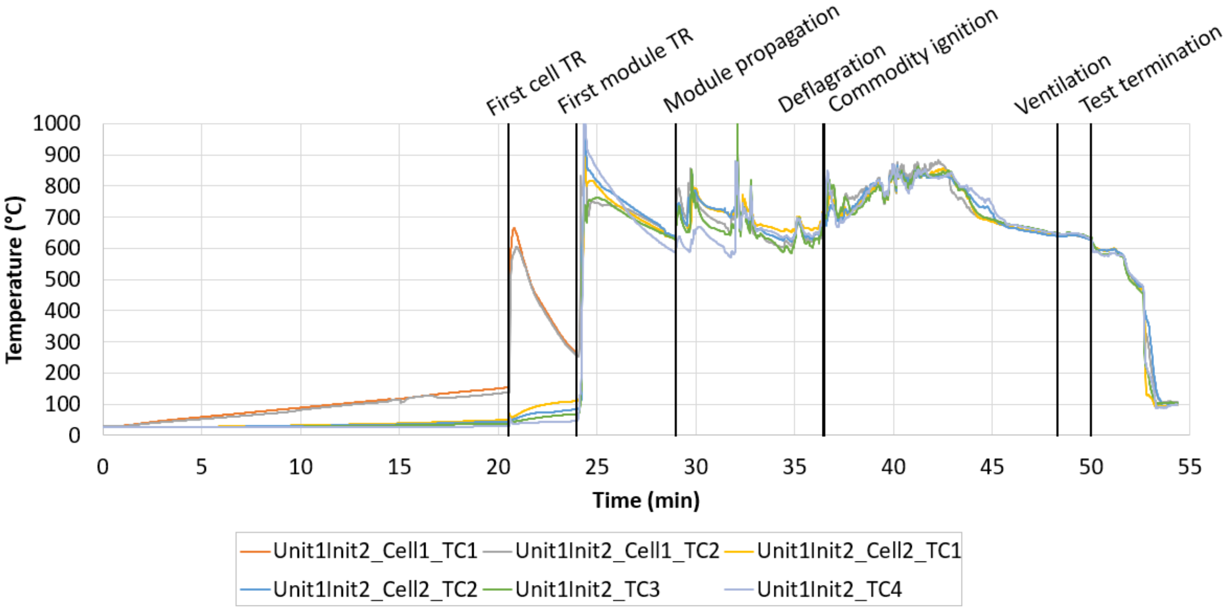

Figure 88 – Temperature measurements in the initiating battery module (“Unit1Init2”)

The battery module beneath the initiating module (“Unit1Init1”) experienced thermal runaway 5 minutes and 37 seconds after propagation through the initiating module. Two and a half minutes later, thermal runaway was observed in another module (“Unit1Mod11”). Thermal runaway was measured in several more modules of Unit 1, moving steadily upwards in the unit, until the resulting accumulated gases in the garage ignited, causing a deflagration 15 minutes and 32 seconds after the first cell thermal runaway. Though all modules were not individually instrumented, it is estimated that 70% of the unit had experienced thermal runaway at the time of the deflagration, as shown through the temperature measurements of Figure 89 and visualization in Figure 90. Thermal imaging of the Unit 1 combined with temperature data suggest that complete propagation was observed in Module 1 through 21, with propagation through 50% of the modules between Module 22 and 48. Thermal images of Unit 1 leading up to the deflagration are included in Figure 91.

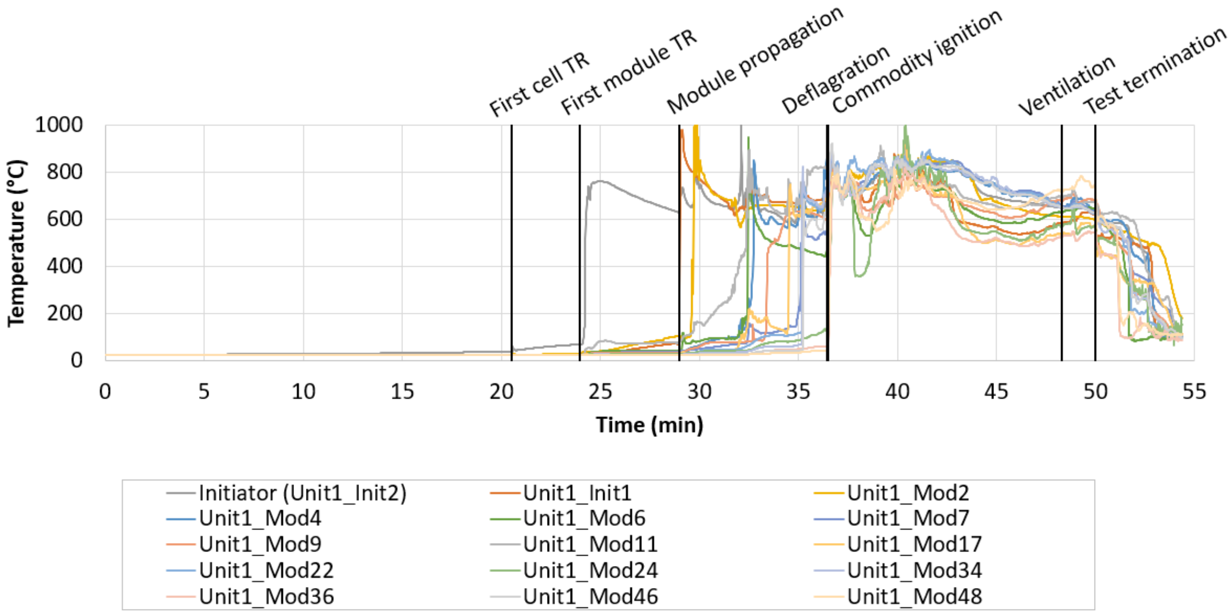

Figure 89 – Temperature measurements within the initiating unit (Unit 1) of Test 2.

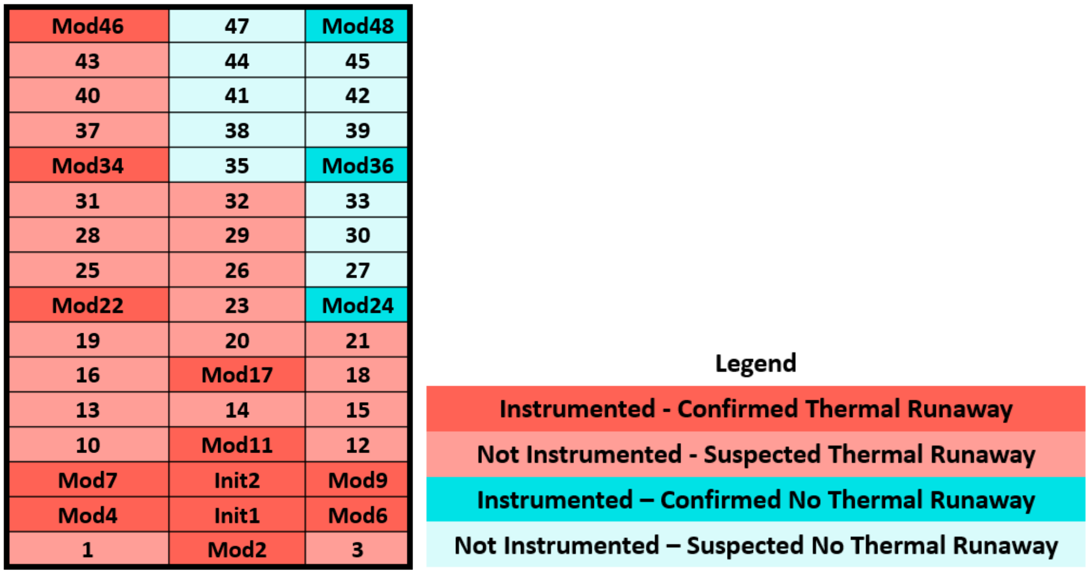

Mod46	47	Mod48
43	44	45
40	41	42
37	38	39
Mod34	35	Mod36
31	32	33
28	29	30
25	26	27
Mod22	23	Mod24
19	20	21
16	Mod17	18
13	14	15
10	Mod11	12
Mod7	Init2	Mod9
Mod4	Init1	Mod6
1	Mod2	3

Legend

Instrumented - Confirmed Thermal Runaway

Not Instrumented - Suspected Thermal Runaway

Instrumented – Confirmed No Thermal Runaway

Not Instrumented – Suspected No Thermal Runaway

Figure 90 – Status of Unit 1 modules at the time of deflagration (36:26, TR + 15:56)

28:59 (TR + 08:29) | 32:30 (TR + 12:00) | 36:25 (TR + 15:31)

Figure 91 – Thermal images of thermal runaway propagation through Unit 1 in Test 1

Within 10 seconds of the deflagration, thermal runaway was observed in the remaining three instrumented modules of Unit 1. Temperatures measured on the exterior of the Unit 1 enclosure increased during the period between the first module-to-module propagation and the deflagration, reaching a maximum measured temperature of approximately 350 °C. Following the deflagration and subsequent commodity box ignition, unit enclosure temperatures rose rapidly to as high as 900 °C, as shown in Figure 92.

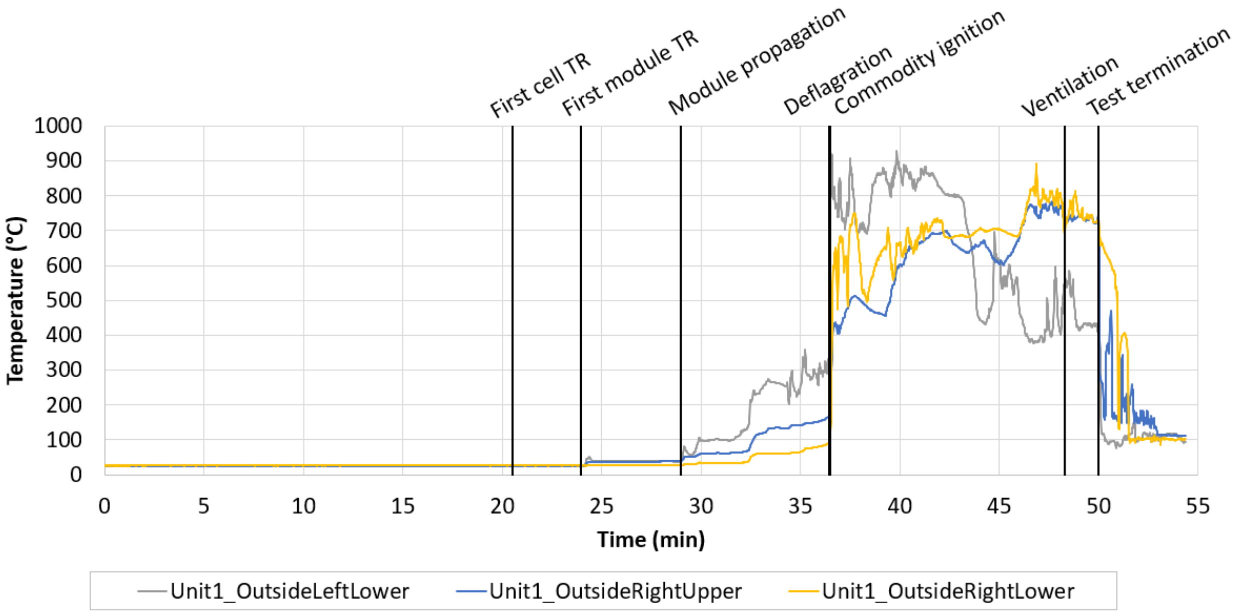

Figure 92 – Unit 1 enclosure exterior temperatures in Test 2.

Exterior enclosure temperatures measured on the center unit, Unit 2, did not increase above 50 °C prior to the deflagration and subsequent commodity box ignition, as pictured in Figure 93. Following the deflagration, upper exterior enclosure temperatures on Unit 2 climbed rapidly to approximately 400 °C. Another sharp increase is observed around 40 minutes which aligns with module temperatures indicative of thermal runaway within Unit 2, as shown in Figure 94. Interior module temperatures of Unit 2 shown in Figure 94 also indicate a high amount of thermal activity directly following the deflagration. Thermal runaway propagation in Unit 2 is identified by temperature and could not be verified by thermal imaging due to high smoke obscuration in the test structure.

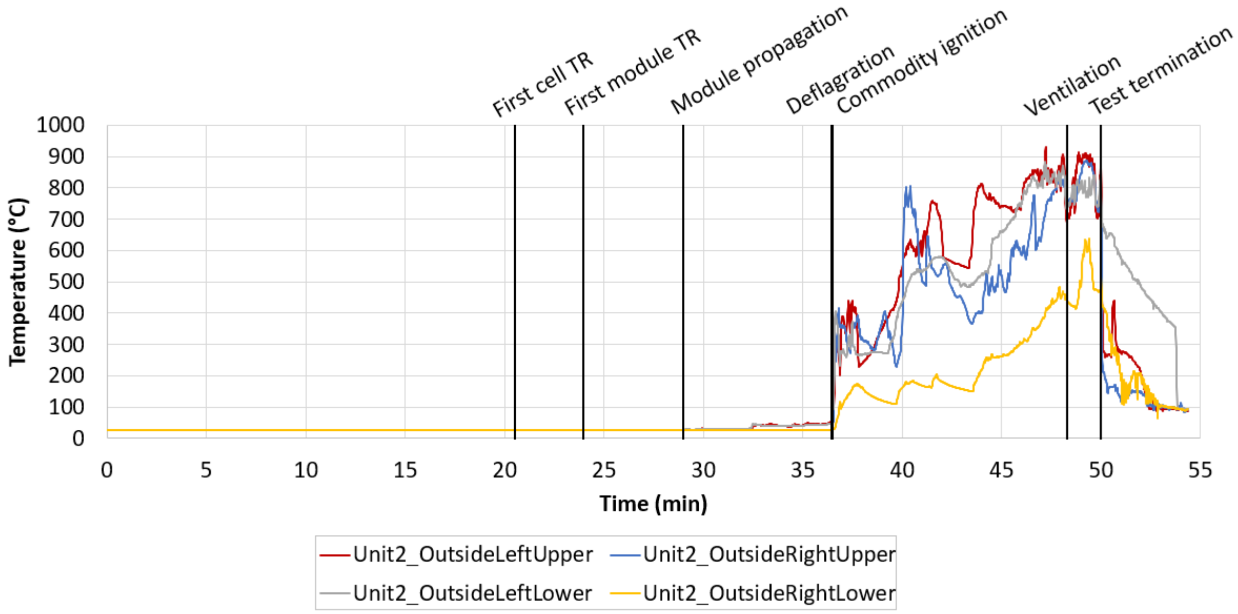

Figure 93 – Unit 2 enclosure exterior temperatures in Test 2.

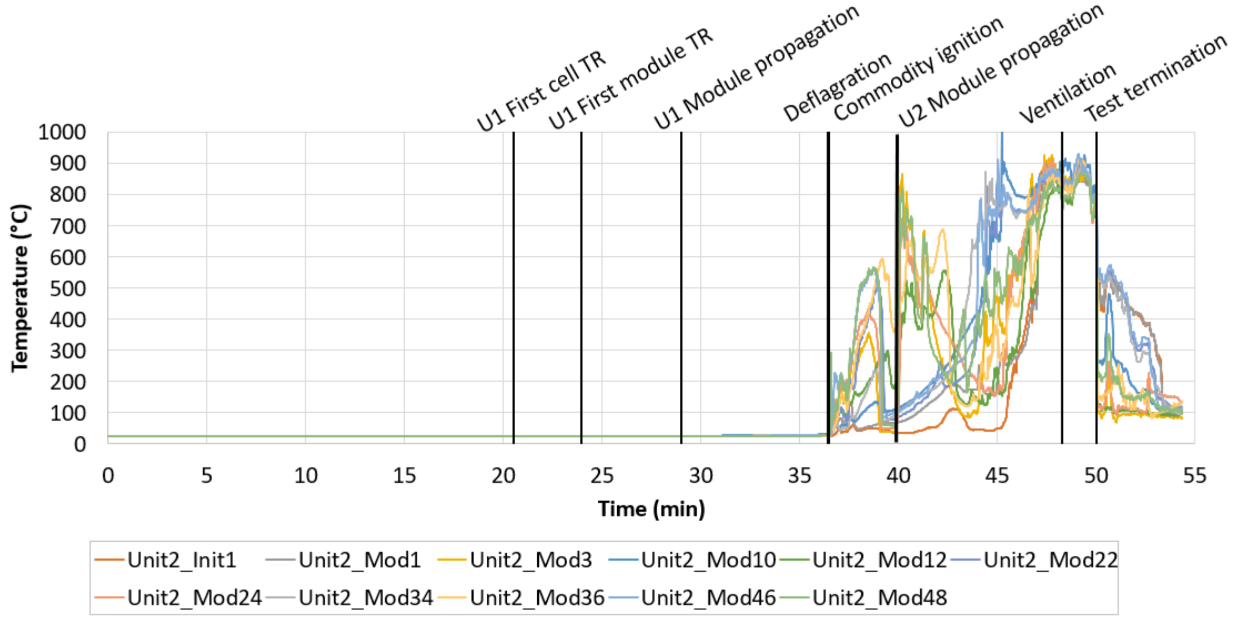

Figure 94 – Temperature measurements within the center unit (Unit 2) of Test 2.

Exterior enclosure temperatures on the rightmost unit, Unit 3, did not show any temperature increase above ambient until the deflagration and subsequent commodity box ignition. For the period between the commodity ignition and test termination, temperatures measured on the outside of Unit 3 increased steadily to 500 °C, as plotted in Figure 95. Temperatures measured on the modules within Unit 3 increased in similarly steady fashion to a maximum of approximately 300 °C with no definitive confirmation of thermal runaway of any cells within the unit, as shown in Figure 96.

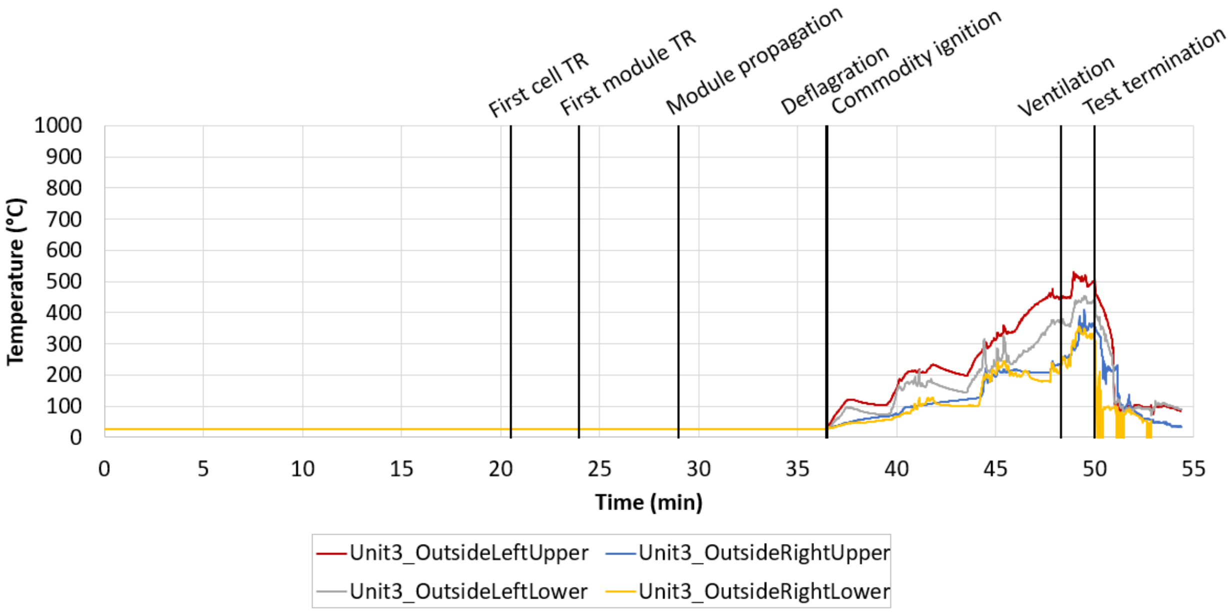

Figure 95 – Unit 3 enclosure exterior temperatures in Test 2.

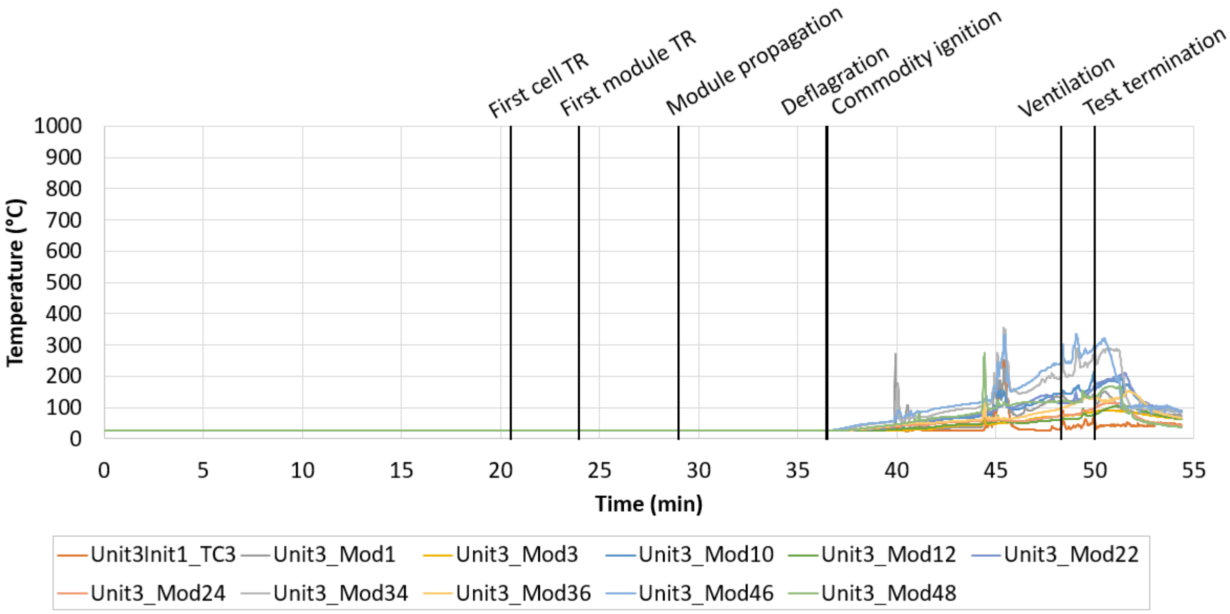

Figure 96 – Temperature measurements within the rightmost unit (Unit 3) of Test 2.

Timing of thermal runaway for all instrumented modules is summarized in Table 7.

Table 7 – Thermal runaway propagation summary for Test 2.

Location	Test Time [MM:SS]	Time Since First Cell TR
Unit1_Init2_Cell1 (First cell)	20:30	00:00
Unit1_Init2 (Full module)	23:57	03:27
Unit1_Init1	28:59	08:29
Unit1_Mod2	29:34	09:04
Unit1_Mod11	32:18	11:48
Unit1_Mod6	32:25	11:55
Unit1_Mod4	32:34	12:04
Unit1_Mod9	33:17	12:47
Unit1_Mod17	34:27	13:57
Unit1_Mod7	34:53	14:23
Unit1_Mod34	35:11	14:41
Unit1_Mod22	35:12	14:42
Unit1_Mod46	35:15	14:45
Deflagration	**36:26**	**15:56**
Unit1_Mod48	36:28	15:58
Unit1_Mod24	36:30	16:00
Commodity box ignition	**36:30**	**16:00**
Unit1_Mod36	36:31	16:01
Unit2_Mod34	39:18	18:48
Unit2_Mod24, Unit 2_Mod48	39:51	19:21
Unit2_Mod3	39:54	19:24
Unit2_Mod46	43:50	23:20
Unit2_Mod10	44:13	23:43
Unit2_Mod22	44:25	23:55
Unit2_Init1	45:08	24:38
Unit2_Mod36	46:05	25:35
Unit2_Mod1, Unit2_Init2	47:00	26:30
Pre-cut Ventilation	**48:17**	**27:47**
Test Termination	**50:00**	**29:30**

5.2.3 Conditions Inside Garage

Gas Temperature

Temperatures measured at the center of the garage did not increase from the first cell and module thermal runaway, as plotted in Figure 97. Following module-to-module propagation at 29 minutes, temperature began to increase to a maximum of 36 °C at the ceiling just prior to the deflagration due to the accumulation of effluent gases from thermal runaway, as pictured in the zoomed-in window of Figure 98.

The deflagration and subsequent fire growth resulted in near instantaneous temperature rise spanning 100 °C at 1 ft off the floor to 700 °C at the ceiling, as shown in Figure 99. Temperatures remained in this range, increasing steadily with increasing burning in the garage. Temperatures increased faster following full operation of the pre-cut opening due to the increased ventilation of the fire. After test termination at 50 minutes, temperatures decreased to ambient as the fire was suppressed.

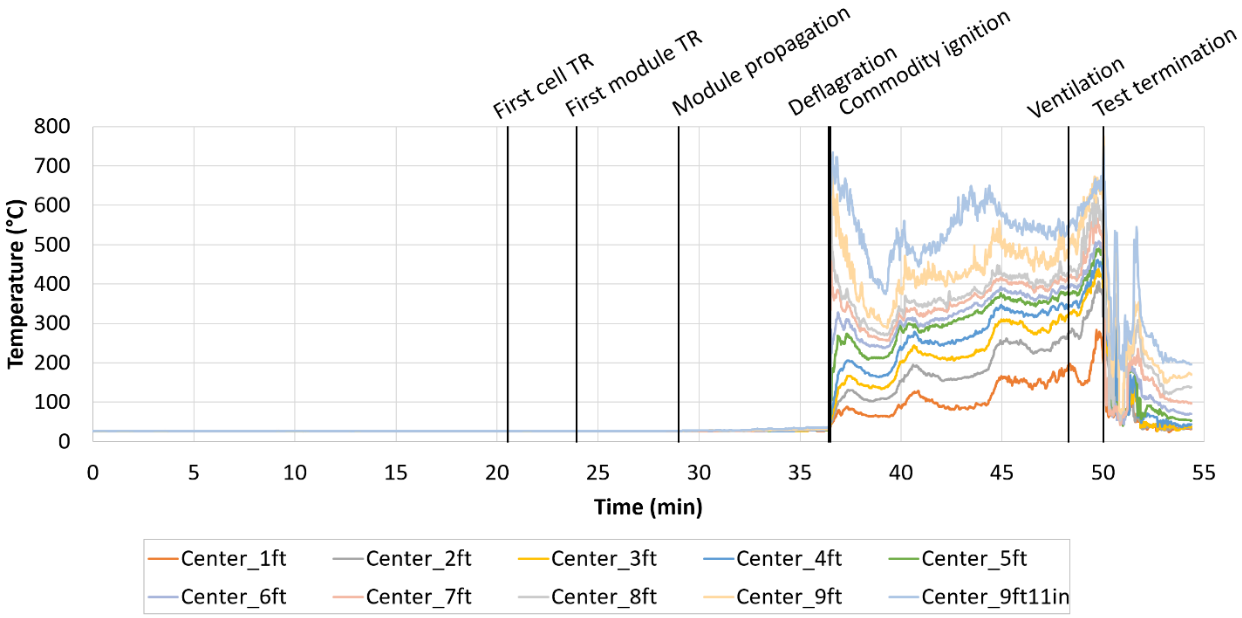

Figure 97 – Temperature inside the garage for Test 2.

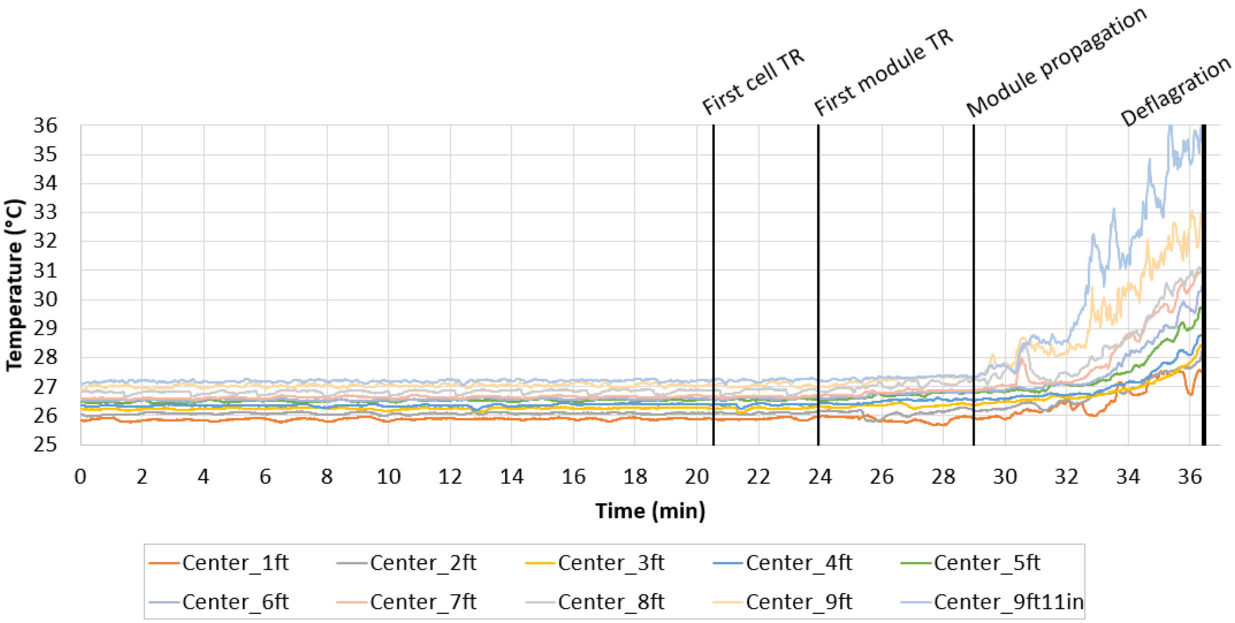

Figure 98 – Temperature inside the garage between 0 and 36 minutes for Test 2.

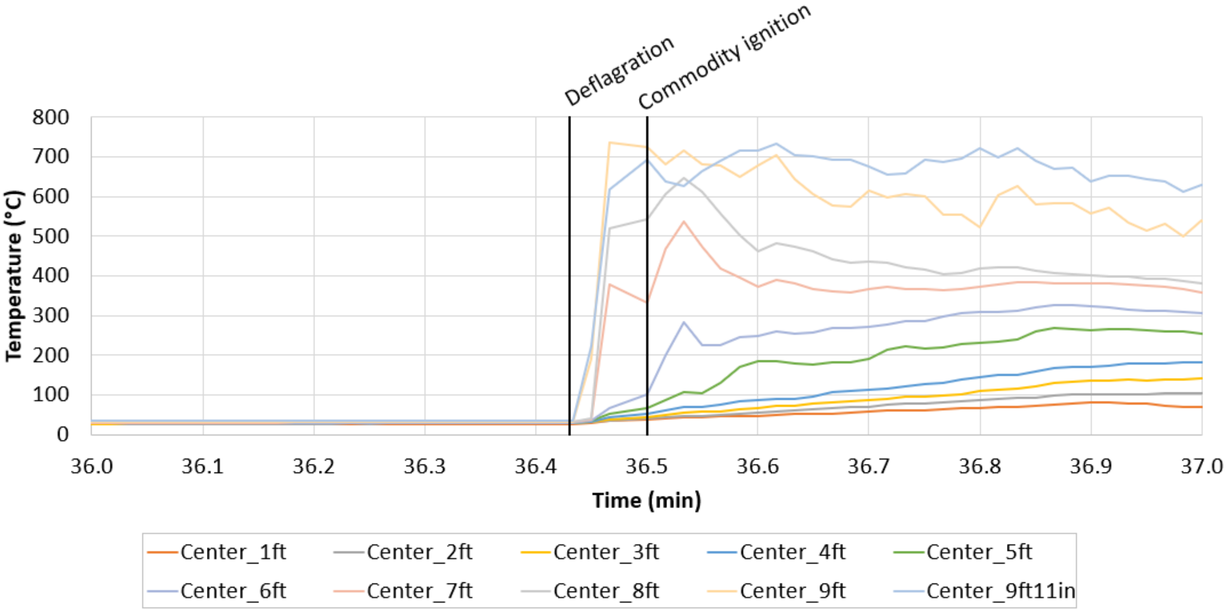

Figure 99 – Temperature inside the garage between 36 and 37 minutes for Test 2.

Gas Concentrations

Oxygen concentration was not significantly reduced from ambient conditions until the deflagration. During the period between the beginning of module-to-module propagation to the deflagration, O_2 concentration was reduced by approximately 0.2 v% as it was displaced by the accumulation of battery vent gases including CO, CO_2, and THC, as shown in Figure 64.

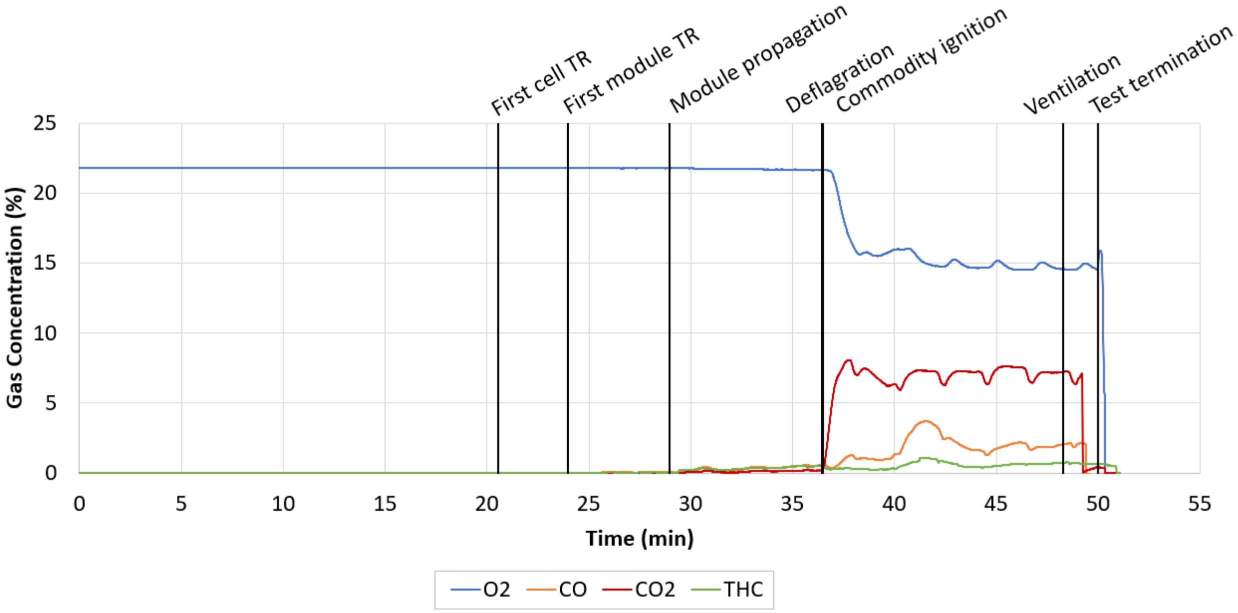

Figure 100 – Interior upper layer gas measurements for Test 2.

Battery vent gases were first measured following thermal runaway propagation through the first module (thirty 18650 component cells). Carbon dioxide measured 0.03 v%, CO measured 0.09 v%, and THC measured 0.05 v%. Following the beginning of module-to-module propagation and before the deflagration, the battery thermal runaway gases increased in concentration to 0.2 v%, 0.6 v%, and 0.6 v% for CO_2, CO, and THC, respectively.

After the deflagration occurred, combustion increased inside the garage, marked by a sharp increase in carbon dioxide to approximately 8 v% and a sharp decrease in oxygen to approximately 15 v%. As the fire became ventilation-limited four minutes later, CO_2 and O_2 remained steady while CO and THC increased to maximum values of 3.7 v% and 1.0 v%, respectively. This timing also lines up with thermal runaway propagation beginning in Unit 2, which would further contribute to the accumulation of these gases.

During ventilation operations, O_2 began to return to the compartment and accumulated gases were reduced. Gas measurements were discontinued as suppression and test termination began.

Explosion Hazards

A deflagration occurred 15 minutes and 56 seconds after the first cell thermal runaway, 36 minutes and 26 seconds after the test began. It is estimated that 70% of the battery modules (1020 individual 18650s) had undergone thermal runaway prior to that moment. Gases sampled from the ceiling measured 0.2 v%, 0.6 v%, and 0.6 v% for CO_2, CO, and THC, respectively, just prior to the deflagration.

Infrared thermal imaging shows the ignition location at the face of the commodity box closest to the bottom left side of Unit 1, as shown in the sequence in Figure 101. At this location, hot gases generated from the ESS impinge directly onto the adjacent cardboard box.

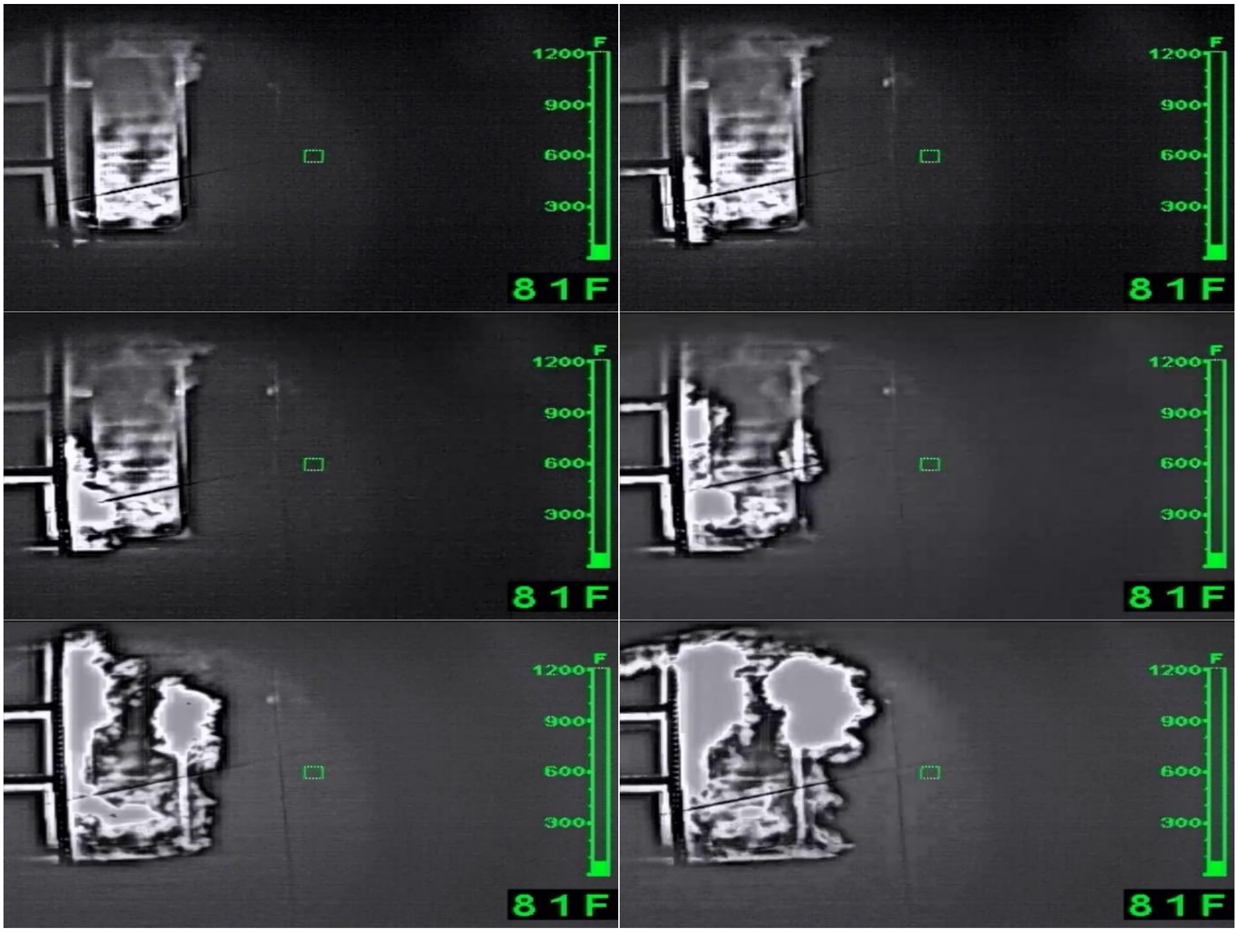

Figure 101 – Thermal image sequence of ignition and deflagration (36:24 to 36:26).

Pressure generated by the deflagration was sufficient to partially dislodge the pre-cut opening from the garage door and eject a stream of smoke and battery gas across a 60-70 ft span of the laboratory. Flames were observed at the garage door opening as well as from conduit openings through the D-side wall of the structure, as shown in Figure 102. The pressure wave was sufficient to push the ceramic wool insulation protecting some instrumentation in the driveway approximately 5 ft away.

Flaming visible from conduit openings on D-side wall  36:26 (TR + 15:56)	Flaming from ventilation cut in garage door 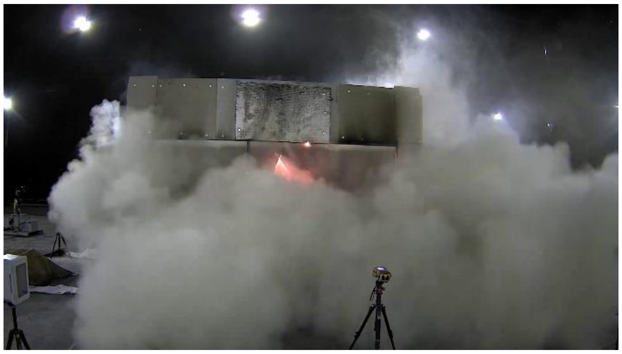 36:27 (TR + 15:57)
Smoke plume pushed 60-70 ft from structure  36:26 (TR + 15:56)	Ceramic fiber insulation thrown from near garage door  36:26 (TR + 15:56)

Figure 102 – Exterior effects of deflagration in Test 2.

5.2.4 Conditions Exterior to Garage

Heat Flux

Heat flux outside the garage door remained at ambient prior to the deflagration. No significant heat flux was measured during the deflagration. The venting pre-cut section of garage door made physical contact with the heat flux gauge stand and knocked it over. Heat flux measurements after the deflagration are not reported because of the movement of the gauge.

Gas Measurements

At the probe outside the garage door, CO_2 and O_2 did not deviate from baseline measurements during initial thermal runaway propagation or immediately following ignition and the resulting deflagration. The CO sensor malfunctioned during Test 2, so CO concentration is not reported. Following fire growth and additional thermal runaways around 39 minutes, O_2 in this location dropped to 15 v% and CO_2 increased to a peak of 4 v%. Concentrations in this location returned to ambient with deviations less than 1 v% as the sampling location was intermittently in and out of the gas plume.

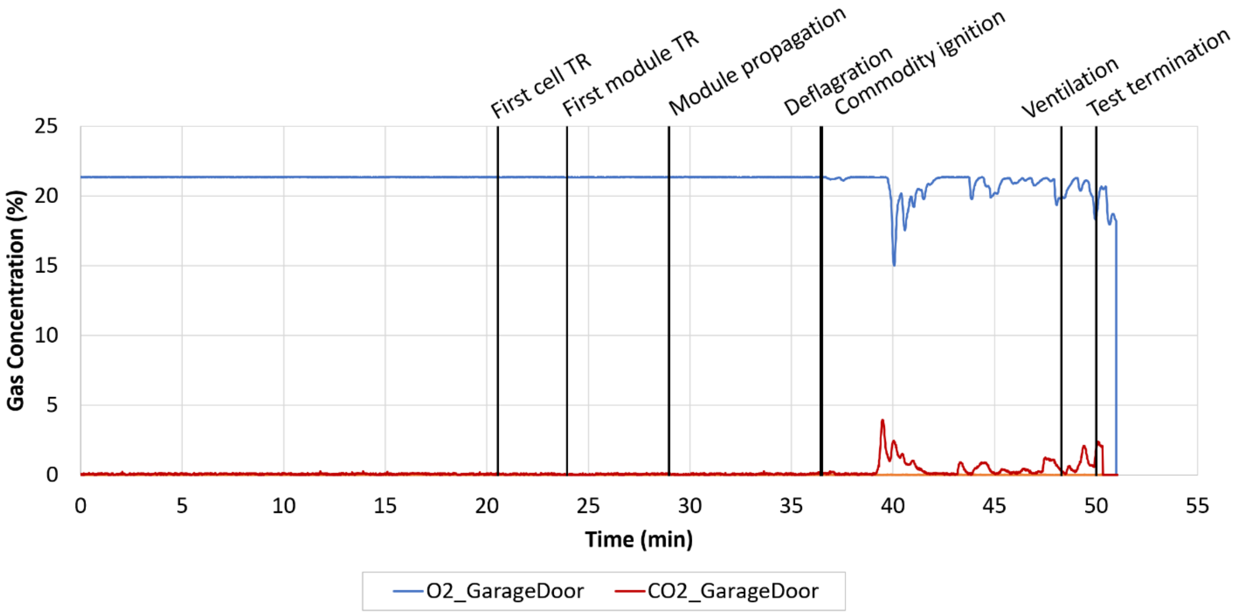

Figure 103 – Exterior gas measurements at the garage door in Test 2.

HF gas was not measured above the low-end calibration limit (0.8 ppm) in Test 2.

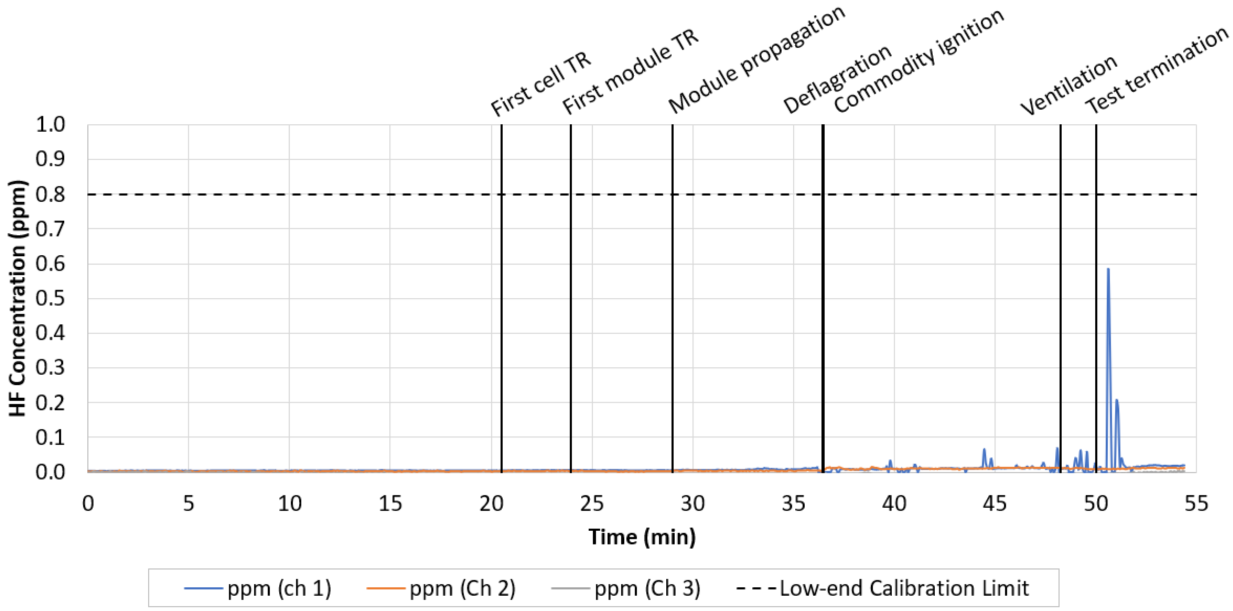

Figure 104 – HF measurements in Test 2.

5.2.5 Size-up Indicators

Visual indicators

Visual indicators from eight moments of interest are included in Figure 106 through Figure 112. Overall, exterior visuals do not conclusively indicate battery involvement or provide warning of an impending deflagration. Visual indicators, however, may be used to identify if a deflagration has occurred, which could indicate the possibility of battery involvement to firefighters.

Figure 105 compares the interior and exterior views of the ESS in a period of active thermal runaway propagation. A cloud of flammable battery gas emanated from Unit 1. Distinctive, low laying vapor clouds provided a clear indication of battery involvement from the interior cameras. Interior IR views show both the low laying cloud and the heat signature of battery thermal runaway in Unit 1. By contrast, exterior visuals do not provide any indication of battery thermal runaway. Smoke and gas are only visible at one location near a penetration used for mounting the ESS, which is unlikely to exist in a typical installation. There is no visual indication of thermal runaway, smoke, or fire near either B-side or C-side access door.

(a) Interior view facing D-wall **(b) IR view through B-wall facing D-wall**

(c) Exterior view from A-D corner **(d) Interior view facing C-wall**

(e) B-side access door **(f) C-side access door**

Figure 105 – Gas accumulation from battery thermal runaway (24:45, TR + 4:45).

Figure 106 captures views around the structure one minute after the images of Figure 105. Interior HD and IR camera views reliably indicate thermal runaway. Smoke and gases are not visible around the perimeter of either B-side or C-side access door. This time aligns with the first exterior view of smoke and gas coming from the edges of the garage door.

(a) IR view through B-wall facing D-wall | (b) Interior view facing C-wall

(c) B-side access door | (d) C-side access door

Figure 106 – Early exterior smoke showing (25:50, TR + 5:20).

Figure 107 is assembled of images taken 5 minutes after Figure 106. Module-to-module thermal runaway propagation continues through Unit 1. At this point, interior camera views are obscured by the accumulation of battery gas inside the garage. IR imaging, by contrast, is able to see through this environment and identify heat signatures from Unit 1 which indicate ongoing thermal runaway behavior. At this point in the process of thermal runaway propagation, battery gas is visible consistently outside the garage. Unlike the low-laying vapor clouds of the interior in Figure 105 and Figure 106, battery gas outside the garage is dispersed and mildly buoyant. No gases were visible around the perimeter of the B-side or C-side access door.

(a) Interior view facing D-wall | **(b) IR view through B-wall facing D-wall**

(c) Exterior view from A-D corner

(d) B-side access door | **(e) C-side access door**

Figure 107 – Exterior view during propagating thermal runaway (30:50, TR + 10:20).

Figure 108 shows four views immediately prior to the deflagration. Interior IR views indicate active thermal runaway but do not provide an indication of the flammability of the environment or likelihood of the deflagration. Exterior images show significant gas leakage from around the garage door and roof of the structure. The buoyancy driven gases emit around all seams and kerfs of the garage door. The gases, which are battery thermal runaway effluent, appear light gray to white and are not distinct from ventilation-limited fire smoke. Traces of battery gas are visible around the seams of the C-side access door. No evidence of smoke is visible around the perimeter of the B-side access door.

(a) Exterior view from A-D corner **(b) IR view through B-wall facing D-wall**

(c) B-side access door **(d) C-side access door**

Figure 108 – Visual conditions immediately prior to deflagration (36:26, TR + 15:56).

Figure 109 shows the environment of the garage 10 seconds after the deflagration. Interior IR imaging shows active thermal runaway activity with surrounding flaming. Exterior views show a significant cloud of gases, vapors and smoke pushed 60-70 ft across the lab. The quantity and positioning of vapor clouds could indicate to a firefighter that a deflagration has recently occurred, and that the situation requires added precautions. Even though the garage door damage was limited, the surrounding environment indicates the occurrence of a deflagration event. Additionally, flaming is visible in penetrations on the D-side wall and small amounts of battery gas is visible around the perimeters of both the B-side and C-side access doors.

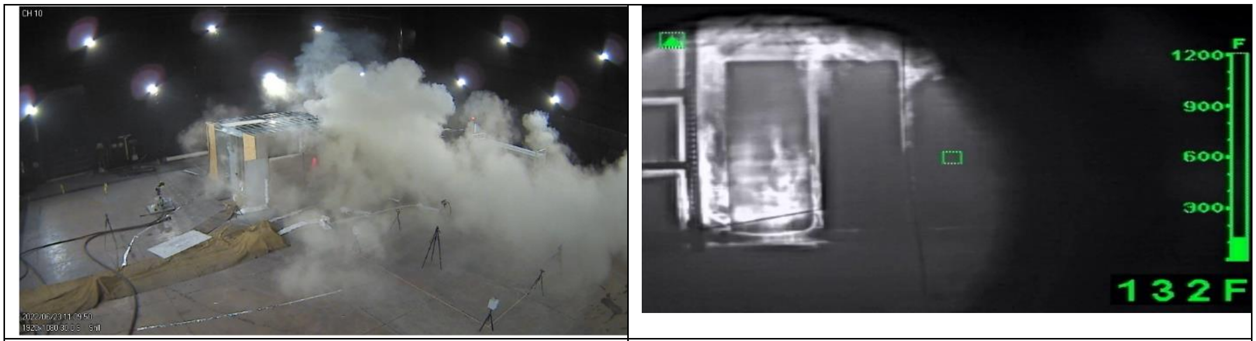

(a) Overhead exterior view | **(b) IR view through B-wall facing D-wall**

(c) B-side access door | **(d) C-side access door**

Figure 109 – Conditions 10 seconds after deflagration (36:36, TR + 16:06).

Figure 110 shows the environment one minute after the deflagration occurred. Interior IR views indicate thermal runaway activity in Unit 1 with flaming combustion of the surrounding commodity boxes. At this point, the battery gas originally pushed from the garage is starting to dissipate. The smoke emanating from the gaps in and around the garage door is at elevated temperature because of the interior fire environment. The smoke is buoyancy driven, light gray in color, and does not provide clear indication of battery involvement. Small amounts of smoke are visible at the upper seams of the B-side and C-side access doors. A smoke plume is starting to emerge from the garage door ventilation opening.

(a) Overhead exterior view | **(b) IR view through B-wall facing D-wall**

(c) B-side access door | **(d) C-side access door**

Figure 110 – Conditions 1 minute after deflagration (37:26, TR + 16:56).

Figure 111 shows the environment around the garage five minutes after the deflagration occurred. At this point, all interior camera views, including IR, are obscured by smoke and provide no differentiation between objects or temperatures throughout the interior. Exterior visuals indicate fire growth inside the garage. The light gray smoke shown in Figure 110 has darkened with the addition of soot from the growing fire. The smoke is driven upwards by the buoyancy of the plume and does not provide a visual suggestion of battery involvement. The exterior smoke from the deflagration is no longer visible. Traces of smoke are visible at the upper edge of the B-side and C-side access doors, which could provide evidence of fire in the garage to an attached structure. The quantity of smoke from the access doors does not provide a reliable indicator of fire size or ventilation conditions.

(a) Overhead exterior view **(b) Interior view facing D-wall**

(c) B-side access door **(d) C-side access door**

Figure 111 – Conditions 5 minutes after deflagration (41:26, TR + 20:56).

Figure 112 shows exterior conditions 3 minutes after the conditions of Figure 111, during a time when thermal runaway propagation was suspected based on temperature measurements inside Unit 2. Visual assessment does not provide an indication of thermal runaway propagation. The buoyancy-driven smoke plume emitted from the gaps in and around the garage door is not visually distinct from the images of Figure 111. Smoke was observed from the upper edge of the B-side and C-side access doors. This smoke does not provide an indication of battery involvement. Interior IR views remain obscured and do not confirm thermal runaway propagation.

(a) Exterior view facing garage door	(b) IR view through B-wall facing D-wall

(c) B-side access door	(d) C-side access door

Figure 112 – View during suspected thermal runaway propagation (44:42, TR + 24:12).

Portable Gas Meters

Figure 113 through Figure 118 provide gas measurement data from the meters for Test 2. Carbon monoxide measurements from the four meters, given in Figure 113, indicated that for approximately 4 minutes prior to the deflagration, up to 200 ppm of CO was measured near the garage door due to leakage of thermal runaway gases from the garage. Prior to the deflagration, CO was measured at the garage door (200 ppm) and C-side access door (20 ppm); CO was not measured at the other two driveway measurement locations. After the deflagration, CO measurement at the garage door meter – which was knocked to the ground as a result of the deflagration – peaked to saturation at 2000 ppm before returning to a baseline of approximately 50 ppm over 4 minutes. The meters in the driveway at 20 ft and 40 ft were physically undisturbed by the deflagration but measured peaks of 275 and 260 ppm, respectively, as the smoke from the deflagration dispersed into the lab, as shown in test video. The C-side service door meter registered a 20 ppm increase in CO following the deflagration.

At the point of test termination, a fog spray pattern of suppression water into the B-side access door pushed a smoke plume out of the garage door V-cut opening. Test video shows the plume engulfing the garage door meter laying on the ground just outside of the garage door. The metered once again peaked at a saturation measurement of 2000 ppm. The other meters in the driveway did not measure a reaction to test termination. The C-side service door meter registered a 10-20 ppm increase during test termination.

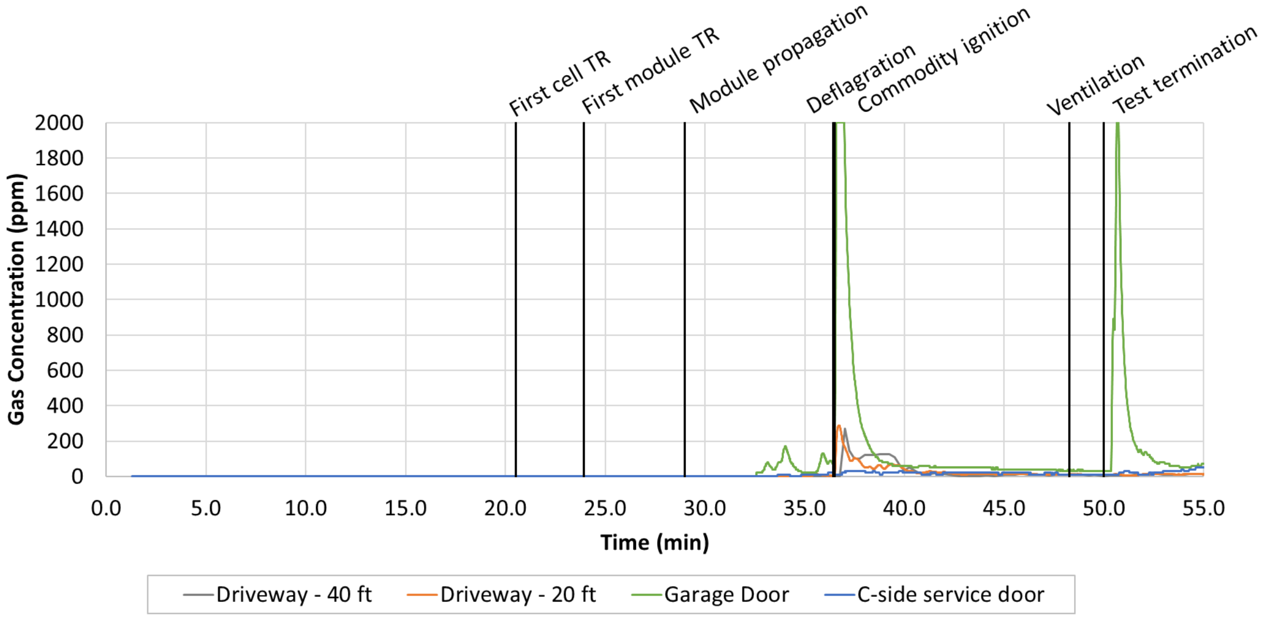

Figure 113 – All portable meter CO measurements in Test 2.

The garage door meter measured peaks of VOCs, LEL and HCN concurrently with the previously discussed peaks of CO, as shown in Figure 114 and Figure 115.LEL did not register above zero prior to the deflagration. Following the deflagration and test termination, the meter registered 870 ppm and 440 ppm of VOCs, respectively. The HCN measurement peaked at 50 ppm during both events. LEL peaked at 26% and 15%, respectively. It is assumed that the measurements made immediately after the deflagration measured the combination of combustion byproducts and non-combusted thermal runaway effluent gases in the ejected smoke. After test termination, the meter measured the products of combustion of the commodity boxes or thermal runaway effluent gases. In the case of HCN, cross sensitivities to CO may have influenced the measurement in both cases, or HCN may have been generated by the burning of the ABS plastic module cases.

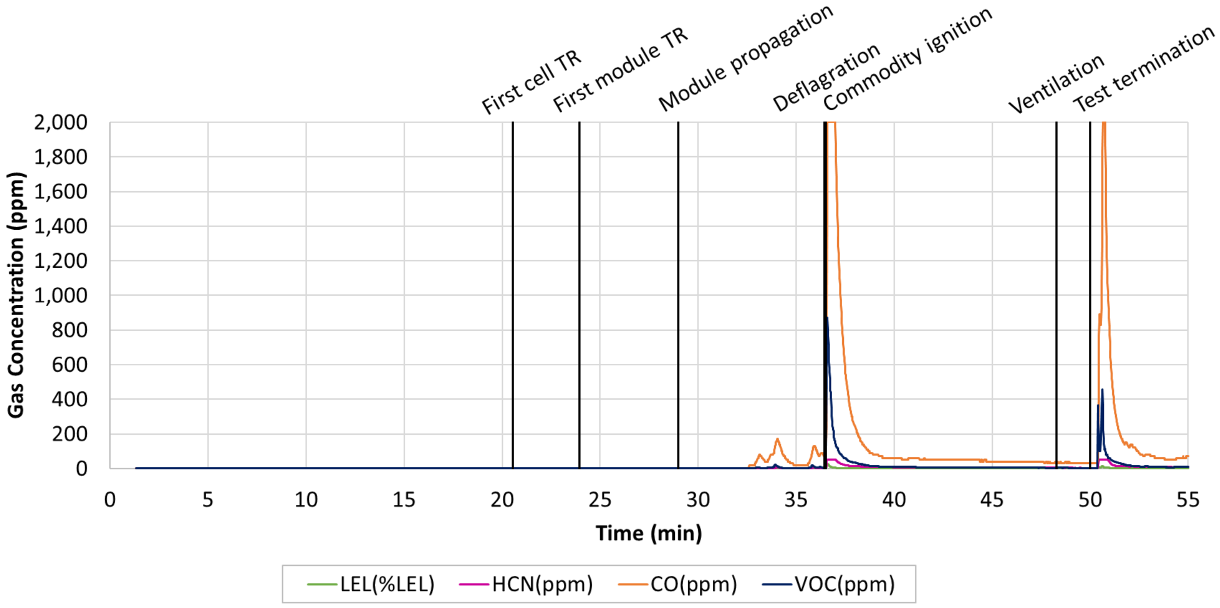

Figure 114 – Portable meter measurements at garage door in Test 2.

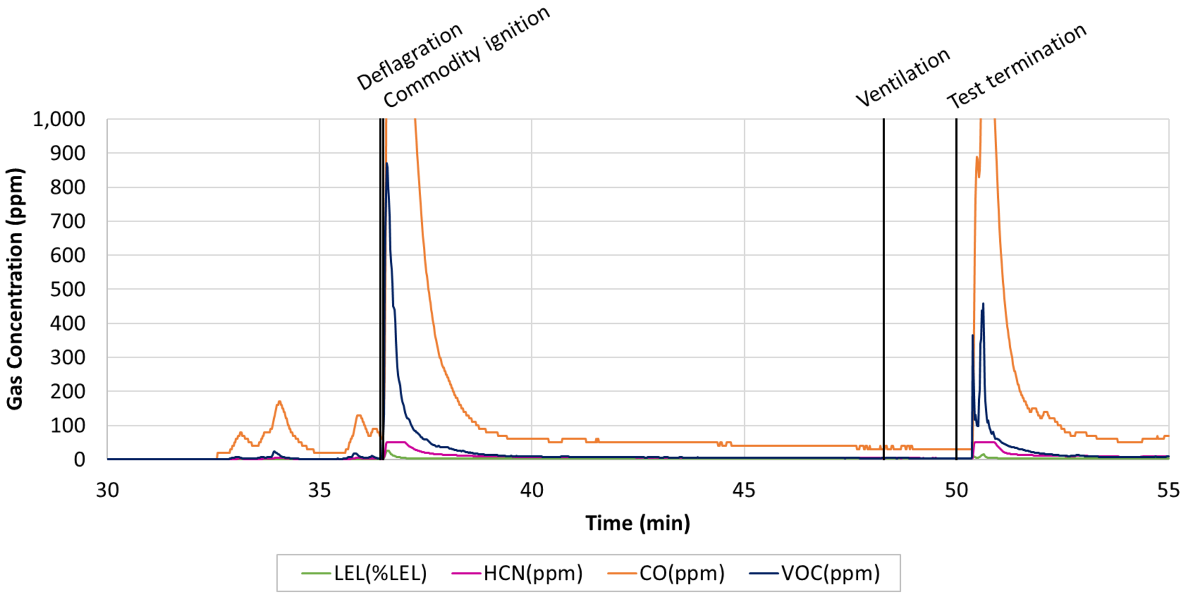

Figure 115 – Portable meter measurements at garage door in Test 2 (zoomed in).

The meter at 20ft down the driveway did not register LEL, H2S or HCN prior to the deflagration, as indicated in Figure 116. Only 17 ppm of CO registered prior to the deflagration. Immediately after the deflagration, the meter registered concurrent spikes of CO and HCN, at peaks of 285 ppm and 20 ppm respectively, due to the plume of combustion products being dispersed down the driveway. Following the simulated fire service intervention and ventilation, levels of CO up to 15 ppm were measured at the meter location for the remainder of the test. LEL and H_2S were never measured above zero in this location for the duration of the test.

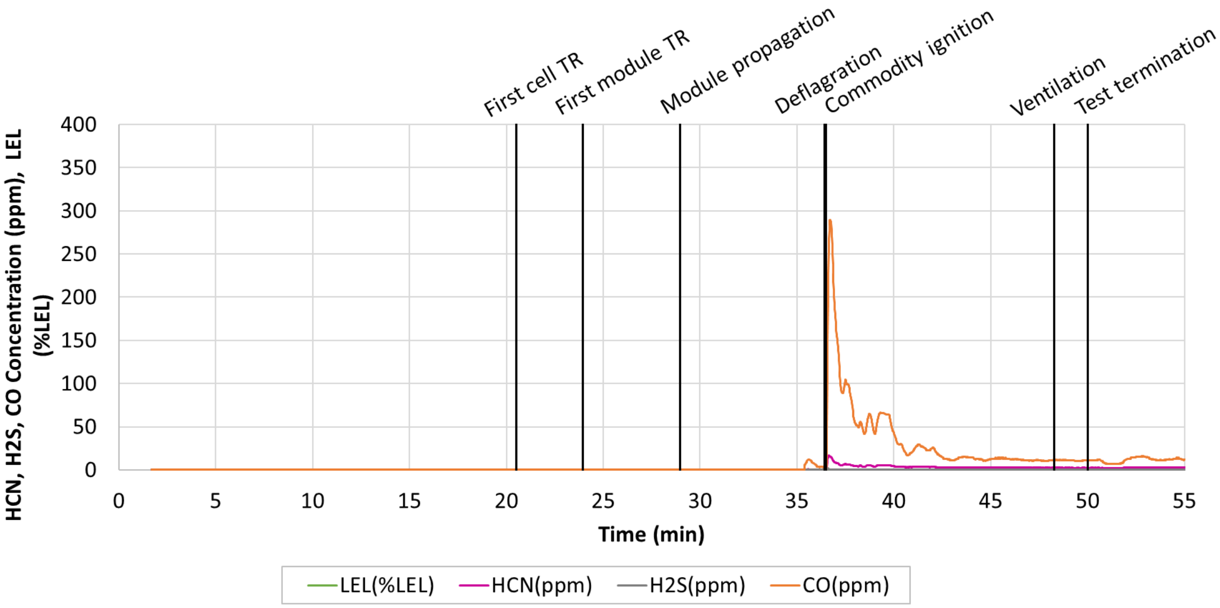

Figure 116 – Portable meter measurements at driveway 20 ft location in Test 2.

The meter at 40 ft down the driveway did not register any gases prior to the deflagration. Following the deflagration, the meter registered a 270 ppm spike of CO due to the plume of combustion products being dispersed down the driveway. This peak is indicated in Figure 117. HCN and H_2S were never measured above zero in this location for Test 2. Following ventilation operations, levels of CO up to 15 ppm were measured at the meter location for the remainder of the test.

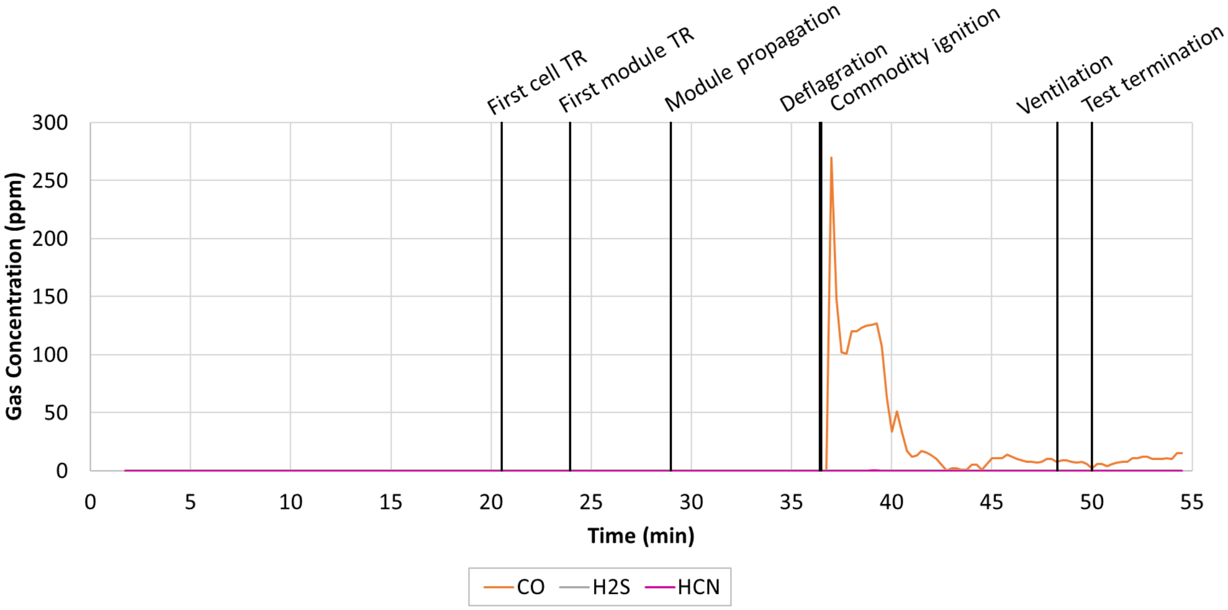

Figure 117 – Portable meter measurements at driveway 40 ft location in Test 2.

The meter by the C-side service door measured small increases in CO and hydrogen below 20 ppm during the period between the beginning of module-to-module thermal runaway propagation and the deflagration (Figure 118). The deflagration caused pressurized gases to leak from the floor, side and ceiling gaps of the C-side door. CO and hydrogen were measured between 10 and 30 ppm during the period between the deflagration and ventilation operations. At the point of test termination, the C-side door was opened and a plume was immediately formed near the meter. The meter was not engulfed in the plume but was near the source of combustion products diffusing into the surrounding air. During the period of test termination, H_2 and CO peaked at 30 ppm and 50 ppm, but it is not clear how these measurements are impacted by cross-sensitivities of the electrochemical sensors.

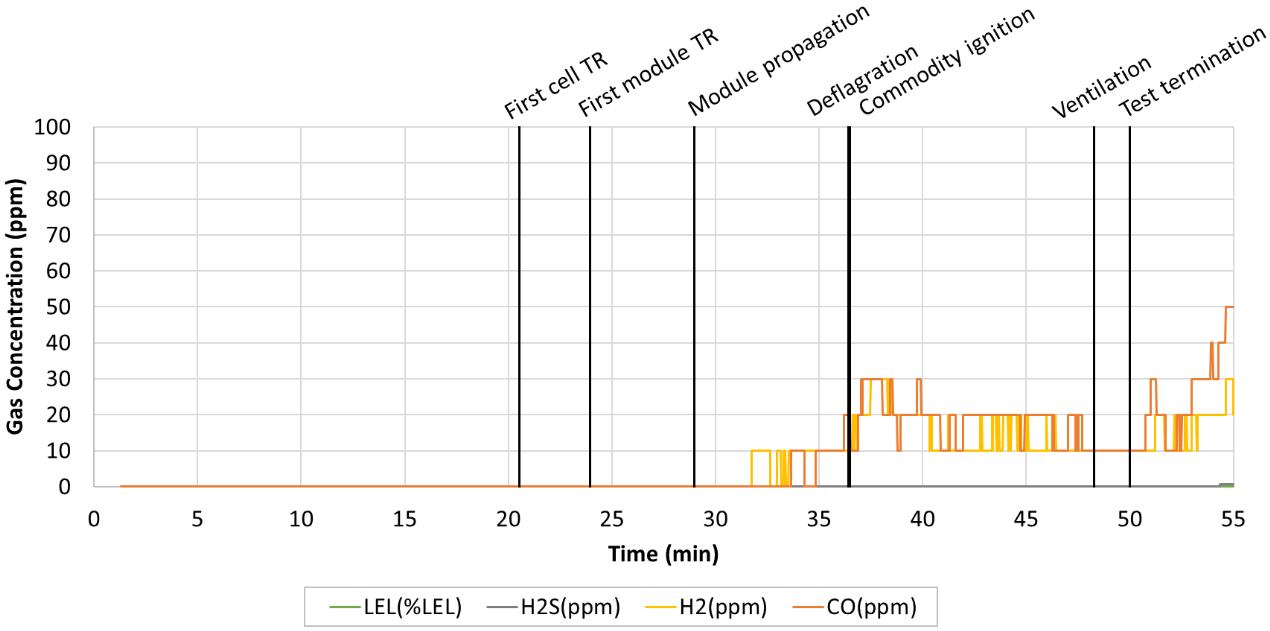

Figure 118 – Portable meter measurements at C-side service door in Test 2.

5.3 Test 3

5.3.1 Timeline

Figure 119 through Figure 122 show a visual sequence of the most significant events that occurred during Test 3. Test 3 was initiated by remotely igniting an ignitor package with an electric match at the center of the bottom edge of the lowest Group A commodity box on the bottom right of the leftmost commodity array. The ignition location is shown in Figure 119.

Figure 119 – Ignition of Group A commodity using an electric match at time 00:01.

As shown in Figure 120, the fire spread vertically through all 4 vertical tiers of stored group A commodity and involved two columns of commodity by 4 minutes and 34 seconds. At this time, the fire had reached its peak heat release rate and vitiation of the flames caused a steady reduction in burning rate.

The exterior surface temperature of the leftmost ESS unit and temperatures of the cells inside were monitored to evaluate whether the cells would enter thermal runaway with the continued proximate but waning thermal exposure. Though the exterior temperature exceeded 200 °C, air gaps between the exterior enclosure, interior plastic enclosures, and the cells prevented the cells from heating beyond 25 °C. At 10 minutes and 18 seconds, a heater installed on a single 18650 cell inside the leftmost ESS was energized and controlled to heat the cell at a rate of 10.8 °F/min (6 °C/min) as a contingency to ensure thermal runaway occurred and the test objective was met. Approximately 9 minutes later, at 19 minutes and 14 seconds, the heated cell entered thermal runaway. The bottom right photo in Figure 120 shows the exterior smoke conditions from the ventilation-limited fire at 19 minutes and 14 seconds.

Underventilation

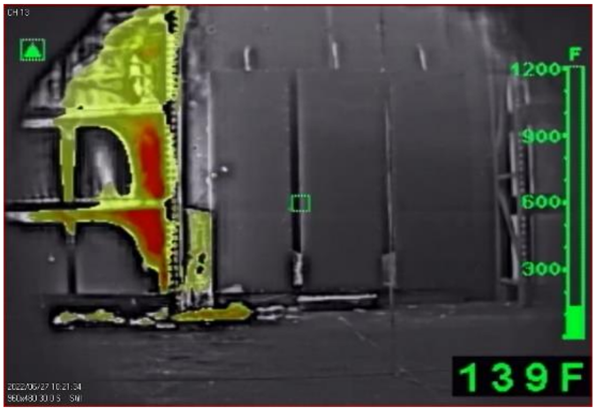

04:34

Heater start

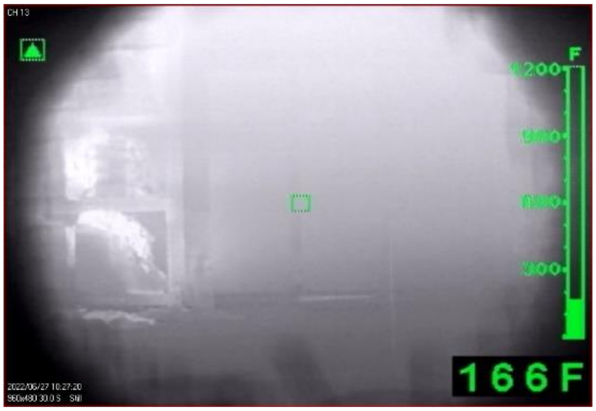

10:18

TR in initiating cell

19:14

Smoke at first TR

19:14

Figure 120 – Sequence of events in Test 3 leading up to 19 minutes of test time.

Eighteen minutes after the first 18650 cell entered thermal runaway, at 37 minutes and 14 seconds, the remaining cells in the initiating module experienced thermal runaway, as shown in the first image of the sequence in Figure 121. The heat added by this first propagation event initiated further thermal runaway events in other modules inside the ESS unit. These events began to occur 4 minutes later, at approximately 41 minutes of test time.

It was determined an appropriate time to simulate fire department vent operation at 51 minutes and 42 seconds based on the number and location of thermal runaways observed through module temperatures, and steadily increasing carbon monoxide and hydrocarbon concentrations which indicated the accumulation of flammable battery gases and the start of underventilation. Simulated vent operation began with igniting the gerb on the right-hand side of the vent kerf. Sparks began ejecting from the gerb within 1-2 seconds from commanded ignition, and the smoke emanating near the top of the kerf ignited within another 1-2 seconds. Ignition of the smoke around the kerf caused ignition of the smoke leaking from top seam of the door, and within 10 seconds, flames traced the perimeter of the door.

Vent opening operations followed the burnout of the second gerb. During vent operations, flaming at the opening increased as the open area of the vent increased. The test was terminated within the next 60 seconds by remotely opening the B-side and C-side doors and initiating suppression remotely, as is shown in Figure 122.

Module-to-module thermal runaway propagation  37:14	First gerb operation  51:42
Ignition of smoke & 2nd gerb  51:51	Vent operation  52:54

Figure 121 – Sequence of events occurring between 19 and 53 minutes of test time.

Figure 122 – Suppression of the test at 53 minutes and 41 seconds.

5.3.2 Thermal Runaway Propagation

As identified in the Test 3 timeline, thermal exposure from the group A commodity fire to the residential ESS enclosure did not cause high enough temperature rise in the battery cells (~180 °C) to cause thermal runaways before the fire became ventilation-limited at 4 minutes and 34 seconds. The peak temperature measured on the surface of the cells inside residential ESS Unit 1 was 106 °C within Module 34 at 10 minutes, as shown in Figure 123.

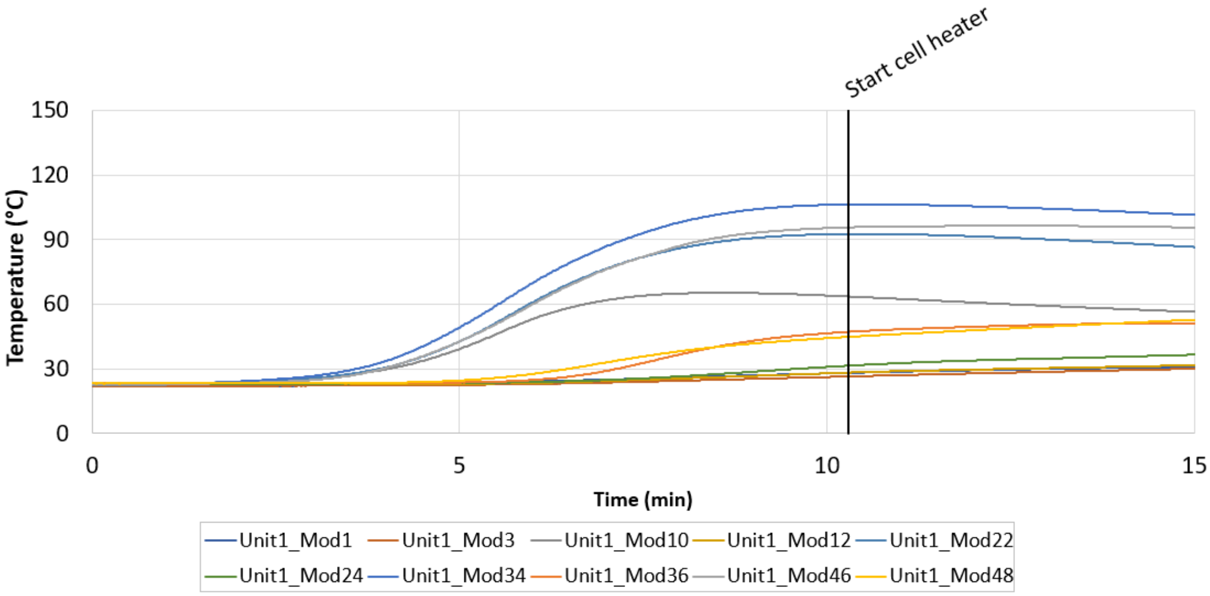

Figure 123 – Surface temperatures of cells inside of residential ESS unit #1.

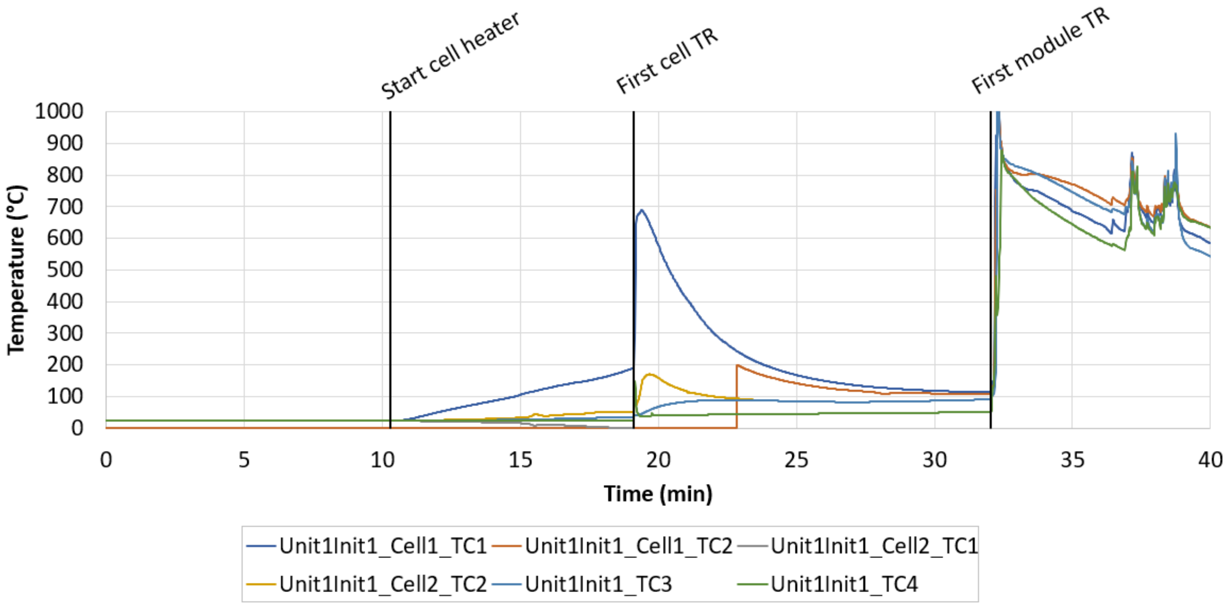

Figure 124 – Surface temperatures of cells inside the initiating module of residential ESS unit #1.

Based on this assessment, it was necessary to energize the flexible film heater installed in the initiating cell of Unit 1 to force thermal runaway in one of the 18650 cells and enable thermal runaway propagation. At 10 minutes and 18 seconds, the heater was energized and controlled to heat the cell at a rate of 10.8 °F/min (6 °C/min), as is shown in Figure 124. Thermal runaway of the heated cell was observed at 19 minutes and 14 seconds.

Thermal runaway propagation to the remaining cells in the initiating module occurred approximately 13 minutes later at 32 minutes and 11 seconds.

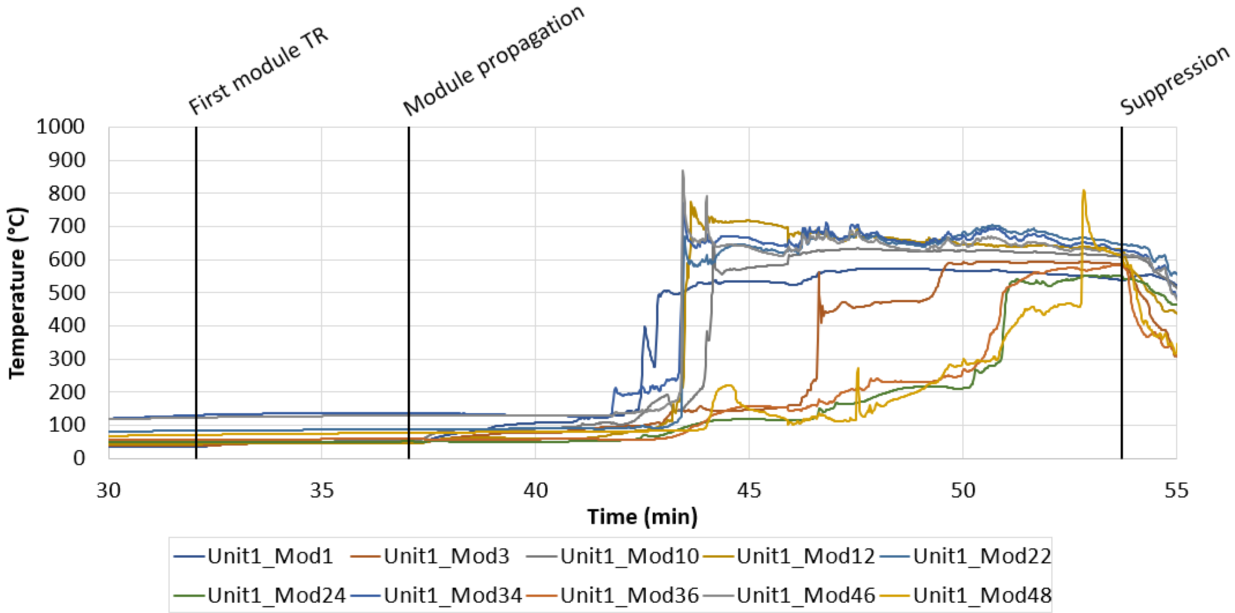

Figure 125 – Surface temperatures of cells contained in residential ESS Unit 1.

Figure 125 documents the surface temperature of the instrumented cells contained inside residential ESS Unit 1 from 15 minutes of test time until the end of the test. The first instance of thermal runaway propagation outside of the initiating module occurred in Module 2, 5 minutes later, at 37 minutes and 4 seconds. Between 42 and 44 minutes of test time, at least 6 modules entered thermal runaway[2]. After 44 minutes of test time, several more thermal runaways occurred prior to the end of the test. The distinct times of observed thermal runaway propagation events are documented in

---

[2] Likely more than 6 modules entered thermal runaway during this period. It is not possible to discern based on the limited thermocouple data and difficulty in distinguishing thermal runaways close in time via the thermal imaging camera view.

Table 8.

Table 8 – Thermal runaway propagation summary for Test 3.

Location	Test Time [MM:SS]	Time Since First Cell TR [MM:SS]
Onset of underventilation	**04:34**	**--**
Unit1_Init1_Cell1 (First cell)	19:07	00:00
Unit1_Init1 (Full module)	32:03	12:56
Unit1_Mod2	37:03	17:56
Unit1_Mod4	40:55	21:48
Unit1_Mod12	42:26	23:19
Unit1_Mod1	42:48	23:41
Unit1_Mod34	43:21	24:14
Unit1_Mod46	43:23	24:16
Unit1_Mod22	43:25	24:18
Unit1_Mod10	43:56	24:18
Unit1_Mod3	46:35	27:28
Unit1_Mod36	50:47	31:40
Unit1_Mod24	50:50	31:43
Gerb 1	**51:42**	**32:35**
Gerb 2	**51:56**	**32:49**
Ventilation start	**52:29**	**33:22**
Unit1_Mod48	52:45	33:38

There were no thermal runaway events in any of the modules located in residential ESS Unit 2 or Unit 3. Figure 126 and Figure 127 show the surface temperatures of cells inside residential ESS Units 2 and 3. Few cells in the units exceeded 100 °C by the end of the test. However, Figure 126 shows that exposure to thermal runaway gas exhausting from Unit 1 and exposure to the temperatures of the hot gas layer were causing an increase in cell temperatures within Unit 2. Cell temperatures at the top of Unit 2 were approximately 130°C by the time of gerb operation and 145 °C at the time of suppression. Peak temperatures in Unit 3 were 91 °C and 106 °C at the same times. Due the rapidly developing compartment fire in the garage post-ventilation, it is likely that thermal runaways would have occurred in Unit 2 followed by Unit 3 shortly after garage door venting had the test not been terminated with suppression operations.

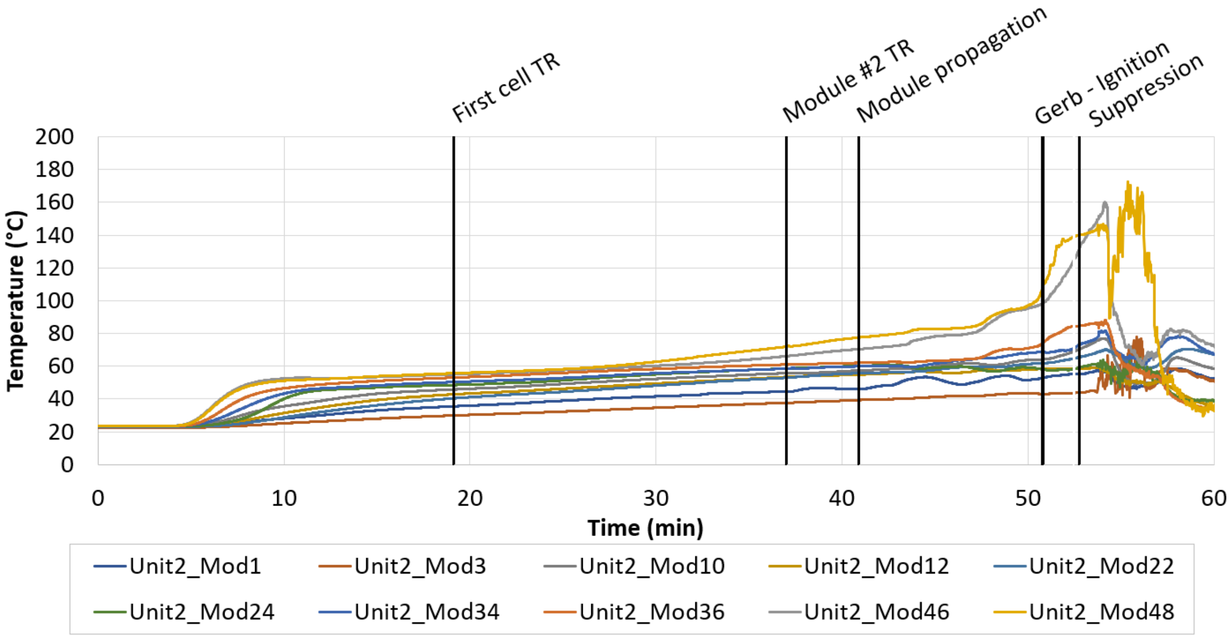

Figure 126 – Surface temperatures of cells in residential ESS Unit #2.

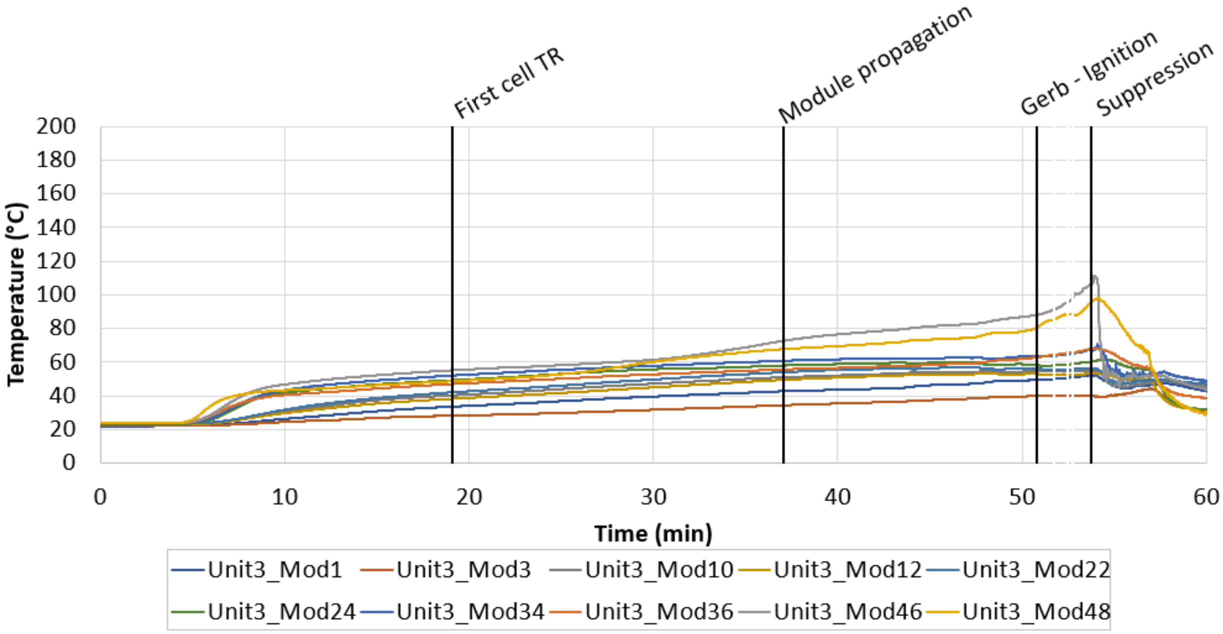

Figure 127 – Surface temperatures of cells in residential ESS Unit #3.

5.3.3 Conditions Inside Garage

Gas Temperature

The ambient gas temperature at the beginning of Test 3 was 24 °C. Gas temperatures begin to increase 1 minute after the electric match was ignited and increased as the fire progressed vertically through the stored Group A commodity. Gas temperatures reached a peak of 310 °C at the ceiling 4 min and 46 seconds after ignition, marking the end of the period of fire growth.

As there was no significant exchange of fire effluent gases with the exterior ambient, the hot gas layer extended to the floor, the flames became vitiated, and the fire entered a decay period immediately after this peak temperature. After approximately 10 minutes of test time, the fire decayed to a quasi-steady and weakly single zone condition governed by the minimal exchange of smoke and ambient air possible through leakage around the two doors and the garage door opening. Under this quasi-steady condition, gas temperatures minimally increased from under 200 °C at 10 minutes to a peak near the ceiling of 240 °C at 43 minutes. This is likely due to wall temperatures increasing, thereby reducing the loss of thermal energy from the interior gases as the ventilation-limited fire continued to burn slowly. After 43 minutes, temperatures decreased as the first ignited Group A commodity boxes burned completely.

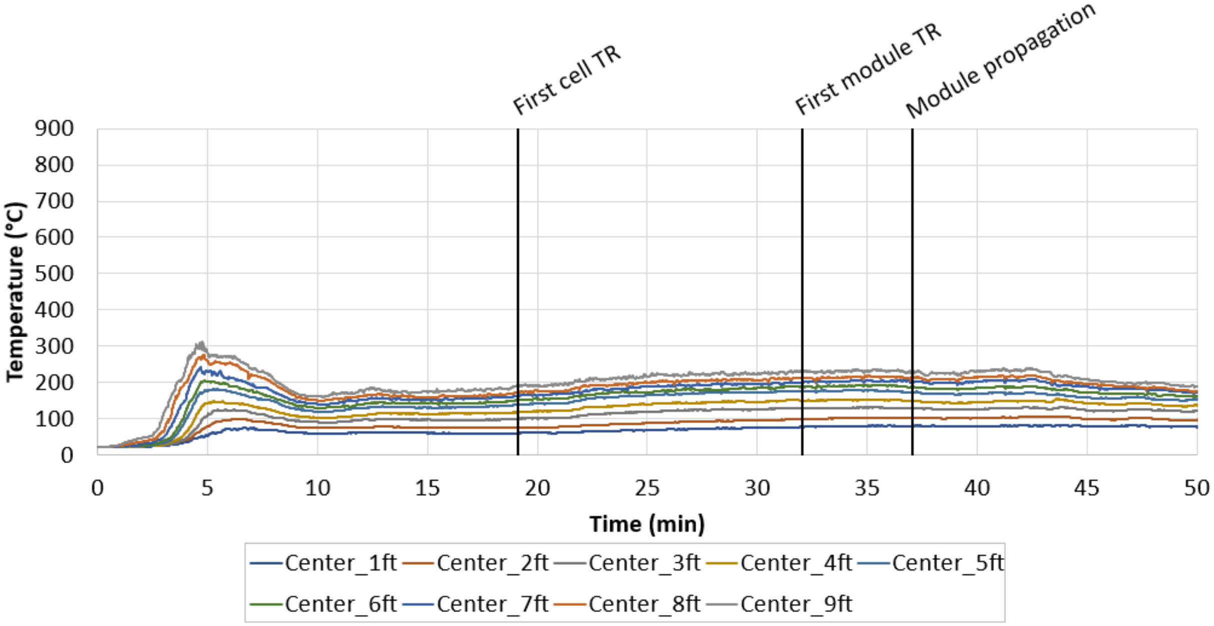

Figure 128 – Gas temperatures measured in the center of the garage during Test 3, from 0 to 50 minutes test time.

At the same time, a significant thermal runaway propagation occurred in Unit 1. The release of heat from the thermal runaway events did not significantly impact gas temperatures since the commodity simultaneously reduced burning.. A visual sequence matching this description is provided in Figure 129.

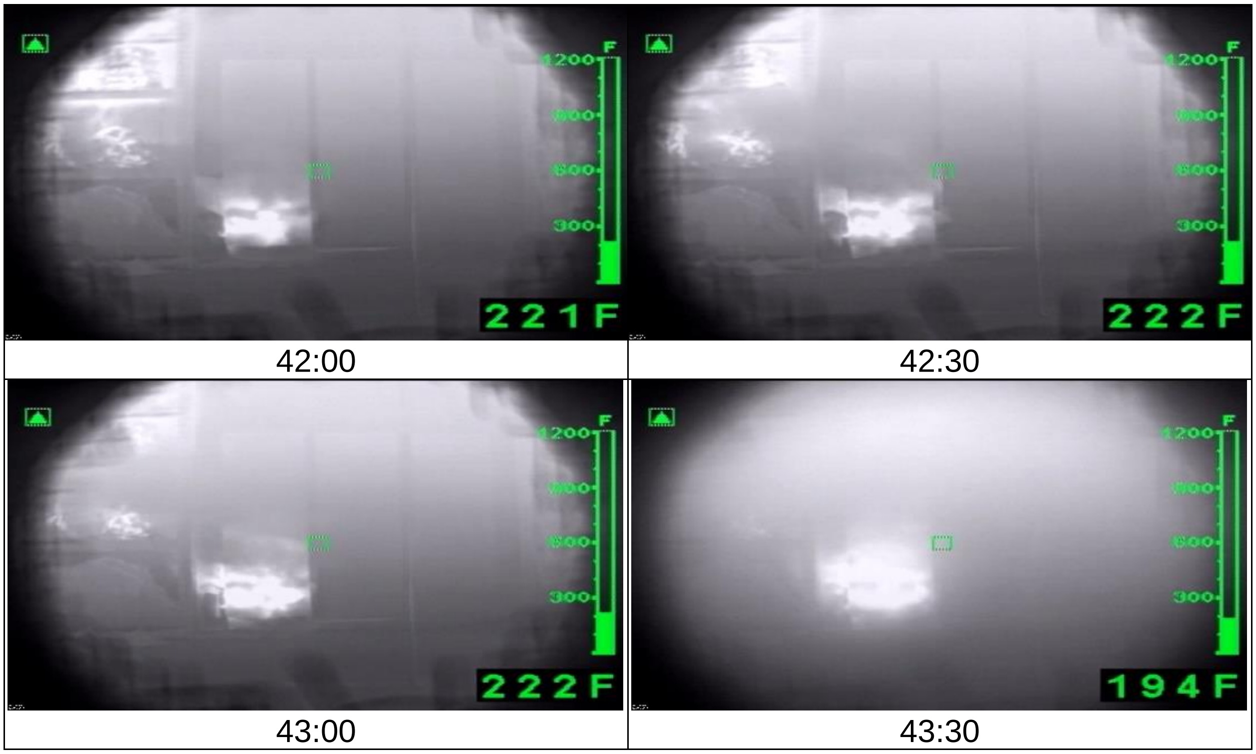

42:00

42:30

43:00

43:30

Figure 129 – 90 second sequence of infrared images showing diminishment of burning in Group A commodity and increase in thermal runaway events.

The period between 50 and 55 minutes of test time is shown in Figure 130, separately from the previous time history, to more clearly display the timing of several thermal runaway propagation events that occurred, as well as the response of the fire to changes in ventilation and suppression. Gas temperatures remained steady, even with several module thermal runaway events, from 50 minutes and until 52 minutes of test time.

Simulated fire department garage door venting operations began at 51 minutes and 42 seconds with ignition of the first gerb. As was shown in Figure 61, sparks from the gerb ignited the smoke emanating from the vent kerfs. This ignition resulted in temporary burning around the top and sides of the garage door opening and sustained burning at the kerfs. Although most of the burning occurred exterior to the structure, temperature measurements in the top 5 ft of the compartment indicate some burning occurred inside, as gas temperatures increased approximately 100 °C before the vent opening began at 52 minutes and 29 seconds.

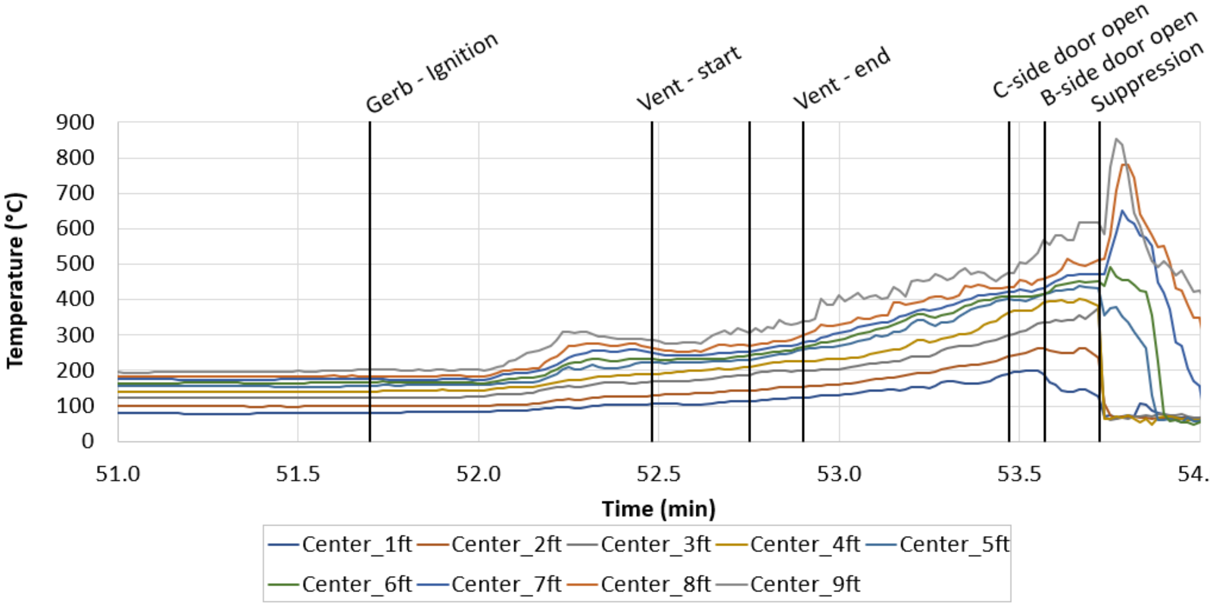

Figure 130 – Gas temperatures measured in the center of the garage during Test 3, from 51 to 54 minutes test time.

The fire at the vent immediately grew with increasing open area as the ventilation procedure progressed over a 30 second period. Temperature measurements in Figure 131 show, and video review confirm, that from the start of the vent opening until 43 seconds later, vent flow is exhausting uni-directionally from the garage beyond a height of 1 ft above the floor. After 53 minutes and 30 seconds, temperatures exhausted from the vent began to reduce because there was less burning immediately at the vent, and more flaming occurred within the garage.

Temperatures at the vent briefly increase again at the time of suppression because of air entrainment from the hose stream into the garage – which fed combustion – and from the evaporation of suppression water in the garage which caused pressure rise to force hot gases out through the vent opening.

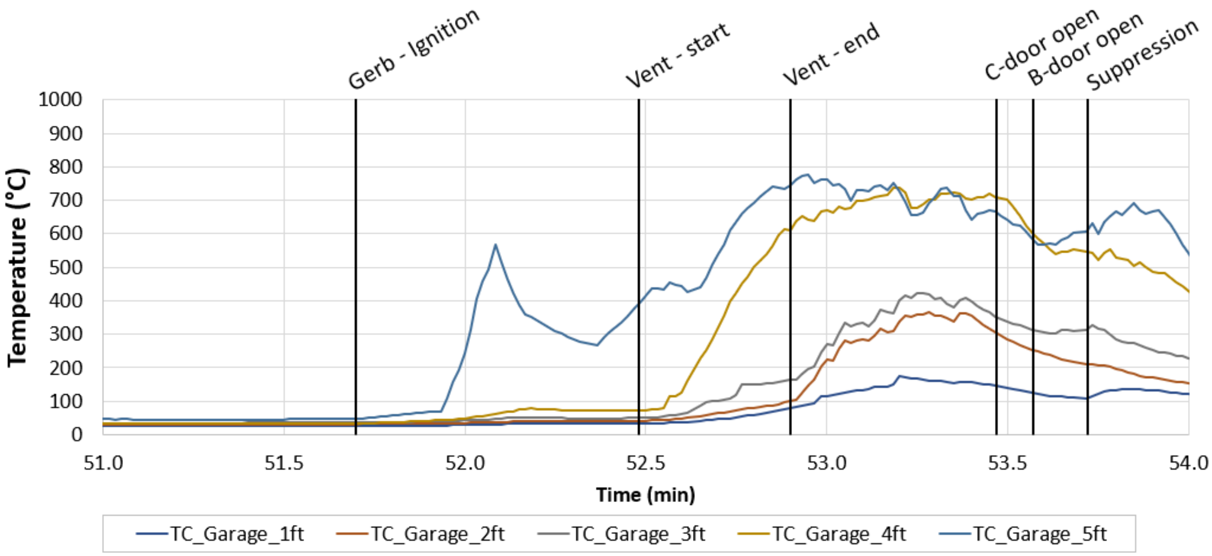

Figure 131 – Gas temperatures measure in the garage door vent during Test 3, from 51 to 54 minutes test time.

Gas Concentrations

After ignition of the Group A commodity, the growing fire consumed O_2 in the closed garage and produced CO and CO_2. Carbon monoxide and carbon dioxide concentrations increased as smoke accumulated. Just before 5 minutes of test time, flames started to become vitiated by the accumulating products of combustion and the fire growth stopped. This aligns with Figure 128 which indicates that temperatures stopped increasing and began decreasing as the fire decayed. At 7 minutes of test time, the fire entered a state of ventilation-limited burning. At the start of this period, O_2 concentration was 13.0 v%, and CO and CO_2 concentrations were 7.1 v% and 1.3 v%, respectively.

Based on infrared video review, the Group A commodity boxes transitioned from flaming into smoldering at approximately 11 minutes. Based on the views from the thermal imaging camera shown in Figure 132, smoldering occurred from approximately 11 minutes until 28 minutes. During this period CO concentration peaked at 2.3 v% and O_2 concentration reduced to 11.3 v%. As the fire transitioned back to limited flaming, the CO concentration reduced, the O_2 concentration remained steady, and the CO_2 concentration increased.

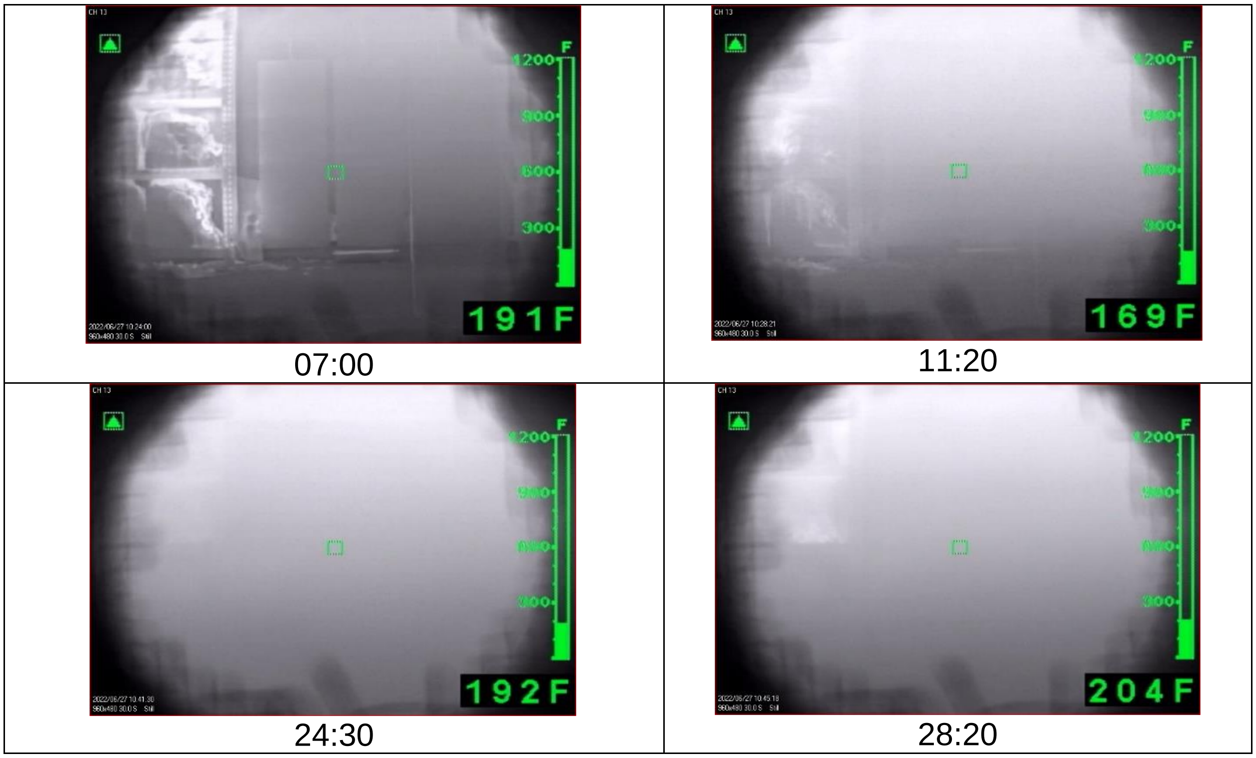

07:00 11:20

24:30 28:20

Figure 132 – Sequence of photographs showing period of transition into vent-limited burning from 11 to 28 minutes of test time.

Two different behaviors affected the gas concentrations after 37 minutes. The ongoing flaming fire in the Group A commodity boxes that had been burning up to this point stopped without igniting the adjacent Group A commodity boxes. Simultaneously, thermal runaway continuously propagated through at least 6 modules within the initiating ESS unit and released unburned gas between 37 minutes and 44 minutes. Subsequently, O_2 increased and CO_2 decreased as the fire waned, while CO and THC increased due to battery gas release. Based on thermal imaging camera video review, several un-instrumented modules experienced thermal runaways sporadically before 51 minutes and 42 seconds, when the gerb was ignited. At this time the O_2, CO, CO_2, and THC concentrations were 14.8 v%, 3.5 v%, 4.4 v%, and 1.4 v%, respectively.

Immediately after the gerb began sparking, the gases venting from the kerfs at the pre-cut opening ignited. Continuous flaming occurred at the kerfs and inside the garage as was visible from the camera looking through the garage door. As a result, the CO and CO_2 concentrations increased until the suppression began at 53 minutes and 42 seconds. Gas concentration measurements were terminated at the start of suppression to prevent saturation of the gas sampling system with water.

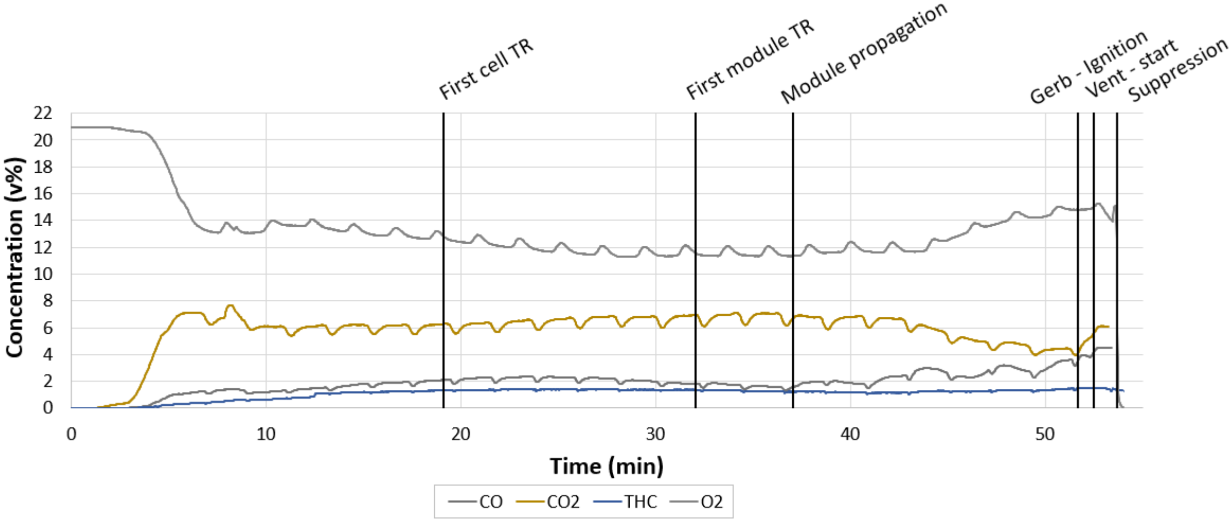

Figure 133 – Gas concentrations measured in the garage during Test 3.

Explosion Hazards

No deflagration or explosion events were observed during Test 3.

5.3.4 Conditions Exterior to Garage

Heat Flux

Heat flux at the front face of the garage door increased to approximately 0.5 kW/m^2 above ambient and remained steady from the time when the fire reached its initial peak after ignition until when the gerb was initiated. Figure 134 shows the heat flux time history of Test 3.

After the gerb was initiated, its sparks ignited the gases venting from the kerfs in the garage door and flaming around the kerfs caused heat flux to peak at 2 kW/m^2. When the vent was operated, existing flames at the vertex of the vent grew with increasing vent area and this caused the heat flux to increase by 55 kW/m^2 in the 25 seconds that it took to completely open the vent. Afterwards, heat flux peaked at 69 kW/m^2 during a period of maximum flaming from the vent.

After the period of unidirectional flow, and as the vent established bi-directional flow, flaming transitioned from the vent into the garage and heat flux began to decrease. The opening of the C-side and B-side doors further contributed to this behavior and heat flux decreased to 36 kW/m^2 at 53 minutes and 41 seconds when suppression was initiated.

Pressurization of the compartment during suppression caused burning gases to exhaust from the garage door vent, which increased heat flux to 48 kW/m^2 for about 15 seconds before decreasing to a range of 10-20 kW/m^2 over the 3 minutes that it took to complete extinguishment.

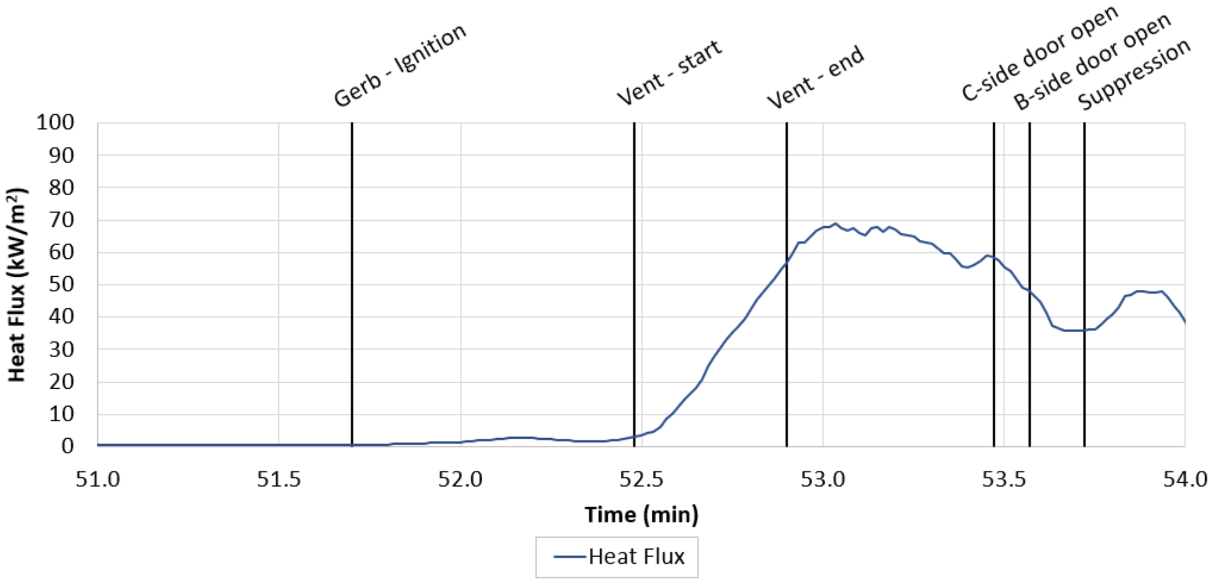

Figure 134 – Heat flux measured in front of the garage door in Test 3.

Gas Measurements

Oxygen, carbon monoxide, and carbon dioxide concentrations at the exterior of the garage door stayed at ambient atmospheric concentrations until the operation of the garage door vent, despite smoke venting from the area near the gas sampling tube, as shown in Figure 135.

Oxygen and carbon dioxide concentrations began changing 20 seconds after the vent was opened in the garage door, although CO concentrations remained at atmospheric background concentrations for the remainder of the test. O_2 decreased to approximately 20.5 v% and CO_2 increased to approximately 0.5 v% until the C-side and B-side doors were opened and burning out of the vent increased. Oxygen and carbon dioxide concentrations reached their relative maximum values of 18.6 v% and 1.1 v% just after the B-side door was opened. Both gas concentrations reduced to zero rapidly after this point as the gas measurement equipment was shut down to prevent the accumulation of moisture during fire suppression.

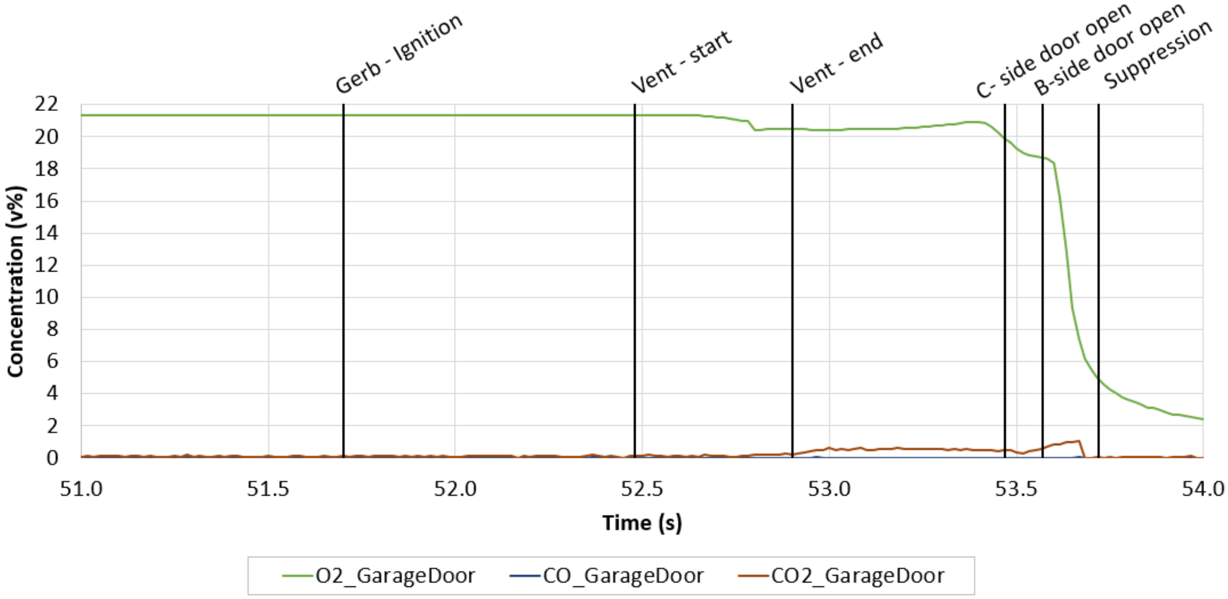

Figure 135 – Exterior gas measurements at the garage door in Test 3.

5.3.5 Size-up Indicators

Visual Indicators

Visual indicators include visual observations and thermal imaging. The thermal imaging camera directed through the B-side wall towards the residential ESS units on the D-side wall provided the most direct view of when thermal runaways were occurring within the garage. Views from this camera were compared with different camera angles from around the exterior of the garage for the test period starting before the first thermal runaway until suppression. The sequence of images shown in Figure 136 - Figure 138 compare the TIC views with an external view from the A-B corner of the garage, which provided the best view of the smoke venting from the garage door.

(a) IR image of interior C-D corner

(b) Overall view

(c) Overall IR image

Figure 136 – Images from first cell thermal runaway (19:14).

(a) IR image of interior C-D corner

(b) Overall view

(c) Overall IR image

Figure 137 – Images from first module thermal runaway (32:11).

(a) IR image of interior C-D corner

(b) Overall view

(c) Overall IR image

Figure 138 – Images from after at least 6 modules experienced thermal runaway within 90 seconds (43:56).

Images are taken from three times: 1) during the first 18650 cell thermal runaway (19:14), 2) during the first module thermal runaway (32:11), and 3) after at least 6 modules experienced thermal runaway within 90 seconds (43:56). The TIC image on the left side of Figure 138 shows a thermal signature at residential ESS Unit 1 after multiple modules have entered into thermal runaway. The venting gases are also visible, but more difficult to distinguish. It was not possible to distinguish the thermal signature of individual 18650 cells undergoing thermal runaway. However, it was possible to identify thermal runaway propagation once multiple module events had occurred and the heat had sufficiently transferred into the residential ESS enclosure walls.

There are no visual indications of these thermal runaways occurring that can be readily discerned from still images taken from the exterior of the garage. For example, the smoke and gases do not appear to change characteristics in terms of volume, opacity, color, or buoyancy. However, while watching the test as it was conducted, and in video review, it is possible to observe transient behavior of the smoke venting under brief pressure pulses associated with the rapid release of gases when modules entered thermal runaway.

The clearest example of this phenomenon that occurred in Test 3 is demonstrated in Figure 139, which shows the smoke venting around the edges of the garage door – not only the vent kerf – at three times separated by two seconds each. In the first image, the neutral plane is seen at the approximate half-height of the door. The neutral plane is indicated in this case by the height above the floor where smoke is escaping from the garage door edges. Two seconds later, in the middle image, during a probable thermal runaway[3], the neutral plane descended to the floor. Another two seconds later, the neutral plane returned to the half-height of the door. A red line has been superimposed over the neutral plane to aid in identifying the neutral plane height. This phenomenon was not seen in Test 1 and is atypical of ventilation-limited fires.


51:28 51:30 51:32

Figure 139 – Short lived transient pressure increase affecting neutral plane height.

A parallel analysis was conducted with IR video collected from outside the garage door, as shown in Figure 136 – Figure 138.. The IR images show the heat through the garage door and identify locations of gas and smoke venting from the structure. There are no visual cues from this footage that indicate battery involvement in terms of thermal runaway occurrence or the accumulation of flammable gases into the hot gas layer.

Figure 136 – Figure 138 demonstrate that there were no thermal effects from the thermal runaways visible from the exterior of the garage during the ongoing thermal runaways.

Further, comparison of the images over time shows that the thermal conditions were governed by the generation of heat from the ventilation-limited Group A commodity fire and that the thermal energy contributed during thermal runaways and any potential burning of flammable battery gases did not alter the thermal picture as viewed in Figure 136 – Figure 138 in any discernable way.

The brief pressure pulsing phenomenon mentioned in the prior video analysis was observable but to a lesser degree. In fact, this phenomenon was only detected after it was first observed in the video analysis and the corresponding thermal imaging video was carefully reviewed several more times.

---

[3] The thermal runaway cannot be verified, as a layer of soot condensed on the TIC lens and completely obscured the thermal imaging view, and the thermal runaway was likely in an uninstrumented module.

Portable Gas Meters

Figure 140 – Figure 142 plot the CO measurements from all four meters during Test 3. During the first 52 minutes of Test 3, during which time the commodity boxes were involved in flaming and only the first ESS module had experienced thermal runaway, a maximum CO level of 30 ppm was measured on any meter. This concentration was measured at the garage door. During this same period and until the end of the test, the two meters located in the driveway displayed a steady increase in CO measurements from zero to approximately 25 ppm as products of combustion from the test diffused into the lab.

Near 52 minutes and 20 seconds, within one minute of gerb activation, the garage door meter and C-side service door meter measured CO concentration peaks of 300 ppm and 100 ppm, respectively. Test video indicates increased visible gas leakage from the compartment during this time. It is possible that gas ignitions by the gerb caused minor overpressures which increased gas leakage from the compartment. A similar peak in CO was measured at the garage door near 53 minutes and 15 seconds. This second peak at the garage door was caused by pulsations in the fire plume emanating from the garage door inverted V-cut vent after it was opened.

At the time of suppression, with both service doors and the garage door vent opened, plumes of gas are pushed out of these openings by the suppression fog stream. These plumes visually envelope the C-side door meter and garage door meter causing saturation measurements (2000 ppm) on both meters.

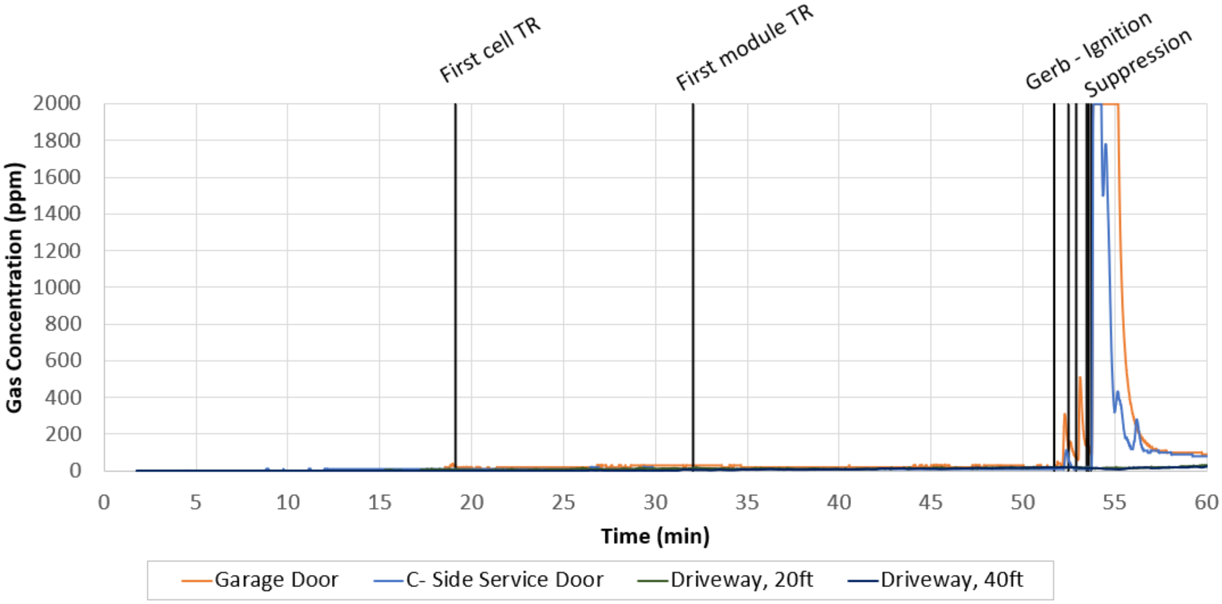

Figure 140 – All portable meter CO measurements in Test 3 (0-2000 ppm).

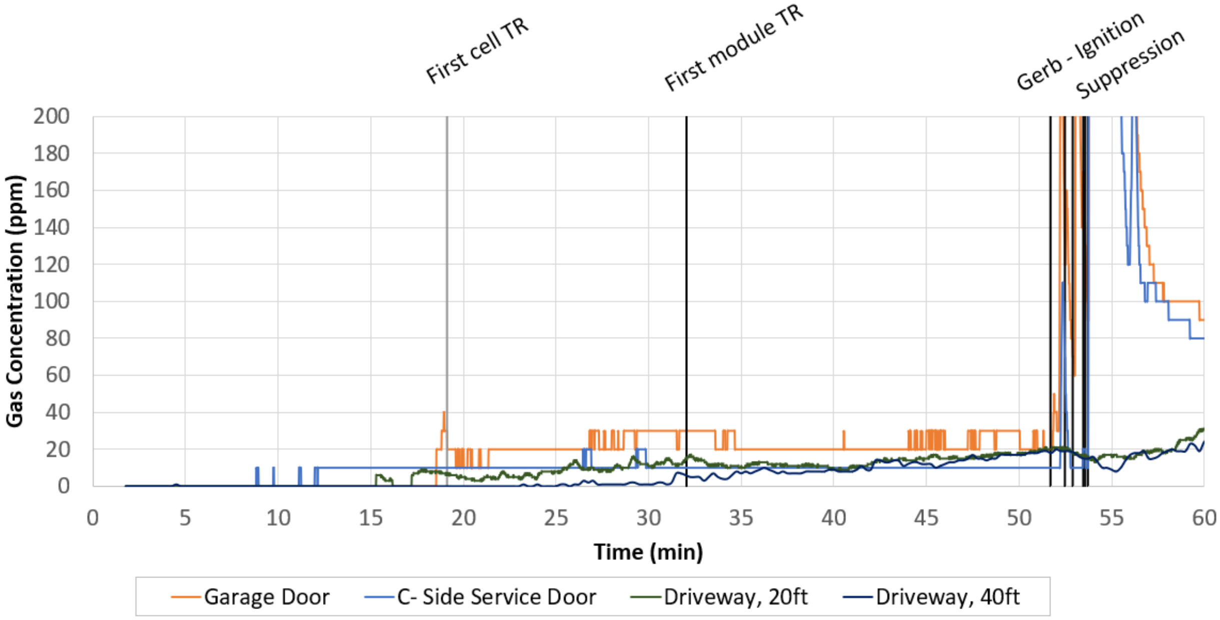

Figure 141 – All portable meter CO measurements in Test 3 (0-200 ppm).

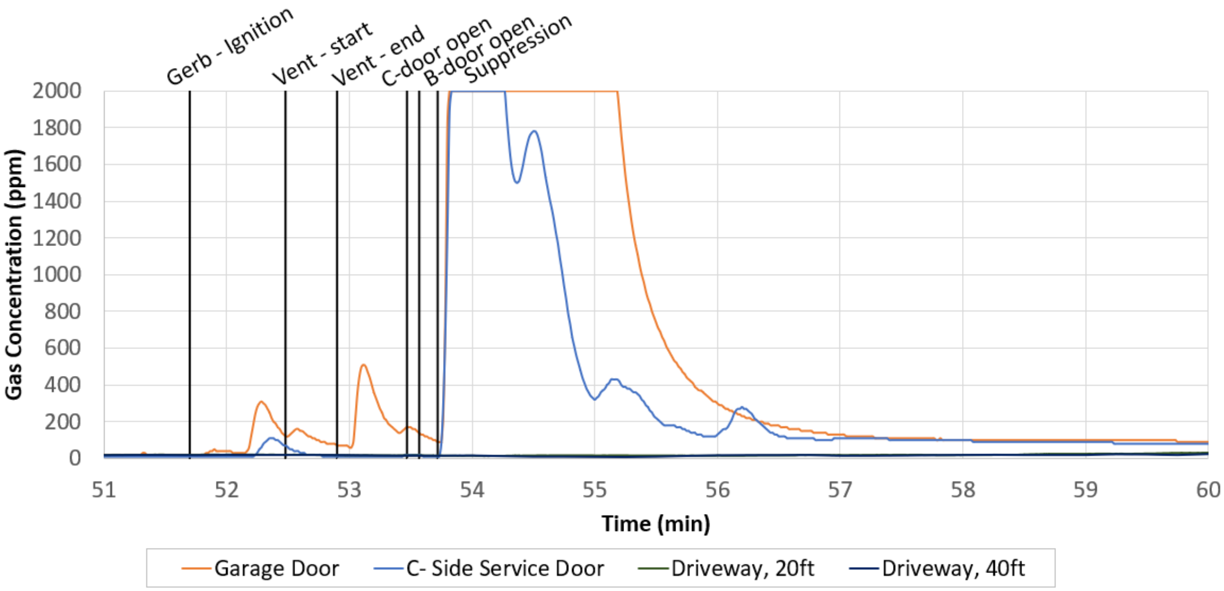

Figure 142 – All portable meter CO measurements in Test 3, for the period between 51 and 60 minutes (0-2000 ppm).

The peaks of CO measured in the garage door meter were accompanied by lesser peaks of HCN, VOCs and LEL (Figure 143 –Figure 145). Before the ventilation sequence, peak measurements were 30 ppm CO, 2 ppm HCN, 8 ppm VOC, and 0 % LEL. Between the beginning of the ventilation sequence and the initiation of suppression, peak measurements were 500 ppm CO, 20 ppm HCN, 320 ppm VOC, and 5 % LEL. During suppression, CO saturated at 2000 ppm, HCN saturated at 50 ppm, VOC peaked at 600 ppm, and LEL readings measured up to 45% LEL.

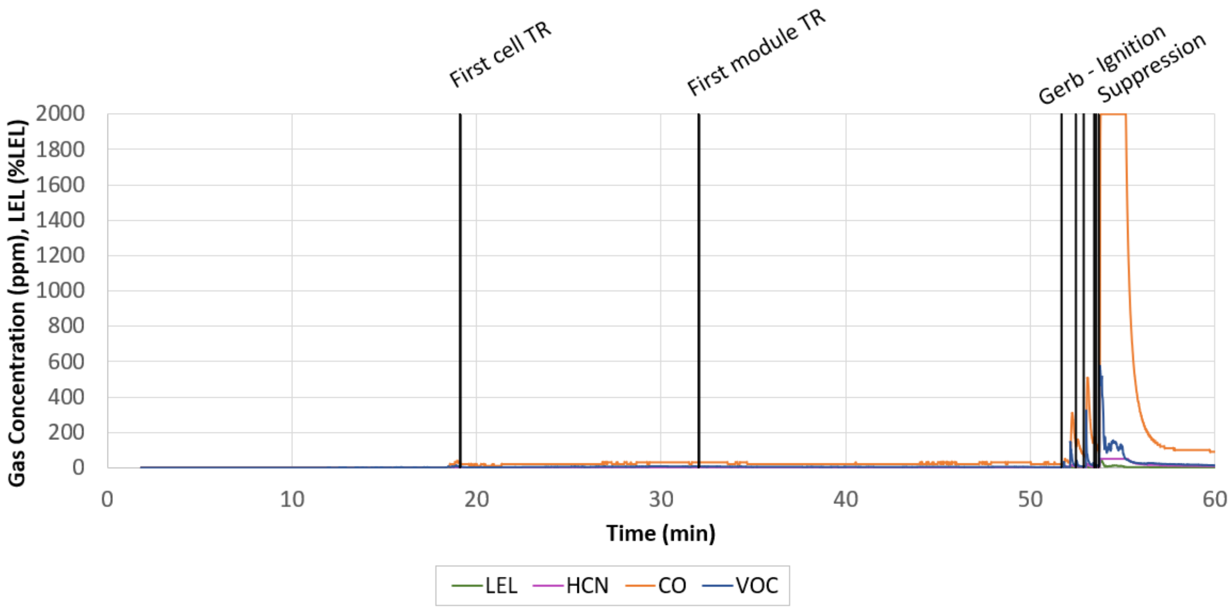

Figure 143 – Garage door meter measurements during Test 3.

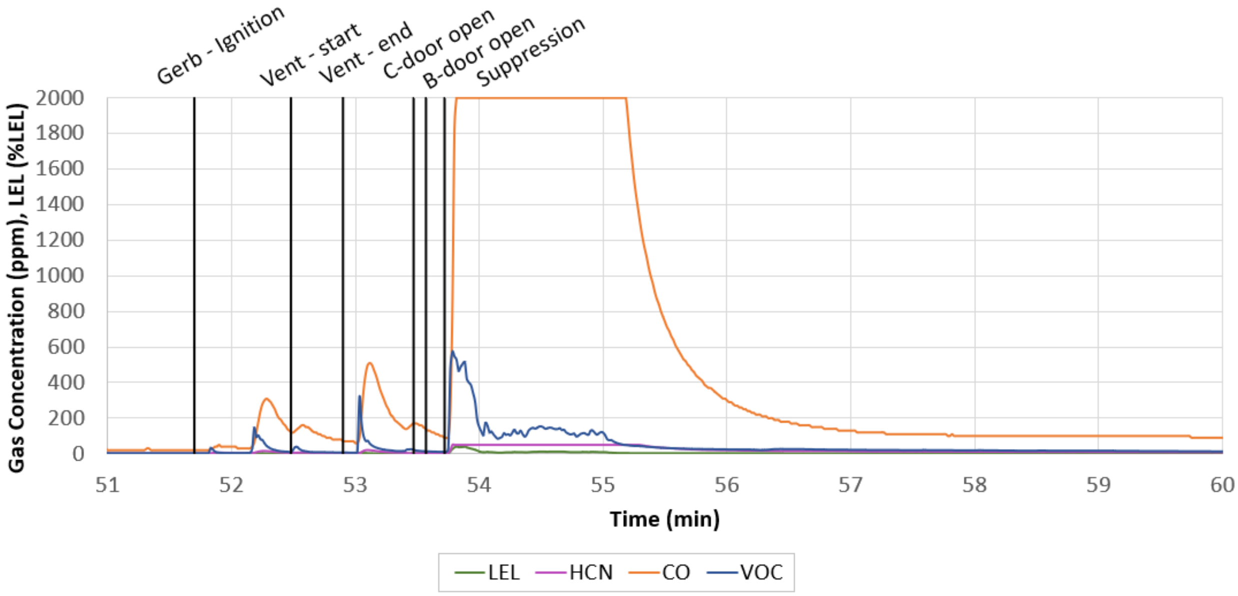

Figure 144 – Garage door meter measurements during Test 3, for the period between 51 and 60 minutes.

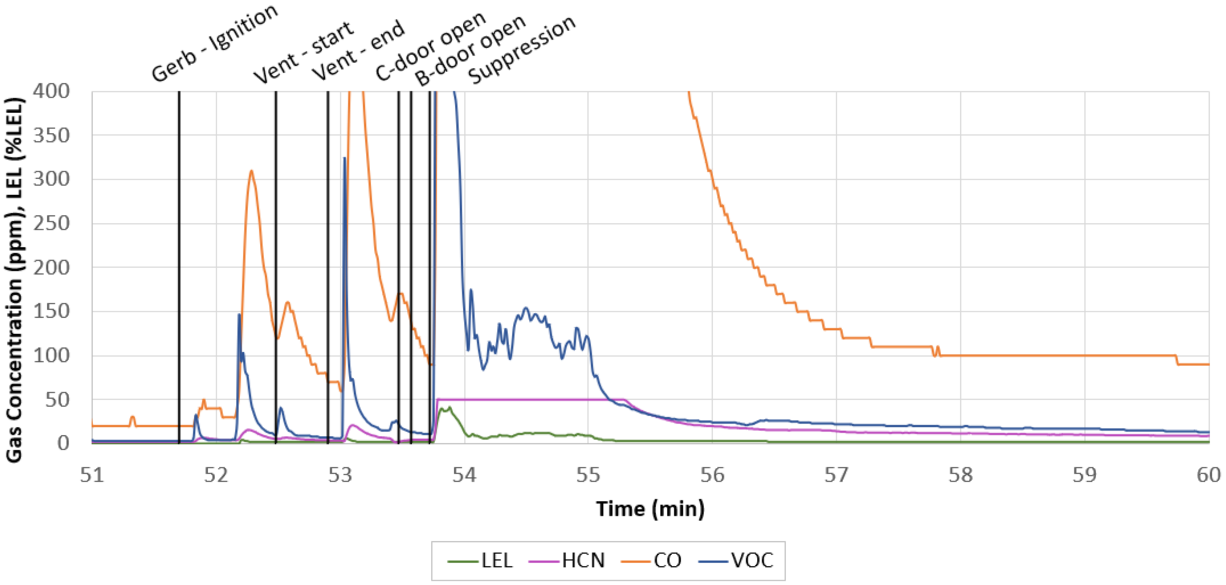

Figure 145 – Garage door meter measurements during Test 3, for the period between 51 and 60 minutes, zoomed in for lower gas concentrations.

Similarly, the peaks of CO measured in the C-side door meter were accompanied by lesser peaks of hydrogen and LEL (Figure 146 and Figure 147). Peak concentrations before the ventilation sequence were 20 ppm CO, 10 ppm H_2, 0 ppm H_2S, and 0 % LEL. No peaks other than CO (110 ppm) were observed during the increased gas leakage that occurred in the window between the first gerb ignition and suppression. During suppression, CO saturated at 2000 ppm, H_2 saturated at 1000 ppm, H_2S peaked at 35 ppm, and LEL peaked at 21 % LEL. For the hydrogen measurement, it is not possible to know the fraction of this measurement that is pure hydrogen versus cross-sensitivity with the presence of CO.

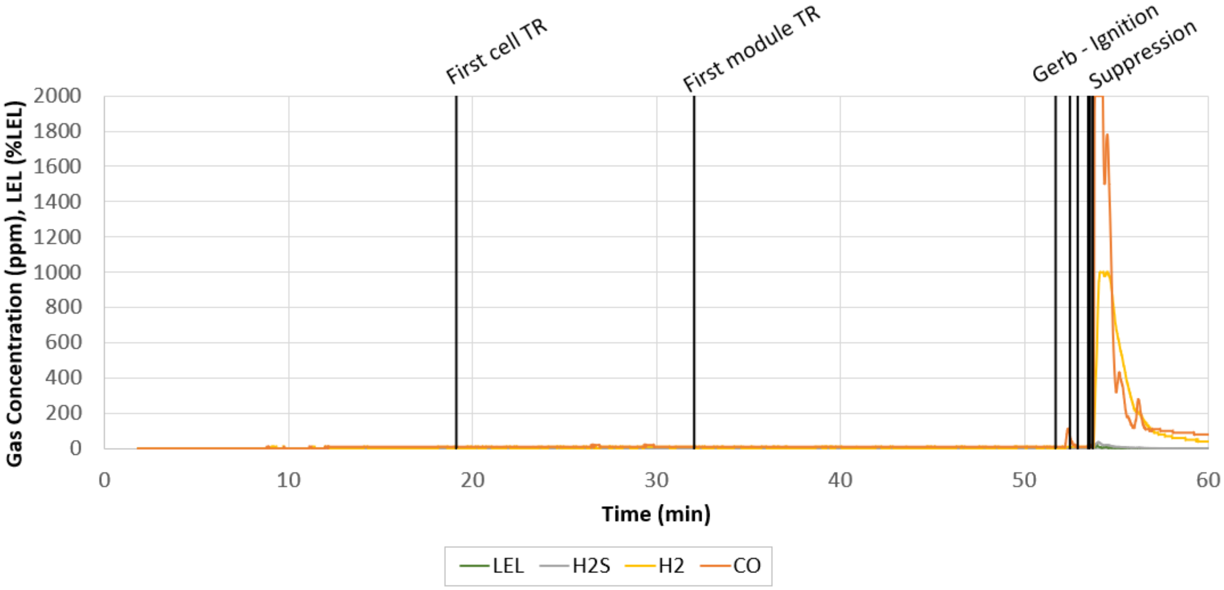

Figure 146 – C-side service door meter measurements during Test 3.

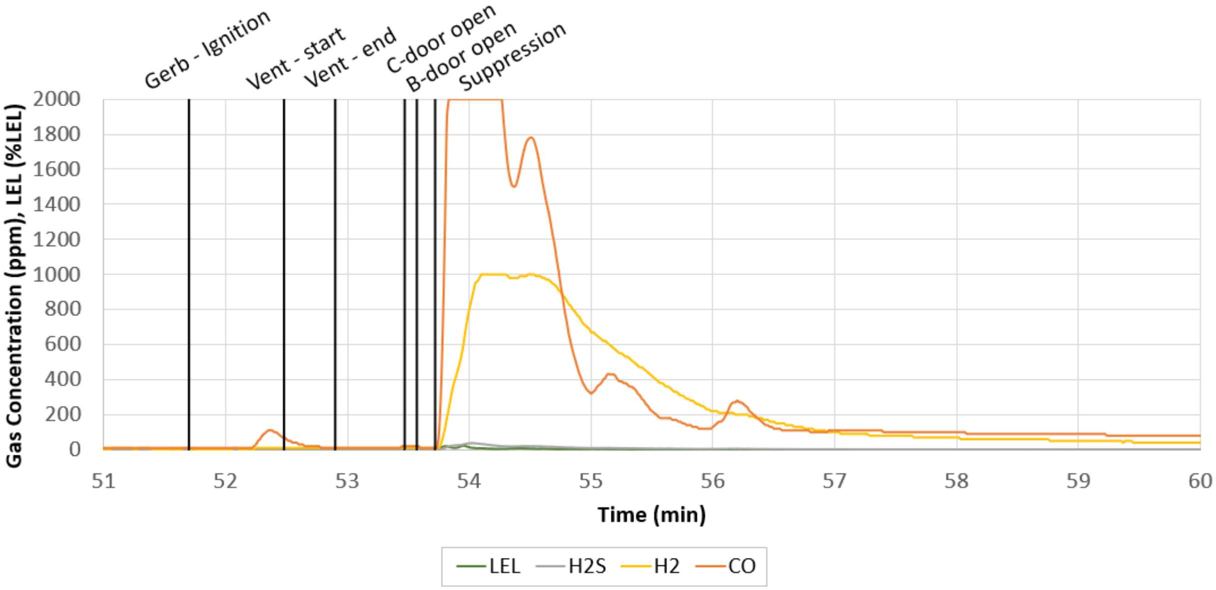

Figure 147 – C-side service door meter measurements during Test 3, for the period between 51 and 60 minutes.

The two meters in the driveway showed parallel trends to each other, as plotted in Figure 148 and Figure 149. During the test, a steady increased in CO was registered by both driveway meters. A similarly steady increase in HCN was registered in the driveway meter at 20 ft (Figure 148). These increases were due to products of combustion from the test diffusing into the lab space and may not be fully representative of measurements in an unconfined environment. In an unconfined environment, lower concentration conditions would likely be present.

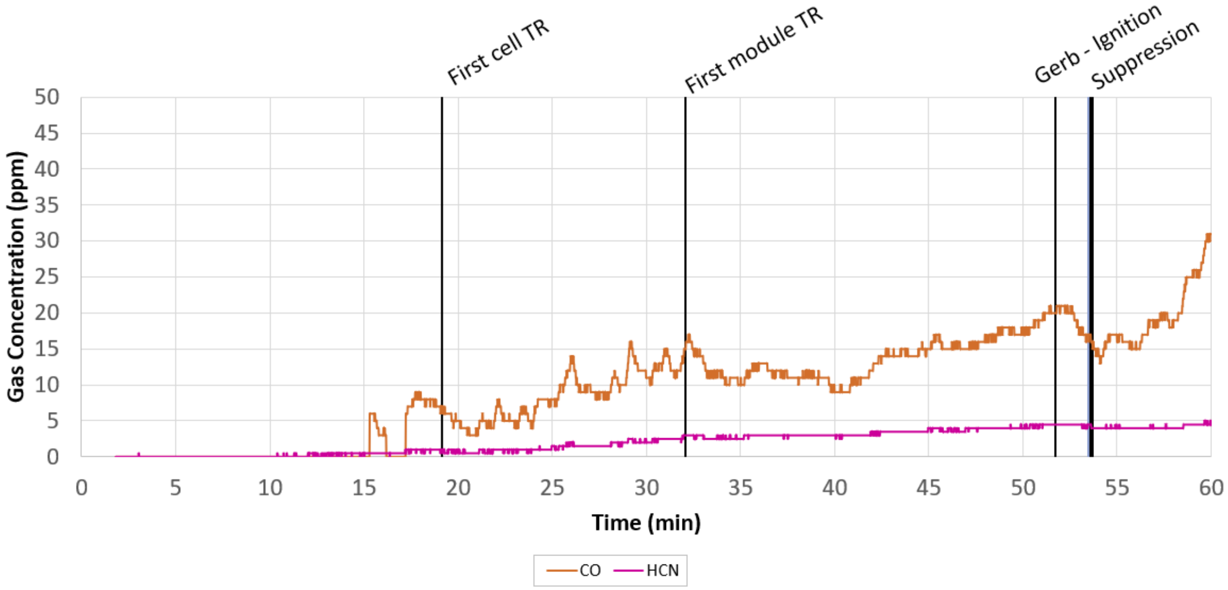

Figure 148 – Portable meter measurements at driveway 20 ft location during Test 3.

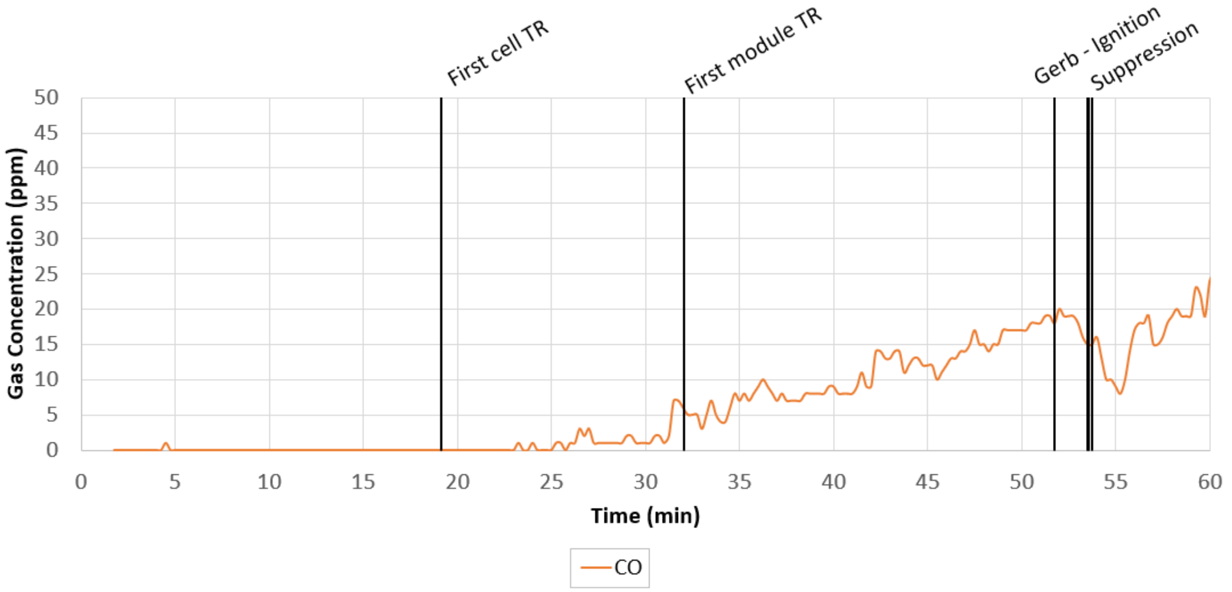

Figure 149 – Portable meter measurements at driveway 40 ft location during Test 3.

5.4 Test 4

5.4.1 Timeline

Figure 150 – Figure 154 show a visual sequence of the most significant events that occurred during Test 4.

Test four was initiated by heating one 18650 component cell (“Unit1Init1_Cell1”) near the bottom of the leftmost ESS unit at 6°C/min for 25 minutes and 21 seconds, at which time thermal runaway occurred in the cell. Battery thermal runaway effluent gases were first observed external to the unit 9 seconds later, as pictured in Figure 150. Approximately 2 minutes later, cell-to-cell thermal runaway propagation was observed by sharp temperature increase within the initiating module (“Unit1Init1”). Ten seconds later, an increase in gas release and thermal signature in Unit 1 was observed. Gas evolved from Unit 1 and accumulated around Unit 1 and all tiers of the adjacent rack of Group A commodity boxes.

First signs of thermal runaway gas venting	Cell-to-cell propagation and gas release
	
25:30 (TR + 00:09)	27:34 (TR + 02:13)
Cell-to-cell propagation and gas release (Infrared view)	Battery gas around ESS unit
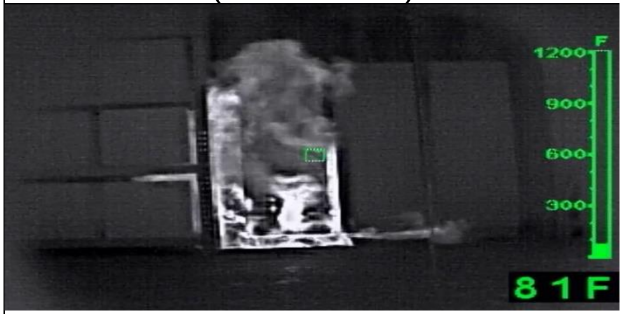	
27:34 (TR + 02:13)	27:40 (TR + 02:19)

Figure 150 – Test events between 25 and 28 minutes of Test 4.

At 27 minutes and 41 seconds, 21 seconds after cell-to-cell propagation was observed, a gerb was activated to ignite the accumulated battery gases, as shown in Figure 151. This was intended to create an early ignition scenario, since Test 2 demonstrated that the batteries can generate viable ignition sources. The ignition of the battery gas resulted in a partial volume deflagration where the garage door was observed to bow out an estimated 2 inches. Gas and flame were observed venting under pressure from conduit openings on the D-side wall. The garage exterior showed no further evidence from the deflagration 2 seconds later.

Accumulation immediately prior to ignition

Ignition

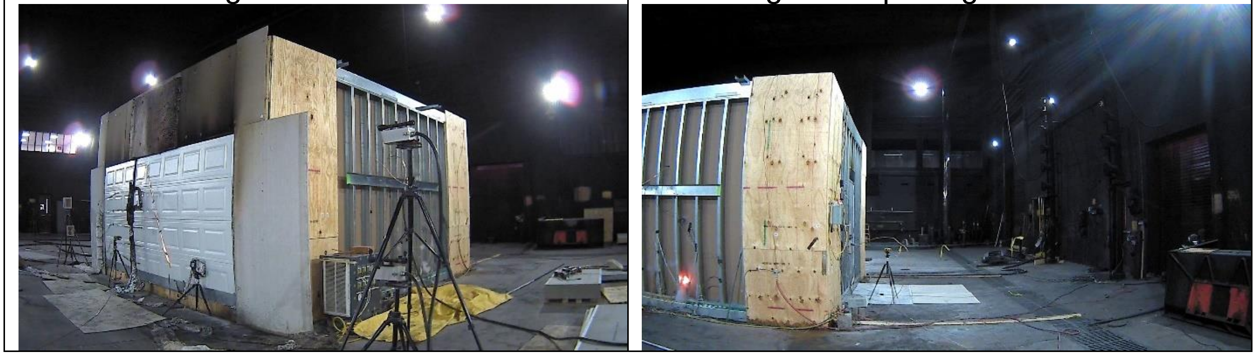

Garage door deflection

Venting from openings on D-side wall

Figure 151 – Battery gas ignition at 27:41 (TR + 02:20).

Sustained flaming was established around Unit 1, as pictured in Figure 152. A smoke layer accumulated near the ceiling with additional battery gas accumulating along the floor. Flaming intensified around 32 minutes as more batteries entered thermal runaway. The first confirmed module-to-module propagation occurred directly above the initiating module (“Unit1Init2”) at 32 minutes and 25 seconds.

Module-to-module propagation continued through Unit 1. During the one-minute span between 35 minutes and 36 minutes, thermal runaway was measured by sharp, sustained temperature increases in all instrumented modules in Unit 1. At approximately 36 minutes, the Group A commodity boxes began to ignite, starting with the column nearest Unit 1.

Sustained flaming around Unit 1  27:55 (TR + 02:34)	Smoke accumulation 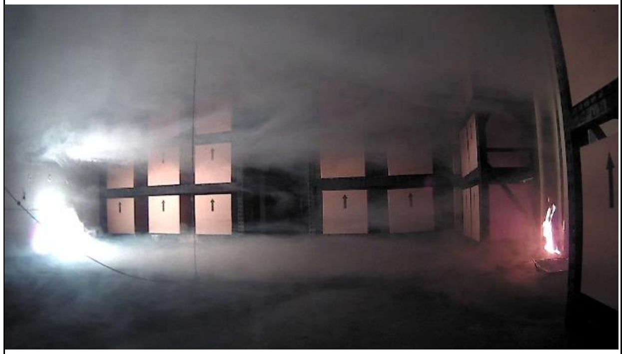 30:55 (TR + 05:34)
Flaming intensifies with module-to-module thermal runaway propagation  32:26 (TR + 07:05)	Column 1, Box 1 ignition (Infrared view) 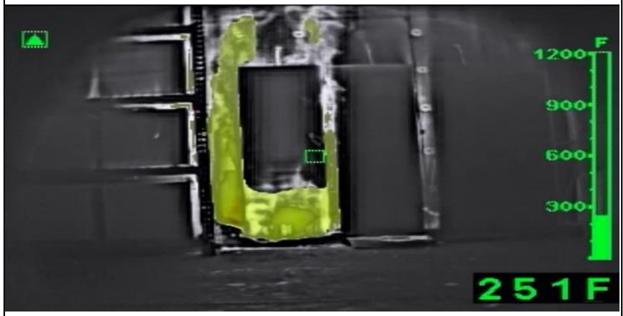 36:03 (TR + 10:42)

Figure 152 – Test events between 27 and 36 minutes in Test 4.

Fire department vent operations were simulated at 43 minutes and 21 seconds based on an established condition of ventilation-limited fire with battery gas contribution to the accumulated hot gas layer. Vent operation began with remote operation of the C-side door which simulated fire department response to an attached garage via the residence. A light gray plume of gas exhausted from the doorway. The garage door vent was not activated during Test 4 ventilation.

Approximately 40 seconds later, smoke was ejected forcefully from the full height of the doorway. The smoke ignited from inside the garage, resulting in a backdraft and sustained flaming out of the doorway. While the flame spread was relatively slow, the fire dynamics match the description of a backdraft.

The influx of fresh air to the garage from the open door resulted in sustained flaming conditions inside the garage with Group A commodity boxes igniting. Near 46 minutes, batteries within Unit 2 underwent thermal runaway and contributed to fire growth. Thermal imaging shows the upper hot gas layer descending. Flaming intensified from the doorway as battery involvement increased.

White/gray smoke venting around garage	Initial plume from vented service door
	
40:00 (TR + 14:39)	43:21 (TR + 18:00)
Backdraft exhausting from C-side door	Sustained flaming from doorway intensifies
	
44:00 (TR + 18:39)	51:36 (TR + 26:15)

Figure 153 – Test events between 40 and 52 minutes of Test 4.

Test termination and suppression began at 54 minutes with remote operation of the B-side door and remote water application for suppression, as pictured in Figure 154.

Figure 154 – Conditions at test termination (54 minutes) in Test 4.

5.4.2 Thermal Runaway Propagation

Test 4 was initiated by heating one 18650 component cell ("Unit1Init1_Cell1") at 10.8 °F/min (6 °C/min) for 25 minutes and 21 seconds, at which time thermal runaway occurred and heater operation was discontinued. Thermal runaway propagation through the rest of the cells in this module (“Unit1Init1”) occurred 3 minutes later, as shown in Figure 155.

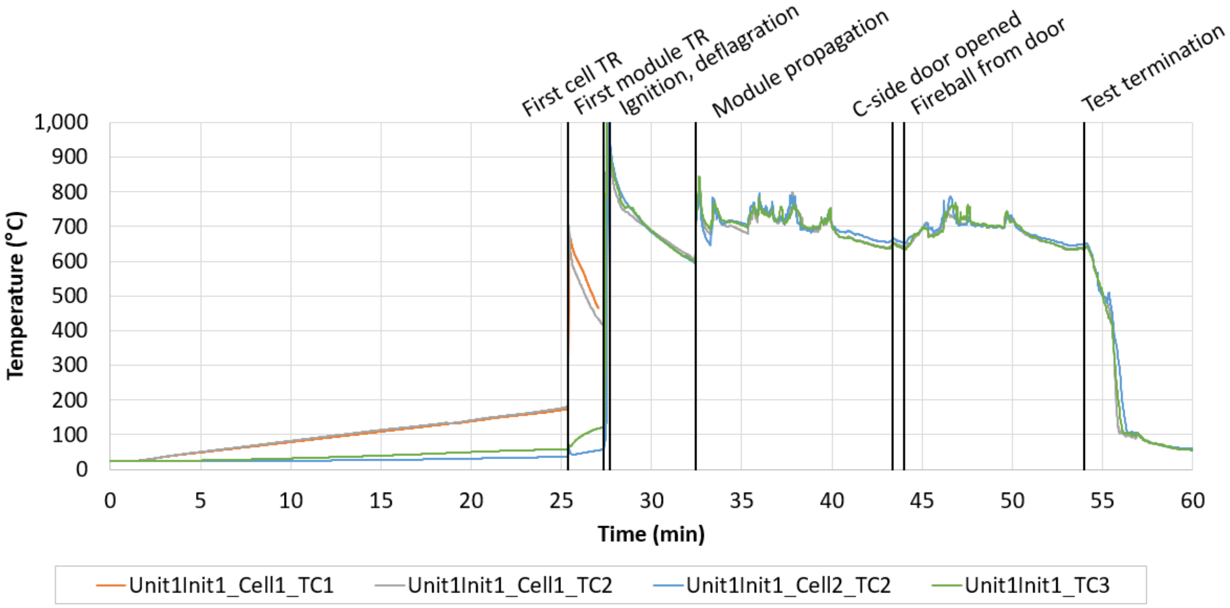

Figure 155 – Temperature measurements in the initiating battery module (“Unit1Init1”).

Twenty-one seconds after propagation within the first module, the accumulated battery vent gases were ignited. Five minutes later, at 32 minutes and 25 seconds of test time, module-to-module propagation was confirmed in the module directly above the initiating module (“Unit1Init2”). The next confirmed thermal runaway occurred in the module directly below the initiating module (“Unit1_Mod2”) within one minute. During the one-minute span between 35 minutes and 36 minutes, thermal runaway was measured by sharp, sustained temperature increases in all instrumented modules in Unit 1, as illustrated in Figure 156.

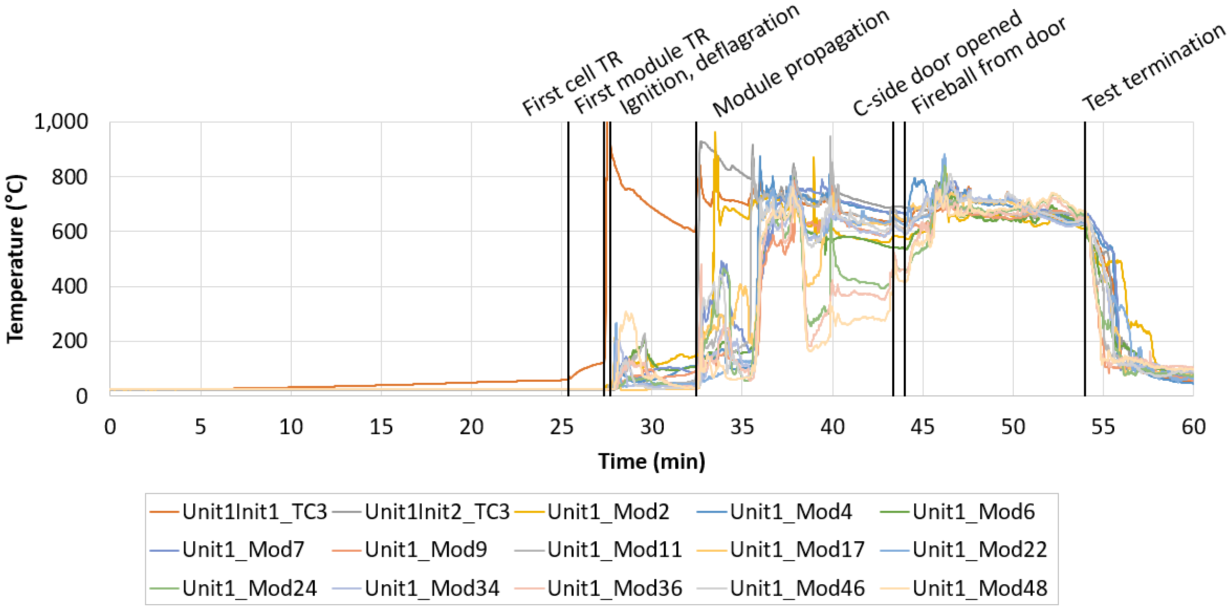

Figure 156 – Temperature measurements within the initiating unit (Unit 1) of Test 4.

Temperature around the enclosure perimeter of Unit 1 did not increase from the first cell thermal runaway. Following ignition, sustained flaming was observed on the lower half of Unit 1. During this time, enclosure perimeter temperatures measured between 100 °C and 200 °C on the lower half and 50 °C to 300 °C on the upper half, as plotted in Figure 157. Module-to-module propagation resulted in increasing fire size and corresponding higher enclosure perimeter temperatures. Peak enclosure temperatures on Unit 1 prior to garage ventilation operations measured near 700 °C. This peak temperature occurred following the period of accelerated thermal runaway between 35 and 36 minutes through the majority of Unit 1.

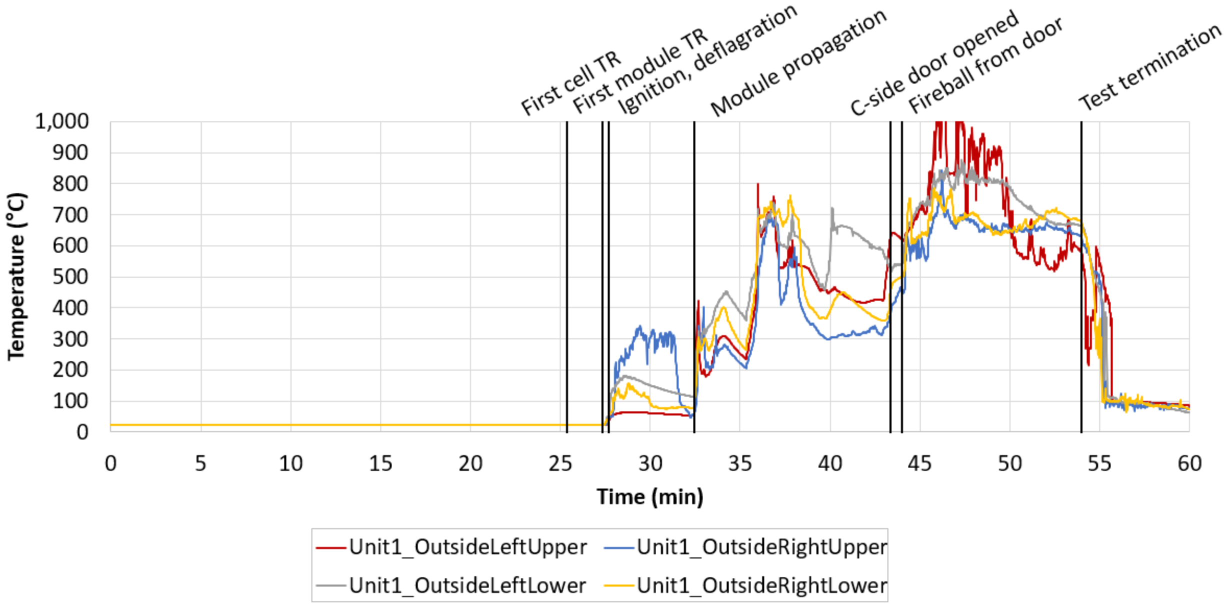

Figure 157 – Unit 1 enclosure exterior temperatures in Test 4.

Enclosure perimeter temperatures on Unit 2 increased momentarily, not exceeding 100 °C, with the first cell thermal runaway and propagation through the initiating module, as shown in Figure 158. Temperatures on the left side of Unit 2, nearest to Unit 1, increased following module-to-module propagation in Unit 1. A spike in temperature exceeding 500 °C was observed on both sides of Unit 2 following the period of accelerated thermal runaway and fire growth from Unit 1 at 35 to 36 minutes.

Near 46 minutes, thermal runaway behavior was observed within Unit 2 which resulted in sustained elevated temperatures between 600 and 800 °C on the outer enclosure of Unit 2. This is aligned with temperature trends within the modules of Unit 2 as illustrated by Figure 159. Thermal runaway was identified in the modules by a sharp, sustained increase in module temperature.

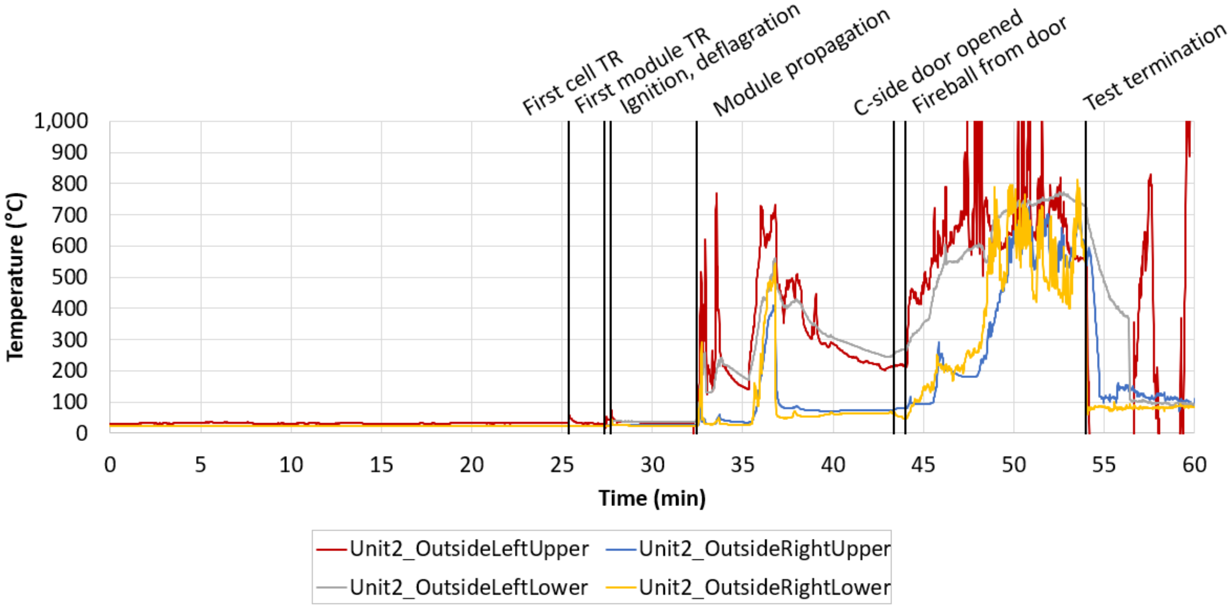

Figure 158 – Unit 2 enclosure exterior temperatures in Test 4.

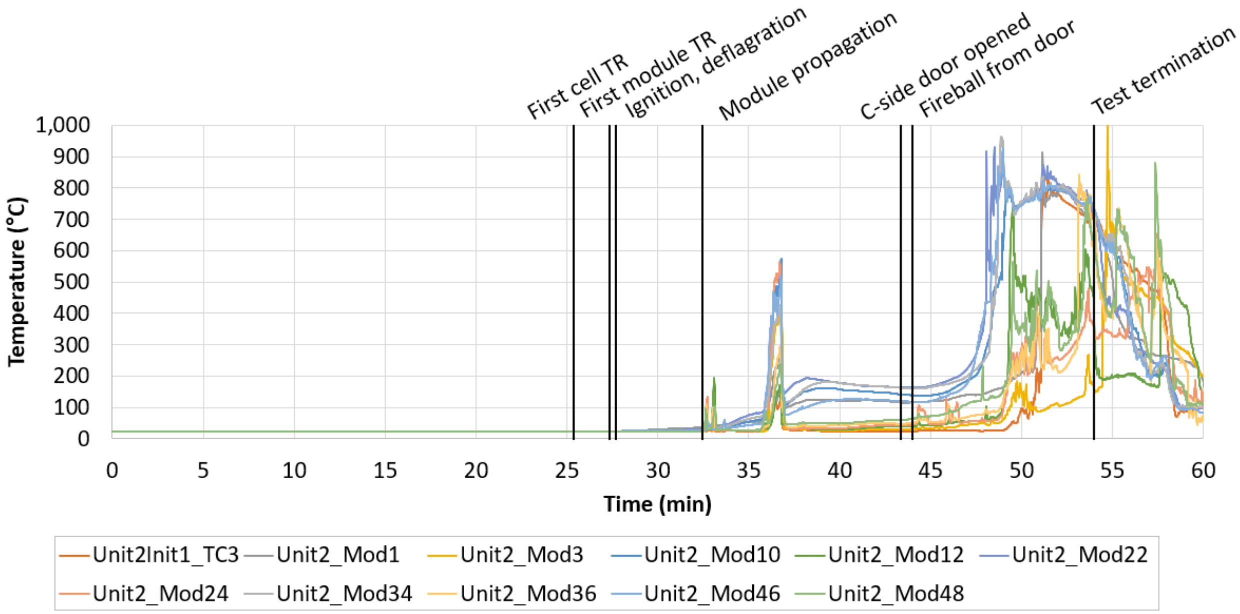

Figure 159 – Temperature measurements within the center unit (Unit 2) of Test 4.

Exterior enclosure temperatures on the rightmost unit, Unit 3, did not show any significant temperature increase above ambient until Unit 1 module-to-module propagation began, as shown in Figure 160. During the period of module-to-module propagation and ventilation of the C-side door, enclosure temperatures for Unit 3 did not exceed 80 °C (which is below the cell venting threshold temperature). Most temperatures measured within the modules of Unit 3 (Figure 161) did not show thermal runaway temperature signatures for the duration of Test 4. However, one instrumented module (“Unit3_Mod34”) had a rapid increase in temperature with sustained temperature above 400 °C, which may have indicated thermal runaway.

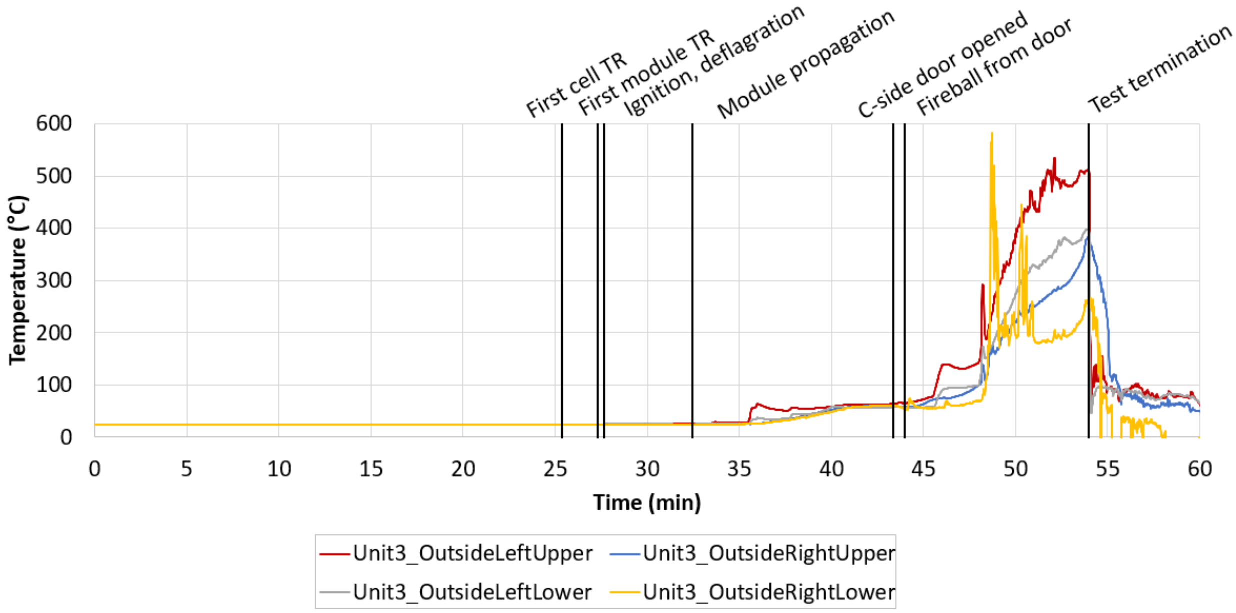

Figure 160 – Unit 3 enclosure exterior temperatures in Test 4.

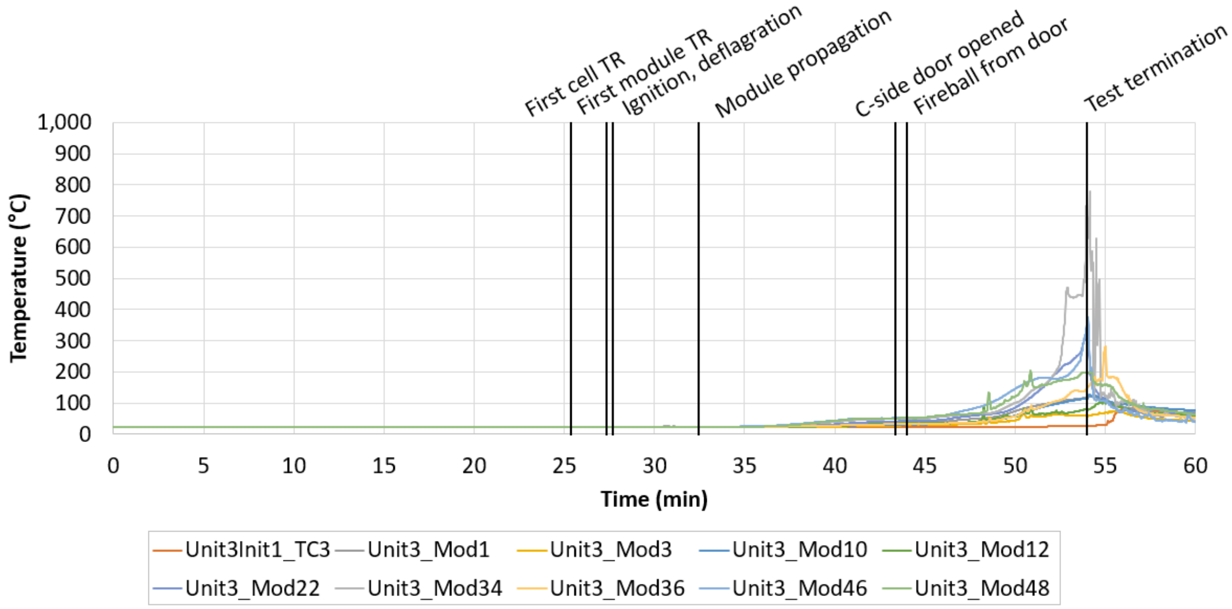

Figure 161 – Temperature measurements within the rightmost unit (Unit 3) of Test 4.

Timing of thermal runaway for all instrumented modules is summarized in Table 7.

Table 9 – Thermal runaway propagation summary.

Location	Test Time	Time Since First Cell TR
Unit1Init1_Cell1	25:21	00:00
Unit1Init1	27:20	01:59
Ignition, partial volume deflagration	27:41	02:20
Unit1Init2	32:25	07:04
Unit1_Mod2	33:16	07:55
Unit1_Mod11	35:24	10:03
Unit1_Mod6, Unit1_Mod24	35:27	10:06
Unit1_Mod36, Unit1_Mod46, Unit1_Mod48	35:31	10:11
Unit1_Mod17	35:36	10:15
Unit1_Mod7	35:38	10:17
Unit1_Mod22	35:39	10:18
Unit1_Mod34	35:42	10:21
Unit1_Mod4	35:44	10:23
Unit1_Mod9	35:49	10:28
C-Side door opened	43:21	18:00
Backdraft	44:00	18:39
Unit2_Mod22	45:47	20:26
Unit2_Mod10	46:04	20:43
Unit2_Mod46	46:44	21:23
Unit2_Mod12	48:14	22:53
Unit2_Mod34	48:15	22:54
Unit2_Mod48	48:52	23:31
Unit2_Mod24	48:54	23:33
Unit2_Mod1	50:33	25:12
Unit2_Unit1	50:57	25:36
Unit3_Mod34 (Possible)	52:29	27:08
Unit2_Mod36	53:04	27:43
Test termination	54:00	28:39
Unit2_Mod3	54:24	29:03

5.4.3 Conditions Inside Garage

Gas Temperature

Gas temperatures measured in the center thermocouple array of the garage are plotted for the test duration in Figure 162 and for the period of greatest activity (25 to 45 minutes) in Figure 163.

Temperatures inside the garage did not increase above ambient after propagation of the first cell. Following ignition of the accumulated gases, temperatures increased to 90 °C at the ceiling before returning near ambient four and half minutes later, at 32 minutes of test time.

Module-to-module propagation increased heat input to the compartment by venting hot gases and burning the flammable gases released. The garage interior temperature increased and decreased in parallel with increasing and decreasing thermal runaway frequency. When the Group A commodity boxes ignited at 36 minutes, temperatures increased to peak compartment temperatures at the ceiling of 400 °C. After 40 minutes and prior to ventilation of the C-side door, the garage fire became ventilation-limited, and temperatures decreased again.

Ventilation of the C-side door resulted in increased burning inside the garage. Temperatures rose rapidly at this point, resulting in flashover conditions with upper layer temperatures at the ceiling reaching 700 °C approximately 40 seconds after ventilation.

Test termination and remote suppression began at 54 minutes which resulted in an immediate temperature drop of 300-400 °C and a gradual decline to ambient afterwards.

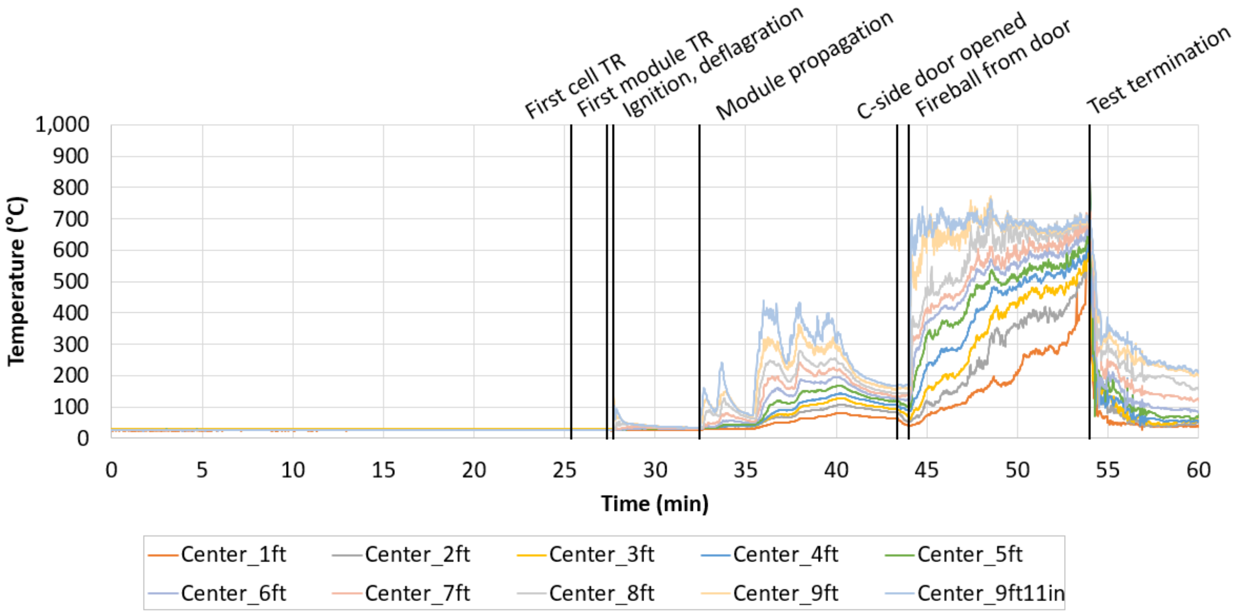

Figure 162 – Temperature inside the garage for Test 4.

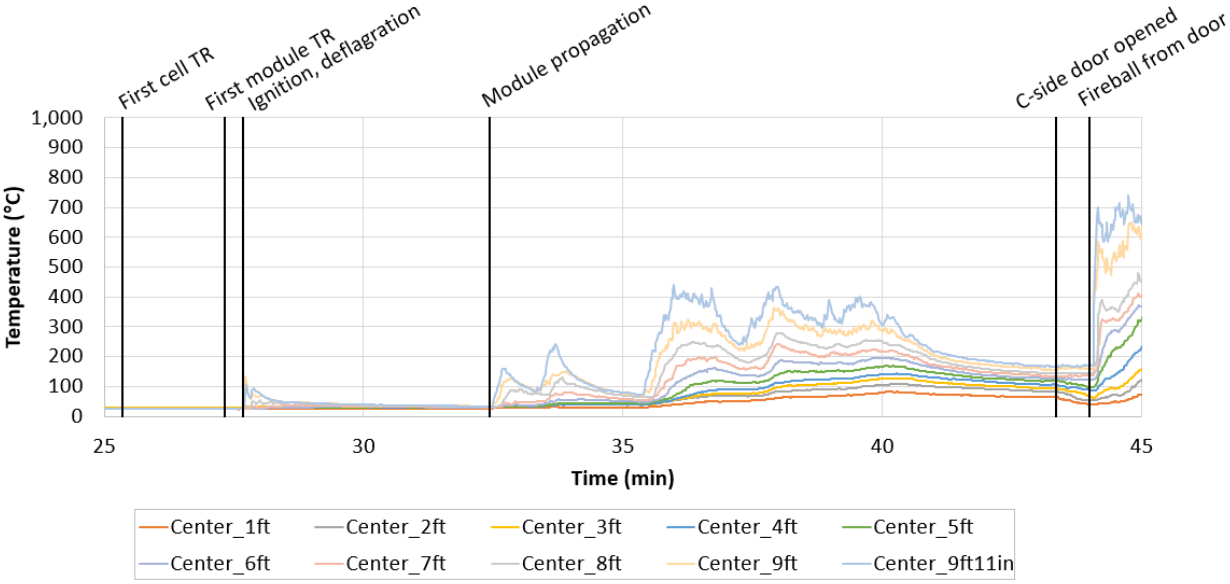

Figure 163 – Temperature inside the garage between 25 and 45 minutes for Test 4.

Gas Concentrations

Gas concentrations in the upper layer of the garage were not changed from initial ambient conditions following the thermal runaway of the first 18650 component cell, as shown in Figure 164. Within 20 seconds of cell-to-cell propagation occurring in the initiating module, a gerb was activated to ignite the accumulated battery vent gases. Combustion byproducts were first measured above ambient conditions in the period between ignition and confirmed module-to-module propagation. In this period, O_2 concentration was reduced by 0.3 v% and CO_2 , CO, and THC were increased to 0.3 v%, 0.07 v%, and 0.02 v%, respectively.

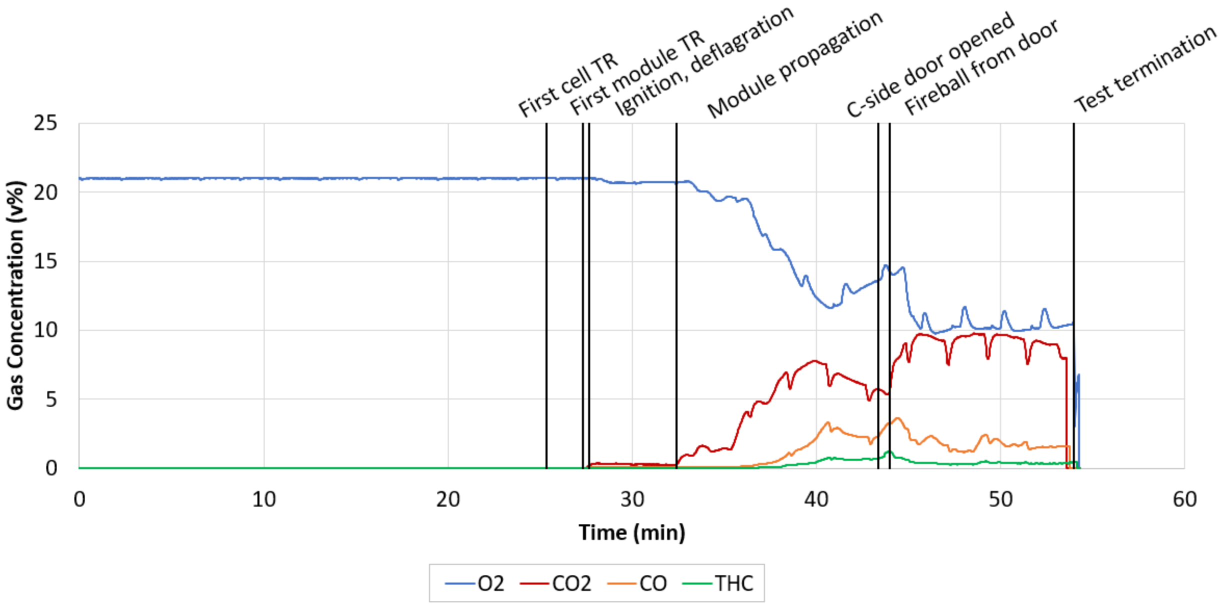

Figure 164 – Interior upper layer gas measurements for Test 4.

Module-to-module propagation was confirmed at 32 minutes and 25 seconds. Module-to-module propagation resulted in generation and subsequent combustion of flammable battery vent gases. This resulted in an increase in $CO_2$and a parallel reduction in O_2 until the fire became ventilation-limited at approximately 41 minutes. During the interval between the beginning of module-to-module propagation and the opening of the C-side door, the lowest O_2 concentration was 11.5 v%. The highest concentrations of CO_2, CO , and THC were 8 v%, 3 v%, and 0.8 v%, respectively.

After the C-side door was opened at 43 minutes and 21 seconds, burning increased within the commodity boxes and the fire quickly became ventilation-limited again at 10 v% oxygen, 10 v% CO_2, 2.5 v% CO, and 0.5 v% THC.

Interior gas measurements were discontinued as test termination procedures commenced.

Explosion Hazards

A partial-volume deflagration resulted from the piloted ignition of battery vent gases surrounding Unit 1 at 27 minutes and 41 seconds. At this time, one module had undergone thermal runaway, equivalent to 30 individual 18650 cells with an estimated gas release of 213 L. The deflagration resulted in a small pressure rise which deflected the garage door an estimated two inches at the center, as pictured in the sequence of Figure 165. The pressure rise did not result in any permanent deformation to the test structure.

Figure 165 – Exterior effects of deflagration (Left – Initial, Right – Peak deflection) in Test 4.

Approximately 40 seconds after the remote operation of the C-side door and the subsequent influx of ambient air, a backdraft occurred which resulted in fire being ejected from the full height of the open door as shown in Figure 153. The event did not result in any observable damage to the structure, but the ejected fire reached several feet out the door.

5.4.4 Conditions Exterior to Garage

Heat Flux

Heat flux at the front face of the garage door did not rise above ambient for the first 35 minutes of Test 4, as plotted in Figure 166. As module-to-module propagation began within Unit 1 and the interior fire grew to ventilation-limited conditions, heat flux measured outside the garage door increased to 0.3 kW/m^2.

After the C-side door was opened, the influx of air supported further burning and the resultant elevated interior temperature conditions radiated through the garage door to a peak of 12 kW/m^2 measured prior to test termination. Heat flux decreased exponentially as test termination operations suppressed the fire.

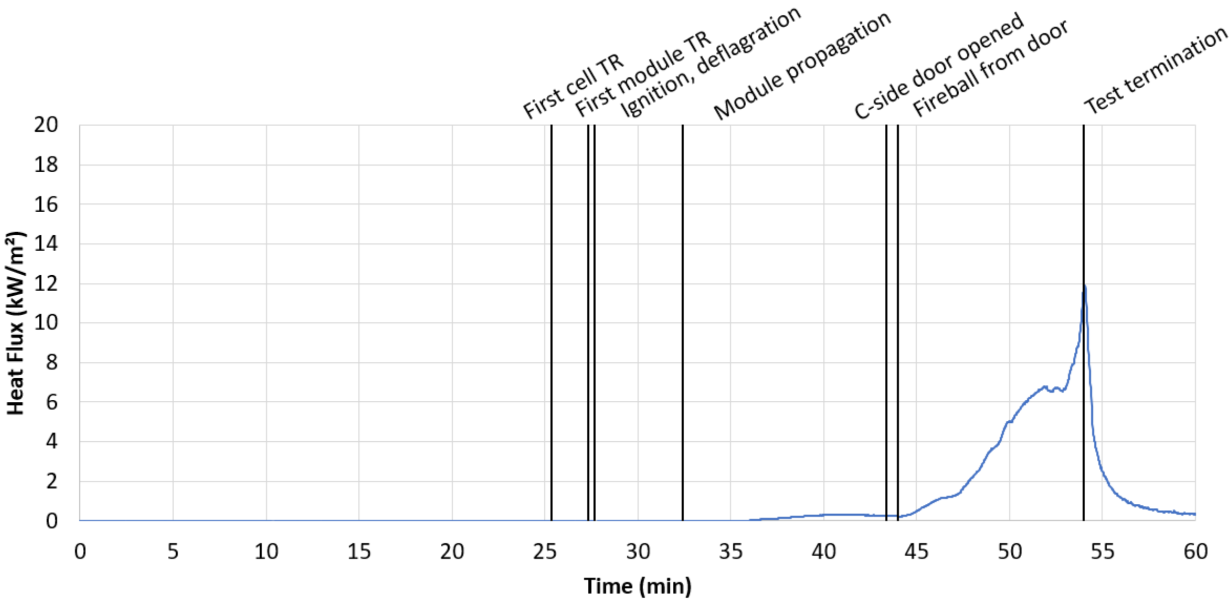

Figure 166 – Heat flux measurement in Test 4.

Gas Measurements

Gas measurements immediately outside the garage door did not deviate from ambient concentrations during the duration of Test 4 as illustrated in Figure 167. The garage door vent was not operated during Test 4, so minimal gas leakage occurred at this location.

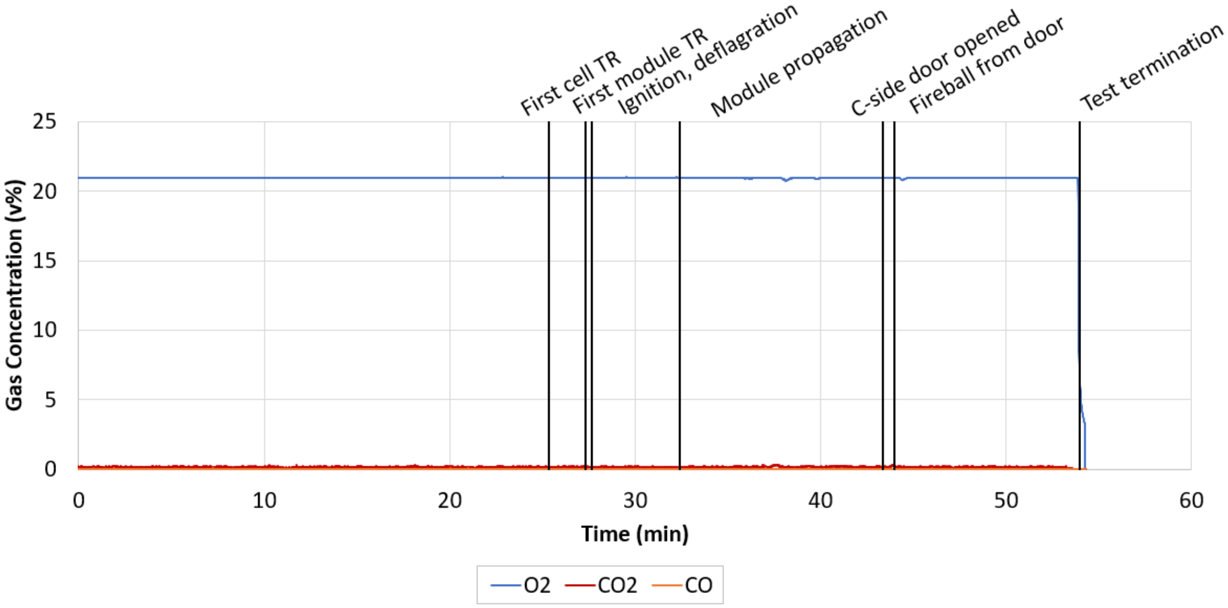

Figure 167 – Exterior gas measurements at the garage door in Test 4.

HF gas was not measured above the low-end calibration limit in Test 4.

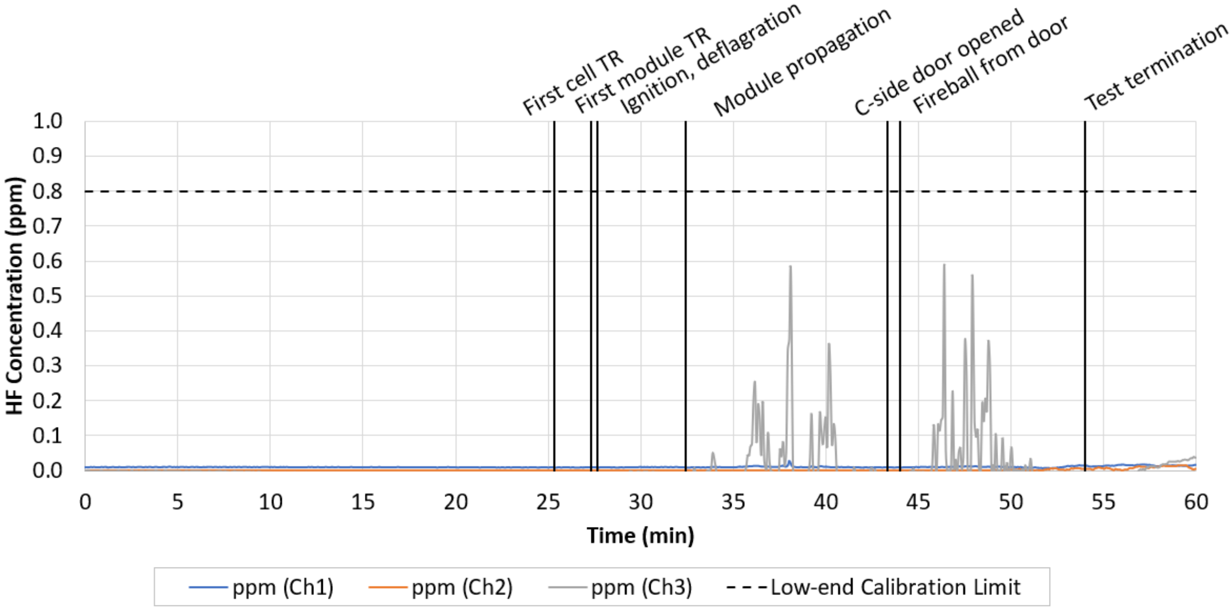

Figure 168 – HF measurements in Test 4.

5.4.5 Size-up Indicators

Visual Indicators

Visual indicators from seven moments of interest are included in Figure 169 through Figure 175. Overall, exterior visuals do not conclusively indicate battery involvement or provide warning of flammable conditions. The introduction of battery gases or battery combustion byproducts did not create a visually distinct signature outside the structure.

Figure 169 illustrates the conditions at peak battery gas accumulation prior to ignition. Interior views that included the ESS, including IR, provide a reliable indication of thermal runaway and identification of the source location. At this moment, no smoke or gas was visible outside the structure from the garage door, B-side door, or C-side door. The IR view of the garage door indicates some heat inside the garage, with a peak of 83 °F. This is within the range of ambient weather conditions for the test day.

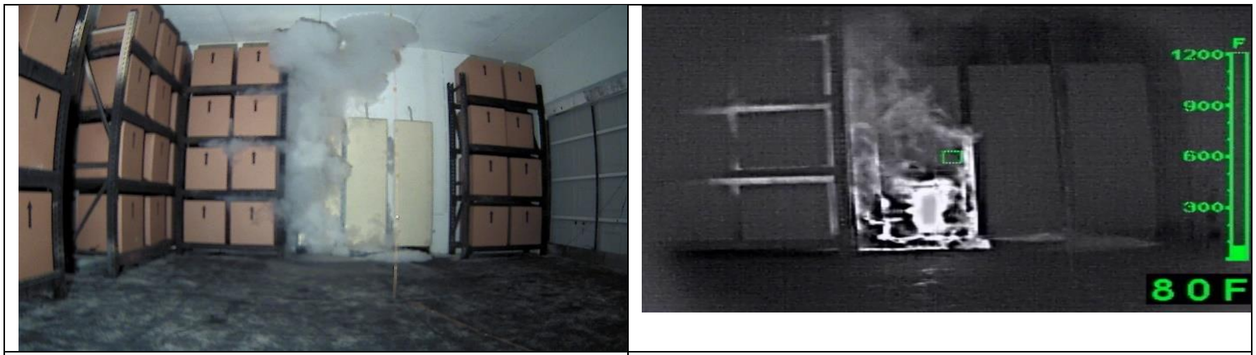

(a) Interior view facing D-wall | **(b) IR view through B-wall facing D-wall**

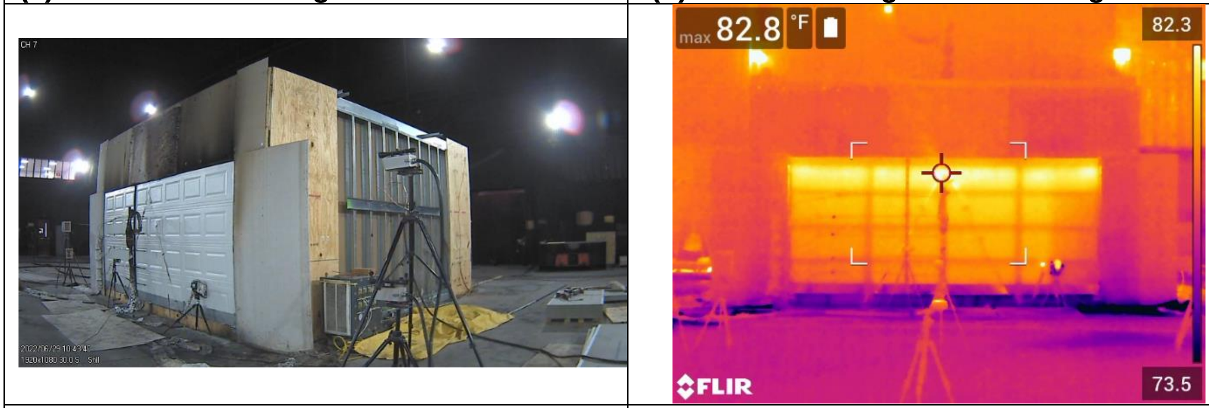

(c) Exterior view from A-D corner | **(d) Exterior IR view of garage door**

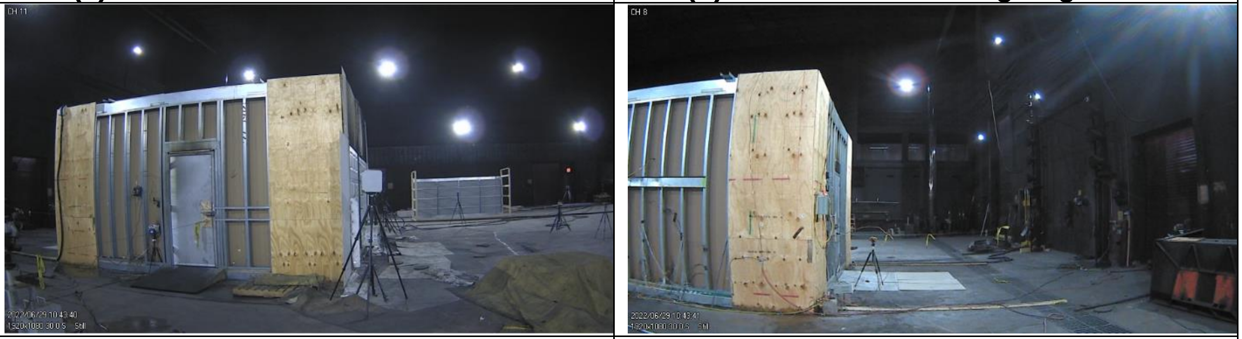

(e) B-side access door | **(f) C-side access door**

Figure 169 – Gas accumulation before ignition (27:40, TR + 02:19).

Figure 170 captured the moment of ignition, 2 seconds after Figure 170. From the interior view, ignition is clear. Similarly, ignition was visible on the D-side wall through a penetration into the structure. It is unlikely that this type of penetration would exist in a residential structure. There were no other external signs of ignition.

(a) Interior view facing D-wall	(b) C-side access door, C-D corner

Figure 170 – Flaming observed at penetrations (27:42, TR + 02:21).

Figure 171 shows different views of the battery fire growth less than one minute after the views in Figure 170. From interior views of the ESS, including the IR view, the presence and location of fire is clear. A smoke layer is developing at the ceiling. This is the first moment where traces of smoke were visible around the garage door external to the structure, as shown in Figure 171(c) and Figure 171(e). Smoke is not visible on the exterior IR view. Heat signature on the exterior IR view is unchanged from the earlier conditions in Figure 105. There is no smoke or gas exiting from the seams around the B-side or C-side doors.

(a) Interior view facing D-wall **(b) IR view through B-wall facing D-wall**

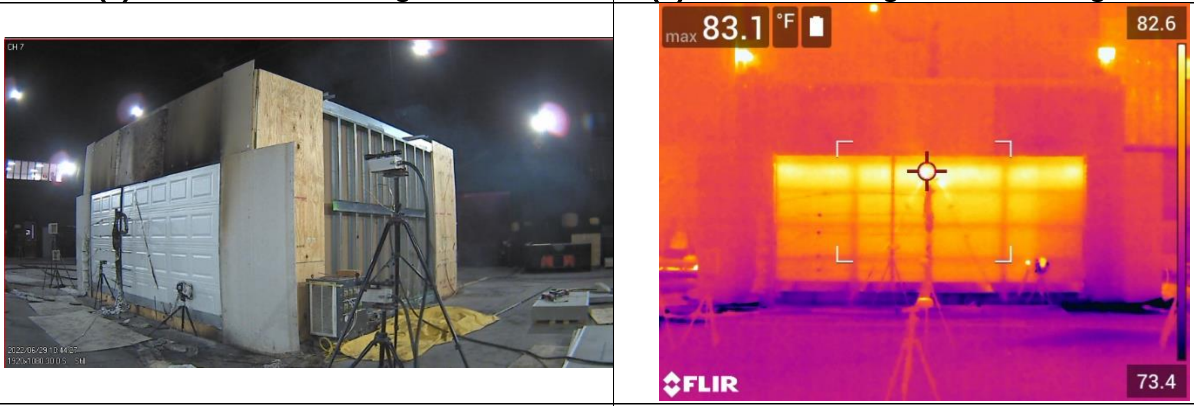

(c) Exterior view from A-D corner **(d) Exterior IR view of garage door**

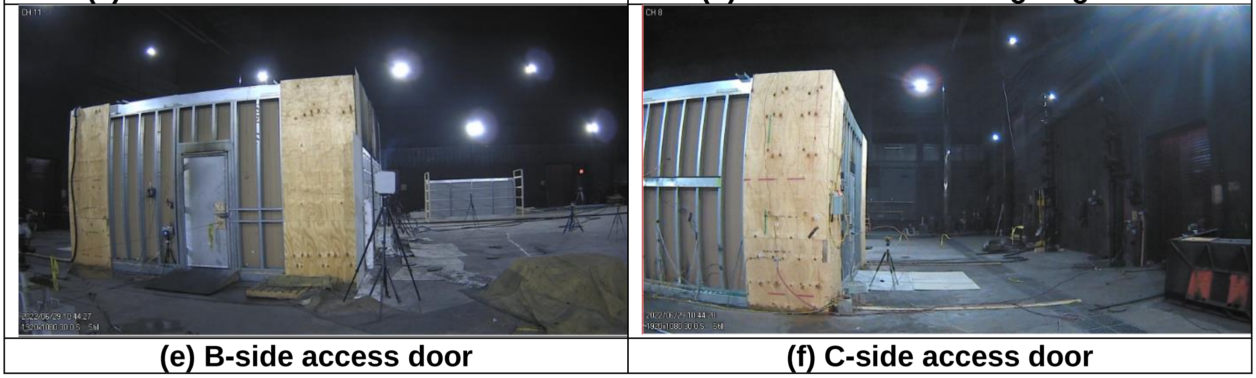

(e) B-side access door **(f) C-side access door**

Figure 171 – Battery fire growth (28:27, TR + 03:06).

Figure 172 illustrates the conditions 4 minutes after Figure 171. At this time, interior views show a stratification of gas and a white vapor cloud behavior that is often associated with battery thermal runaway. The IR interior view does not provide a visual of stratification but does show the location and occurrence of thermal runaway in the ESS, as the ESS is the only item involved in the fire at this time. From the exterior, smoke is visible around the edges of the garage door, as seen in Figure 172(c) and Figure 172(e). The smoke and gas external to the structure is light gray and buoyancy-driven upwards from the structure. Smoke and gas are not visible on the IR view of the garage door. The IR view shows a peak temperature of 102 °F. This is a 19 °F increase from the previous image. Someone watching this IR view would be able to recognize the increase in heat and possible fire inside the garage but would not be able to discern battery involvement. No smoke or gas was observed around the perimeter of the B-side or C-side doors.

(a) Interior view facing D-wall **(b) IR view through B-wall facing D-wall**

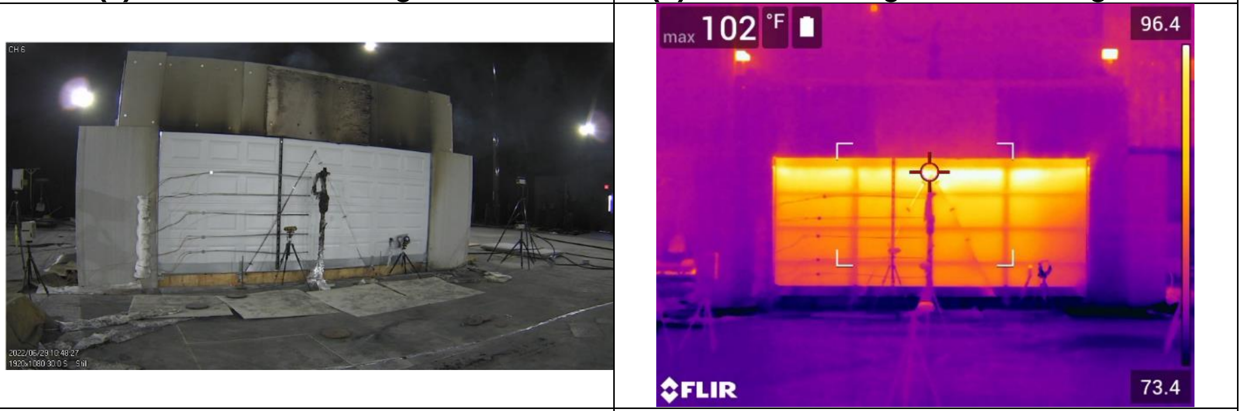

(c) Exterior view from A-D corner **(d) Exterior IR view of garage door**

(e) B-side access door **(f) C-side access door**

Figure 172 – Ignition and gas stratification (32:26, TR + 07:05).

Figure 173 documents the conditions of the garage immediately prior to ventilation of the C-side door, 11 minutes after the conditions of Figure 172. Interior visibility, even on the IR camera, is sufficient only to confirm the presence of heat, fire, and smoke but cannot differentiate the location of any individual objects. Outside the structure, there is significant smoke and gas emitting from the seams of the garage door. This plume is visible on both the standard and IR cameras. There is smoke emitting from the top seam of both the B-side and C-side door. The smoke plumes are light gray and buoyancy-driven upwards. There is no visible signature to confirm or suggest battery involvement at this instance.

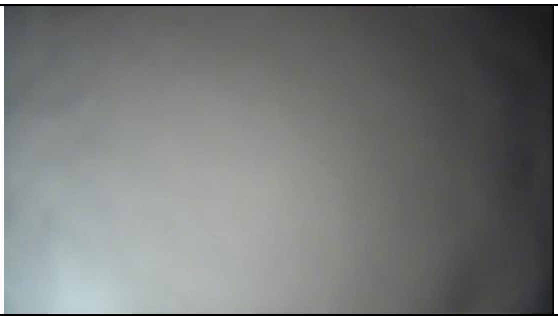	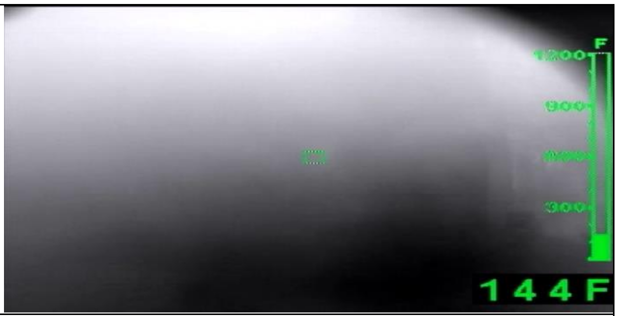
(a) Interior view facing D-wall	**(b) IR view through B-wall facing D-wall**
	
(c) Exterior view from A-D corner	**(d) Interior view facing C-wall**
	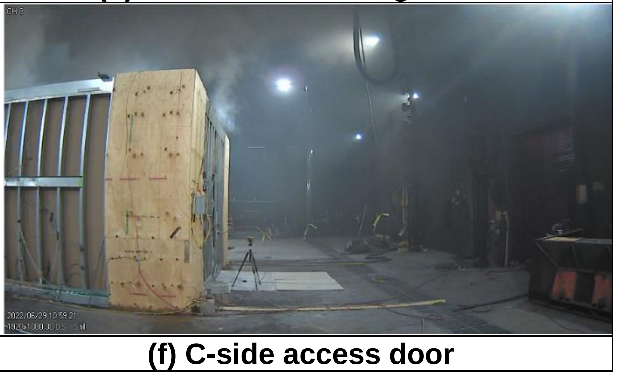
(e) B-side access door	**(f) C-side access door**

Figure 173 – Conditions prior to opening C-side door (43:21, TR + 18:00).

Figure 174 shows the conditions around the garage immediately after the C-side door was ventilated, 2 seconds after the images of Figure 173. The smoke leakage around the garage door continued to be light gray and buoyancy driven, with similar intensity to the previous images. The IR view shows continued smoke emission around the garage door as well as the hot smoke plume extending from the open C-side door. Small amounts of smoke continue to leak from the upper edge of the B-side door. The smoke plumes visible in Figure 174 are consistent with ventilation-limited fire smoke and do not provide specific indication of battery involvement.

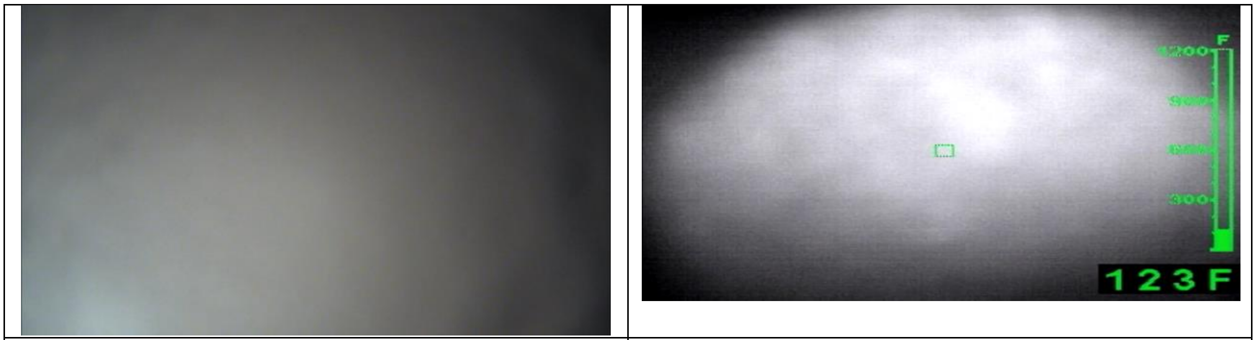

(a) Interior view facing D-wall **(b) IR view through B-wall faing D-wall**

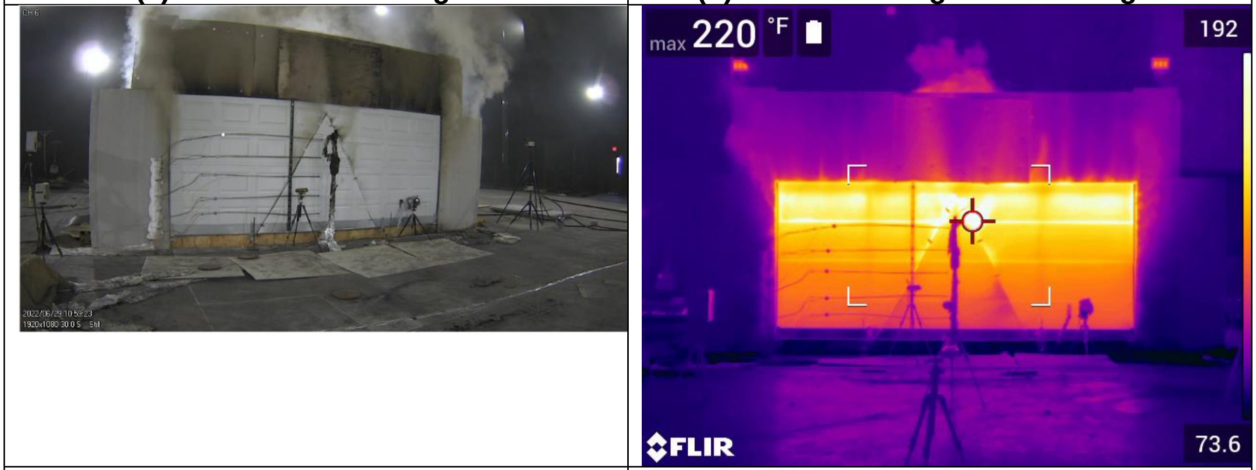

(c) Exterior view from A-D corner **(d) Exterior IR view of garage door**

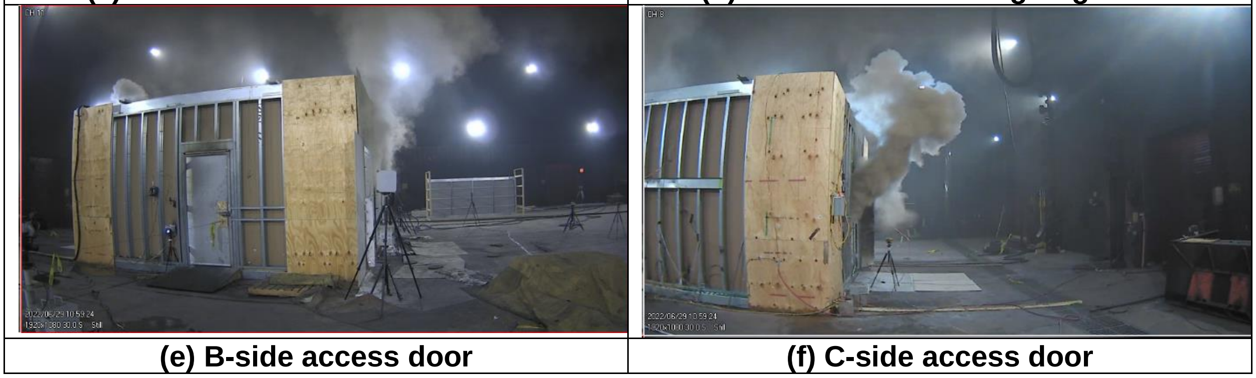

(e) B-side access door **(f) C-side access door**

Figure 174 – Conditions immediately after opening door (43:23, TR + 18:02).

Figure 175 captures images less than one minute after the images of Figure 174. Rapid flame spread generated pressure which pushed gas and flames from the garage moments after these images. Interior IR views were viable again following ventilation of the C-side access door. Ventilation increased visibility by allowing smoke to clear from the structure. IR views show the heat of Unit 1 and the flaming or smoldering condition of the commodity boxes. The smoke showing outside of the structure continued to be light gray in color with increasing plume opacity. Small amounts of smoke were emitted from the top edge of the B-side access door. Smoke plume color and consistency alone do not indicate battery involvement or the flammability of the mixture.

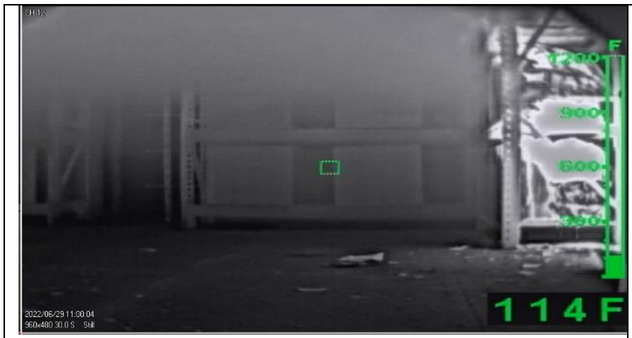

(a) IR view through garage door facing C-wall

(b) IR view through B-wall facing D-wall

(c) Exterior view from A-D corner

(d) Exterior IR view of garage door

(e) B-side access door

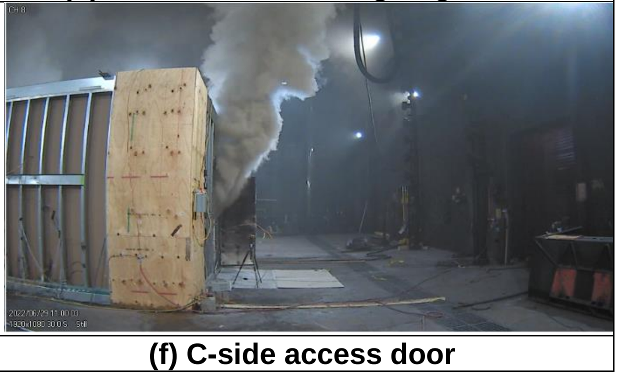

(f) C-side access door

Figure 175 – Conditions prior to backdraft (44:03, TR + 18:42).

Portable Gas Meters

During Test 4, oxygen concentrations remained at ambient for the duration of the test.

Figure 176 - Figure 182 provide gas measurement data from the meters for Test 4.

Carbon monoxide measurements from the four meters indicate that near the garage door, CO concentrations peaked near 225 ppm during a period of activity between the first module propagation and the opening of the C-side door.

The backdraft resulting from opening the C-side door was registered by the C-side door meter, which measured a CO peak of 360 ppm. Test video indicates that the meter was engulfed by the fire plume at this point in time. A 40 ppm increase in CO was also registered at the garage door meter at this time, likely due to the pressurization of the garage during the backdraft.

Up to 8 minutes before and after test suppression, the diffusion of combustion gases into the lab was registered by a steady increase in CO the three pump-driven meters.

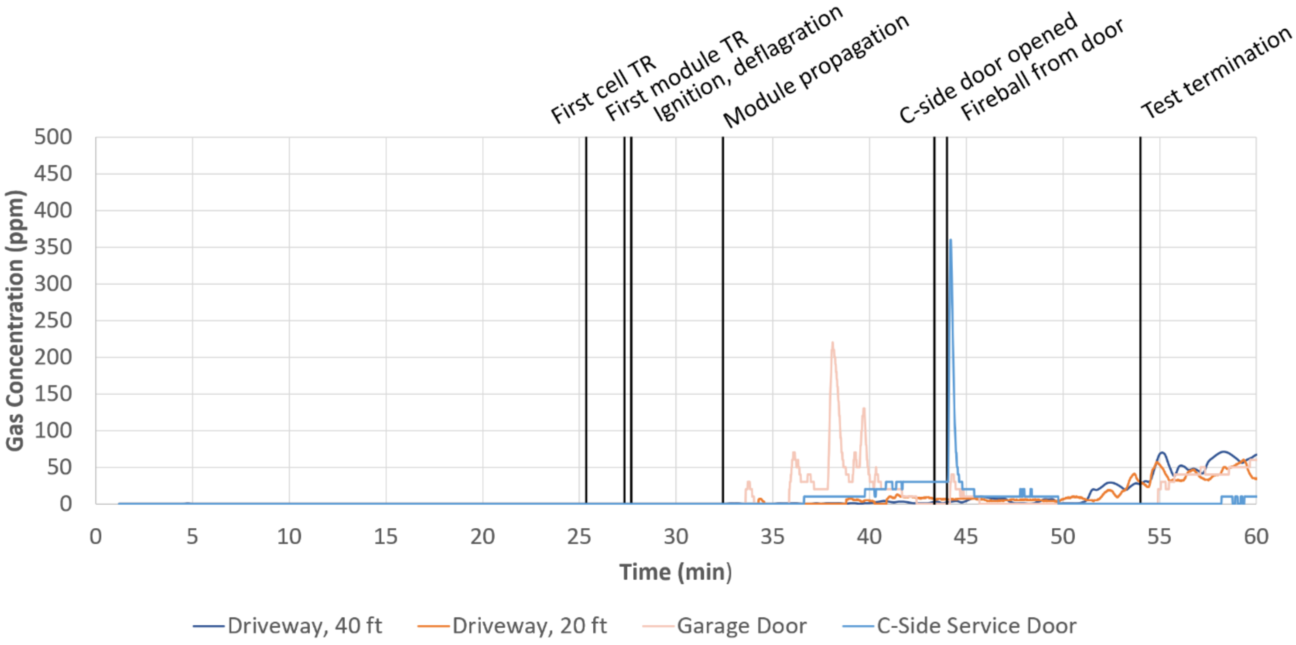

Figure 176 – All CO measurements in Test 4.

At the garage door, the patterns created in the CO measurement by gases puffing from the garage door seams during period of thermal runaway propagation were mirrored in the HCN and VOC measurements (Figure 177 and Figure 178). Peaks of HCN and VOC at 10 ppm and 7 ppm, respectively, were measured during this time. When the backdraft occurred, another set of 5 ppm peaks in HCN and VOC were measured. Similar to the measurements from the previous 10 minutes of test time, these peaks were caused by pressurization of the garage puffing gas from the garage door seams.

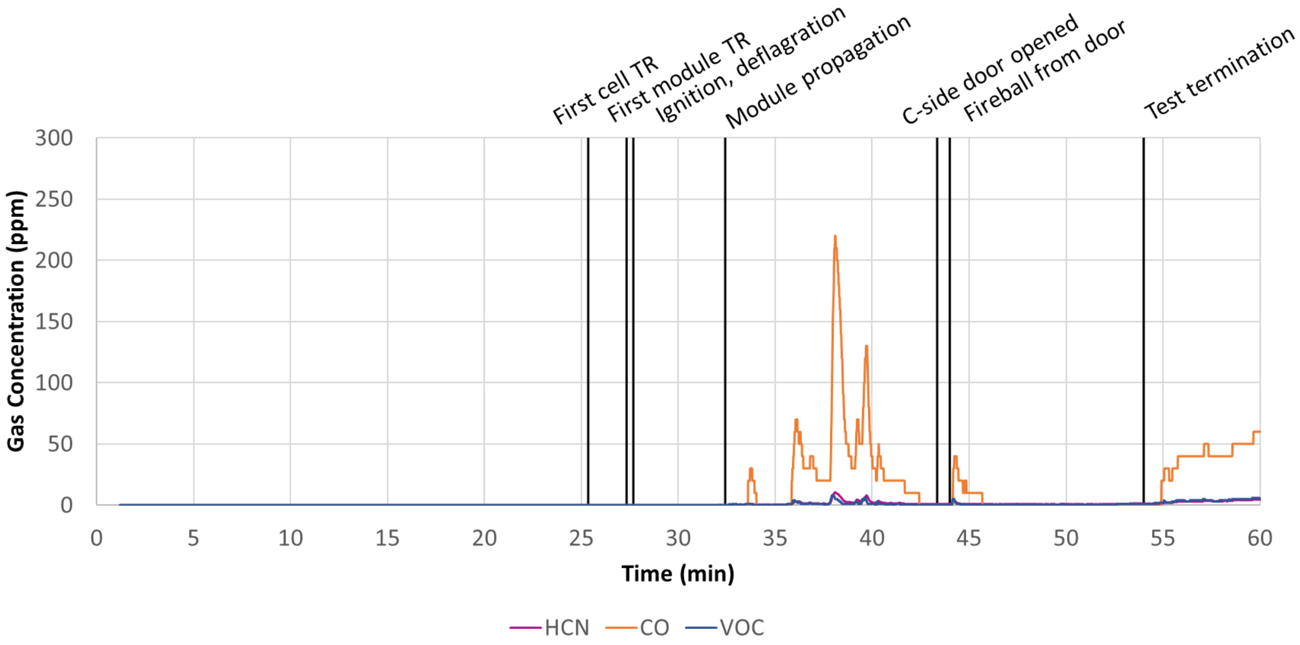

Figure 177 – Measurements at garage door in Test 4 (0-300 ppm).

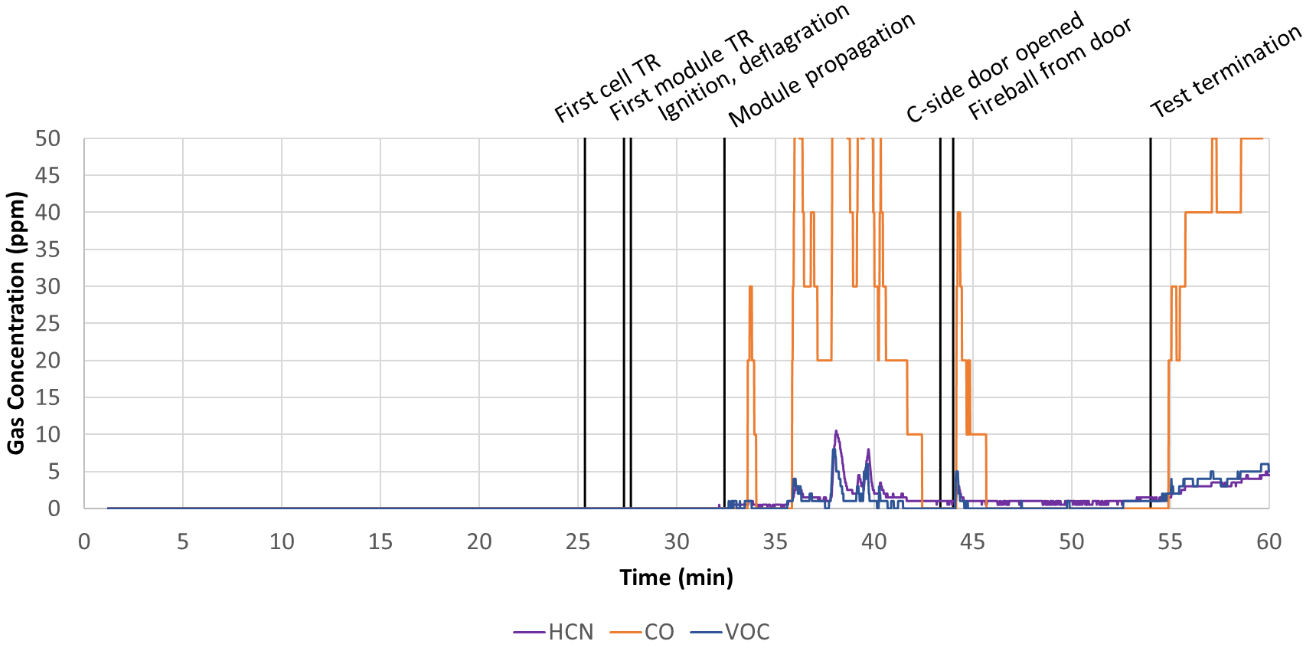

Figure 178 – Measurements at garage door in Test 4 (zoomed in to 0-50 ppm).

At the two meters located at 20 ft and 40 ft along the driveway (Figure 179 and Figure 180), steady increases in CO were registered starting during the time period of thermal runaway propagation in Unit 1 between the ignition and the opening of the C-side door. Within 5 minutes before test termination and after test termination, CO concentrations increased at a higher rate. The two meters registered peak CO concentrations of 60 ppm and 70 ppm, respectively, during the last 10 minutes of test time. HCN measurement in the meter at 20 ft registered a similar pattern to CO, except with a lower peak near 7 ppm. No HCN was registered at the meter at 40 ft.

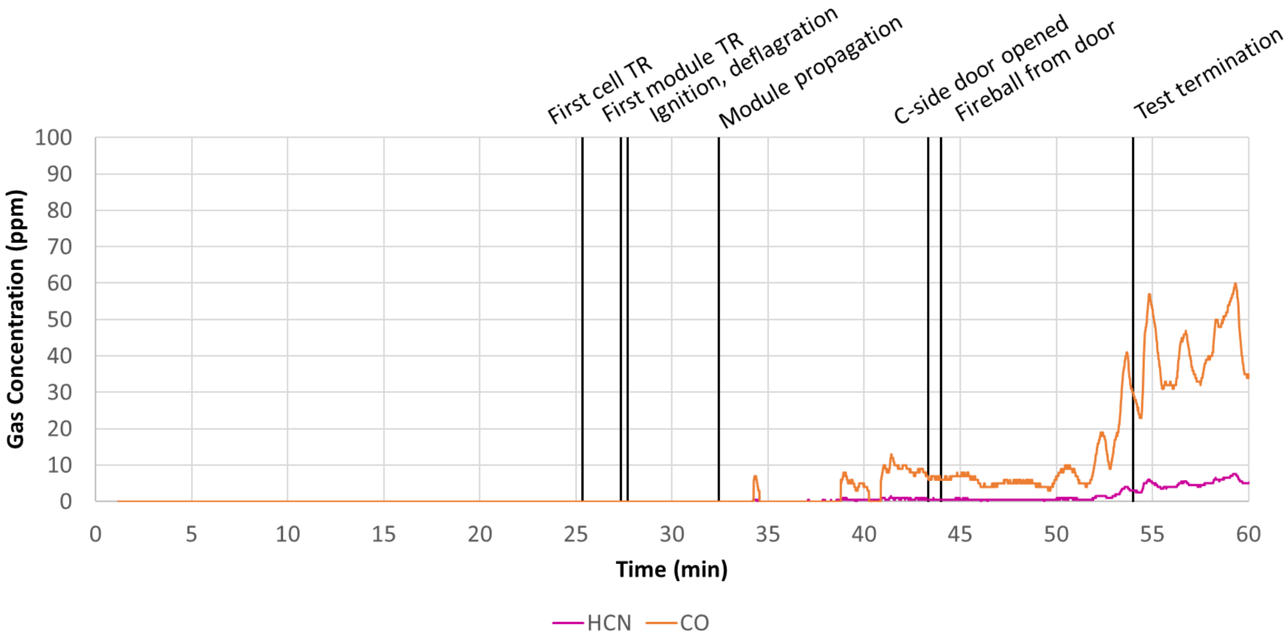

Figure 179 – Measurements at driveway 20 ft location in Test 4.

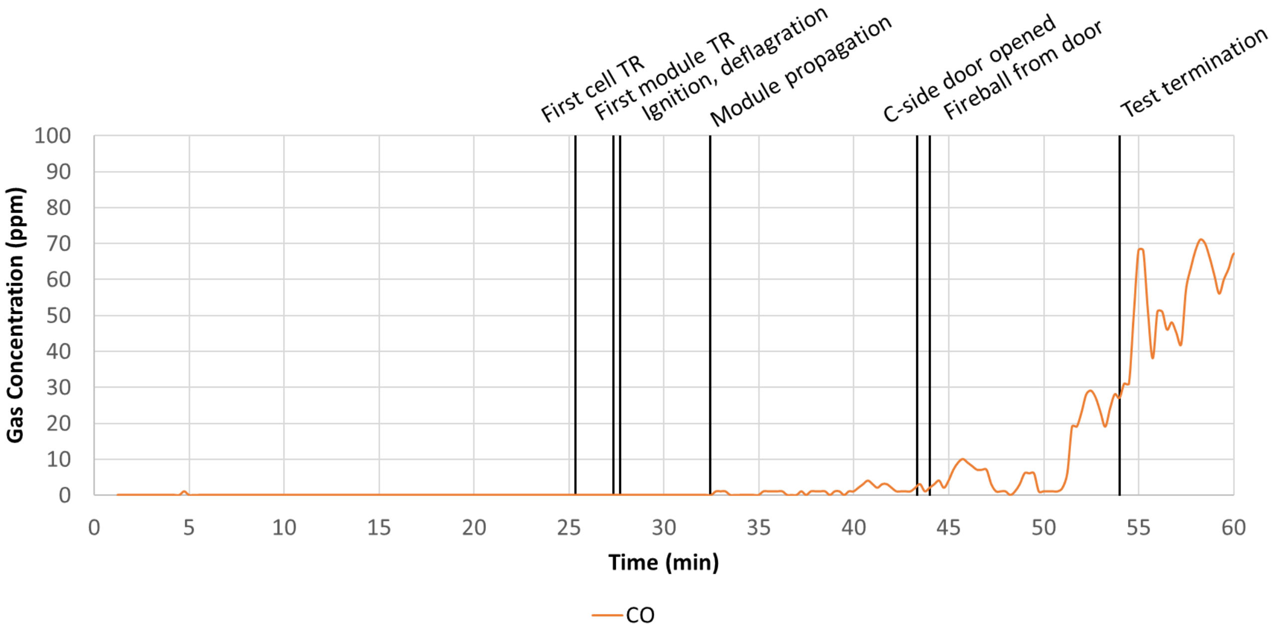

Figure 180 – Measurements at driveway 40 ft location in Test 4.

For approximately 7 minutes prior to the C-side door being opened, gas leakage from the compartment was registered by the CO and hydrogen sensors up to 30 ppm on the meter located outside the C-side door. Due to the cross sensitivity of the H_2 sensor with CO, it is inconclusive as to the fraction of the H_2 spike during the backdraft that was due to CO saturation or the presence of H_2. However, it is known that the thermal runaway effluents from the batteries used in this test contain H_2. The meter registered peaks in CO and H_2 when smoke and flames ejected from the door 40 seconds after the door was opened (Figure 181 and Figure 182). Hydrogen measurement saturated at 80 ppm during this time. For the first 40 seconds after the C-side door was opened and before the backdraft, the meter was not within the influence of the plume per video review. Small peaks of HCN and VOCs, in the range of 5 ppm, were also registered.

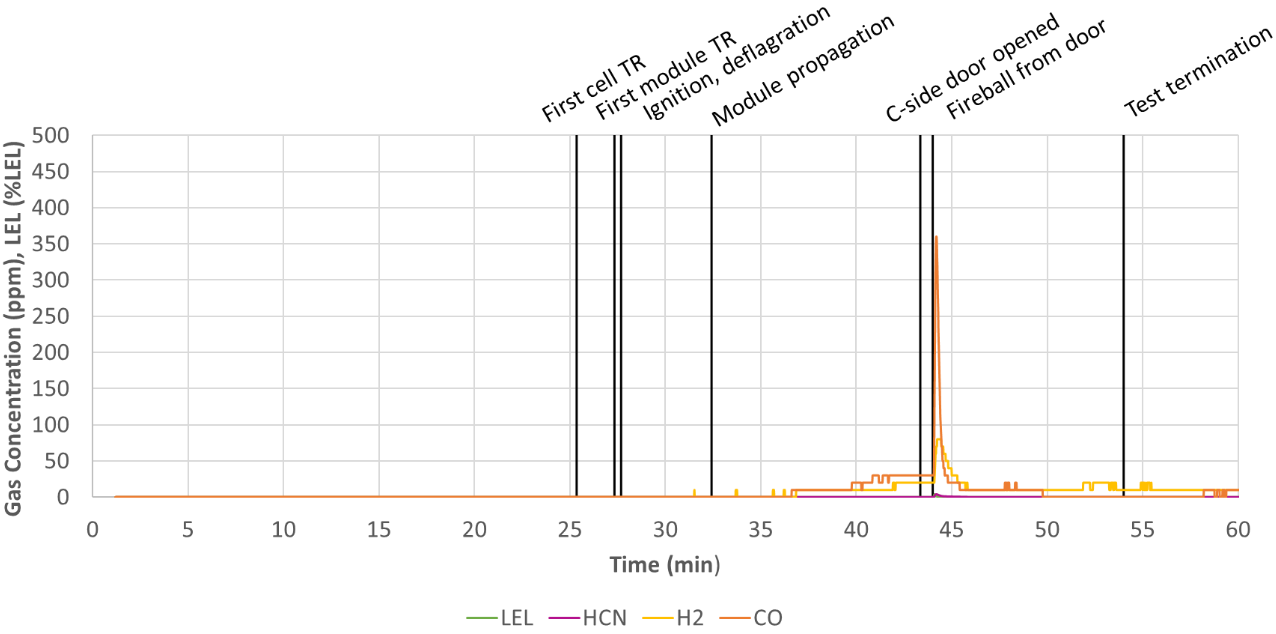

Figure 181 – Measurements at C-side rear door in Test 4.

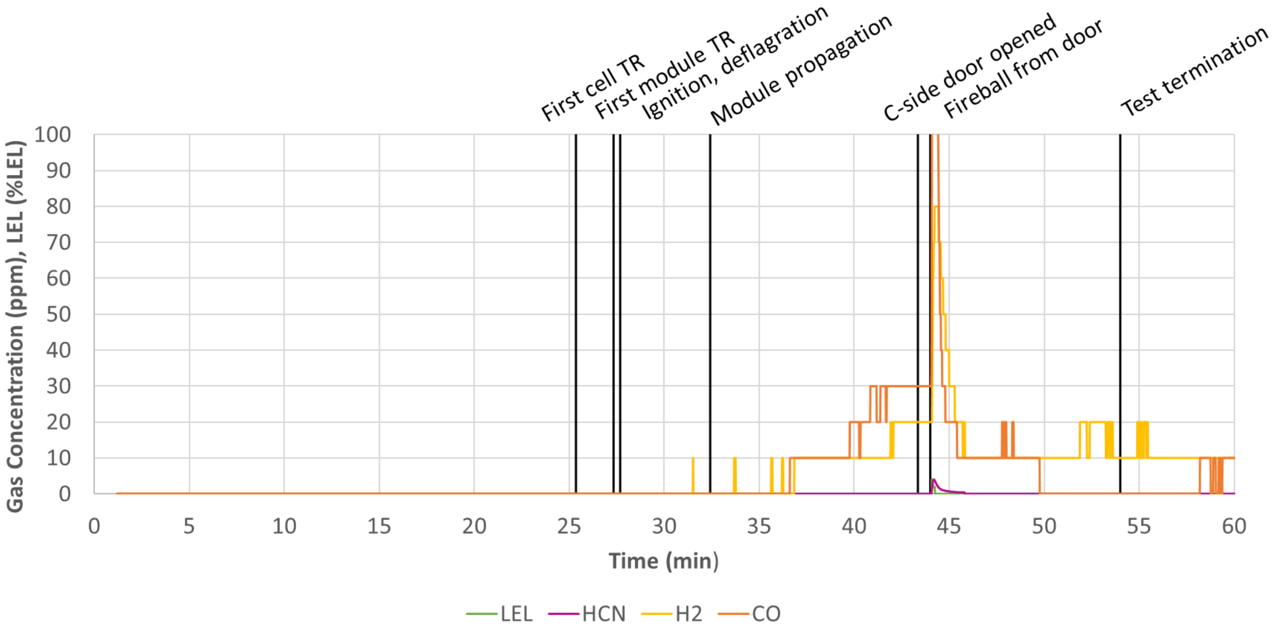

Figure 182 – Measurements at C-side service door in Test 4 (zoomed in).

6 Discussion of Results

The test series results are discussed with a focus on hazards relevant for fire service size-up and tactical considerations.

6.1 Impact of Li-ion Battery Involvement on Fire Growth Rate

Starting from the first thermal runaway, fire growth rates driven by batteries were both faster and slower than the fire growth rate of the Group A commodity alone. This is an important consideration when evaluating the risk from fires that start from li-ion batteries because li-ion battery driven fire growth depends on the rate of thermal runaway propagation, whether the battery gas ignites during thermal runaway, and the ignition of secondary items by the battery.

Rates of thermal runaway propagation are unique from li-ion product to li-ion product and depend on multiple variables. Fire growth of a li-ion product can be slow in products designed to prevent thermal runaway or extremely fast with products without design considerations for preventing thermal runaway propagation. Therefore, a common approach of assuming a t^2 growth rate for a fire cannot be appropriately applied when fires are initiated by a li-ion battery. For the firefighter, this means incipient fires, well-developed fires, and explosion hazards followed by fires should all be considered when responding to li-ion battery-initiated incidents.

In Tests 1 and 3, when the commodity was the first item ignited, the commodity fires caused underventilation of the garage in approximately 5 minutes (5 minutes and 18 seconds, 4 minutes and 34 seconds, respectively).

The fire in Test 2 grew extremely quickly once ignited; although, battery gas vented in Test 2 for over 15 minutes before ignition. Accumulated battery gas burned as it deflagrated over several seconds, which ignited most of the contents in the garage. Prior to ignition, there was no appreciable temperature rise above ambient in the garage due to the ongoing thermal runaways. The ensuing fire reached a ventilation-limited condition within 1 minute, even with additional ventilation introduced when the deflagration partially opened the pre-cut opening in the garage door.

The fire in Test 4 grew more slowly than either Test 1 or Test 3. Battery vent gases were ignited using a gerb once thermal runaway occurred in the initiating module, which caused steady sustained flaming of the ESS unit without any fire growth. Approximately 5 minutes passed before a second module experienced thermal runaway, which increased flaming. The increased flaming caused more rapid progression of thermal runaway propagation through several modules. Three and a half minutes later, or eight and half minutes after the first thermal runaway, the adjacent Group A commodity ignited. Once the battery fire involved nearby combustibles, the fire growth rate was dominated by the Group A commodity.

6.2 Impact of Battery Gas on Smoke Flammability

Test 1 was used as a baseline case to examine whether rotary rescue saw operation could impact the conditions of the fire by igniting smoke venting from the garage. There was no ignition of the accumulated smoke from an under-ventilated fire when the showers of sparks from the two gerbs were activated to simulate rotary rescue saw operation.

Test 2 demonstrated the higher ignition propensity of battery gas compared to the accumulated underventilated fire smoke of Test 1. Thermal runaway propagation in Test 2 resulted in both a significant accumulation of flammable battery gas and an ignition source that caused a deflagration. The deflagration took place before the time when a pyrotechnic was planned to provide an ignition source.

The strength of the ignition source is not known, but some energetic component of thermal runaway (e.g., elevated gas temperature, an ember, an arc, etc.) caused the ignition of the vented battery gas. While the minimum ignition energy (MIE) of the battery vent gas mixture in these experiments has not been measured, the MIEs for hydrogen, CO, methane, and typical hydrocarbons are presented in Table 10. Given these low MIEs, potential ignition sources in residential spaces include appliances (piloted gas-powered equipment, appliances, etc.) garage door openers, and electrical switches, in addition to battery ejecta.

Table 10 – Minimum ignition energies [38].

Gas	Minimum Ignition Energy (mJ)
Hydrogen (H_2)	0.03
Carbon monoxide (CO)	<0.3
Methane (CH_4)	0.71
Ethylene (C_2H_4)	0.114
Propane (C_3H_8)	0.5
Butane (C_4H_{10})	0.25

Test 1 showed that simulated rotary rescue saw operation is unlikely to ignite the smoke from a ventilation-limited fire. By contrast, Test 3 demonstrated that the unburned battery gas from li-ion thermal runaway can increase the ignition propensity of the hot gas layer and the smoke of a ventilation-limited fire. The smoke exhausting from the garage vent kerfs ignited immediately upon contact with the pyrotechnic sparks used to simulating rotary rescue saw operation in Test 3.

Test 4 also demonstrated an increase in the flammability of the hot gas layer. When the C-side door was opened, ambient air exchanged with smoke from the garage for 40 seconds. During this time, a flammable mixture formed between the hot gases in the compartment and the incoming gravity current of cooler outside air, resulting in a backdraft. The backdraft vented smoke and fire through the full height of the doorway. This lasted for approximately 5 seconds.

6.3 Impact of Ventilation

Given the flammability of the gas mixture, as discussed in Section 6.1, the impact of ventilation operations and influx of fresh air is critical because the interior environment may experience a deflagration or a rapid transition to flashover.

The smoke in Test 3 immediately ignited during simulated vent operations when the smoke contacted the simulated saw sparks. This is atypical for ventilation-limited fires, particularly for such low gas temperatures (< 300 °C). In Test 1, external flaming was not observed until gas temperatures exceeded 300 °C and only after 12 minutes of fire growth after the vent was fully opened. In contrast, the fire immediately grew once the garage door was vented during Test 3. Further, from the beginning of the vent operation until approximately 40 seconds after the end of vent operation, gases vented unidirectionally out from the opening and burned. There was no exchange of outside air into the compartment.

Experiments conducted by UL in 2020 [39] in a simulated walk-in containerized li-ion energy storage system also demonstrated a rapid increase in flaming in similar conditions. Accumulated battery gases in one experiment caused a rapid transition to flashover within 20 seconds of ventilation of the container door.

Test 4 demonstrated the potential for a deflagration or backdraft in response to ventilating a ventilation-limited garage fire involving li-ion thermal runaways. Conditions were similar to those at the time of vent operation in Test 3; gas temperatures were below 200 °C. Approximately 40 seconds after simulating the opening of the door between the house and garage, adequate exchange of ambient air and mixing cause ignition of the smoke inside the garage. The pressure rise from the backdraft in the garage caused fire to eject through the full height of the doorway for a duration of approximately 5 seconds. Under similar conditions, although without any active burning, a change in ventilation associated with opening a door to an ESS in Surprise, Ariz., led to the explosion of the ESS [40].

In contrast to a rapid increase in flaming seen in Test 3, and the deflagration observed in Test 4, the ventilation of the garage door in Test 1 resulted in a comparably slow increase in fire size.

6.4 Deflagration Hazards

Flammable gases released by thermal runaways can create explosion hazards. Three different types of deflagration scenario can develop when thermal runaway propagation occurs in an ESS installed in a garage:

1. *Partial volume deflagration* - Thermal runaway propagation releases a sufficient volume of unignited flammable battery gas to form a flammable battery gas and air mixture in a volume around the ESS unit, resulting in a deflagration when a viable ignition source is introduced.
2. *Full volume deflagration* - Thermal runaway propagation releases a sufficient volume of unignited flammable battery gas to form a flammable battery gas and air

mixture in the entire volume of the structure, resulting in a deflagration when a viable ignition source is introduced.

3. *Backdraft* - Thermal runaways occur during (and potentially as a result of) a vent-limited room and contents fire and contribute a sufficient volume of unignited flammable battery gases to the hot gas layer, resulting in a deflagration, when ambient air mixes into the room following a change in ventilation. The ignition source is presumably the fire.

Regardless of which scenario produced the explosion potential, all three scenarios can produce hazards of flaming and projectiles (e.g., glass fragments, metal, wood).

The first deflagration scenario was demonstrated in Tests 2 and 4: partial volume deflagration.

In Test 2, thermal runaway propagated through approximately 70% of the initiating unit before the accumulating gases were ignited by a spark or heat from the thermal runaways. Two estimates of the gas accumulation in the garage are possible with the available data. Based on the estimate that 70% of the module experienced thermal runaway, and that each module released 213 L of gas each as calculated using the cell gas release volume from Table 2, then approximately 7,200 L of gas was released into the garage. This corresponds to a concentration of 6.3 v% assuming the gases and room air are well-mixed, which is 71 % of the LFL for the battery gas mixture.

Second, battery gas volume can be estimated from the gas concentrations measured at the ceiling at the time of ignition if it is assumed that the 15-minute period of thermal runaways provided enough time for mixing with room air. Table 11 shows that estimated battery gas volumes between 1000 L to 2000 L[4] were released, corresponding to 10 to 20% of the LFL assuming the garage is well-mixed.

Table 11 – Estimated battery gas volume in garage at ignition based on gas concentration measurements.

Species	Concentration at Ignition [v%]	Battery Gas Mixture Species Concentrations [v%]	Extrapolated Battery Gas Concentration [v%]	Estimated Battery Gas Volume [L]
CO	0.6	36.2	1.7	1877
CO_2	0.2	22.1	0.9	1025
THC	0.6	10	6.0	6796
O_2	0.2	-	1.0	1081

---

[4] The estimate using THC appears high because the FID was calibrated using propane. Hydrocarbons with more than 3 carbon atoms likely caused an over-counting of THC concentration.

Differences in the estimates based on the first and second approach are likely because leakage was not negligible and uniformly well-mixed is not an appropriate assumption for the gas concentration in garage.

Given these two estimates of release volume, the deflagration in Test 2 must have been a partial volume deflagration. The battery gas release volume was not large enough to exceed the LFL and create a full volume deflagration hazard even with the well-mixed and zero leakage assumptions. The measured gas concentration demonstrates that the actual battery gas concentration at the ceiling was lower than some region around the ESS unit, where the gas concentration was between the flammability limits. The long duration of the total gas release enabled the gas to disperse across the room. Therefore, much of the gas in the room is likely below the LFL and does not participate in the deflagration.

As part of the test design, the garage door vent also blew out during the deflagration at an unknown pressure without also operating the entire garage door as a deflagration vent. The whole garage door was designed as a deflagration vent to operate at 1 kPa. Because only the inner vent partially opened and the whole door remained attached, it is assumed that the pressure rise did not exceed 1 kPa due to venting. Therefore, there is no means to quantify the explosion hazard using typical hand calculations. However, Test 2 demonstrated that a partial volume deflagration can create significant projectile, heat and toxicity hazards to firefighters in the driveway.

Test 2 demonstrated that, while unlikely to occur, a full-volume deflagration may be possible with complete thermal runaway propagation before ignition if there was little to no leakage from the garage. A conservative estimation of the maximum amount of gas that could be developed from the custom ESS used in this project is 10,224 L, which would result in a well-mixed battery gas concentration of 9.0 v%, which is above the LFL for the garage by 0.1 v%. Test 2 also demonstrates that the severity of a deflagration hazard may be heavily dependent on timing and that the timing itself can be unpredictable.

Early in Test 4, a partial volume deflagration was confirmed visually from interior video camera views. A pyrotechnic was used to ignite the gases that exhausted from the initiating unit at the completion of thermal runaways in the initiating module. Unlike in Test 2, the battery gas had only mixed with air in a local volume around the ESS unit, so the corresponding battery gas measurements at the ceiling at the time of ignition were negligible. Based on the former method applied to the estimation of battery gas release from Test 2, it is estimated that 213 L of gas was released in Test 4 up until the time of ignition (i.e., the gerb was operated immediately after 1 complete module thermal runaway).

The Adiabatic Mixing Explosion Model (AMEM) created by Ogle [41] can be used to quantify the explosion hazards for the gas release volume estimated for Test 4. A conservative estimate of the maximum pressure that could be developed in the garage was calculated to be 3 kPa (0.44 psig). The calculation assumes the constant volume burning of all the battery gas followed by adiabatic mixing of the burned gas with the surrounding air.

Table 12 shows that an AMEM calculated pressure of 3 kPa roughly corresponds to a level of damage where windows could be shattered. The construction of the test structure makes it difficult to estimate the actual pressure developed during the deflagration, but it is estimated to be less than or equal to 1 kPa since there was permanent deformation in the garage door and several explosion venting fasteners were found to have operated in the overall garage door construction. Given that 1 kPa was developed from 0.4 kWh worth of li-ion battery, it is reasonable that the thermal runaway propagation of several modules could produce enough flammable gas to detach a garage door (7 – 15 kPa) or cause structural damage (15 – 20 kPa).

The maximum extent of possible explosion hazard is not clear, since the AMEM calculation tends to be conservative and many variables ultimately influence explosion severity (e.g., release volume, mixing with air, ignition location, turbulence, combustion efficiency, etc.). Further experiments should be conducted to better understand the potential explosion severity of different battery gas release scenarios in a test structure more representative of typical residential construction.

Table 12 – Pressure damage thresholds [42].

Pressure (kPa)	Damage Description
3.5-7	Small and large windows usually shattered
7-15	Wood and aluminum panel fasteners fail; panels buckle or blow out
15-20	Unreinforced concrete and cinderblock walls shattered
20	Steel frame buildings distorted and pulled away from foundations
20-28	Self-framing steel panel building demolished
35-50	Nearly complete destruction of houses

The third deflagration scenario was also demonstrated in Test 4: deflagration during a ventilation-limited fire.

After the early partial volume deflagration, the ensuing propagation of thermal runaway and flaming caused the ignition of the Group A commodity and a ventilation-limited fire. As was shown in the Test 4 results summary, thermal runaways continued to occur while the fire was ventilation-limited, which added flammable battery gases to the hot gas layer. When the C-side door was opened, laboratory ambient air exchanged bi-directionally with smoke from the garage. After 40 seconds, enough oxygen had mixed within the garage to create a flammable mixture. A deflagration front visible within an internal IR camera moved throughout the compartment and at the same time, fire ejected through the full height of the open door. Given that the whole garage door deflagration vent did not operate, pressure generated did not exceed 1 kPa.

6.5 Visual Indications of Li-Ion Battery Involvement in Fire

Distinct visual characteristics can identify battery gas accumulation within an enclosed space if there is visibility into the interior of the space. In Tests 2 and 4, there was a clear accumulation of a whitish gray denser-than-air layer at the floor and an accumulation of whitish gray lighter-than-air gas layer at the ceiling. This was more evident in Test 2 than in Test 4, as more battery gas was released in Test 2 before self-ignition. However, this two-layer condition lasted in Test 4 after ignition until all visibility was lost due to the fire producing smoke. Such visual conditions as in Test 2, or in Test 4 prior to the ignition, represent an immediate risk of ignition followed by flash fire and/or deflagration.

In Test 4, the battery gas release was ignited after one module experienced thermal runaway which resulted in a partial volume deflagration. There were no exterior indicators of thermal runaway visible at the time of ignition.

In Test 2, battery gas also accumulated within the garage in a sufficient quantity to cause a partial volume deflagration hazard before any gases could be observed outside the structure. However, gas accumulation continued for more than 15 minutes without ignition. During this time the heavier vapors within the battery gas spread radially out from the garage low to the ground as it leaked from around the seams of the garage door, while other gases remained neutrally buoyant and “hung in vapor clouds”. This is likely driven by the densities of the different species comprising the battery gas at ambient temperature, as the thermal runaways did not produce enough heat to drive movement of the battery gas via buoyancy. However, it is important to consider that wind velocity and direction could significantly impact these characteristics as exterior visual indicators. Under wind-driven conditions, this indicator may appear as steam, ventilation-limited fire smoke, or may not appear visible around a structure at all.

There are no reliable visual indicators of thermal runaway during an active compartment fire. The temperatures imparted by the fire plume negate the observable buoyancy behavior of the battery gas. The soot from the burning of ordinary combustible material conceals the recognizable lighter color of the thermal runaway effluent.

Intermittent and irregularly timed “puffing” behavior, where smoke and gases vented from seams in the garage envelope under pressure, could be observed under repeated scrutiny during video review of Tests 3 and 4 when there was propagation of thermal runaway either before or during a fire in the garage. This was suspected during the administration of the test but was difficult to verify real-time even under laboratory conditions. It was more difficult to observe this phenomenon using the IR cameras than it was to observe it directly with the naked eye. Large cells in thermal runaway, or very rapid propagation of thermal runaway may consistently produce enough volume to visibly pressurize the garage. However, it is not feasible that enough attention can be paid to smoke puffing behavior on a busy fireground for this characteristic to be identified reliably. As with the observation of unburned battery gas, other on-scene factors such as terrain, wind velocity and wind direction may also complicate evaluation of puffing behavior. This visual should not be relied upon, but should intermittent puffing at irregular intervals be observed, this may indicate the propagation of thermal runaway through cells in a li-ion battery.

6.6 Detection of Thermal Runaways with Portable Gas Meters

Table 13 shows the gas concentrations measured by the portable gas meters in Tests 1 – 4. When comparing peak gas concentrations from the test with no batteries (Test 1), against the three tests with batteries (Tests 2-4), there are no uniquely high gas concentrations that indicate the presence of batteries in thermal runaway prior to either the simulated fire department venting of the garage door in Tests 3 and 4 or the deflagration in Test 2. In other words, the peak gas concentrations observed from the fire with no batteries (Test 1) were similar to the peak gas concentrations from when there was effluent accumulating from batteries in thermal runaway with no fire (Test 2), and when many batteries (12 or more modules) entered thermal runaway during a fire (Test 4). Furthermore, while the sensors in the portable gas meters gave a constant zero signal with no discernable noise (according to the meter output) when the ambient air was known to be clear of smoke and gases, the measured concentrations of HCN and VOCs were at the bottom of the detection limit for the sensors and may not be accurate measurements.

Compared with other measurement locations, gas concentrations were always the highest near the garage door. As was demonstrated in Test 2, the area near the garage door is a dangerous location to collect gas measurements with a portable gas meter due to the potential for a deflagration hazard.

Table 13 – Gas concentrations measured at the time of venting or deflagration (Test 2), and the peak gas concentration measured prior to that time in parentheses.

Gas Species	Test 1 (t=vent) [ppm]	Test 2 (t=deflagration) [ppm]	Test 3 (t=vent) [ppm]	Test 4 (t=vent) [ppm]
CO	0 (140)	60 (170)	20 (30)	0 (225)
LEL	0 (0)	0 (0)	0 (0)	0 (0)[5]
HCN	1.5 (9)	2 (5)	2 (2)	1 (10.5)
VOC	0 (5)	2 (24)	3 (5)	0 (8)

---

[5] The meter with the LEL measurement was located at the C-side door during Test 4.

6.7 Detection of Residential Explosion Hazards

Detection of a potential explosion hazard is not possible in residential garages based on the current requirements for detection equipment in the codes. There are no code provisions in North America that require the installation of devices capable of detecting the explosion hazard exhibited in Test 2. The U.S. Fire Administration recommends [43] that heat alarms be installed in garages, and code provisions for heat alarms have been debated in California [44]. The conditions in Test 2 demonstrated that there would not likely be a detectable rise in temperature prior to a deflagration. However, a heat alarm would likely operate and provide valuable warning time should a fire start in the contents of a garage, or if an ESS in thermal runaway ignited upon thermal runaway or before an explosion hazard could develop.

Smoke, CO, and H_2 detection is not required by codes to be installed in garages, nor are they viable means of detection. It is well understood that the operation of vehicles and equipment in the garage can cause nuisance alarms with these detection technologies. Subsequently, thermal runaway off gassing incidents are not likely to be detected by typical fire detection equipment within the habitable space of the home and may also not be detected by home occupants until after gas ignition, as occurred in an EV thermal runaway in Montreal, Canada in 2019 [45], [46] and Erie, Colorado, USA in 2023 [26].

Combustible gas detectors may be a viable means of thermal runaway early warning in garages. In 2020, NFPA published NFPA 715: Standard for the Installation of Fuel Gases Detection and Warning Equipment [47] based on a 2018 request from the American Gas Association for an installation standard for combustible gas detectors [48]. Research is needed to determine the most effective technologies, appropriate locations for detecting battery gases from residential ESS, and possible nuisance activation issues. However, residential gas detectors, which typically alarm in the range of 10 v% to 25 v% of LFL for hydrocarbon gases [49], may be a viable technology for providing homeowners with an early warning for evacuation.

Battery management systems within ESS products may have the capability to detect thermal runaways as they occur and possibly even provide advanced warning. However, the fire codes and standards community has not accepted BMS signal outputs to alarm equipment because BMS and its associated sensors are not currently evaluated for their reliability in the same way as fire detection and alarm equipment. Further, ESS fire incidents have been previously attributed to BMS failures, and so BMS are often characterized by the fire codes and standards community as a single point of failure.

6.8 Detection of Hydrogen Fluoride (HF)

In all four tests, HF was not measured above the minimum detection limit of the TDLAS, 0.8 ppm, in the driveway area exterior to the garage. Given the path dependent nature of the measurements, these measurements considered an average concentration across the width of the driveway between the instrument's emitters and receivers, which were installed across the representative driveway. This low-end calibration limit is below the critical concentrations for exposure limits, as shown in Table 14.

Though the hydrogen fluoride concentration was below the calibration limit of the instrument as well as below any of the cited exposure limits, SCBA respiratory protection is essential due to the potential for other toxic combustion byproducts, particularly carbon monoxide, as well as the potential for deflagration or rapid fire growth conditions.

Table 14 – Concentration thresholds for HF

Metric	Concentration	Source
OSHA Permissible Exposure Limit (PEL)	3 ppm Time-Weighted Average (TWA)	[50]
NRC Emergency Exposure Limits (EEL)	60-minute: 8 ppm 30-minute: 10 ppm 10-minute: 20 ppm	[50]
Immediately Dangerous to Life and Health (IDLH)	30 ppm	[50]

7 Fire Service Size-Up and Tactical Considerations

This research project was intended to evaluate the impact of lithium-ion residential energy storage systems as a source of a fire or explosion hazard, or when they become involved in a room and contents fire. However, other products (e.g., electric vehicles, micro mobility devices) may contain quantities of li-ion cells sufficient for impacting fire and explosion hazards in the same manner. The following considerations may be applicable to those battery devices, though the specific features and constraints of these other scenarios were not included in the test program design. It should be recognized that these considerations are not a complete set of recommendations for responding to garage fires. Given the tendency of garages to act as a storage area and chemical inventory for homeowners, the considerations from this research are intended to augment tactical considerations for other hazards that may be present in residential garages.

A. When li-ion batteries undergo thermal runway without burning, an explosion hazard begins to develop. The timing of a battery gas explosion is unpredictable. The severity of a battery gas explosion is dependent on gas quantity.

If thermal runaway occurs and releases unburned battery gas, an explosion hazard from a partial volume deflagration begins to develop. The severity of the potential explosion hazard increases as thermal runaway propagation continues without flaming.

24:01 (TR + 03:31)

25:13 (TR + 04:43)

26:22 (TR + 05:52)

29:43 (TR + 09:13)

30:50 (TR + 10:20)

36:34 (TR + 16:04)

Figure 183 – Increasing explosion hazard with ongoing thermal runaway propagation.

Test 2 demonstrated that thermal runaway propagation in a lithium-ion battery produces both an adequate quantity of gas to create an explosion hazard and several types of ignition sources with adequate energy to ignite the released gas. Imagery from the thermal imaging camera showed the ejection of sparks from the ESS unit. Temperature measurements inside the ESS unit gases venting at temperatures above the autoignition temperature of the battery gas components [51] and likewise, the metal surfaces of the ESS unit may have been heated enough by the cells in thermal runaway to act as an ignition source.

Whether ignition occurs ultimately depends on an ignition source being present in a region where the battery gas is within its flammability limits. Given an ongoing release of battery gas and the constant production of viable ignition sources, it should be assumed that an ignition will eventually occur.

When the batteries ignited in Test 2, the accumulated gas produced a partial volume deflagration. The ongoing release of white/gray battery gas followed by a deflagration are the same conditions that caused an explosion of a battery energy storage system in Surprise, AZ [40] and more recently, a residential garage explosion in Erie, CO [26]. The buildup of gases and deflagrations were also observed several times in experiments conducted by UL in 2020 [39].

Many factors beyond the volume of the gas release also determine explosion severity, such as the how well the gas mixes with room air, the room volume, turbulence, ignition source strength, and the flammability properties of the battery gas. Based on how the test structure was built, the partial volume deflagration in Test 4 created less than 1 kPa or it would have otherwise ruptured the garage door. However, conservative hand calculations suggest up to a maximum of 3 kPa could have been developed, which is enough pressure to shatter windows.

The development of a partial volume deflagration hazard was observed several times in a series of 3 experiments run by UL in 2020 to examine the hazards of thermal runaways in walk-in containerized li-ion ESS [39]. The volume of the container was approximately the same as a 1-car garage. In the first experiment, the batteries in thermal runaway released and ignited a similar volume of battery gas to Test 4 and the partial volume deflagration generated 2 – 4 kPa.

It is recommended that firefighters do not approach a room with suspected ongoing and unignited battery gas release from li-ion batteries in propagating thermal runaway.

B. A significant explosion hazard can develop before any exterior indicators (visual or measurable) are shown.

In Test 4, a partial volume deflagration involving 0.3 kWh of batteries in thermal runaway (1 module, or 2% of the total quantity of cells in the ESS unit) generated approximately 1 kPa of pressure and permanently deformed the garage door outward. The gas was released from only 20 seconds of thermal runaway behavior. One kilopascal would likely break windows, potentially causing shrapnel.

While Test 4 involved a forced ignition, a thermal runaway-ignited deflagration occurred in a 20 ft. shipping container involving the thermal runaway of a module of the same size in a 2020 UL test series. The volume of that container is roughly equivalent to a 1-car garage. In that test, there were also no external indicators of thermal runaway or an explosion hazard. A higher pressure of 2 kPa – 4 kPa bent door hardware and forced open the container door. It is likely more significant damage would occur in a 1-car garage scenario. This indicates that explosion hazards also existed in Test 2 between the beginning of thermal runaway propagation and exterior visual indication that battery gas was being released from the garage.

The explosion incident in Erie, CO, as described in Section 2 of this report, is an example that a significant explosion hazard can develop and even occur without any prior exterior indicators. At that incident, it was known that the garage was filled with smoke, but due to the visual similarity between ordinary smoke and unburned battery gas, the explosion hazard was not recognized. When the explosion occurred, the garage door was thrown from its opening and contacted the helmet of the incident commander as it traveled down the driveway. Given the condition of the garage at the time of arrival, hazard could also have occurred during size-up with no prior indication [26].

.

Figure 184 – Still image of garage door contacting incident commander during explosion incident in Erie, CO.

C. Unburned battery gas ignites readily and can increase the flammability of the smoke in a ventilation-limited fire.

Although unburned battery gas has distinct visual and olfactory characteristics, it can appear similar to, and potentially be mistaken for, smoke from a room and contents fire. It is important to be aware that sparking hand tools and powered saws for cutting ventilation holes can create ignition sources for unburned battery gas. No intentional ignition sources were introduced into Test 2, which demonstrated that even ignition sources provided by thermal runaway itself can ignite unburned battery gas unpredictably.

Enough batteries had gone into thermal runaway during the vent-limited phase of the fire in Test 3 to increase the flammability of the smoke inside the garage. When rotary rescue saw cuts were simulated with a gerb, the smoke ignited immediately upon contact with the sparks, and flames spread around the perimeter of the garage door from which smoke was venting.

D. Without active fire, lithium-ion battery thermal runaways may be recognizable by white/gray battery gas leaking from the structure and forming low-hanging vapor clouds.

White/gray gas and vapor was first observed leaking out from around the garage door after it had first accumulated inside the structure for several minutes of thermal runaway propagation in Test 2. White/gray gases and/or vapors are only produced from the batteries when they experienced thermal runaways without burning, so continued leakage of these from a structure may indicate ongoing thermal runaways and that the batteries have not yet ignited. It is critical to recognize that this smoke appearance and related potential deflagration hazard is contrary to previous size-up guidance that implies “lazy” or non-turbulent white smoke is an incipient fire, and does not cover this potential deflagration risk [52].

It should be considered that environmental conditions such as wind velocity and direction, terrain, and lighting conditions may impair the ability to identify the distinct battery thermal runaway effluent. Structural factors include the tightness of the seal around the garage door and any penetrations through the exterior walls. Figure 185 shows an example of the conditions observed in Test 2, in another UL experiment in 2020, and at the scene of the explosion in Surprise, AZ.

Test 2 (this series) Test 3 in 2020 UL series [39] Surprise, AZ [1]

Figure 185 – Sequence of images from different instances of accumulated battery gas leaking from structures.

E. With or without active fire, stratification of smoke at the ceiling and at the floor indicates the thermal runaway of li-ion batteries.

The components of battery gas stratify near the ceiling and the floor in a room where batteries are experiencing propagating thermal runways. This tends to leave a characteristic visible region between a smoky layer at the floor and a smoky layer at the ceiling. As thermal runaways do not release as much thermal energy as a flaming fire, there is not as much thermally driven gas movement. As such, the gases may appear stagnant or slow-moving. This distinctive two-layer accumulation of lighter gases near the ceiling and heavier gases and vapors along the floor was clearly present in Test 2 as is shown in Figure 183. It is important to recognize that this can represent an immediate flash fire or deflagration hazard.

Test 4 demonstrated that even after a transition to flaming (including a possible deflagration), the layer of battery gas near the floor may still be recognizable and unique to a post-thermal runaway condition. Figure 186 provides two different viewing angles from Test 4 demonstrating this phenomenon.

Figure 186 – Visual indication of thermal runaways in Test 4: hot gas layer developing at ceiling and a clearly defined smoke layer remains at the floor.

F. With an active fire, there are no reliable visual or thermal imaging indicators to confirm battery involvement from the exterior of the structure.

Despite battery gas from thermal runaways being distinct on its own, the indication of batteries in thermal runaway was obscured by heat and smoke when the room and contents were involved in fire, as demonstrated with Test 3 and Test 4. Soot created from the combustion of ordinary combustible materials will likely obscure the whitish/gray appearance of the battery gases and significant temperature rise from the fire will result in buoyancy driven movement. Some behavior of smoke “puffing” out from seams around the garage door was observed, but the behavior was very short lived and may not be noticed or could be mistaken for wind driven behavior. Infrared views did not provide any additional detail that was not visible to the naked eye, and the “puffing” behavior was less observable in IR. Should this “puffing” behavior be observed, firefighters should be aware that battery-gas influenced fire dynamics, including backdraft hazards, are possible.

G. Portable gas meters are not effective for determining whether a garage fire is involves li-ion batteries.

There was no clear indication whether batteries were involved in the garage fire when portable gas meters were used to measure the gas concentrations near the garage door. The peak gas concentrations observed from the fire with no batteries (Test 1) was similar to the peak gas concentrations when many batteries (12 or more modules) entered thermal runaway during a fire (Test 4).

H. During size-up, additional indicators for residential energy storage system installation should be considered beyond smoke appearance.

During size-up, additional indicators beyond the appearance of any battery gas from thermal runaway should be considered to assess the likelihood of battery involvement. Potential indicators that suggest a residence may have an energy storage system installed include the presence of a photovoltaic system, an additional connection at the electric meter, or an electric vehicle. These pieces of equipment may also be identified by their labeling if mounted on the exterior of the structure. If present, the homeowner or resident may also be interviewed to identify the presence or specific location of an energy storage system. Roofing should be closely scrutinized, as it may be challenging to recognize building-integrated photovoltaic panels (i.e., “solar shingles”). Therefore, firefighters should be additionally observant about the introduction of residential energy storage systems in their response coverage areas. Fire departments should consider updating their dispatch cards to include questions that develop pertinent information regarding batteries and photovoltaic systems on the property.

Sounds and smells may also indicate the presence of lithium-ion batteries in thermal runaway. In a Federal Aviation Administration database [53] full of hundreds of li-ion battery incidents, the sound of thermal runaway is described as “popping”, “clapping”, “banging” and “hissing.” The smells of thermal runaways are repeatedly described as “electrical” and “plastic.”

Improvements to battery awareness are also possible before an incident occurs. It may be possible to review permits for the installation of ESS, PV and EV chargers, but this capability will vary from jurisdiction to jurisdiction. An additional possibility is to incorporate questions about whether batteries are installed in a residence or believed to be involved in the fire.

I. Firefighters are at greatest risk for explosion hazards in the driveway and at doors, windows, and other vent points. Do not park fire apparatus or stage crews in front of garage door.

As observed by the forceful gas ejection and garage door damage in Test 2, a deflagration of accumulated battery gas can risk harm to fire fighters in the driveway or other potential vent locations, including windows or doors. The peak pressure is not known for Test 2, but a partial volume deflagration involving approximately 2% (or 0.4 kWh) of the cells in the initiating ESS unit in Test 4 demonstrated that a small volume of battery gas (~213 L) can generate pressures high enough (1-4 kPa) to shatter windows.

Larger battery gas release volumes than what was observed in Test 4 can create higher explosion pressures, detach garage doors, and potentially cause structural damage. Detailed damage information is not available, but two electric vehicle battery thermal runaway incidents that resulted in garage explosions ejected the garage doors tens of feet from the residences. Further data is needed to improve the understanding of the relationship between the amount of gas released from a battery versus explosion hazard severity in residential structures including a better understanding of whether the structure will be damaged by the explosion (i.e., creating additional areas of hazards to firefighters) or if the garage door provides adequate pressure relief capacity.

J. Do not approach or enter to take portable gas meter measurements if there is a suspected case of batteries in thermal runaway and there are no indicators of an active fire.

Measurements from this test series demonstrated that portable gas meter measurements taken from the exterior of the garage cannot provide a reliable indication of an explosion hazard within. The LEL % measurement, which might be anticipated to be most relevant to determining whether an explosion hazard is present, was zero at the garage door location in all tests. Carbon monoxide, and to a lesser extent VOC concentrations, were elevated when cells were in active thermal runaway propagation, but the concentrations were not appreciably different from the baseline in Test 1 when no batteries were involved.

To get to the locations where these measurements were taken an entry team would have to get close to the garage, exposing them to blast wave, flame, and projectile hazards. In a previous set of tests run in 2020 [39], deflagrations were observed as early as 30 seconds after the start of thermal runaway, prior to any of the interior or exterior portable gas meters indicating an increase in flammable gas concentrations and prior to the development of a visible vapor cloud.

An explosion is most likely to occur during active thermal runaways, which adds both further unburned gas and potential ignition sources to the garage. For example, in Test 2, an explosion occurred without any otherwise recognizable warning that an explosion was about to occur. Use of a portable gas meter near the door in this case could have caused serious injury or even death to the user. Distance away from the garage (as demonstrated) and wind will diminish or prevent any potentially useful gas concentration measurements. These same observations were made in a series of walk-in containerized lithium-ion battery experiments conducted by UL in 2020 [39].

The deflagration event in Tests 2 occurred after a vapor cloud had started to form on the exterior of the garage, and exterior portable gas meters measured flammable gas concentrations higher than zero.

Two real world incidents also demonstrate this point. At an ESS explosion in Surprise, AZ the battery gas concentration exterior to a structure with batteries in thermal runaway reduced below levels associated with HAZMAT and explosion hazards. Approximately 3 minutes after the door was opened, outside air had mixed with battery gases to create a flammable mixture and a severe explosion injured 4 firefighters near the door from which gas concentrations we being measured [40]. More recently, an explosion occurred due to an electric battery thermal runaway in a garage in Erie, CO [26]. It is not known if there were any gas measurements collected, but the scene was sized-up with “nothing showing.” The explosion caused the garage door to become a projectile, which narrowly missed a fire fighter standing nearby.

K. Because conditions can change rapidly, full structural PPE with SCBA should be donned before performing size-up. PPE should also be worn in the vicinity of heat impacted batteries until removed from the scene.

This test series demonstrated that it will likely be difficult to recognize any indications that li-ion batteries have generated an explosion hazard or are significantly involved in a room and contents fire. Tests 2 and 4 made clear that conditions can change quickly during a deflagration or rapid increase in fire growth.

Test 2 demonstrated that following deflagration, the driveway can become an area of high risk for respiratory hazards during size-up or preparation for entry by ejecting accumulated smoke and battery gas tens of feet from the structure. High concentrations of toxic gases built up emphasize the need for breathing protection at the level of SCBA. The speed of the hazard development precludes donning protective equipment after the fact. In deflagration, projectiles and thermal hazards may be hazards as well. Structural PPE is not intended for protection from projectile hazards but may reduce thermal hazards sufficiently. Test 4 demonstrated that adding ventilation to a li-ion battery involved fire may create rapid fire growth conditions which preclude donning protective equipment.

It is critical that fire fighters wear adequate PPE when working around heat-impacted batteries during suppression, overhaul, and any protracted scene examination. Any time a lithium-ion battery is heat-impacted, firefighters should anticipate the potential for sudden and unpredictable thermal runaways. Thermal exposure may damage the delicate internal structure of a battery and cause the battery to re-ignite at unpredictable times. The development of smoke and fire from a heat-impacted battery may create life-threatening exposures faster than proper PPE can be donned, therefore it is critical to wear appropriate PPE before handling or working near heat-impacted batteries.

L. Because conditions can change rapidly, hose lines should be pre-deployed, charged, and ready for operations before ventilation or entry when li-ion thermal runaways are suspected. Hose lines should remain available to manage reignition/thermal runaway of heat impacted batteries until removed from the scene.

Venting a garage fire that involves a significant quantity of li-ion batteries in thermal runaway can result in exceptionally fast fire growth and/or a backdraft. Fire fighters should confirm all residents have evacuated from the structure prior to making entry into the home. When fire fighters are conducting search operations, firefighters need to be aware that pressure due to a backdraft may damage the fire-resistant barrier between the garage and living space, enabling fire spread from the garage into the home. This could occur behind their operations.

The results of these tests emphasize the need to treat manual ventilation of a fire that may involve ESS with additional caution. Flammable gas accumulation hazards can exist whether there is visible evidence of thermal runaways or no clear indication of thermal runaways.

Fire fighters should anticipate the potential for ignition of accumulated thermal runaway effluent gases and rapid transition to flashover and/or a backdraft following changes in ventilation when the involvement of a residential ESS unit in a garage fire is suspected. Both a rapid increase in flaming (Test 3) and a backdraft (Test 4) were observed in this test series as a result of changing ventilation.

Test 3 demonstrated enhanced flammability of the smoke when it ignited during simulated saw operation. Once flaming started, any increase in the vent area immediately resulting in an increase in the size of the fire venting through the garage door. Battery gas can increase the flammability of smoke from ventilation limited fires.

Test 4 demonstrated that introducing air into a ventilation limited garage fire involving an ESS unit may result in a backdraft. These findings are consistent with the findings published by UL in 2020 regarding containerized ESS installations [39].

Reignitions were not observed in this testing because the batteries were managed with extreme safety conservatism. Test termination procedures included immediately flooding the battery unit enclosures prior to initiating room fire suppression. While water may cause shorting, which could lead to thermal runaways later, this hazard was managed by immediately disconnecting the units from the structure and expediently moving the affected units to a electrolyte enhanced water bath for managing thermal runaways and dissipating stranded energy. Extreme caution should be exercised in real incidents to consider reignitions of heat impacted batteries that have not been removed from the structure and fire fighters must not put themselves in a position where a heat-impacted battery is in their path of egress during a reignition.

Fire departments should also consider the potential longevity of resource deployment during incidents involving li-ion batteries in structures. The potential for re-ignitions may create extended timelines in which resources must remain committed to post incident standby and are not available for use in other responses.

8 References

[1] C. M. Fleischmann and Z. Chen, “Defining the Difference between Backdraft and Smoke Explosions,” *Procedia Engineering*, vol. 62, pp. 324–330, 2013, doi: 10.1016/j.proeng.2013.08.071.

[2] Underwriters Laboratories Inc., “ANSI/CAN/UL 9540A: Standard for Safety Test Method for Evaluating Thermal Runaway Fire Propagation in Battery Energy Storage Systems.” Underwriters Laboratories Inc., 2019.

[3] National Fire Protection Association and Explosion Protection Systems, *NFPA 68: standard on explosion protection by deflagration venting.* 2018.

[4] John Warner, *The Handbook of Lithium-Ion Battery Pack Design*. Elsevier, 2015.

[5] “29 C.F.R. 1910.120 - Hazardous waste operations and emergency response.” Accessed: Jul. 13, 2023. [Online]. Available: https://www.osha.gov/laws-regs/regulations/standardnumber/1910/1910.120

[6] H. R. Ludwig, S. G. Cairelli, and J. J. Whalen, “Documentation for immediately dangerous to life or health concentrations (IDLHs),” National Institute for Occupational Safety and Health. Division of Standards Development and Technology Transfer., May 1994.

[7] “Residential Energy Storage Market by Power Rating (3–6 kW & 6–10 kW), Connectivity (On-Grid & Off-Grid), Technology (Lead–Acid & Lithium-Ion), Ownership (Customer, Utility, & Third-Party), Operation (Standalone & Solar), Region - Global Forecast to 2024,” Markets and Markets, Apr. 2019. [Online]. Available: https://www.marketsandmarkets.com/Market-Reports/residential-energy-storage-market-153284325.html

[8] “Battery Energy Storage Market Size, Share & COVID-19 Impact Analysism By Type (Lithium-Ion Battery, Lead Acid Battery, Flow Battery, Others), By Connectivity (Off-Grid, On-Grid), By Application (Residential, Non-Residential, Utility, Others), By Ownership (Customer-Owned, Third-Party Owned, Utility-Owned), By Capacity (Small Scale {Less than 1 MW}, Large Scale {Greater than 1 MW}), and Regional Forecast, 2022-2029,” Fortune Business Insights, Mar. 2022. [Online]. Available: https://www.fortunebusinessinsights.com/industry-reports/battery-energy-storage-market-100489

[9] A. David, “Residential Energy Storage: U.S. Manufacturing and Imports Grow Amid Rising Demand,” Office of Industries, U.S. International Trade Commission, Washington, DC, No. ID-077, Jul. 2021.

[10] S. Ray, “Solar power and batteries account for 60% of planned new U.S. electric generation capacity,” U.S. Energy Information Administration, Mar. 2022. Accessed: May 12, 2022. [Online]. Available: https://www.eia.gov/todayinenergy/detail.php?id=51518

[11] S. Enkhardt, “Senec remotely switches off its residential batteries after explosion in Germany,” p. 7.

[12] S. W. R. Aktuell, “Nach Explosion in Bodnegg: Hersteller nimmt Stromspeicher wieder in Betrieb,” swr.online. Accessed: May 16, 2022. [Online]. Available: https://www.swr.de/swraktuell/baden-wuerttemberg/friedrichshafen/stromspeicher-gehen-schrittweise-wieder-in-betrieb-100.html

[13] “Standby mode | SENEC.” Accessed: May 16, 2022. [Online]. Available: https://senec.com/de/standby-modus

[14] “Explosion eines Batteriespeichers sorgt für Kellerbrand – diesmal kein Senec-Speicher,” pv magazine Deutschland. Accessed: May 16, 2022. [Online]. Available: https://www.pv-magazine.de/2022/05/09/explosion-eines-batteriespeichers-sorgt-fuer-kellerbrand-diesmal-kein-senec-speicher/

[15] Redaktion, “Anlage war fast neu: Batterie für Photovoltaik explodiert - 100.000 Euro Schaden durch Brand in Unterfranken,” *inFranken.de*, Wohnhausbrand, Germany, Jul. 19, 2018. Accessed: Mar. 28, 2022. [Online]. Available: https://www.infranken.de/lk/wuerzburg/anlage-war-fast-neu-batterie-fuer-photovoltaik-explodiert-100-000-euro-schaden-durch-brand-art-3550416

[16] Redaktion, “Grub am Forst: Speicherbatterie löst Explosion aus,” *Neue Presse*, Coburg, Germany, Sep. 04, 2020. Accessed: Mar. 28, 2022. [Online]. Available: https://www.np-coburg.de/inhalt.laenderspiegel-grub-am-forst-speicherbatterie-loest-explosion-aus.135ae409-ffc6-453d-b0b8-b1d653e03752.html

[17] S. W. R. Aktuell, “Herstellerfirma zieht Konsequenzen nach Explosion von Batteriespeicher,” swr.online. Accessed: May 16, 2022. [Online]. Available: https://www.swr.de/swraktuell/baden-wuerttemberg/friedrichshafen/nach-explosion-in-bodnegg-zieht-firma-konsequenzen-100.html

[18] “Senec setzt auf maximale Sicherheit – Neuer Zwischenfall gemeldet,” pv magazine Deutschland. Accessed: May 16, 2022. [Online]. Available: https://www.pv-magazine.de/2022/04/28/senec-setzt-auf-maximale-sicherheit-neuer-zwischenfall-gemeldet/

[19] C. B. C. News ·, “Electric car catches fire and explodes in Île-Bizard garage | CBC News,” CBC. Accessed: May 13, 2022. [Online]. Available: https://www.cbc.ca/news/canada/montreal/electric-car-catches-fire-and-explodes-in-%C3%AEle-bizard-garage-1.5227665

[20] A. Cramer, “‘Battery bunker’ burns in Brown’s Canyon,” p. 2.

[21] “Warning about maintaining solar panel batteries after Adelaide house badly damaged in fire,” *ABC News*, Feb. 13, 2022. Accessed: May 16, 2022. [Online]. Available: https://www.abc.net.au/news/2022-02-13/adelaide-house-fire-linked-to-solar-panel-batteries/100826624

[22] “横浜・港北区の住宅で火事　ソーラーパネル蓄電池の火を、家人が目撃（カナロコ by 神奈川新聞）,” Yahoo!ニュース. Accessed: May 16, 2022. [Online]. Available: https://news.yahoo.co.jp/articles/737c2ab3a8998b78d2e1526ebe37e51569f45887

[23] “Explosion im Kreis Calw: Feuerwehrleute haben Riesen-Glück,” SWR3.de. Accessed: May 13, 2022. [Online]. Available: https://www.swr3.de/aktuell/nachrichten/kreis-calw-batteriespeicher-explodiert-100.html

[24] D. Brooks, “NewHampshire.pdf,” *Concord Monitor*, Concord, NH, Dec. 21, 2022. Accessed: Jan. 04, 2023. [Online]. Available: https://www.concordmonitor.com/battery-fire-sanbornton-nh-49277924

[25] Fire and Rescue New South Wales, “FIRE AND RESCUE NSW INVESTIGATORS DETERMINE A FAULTY LITHIUM ION BATTERY CAUSED A VILLA FIRE AT EPPING - VIDEO - EPPING,” Fire and Rescue NSW. Accessed: Apr. 13, 2023.

[Online]. Available: https://www.fire.nsw.gov.au/incident.php?record=recGkTV93cx6ZN0gA

[26] Mountain View Fire Rescue [@MVFireRescue], “It was a scary moment for our crews this morning on a call in Erie. Report came in as a structure fire with smoke in the home. Turned out to be a hybrid on fire, which lead to a small explosion from the battery. Full details are in the infographic. https://t.co/GyhIwTbAhq,” Twitter. Accessed: Apr. 12, 2023. [Online]. Available: https://twitter.com/MVFireRescue/status/1645910121271406593

[27] *2021 IRC: international residential code for one- and two-family dwellings*, 2021 edition. Country Club Hills, IL: International Code Council, Inc., 2020.

[28] International Code Council, *IFC: International fire code, 2021*. 2020.

[29] Underwriters Laboratories Inc., “ANSI/CAN/UL 9540:2020 Standard for Safety for Energy Storage Systems and Equipment.” Feb. 27, 2020.

[30] “NFPA 855 - Standard for the Installation of Stationary Energy Storage Systems.” 2020.

[31] V. Salandro, “When It Comes to Garages, Buyers Want Space for at Least Two Cars,” *Builder Magazine*, pp. 1–5, Oct. 30, 2018.

[32] “Residential Building Garage Fires (2009-2011),” *U.S. Fire Administration*, vol. 14, no. 12, p. 11, Nov. 2013.

[33] B. Gustin, “Fire Tactics for Attached Garages.” Fire Engineering University.

[34] “Fighting Fire in Attached Garages,” Firefighter Nation. [Online]. Available: https://www.firefighternation.com/firerescue/fighting-fire-in-attached-garages/

[35] National Fire Protection Association and National Fire Protection Association, *NFPA 13 standard for the installation of sprinkler systems, 2019.* 2018.

[36] A. Barowy, A. Schraiber, and R. Zalosh, “Explosion protection for prompt and delayed deflagrations in containerized lithium-ion battery energy storage systems,” *Journal of Loss Prevention in the Process Industries*, vol. 80, p. 104893, Dec. 2022, doi: 10.1016/j.jlp.2022.104893.

[37] “Open Path Gas Detection | Boreal Laser.” Accessed: Apr. 21, 2023. [Online]. Available: https://boreal-laser.com/

[38] HAZCALC, “MIE - Minimum Ignition Energy.” Accessed: Apr. 17, 2023. [Online]. Available: https://hazcalconline.com/wp-content/uploads/2021/09/2021-MIE-list.pdf

[39] A. Barowy, A. Klieger, J. Regan, and M. McKinnon, “UL 9540A Installation Level Tests with Outdoor Lithium-ion Energy Storage System Mockups,” UL LLC, Northbrook, Illinois, Apr. 2021.

[40] M. B. McKinnon, S. DeCrane, and S. Kerber, “Four Firefighters Injured In Lithium-Ion Battery Energy Storage System Explosion - Arizona,” p. 66.

[41] R. Ogle, “Explosion hazard analysis for an enclosure partially filled with a flammable gas,” *Process Safety Progress*, vol. 18, pp. 170–177, Apr. 2004, doi: 10.1002/prs.680180310.

[42] *Guidelines for Vapor Cloud Explosion, Pressure Vessel Burst, BLEVE, and Flash Fire Hazards*, 2nd ed. Center for Chemical Process Safety.

[43] “Home garage fire safety outreach materials,” U.S. Fire Administration. Accessed: Apr. 04, 2023. [Online]. Available: https://www.usfa.fema.gov/prevention/outreach/garage_fires.html

[44] “2019 California Residential Code section R327.7 for Heat Detection for Energy Storage Systems,” CAL FIRE, Jul. 2021.
[45] “Hyundai Kona Electric Explodes, Blows Hole In Garage: Cause Unknown,” InsideEVs. Accessed: Apr. 04, 2023. [Online]. Available: https://insideevs.com/news/362202/hyundai-kona-electric-explodes-canada/
[46] E. C. Evarts, “Hyundai Kona Electric explodes in Montreal garage,” p. 20.
[47] National Fire Protection Association, “NFPA 715: Standard for the Installation of Fuel Gases Detection and Warning Equipment.” National Fire Protection Association, 2022.
[48] “NFPA Journal - Early Warning, November/December 2020.” Accessed: Apr. 12, 2023. [Online]. Available: http://www.nfpa.org/News-and-Research/Publications-and-media/NFPA-Journal/2020/November-December-2020/Features/Gas
[49] S. Davis, D. Engel, and J. Pagliaro, “Combustible Gas Dispersion in Residential Occupancies and Detector Location Analysis,” Fire Protection Research Foundation, 2020.
[50] National Institute for Occupational Safety and Health, “Hydrogen Fluoride (as F).” Centers for Disease Control and Prevention, 1994. Accessed: Aug. 08, 2023. [Online]. Available: https://www.cdc.gov/niosh/idlh/7664393.html
[51] “Fuels and Chemicals - Autoignition Temperatures.” Accessed: Apr. 18, 2023. [Online]. Available: https://www.engineeringtoolbox.com/fuels-ignition-temperatures-d_171.html
[52] “David Dodson: The Art of Reading Smoke - Fire Engineering: Firefighter Training and Fire Service News, Rescue.” Accessed: Aug. 07, 2023. [Online]. Available: https://www.fireengineering.com/leadership/david-dodson-the-art-of-reading-smoke/
[53] “Workbook: LithiumBatteries.” Accessed: Apr. 17, 2023. [Online]. Available: https://explore.dot.gov/t/FAA/views/LithiumBatteries/IncidentDetails?%3Aembed=y&%3AisGuestRedirectFromVizportal=y
[54] “Electrochemical type - Operating principle - Technology - FIGARO Engineering inc.” Accessed: Jul. 13, 2023. [Online]. Available: https://www.figaro.co.jp/en/technicalinfo/principle/electrochemical-type.html
[55] “RAE Systems Technical Note TN-114: Sensor Specifications and Cross-Sensitivities,” RAE Systems, 2018.
[56] “ID 0802-91-MC / ALTAIR® 5X Multigas Detector,” MSA, Cranberry, MA, 2011.
[57] “Ventis Pro Series Product Manual, Edition 9,” Industrial Scientific, Pittsburgh, PA, 2017.
[58] “Sensor Technology - Delphian Corporation.” Accessed: Jul. 13, 2023. [Online]. Available: https://delphian.com/sensor-tech.htm
[59] “What You Need to Know about Sensor Poisons and Inhibitors.” Accessed: Jul. 13, 2023. [Online]. Available: https://www.indsci.com/en/blog/what-you-need-to-know-about-sensor-poisons-and-inhibitors
[60] “Application Note AP-219: Using Pids For 10% Of Lel Decisions,” RAE Systems, 2010.
[61] “Technical Note TN-106: A Guideline for PID Instrument Response,” RAE Systems, 2018.

[62] "Technical Note TN-169: Theory and Operation of NDIR Sensors," RAE Systems, 2002.
[63] A. Dey, "Semiconductor metal oxide gas sensors: A review," *Materials Science and Engineering: B*, vol. 229, pp. 206–217, Mar. 2018, doi: 10.1016/j.mseb.2017.12.036.

Appendix A: Development Tests of ESS Unit

Module

Each residential mockup unit consisted of 48 modules. Each module included 30 individual 18650-format cells in a plastic enclosure. One cell (“1” in Figure 187) in the mockup module was heated to thermal runaway with a film heater at 6 °C/min.

The subsequent thermal runaway propagation and fire size was measured by oxygen consumption calorimetry, as reported in Figure 188. The peak heat release rate was 300 kW for less than 10 seconds. The condition of the module at the moment of peak heat release rate is shown in Figure 189.

Figure 187 – Module construction (left) and assembly (right).

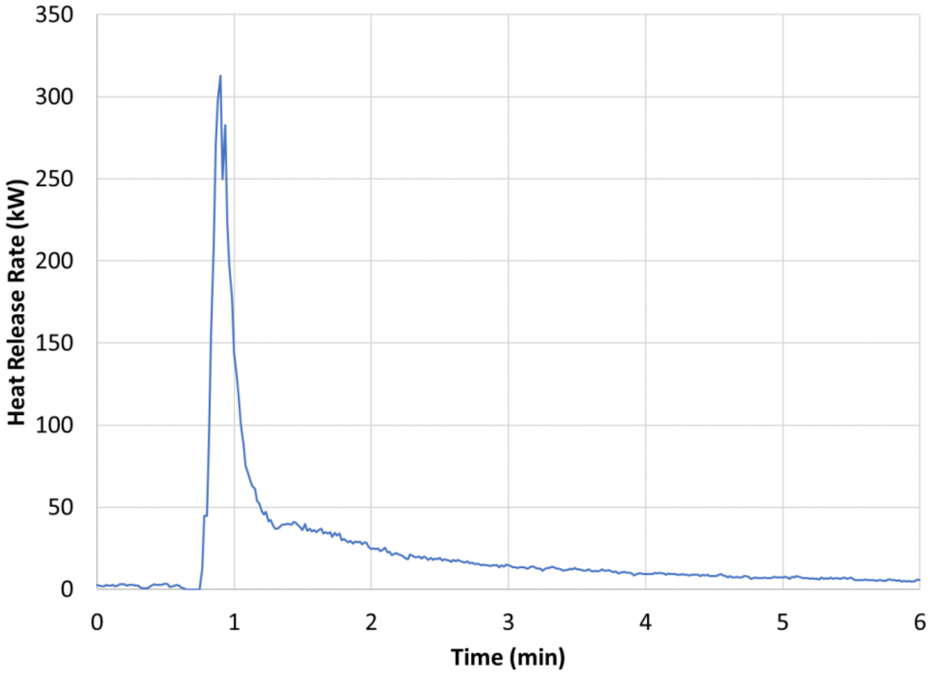

Figure 188 – Module heat release rate.

Figure 189 – Photo of module at peak heat release rate.

Unit

Several design features were included in this design based on a review of commercially available products. These features include:

- Wall-mounted
- Steel enclosure
- Equipment space for a BMS/Inverter
- Openings for conduit interconnection or ventilation near the BMS area
- Rectangle shape with thin profile
- Dividers between collections of component cells

The unit was designed to create a condition of module-to-module thermal runaway propagation.

Two tests were conducted with the unit to characterize its performance in advance of the large-scale tests presented in this report. Scenario 1 was initiated with thermal runaway in a cell with observation of the resultant thermal runaway propagation, unit-to-unit thermal runaway propagation, and unit-to-Commodity fire spread. Scenario 2 was initiated with ignition of the Group A Commodity with observation of thermal runaway initiation and propagation to a partially populated ESS unit.

Scenario 1 – Event development initiated by thermal runaway

Scenario 1 included two ESS units. The units were spaced 3 inches apart from cover to cover (4 inches apart between the interior battery modules). The target array of Group A commodity was located 36 inches away. Thermal runaway was initiated in one cell within one module (“Init 1”). The test setup is pictured in Figure 190 with instrumentation layout in Figure 191 and Figure 192 for the initiating unit and target unit, respectively.

Figure 190 – Interior of ESS units (left) and complete test setup (right) for Scenario 1.

The first cell entered thermal runaway following 32 minutes and 11 seconds of external heating. Once the rest of the cells in the module underwent thermal runaway, 9 minutes and 23 seconds later, the battery vent gases and ESS unit materials ignited. Thermal runaway propagated module-to-module through the bottom quarter of modules, as indicated by the thermal runaway timeline included in Table 15. Fourteen (14) minutes and 50 seconds after the first cell thermal runaway, the target stack of commodity boxes ignited on the face closest to the ESS unit. Peak heat release of 5,000 kW was reached within four minutes of commodity ignition. Fire size at key moments of the test are highlighted in Figure 194. This accelerated thermal runaway propagation through the unit.

Approximately three minutes after the commodity boxes ignited, the modules of the left target unit experienced thermal runaway. Complete burnout occurred around 65 minutes of test time, approximately a half hour since the first cell thermal runaway, as plotted in Figure 193. Post test condition of the ESS units and commodity boxes are pictured in Figure 195.

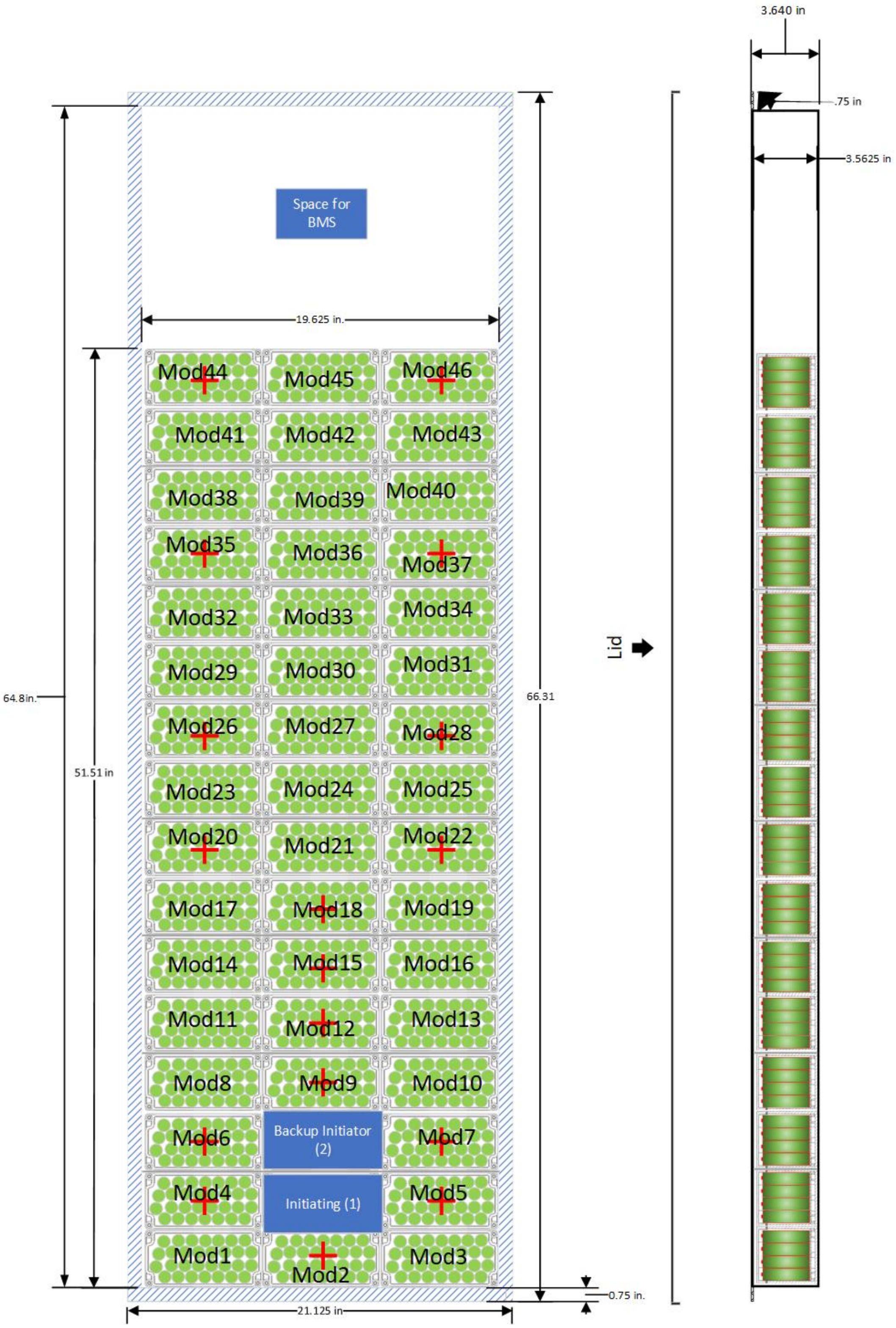

Figure 191 – Initiating unit instrumentation layout.

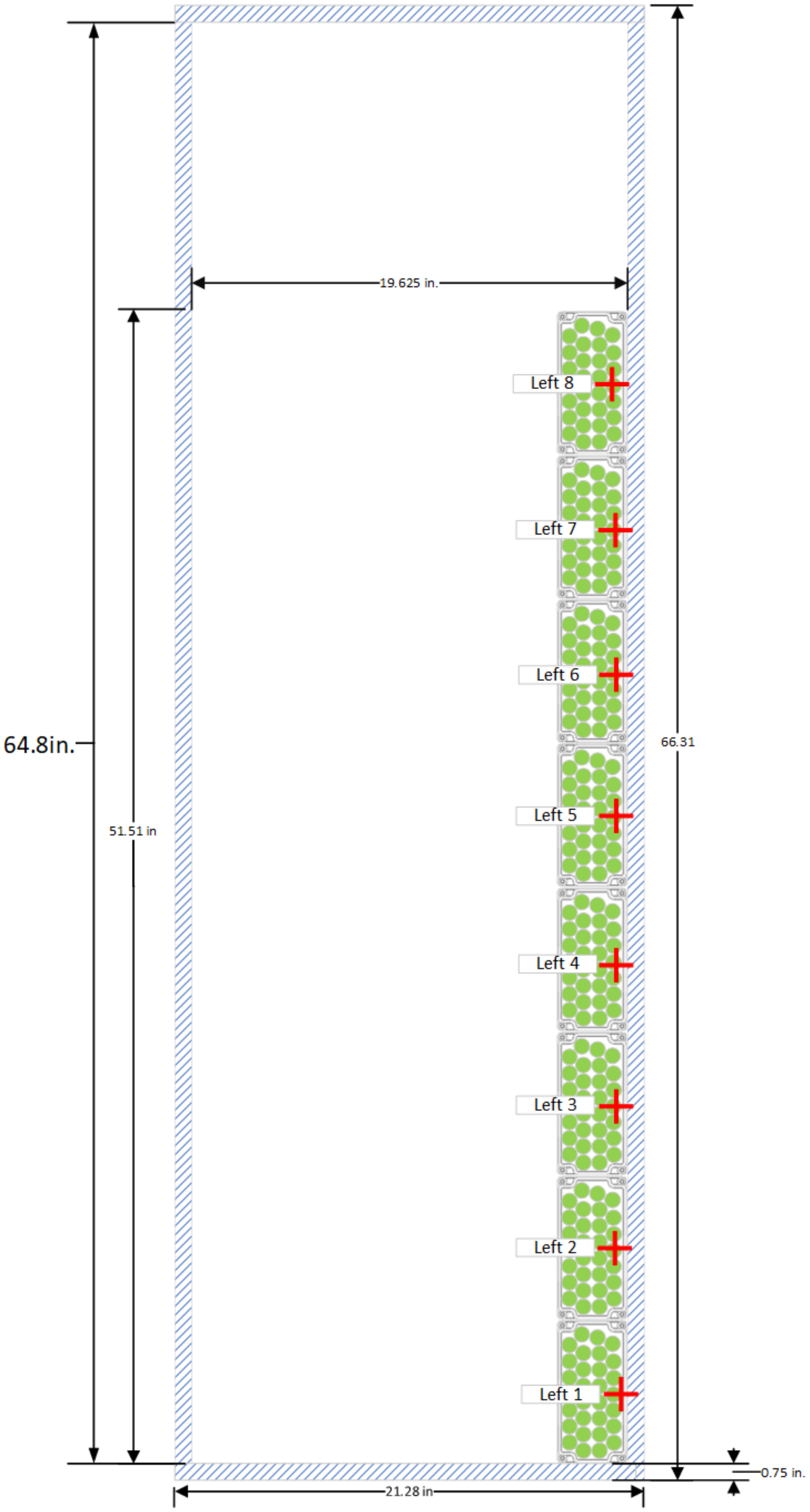

Figure 192 – Left target unit instrumentation layout used in Scenario 1 and Scenario 2.

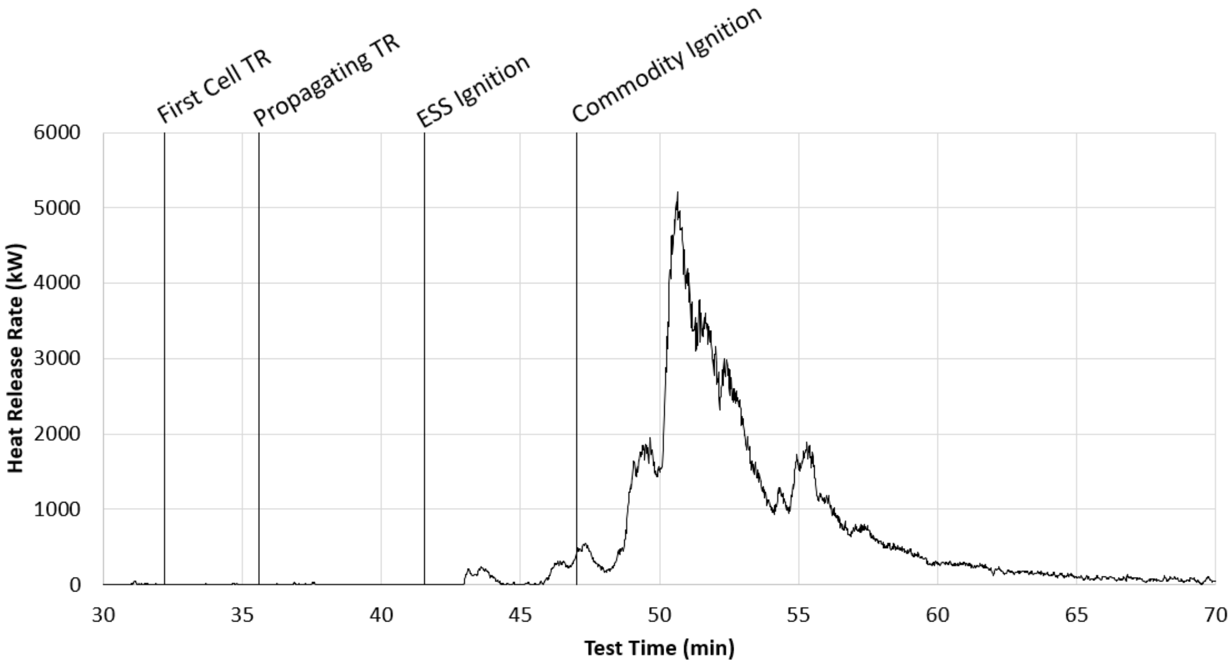

Figure 193 – Heat release rate from the first cell thermal runaway to the end of the test in Scenario 1.

Table 15 – Timing of thermal runaway and major test events in Scenario 1.

Thermal Runaway Location/Event	Time (MM:SS)	Time since first TR (MM:SS)
Init 1	32:11	00:00
ESS Ignition	41:34	09:23
Init 2, Mod 2	42:55	10:44
Mod 5	45:39	13:28
Mod 9	45:56	13:45
Mod 4	46:35	14:24
Commodity Box Ignition	47:01	14:50
Mod 7, Mod 20	47:14	15:03
Mod 26, Mod 28, Mod 35, Mod 37, Mod 46	47:15	15:04
Mod 15	47:43	15:32
Mod 44	48:35	16:24
Mod 12	48:40	16:30
Mod 18, Mod 22	50:11	18:00
Left 2, Left 3, Left 4, Left 5, Left 6, Left 7, Left 8	50:29	18:19
Left 1	51:56	19:45

Gas venting from ESS unit
(TR + 03:31)

Ignition at bottom corner of ESS
(TR + 09:23)

Flaming of ESS during active thermal runaway
(TR + 10:43)

Ignition of Commodity boxes
(TR + 14:50)

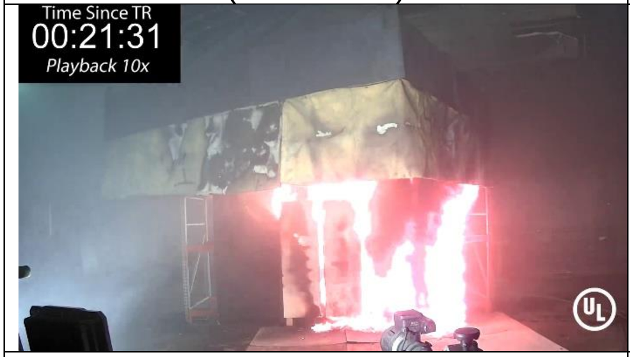

Fire growth and propagation into adjacent unit (TR + 21:31)

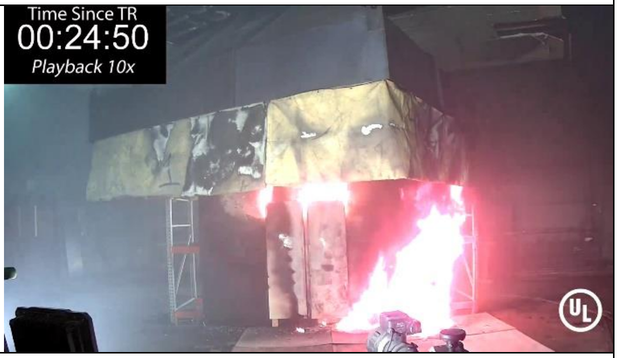

Fire decay and continued thermal runaway (TR + 24:50)

Figure 194 – Images showing test progression in Scenario 1.

Figure 195 – Post-test condition of ESS units and Commodity boxes in Scenario 1.

Scenario 2 – Event development initiated in ignition of Group A Commodity

Scenario 2 included one ESS target unit positioned 36 inches to the left of an array of Group A commodity. The test was initiated by igniting the bottom commodity box on the face nearest the ESS with an electric match. The test setup is pictured in Figure 196. The target unit is instrumented in the same layout as the left target of Scenario 1 (Figure 192).

Figure 196 – ESS unit interior (left) and complete setup (right).

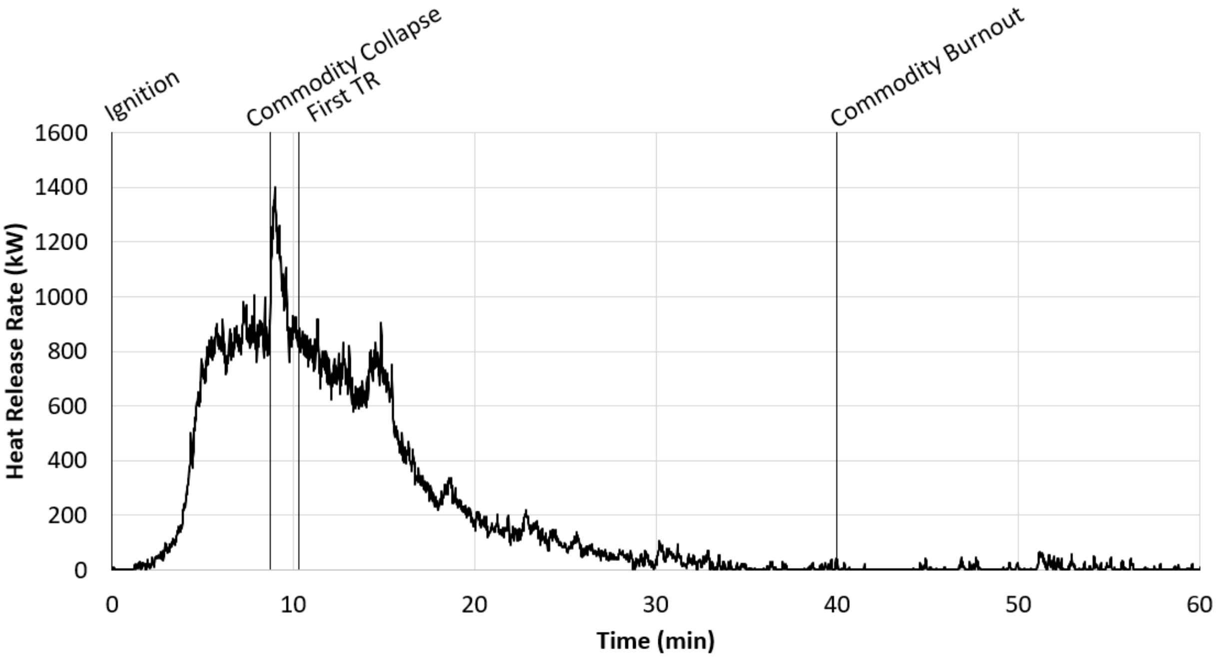

Figure 197 – Heat release rate from the first cell thermal runaway to the end of the test in Scenario 2.

Ignition occurred in the lowest inner face of the commodity stack. After 8 minutes and 43 seconds of fire growth, the stack collapsed towards the ESS unit. Peak heat release rate of 1,400 kW occurred immediately after the stack collapsed. Approximately 90 seconds after the collapse, thermal runaway occurred in the lowest module of the ESS unit. Thermal runaway propagated through the next three lowest modules within one minute. These four modules were directly adjacent to the collapsed boxes. Seven (7) minutes later, thermal runaway occurred in the next lowest module, “Target 5”. Propagation continued upwards with propagation times noted in

Table 16. Thermal runaway occurred in the final module, “Target 8” nearly 10 minutes after burnout of the commodity boxes. Images from key test events are included in Figure 198. Post-test condition is pictured in Figure 199.

Table 16 – Timing of thermal runaway and major test events in Scenario 2.

Thermal Runaway Location/Event	Time (MM:SS)
Commodity Box Ignition	00:00
Commodity Box Stack Collapse	08:43
Target 1	10:17
Target 4	10:19
Target 3	10:34
Target 2	10:58
Target 5	17:24
Target 6	22:03
Target 7	30:00
Commodity Box Burnout	40:00
Target 8	49:39

Note: If the ESS had been fully populated, these propagation times would likely be different.

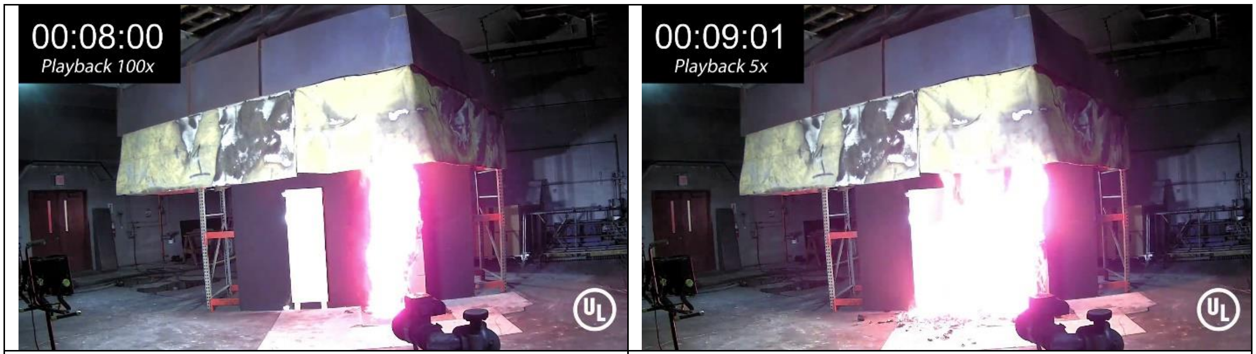

Commodity fire growth before ESS involvement (08:00)

Commodity fire growth and collapse of stack (09:01)

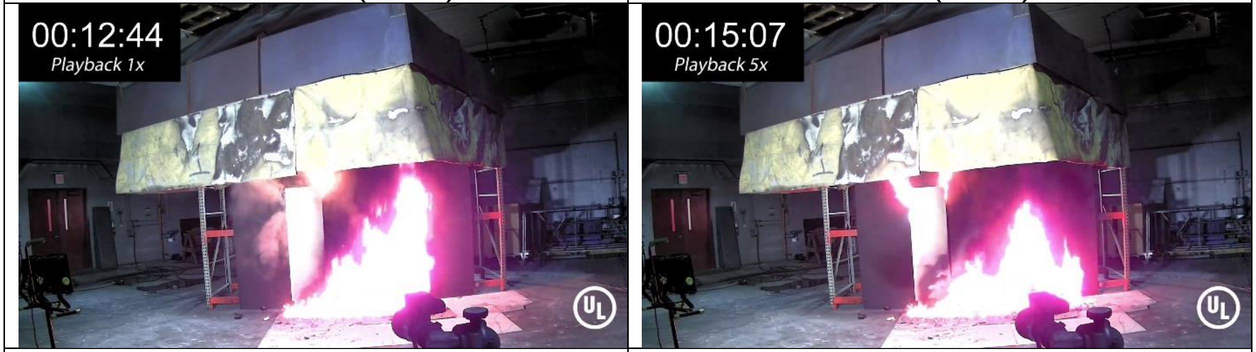

Commodity fire growth and thermal runaway in ESS (12:44)

Continued thermal runaway and flaming from ESS (15:07)

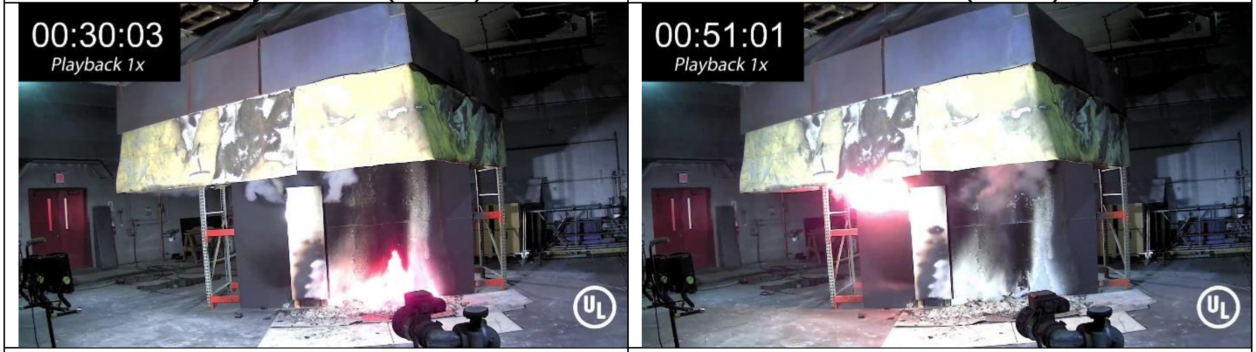

Continued thermal runaway and decay of fire from commodity boxes (30:03)

Thermal runaway in final module after burnout of commodity boxes (51:01)

Figure 198 – Images showing test progression in Scenario 2.

Figure 199 – Post-test condition of ESS unit and Commodity boxes in Scenario 2.

Appendix B: Portable Gas Meter Technologies

This Appendix describes the operating principles of the various technologies used in the portable gas meters used in this investigation.

Electrochemical

Electrochemical sensors consist of at least three distinct components. These components include a sensing electrode, a counter electrode, and an ion conductor between the two electrodes. The operating principle of electrochemical gas sensors involves the reduction or oxidation of a target gas at the sensing electrode, which generates an electric potential or the flow of current through the ion conductor to the counter electrode. Electrochemical sensors may be the amperometric type, in which the measurand is the current between the electrodes, or the potentiometric type, in which the measurand is the electric potential between the two electrodes [54].

To relate the current or electric potential between the electrodes to a specific target gas concentration, the rate of gas flow to the sensing electrode must be controlled. This is often achieved using a diffusion film or a pinhole. The flow control mechanism may also incorporate filters to selectively allow gas species to come in contact with the sensing electrode. The flow control mechanism is a possible point of failure or source of uncertainty for electrochemical sensors that have been exposed to atmospheres that compromise the integrity of the mechanism. Silicon vapors, sulfuric acid gas, and excessive condensation of water vapor may foul the permeable diffusion film. Additionally, salt-water spray, basic gases, dust or oil mist, and frozen water may permanently affect the ability of the sensor to accurately measure gas concentrations.

Due to the relative simplicity of electrochemical gas sensors and the inability to completely filter out unwanted gas species, electrochemical sensors often suffer from cross-sensitivities in which the presence of a non-target gas interferes with the measurement and indicates an erroneously higher or lower target gas measurement. Table 5 (in the body of the report) shows cross sensitivities for the gases of interest within the sensors of RAE meters used in this work [55]–[57].

Electrochemical sensors are a low-cost and low-power option for measuring oxygen concentration as well as low-level concentrations of toxic gases (on the order of parts per million (ppm)). These advantages make electrochemical sensors ideal for portable multi-gas meters used by firefighters and HAZMAT personnel. These advantages must be weighed against the limitations and cross-sensitivities of specific electrochemical sensors when determining which meters and sensors to use during an emergency response.

Catalytic Bead

A catalytic bead sensor is comprised of a small catalytic bead supported by an electrically conductive wire. The catalyst facilitates combustion of a mixture of gases and vapors at temperatures significantly lower than would typically be required for combustion. Local combustion of the gas mixture on the surface of the catalytic bead increases the temperature of the wire in proportion to the concentration of a specific flammable gas in the mixture, which affects the electrical conductivity of the wire in a predictable way [58]. Catalytic bead sensors are typically only suitable for measuring the concentration of flammable gases up to the lower explosive limit (LEL).

Catalytic bead sensors can only provide an accurate assessment of the concentration of a gas when a single, known flammable gas is present in a mixture. This technology does not allow for identification and quantification of an unknown gas species or mixture. Most catalytic bead sensors are calibrated to a specific flammable gas (typically methane, propane, or pentane) and correction factors are used to convert a measurement from the calibration basis to the measured gas species basis. Table 17 shows a chart with listed correction / cross-sensitivity data for a catalytic bead sensor calibrated with methane [55]. Additionally, most catalytic bead sensors are affected by elevated gas temperature and are not typically used in high temperature environments.

Table 17 – Correction factors for a catalytic bead LEL sensor calibrated for Methane.

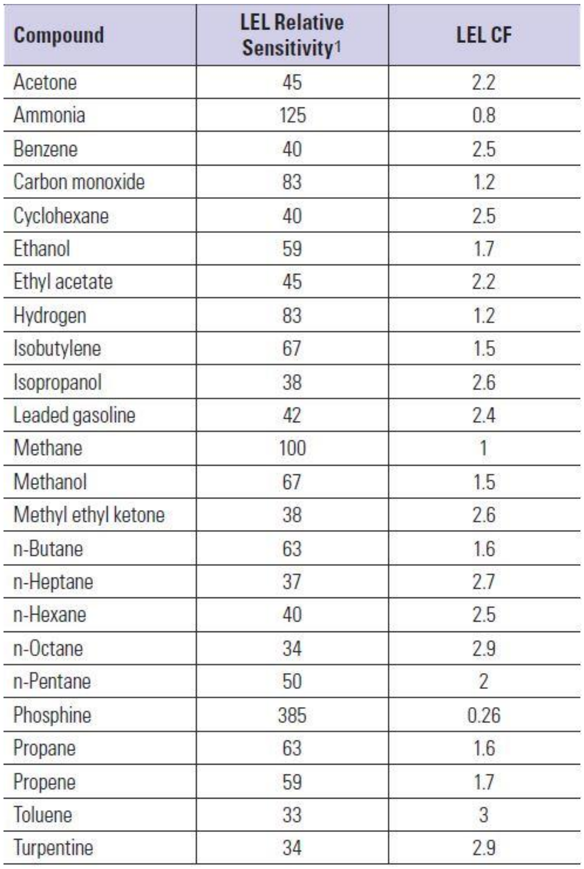

Compound	LEL Relative Sensitivity[1]	LEL CF
Acetone	45	2.2
Ammonia	125	0.8
Benzene	40	2.5
Carbon monoxide	83	1.2
Cyclohexane	40	2.5
Ethanol	59	1.7
Ethyl acetate	45	2.2
Hydrogen	83	1.2
Isobutylene	67	1.5
Isopropanol	38	2.6
Leaded gasoline	42	2.4
Methane	100	1
Methanol	67	1.5
Methyl ethyl ketone	38	2.6
n-Butane	63	1.6
n-Heptane	37	2.7
n-Hexane	40	2.5
n-Octane	34	2.9
n-Pentane	50	2
Phosphine	385	0.26
Propane	63	1.6
Propene	59	1.7
Toluene	33	3
Turpentine	34	2.9

Because the operation of catalytic bead sensors depends on combustion of the sample gas mixture at the bead surface, this technology is only suitable in oxygen-containing atmospheres. Additionally, vitiated oxygen conditions and samples with a gas mixture concentration above the LEL may result in erroneously low measurements. The catalyst may lose sensitivity due to catalyst poisoning from specific trace gases. Common catalyst poisons include silicone, halocarbons, and metallo-organic compounds.

Catalytic bead sensors are particularly susceptible to poisoning and inhibitors. Sensor poisons are chemicals or substances that react directly with the heated catalyst to permanently damage the sensor. Inhibitors are chemicals that can temporarily affect the sensitivity of the sensor, and if a mixture of gases is combustible and contains an inhibitor, the sensor may not be able to detect the combustible gases. Some of the most common potential inhibitors are halogenated compounds, which include many clean agents that are available for suppression [59].

Photoionization Detector (PID)

PIDs involve shining an ultraviolet (UV) light through a sample gas. If the photon energy of the UV light used in the PID is greater than the ionization energy of the target gas molecules, the molecules are ionized (electrons are ejected from the molecules). The ejected electrons are collected on charged grids and produce an electric current, which is proportional to the amount of gas in the sample [60]. Gases with ionization energies higher than the lamp photon energy are typically not detected.

PIDs are useful because they are sensitive to volatile organic compounds (VOCs) that may be flammable or toxic but are not typically measured using a targeted electrochemical sensor and may detect these compounds at sub-ppm concentrations. Different UV lamp photon energies allow for either a wider range of gases detected (higher energy) or a more sensitive detector with a more selective list of possible gases detected (lower energy). This technology is unable to identify components of an unknown gas mixture but can indicate the presence and total concentration of VOCs within the range of ionization energies suitable for the UV lamp. Common compounds expected to be detected by a 10.6 eV lamp have been tabulated by the manufacturers [61].

Non-Dispersive Infrared (NDIR)

NDIR sensors consist of a polychromatic light source, a detector, and a filter to selectively allow light with a specific band of wavelengths through to the detector. As infrared light interacts with gas molecules, a portion of the light is absorbed by the molecules, resulting in vibrations that increase the temperature of the gas. The amount of infrared light absorbed by the gas sample is directly proportional to the concentration of the target gas in the sample [62].

Specific chemical bonds absorb a unique wavelength of light in the infrared spectrum. The carbon dioxide covalent bonds absorb infrared light at 4.26 microns, and the carbon-hydrogen covalent bond common in hydrocarbons has a strong absorption peak from 3.3-3.5 microns. Detectors designed to measure concentrations of each of these gases incorporate a filter to allow light in these wavelength ranges to the detector.

NDIR detectors designed to measure hydrocarbon concentrations are not selective and are incapable of identifying specific gas species. Two advantages of NDIR sensors for LEL monitoring over catalytic bead sensors are that the sample gas atmosphere is not required to contain oxygen, and the sensor may be able to measure flammable gas concentrations above the LEL.

Solid-State (Metal-oxide Semiconductor)

Solid-state sensors, also known as metal-oxide semiconductor sensors, are comprised of a thin layer of metal oxide on the surface of a non-conductor. The semiconductor layer connects two electrodes. In normal ambient air, electrons in the metal oxide are attracted toward oxygen, which is adsorbed at the surface of the semiconductor. This effectively results in no current flow through the semiconductor.

When a target gas from the atmosphere is present at the sensing surface, some of the absorbed oxygen is reduced by the target gas molecules, which frees up electrons in the semiconductor. These free electrons effectively decrease the electrical resistance and allow current flow. The electrical resistance of the semiconductor varies logarithmically with the gas concentration [63].

This technology is sensitive but inherently non-specific and cannot be used to identify the components in an unknown gas mixture. The sensitivity of the semiconductor sensor may be affected by humidity and temperature. This technology can only be used in an atmosphere with oxygen, and vitiated conditions may result in erroneous readings.